THE UNIVERSITY OF CALGARY

An Experimental Investigation of the Flow Structure and Stability Limits of Jet Diffusion Flames in a Co-flowing Oxidizing Stream

by

Nancy Papanikolaou

A DISSERTATION

SUBMITTED TO THE FACULTY OF GRADUATE STUDIES

IN PARTIAL FULFILMENT OF THE REQUIREMENTS FOR THE

DEGREE OF DOCTOR OF PHILOSOPHY

DEPARTMENT OF MECHANICAL ENGINEERING

CALGARY, ALBERTA

MAY 1998

© Nancy Papanikolaou 1998

National Library of Canada
Bibliothèque nationale du Canada

Acquisitions and Bibliographic Services
Acquisitions et services bibliographiques

395 Wellington Street
Ottawa ON K1A 0N4
Canada

395, rue Wellington
Ottawa ON K1A 0N4
Canada

Your file Votre référence

Our file Notre référence

The author has granted a non-exclusive licence allowing the National Library of Canada to reproduce, loan, distribute or sell copies of this thesis in microform, paper or electronic formats.

L'auteur a accordé une licence non exclusive permettant à la Bibliothèque nationale du Canada de reproduire, prêter, distribuer ou vendre des copies de cette thèse sous la forme de microfiche/film, de reproduction sur papier ou sur format électronique.

The author retains ownership of the copyright in this thesis. Neither the thesis nor substantial extracts from it may be printed or otherwise reproduced without the author's permission.

L'auteur conserve la propriété du droit d'auteur qui protège cette thèse. Ni la thèse ni des extraits substantiels de celle-ci ne doivent être imprimés ou autrement reproduits sans son autorisation.

0-612-31062-0

Canada

Abstract

The blowout limits of non-premixed jet flames issuing into a co-flowing oxidizing stream were experimentally studied with methane as the primary jet fuel. The experiments were conducted on two different types of nozzles (i.e., long tubes and short nozzles) of various discharge diameters and ellipticity. There were two distinct regions in which the flame extinguished as either a lifted flame or an attached flame, depending on the value of the co-flowing stream velocity. The flame blew out as a lifted flame in low co-flowing stream velocities while attached flame blowout occurred at relatively higher co-flowing stream velocities.

For a constant jet discharge area, a variation in the nozzle configuration had little effect on the blowout limits of lifted flames but it did play a significant role in the stability of attached flames. The range of co-flowing stream velocities, in which jet diffusion flames can be stabilized without additional external devices, was extended with an increase in the thickness of the nozzle lip. The stability limits of attached flames were also dependent on the ellipticity of the nozzle and an optimum aspect ratio with respect to the blowout limits was observed.

The effect of changes in the jet fuel composition on the blowout limits was also studied. The introduction of hydrogen as an additive in the methane jet significantly improved the blowout limits in both the lifted and attached flame regions. The addition of diluents into the methane jet decreased the stability of lifted jet flames and, to a much lesser degree, of attached flames.

Also, an investigation of the effect of an auxiliary fuel premixed with the co-flowing air stream on blowout limits of jet diffusion flames using nozzles of different geometries was also conducted. Methane, propane, ethylene and hydrogen were employed as the auxiliary fuels. The addition of small concentrations of auxiliary fuels improved the

blowout limits; however, at higher auxiliary fuel concentrations, the blowout limits either increased or decreased depending on the co-flowing stream velocity and the type of auxiliary fuel employed.

To explain the experimental trends observed for the blowout limits, the flow structure of cold and ignited jets issuing into a co-flowing stream of air or very lean air and methane mixtures was experimentally investigated using a laser Doppler velocimeter. These tests were conducted with a circular jet and elliptic jets of aspect ratios of 1.38 and 1.60. The time-averaged velocity and turbulence intensity in the axial and radial direction were measured for a range of co-flowing stream velocities. It was found that the phenomenon of axis-switching was dependent on the operating conditions.

Acknowledgements

This dissertation is the result of the vision, support and interest of many people. The following list is not exhaustive, nor does it include all of the contributions of the individuals named. It is a sincere attempt to at least identify the chief areas in which each contributed.

I would like to express my appreciation to my supervisor, Dr. I. Wierzba, for initiating this project and for her valuable suggestions and unwavering encouragements thereafter. I am deeply grateful for her painstaking task of editing the dissertation.

I would also like to thank Dr. Karim for the constructive suggestions and criticisms at various stages of the work and for the use of certain equipment.

The laboratory work was supported by R. Gustafson, A. Moerhle and G. East. I would like to acknowledge especially the technical assistance of B. Ferguson. The success of the LDV measurements is a testimonial of his tenacity and technical competence.

I am grateful to Massoumeh Karbassi for her encouragements and invaluable help in computer programming. I would also like to acknowledge the contributions of previous students in the Department of Mechanical Engineering (P. Samuels, M.A. Hanna, D. Mohindra and M.M. Metwally) who had worked on the similar topic.

The financial support of the University of Calgary, Natural Science and Engineering Research Council of Canada, Zonta International Foundation, Killam Foundation and the Alberta Heritage Fund are also acknowledged.

I wish to thank my family, particularly my parents, for their unlimited support and comforting words during times of frustration.

Table of Contents

Approval Page ii

Abstract iii

Acknowledgements v

Table of Contents vi

List of Tables viii

List of Figures ix

List of Symbols xvii

CHAPTER 1. INTRODUCTION 1
1.1 General 1
1.2 Objectives 3

CHAPTER 2. LITERATURE REVIEW 5
2.1 General 5
2.2 Experimental Studies of Flame Stability 5
2.2.1 Flow Structure 11
2.3 Theoretical Studies of Flame Stability 14

CHAPTER 3. APPARATUS AND EXPERIMENTAL PROCEDURE 20
3.1 Experimental Set-up 20
3.2 Flow Metering 22
3.3 Jet Nozzles 22
3.4 Laser-Doppler Velocimeter 25
3.5 Temperature Measurements 30
3.6 Schlieren System 31
3.7 Gas Analysis Measurements 31
3.8 Experimental Procedure 31

CHAPTER 4. RESULTS AND DISCUSSION: BLOWOUT LIMITS 34
4.1 General 34
4.2 Effect of Co-flowing Stream Velocity 34
4.3 Effect of Nozzle Geometry 35
4.4 Effect of Jet Fuel Additives 46

4.5 Effect of Auxiliary Fuel in the Co-flowing Air Stream 49
4.6 Limiting Stream Velocity 68
4.7 Nondimensional Correlations 72

CHAPTER 5. RESULTS AND DISCUSSION:
VELOCITY FIELD MEASUREMENTS 79
5.1 Effect of Co-flowing Stream Velocity 79
5.2 Effect of Jet Discharge Velocity 107
5.3 Effect of Hydrogen Addition 120
5.4 Effect of Auxiliary Methane in the Co-flowing Air Stream 123
5.5 Effect of a Diluent in the Co-flowing Air Stream 123
5.6 Effect of Jet Nozzle Ellipticity 126
5.6.1 Cold jet 126
5.6.2 Attached Flames 151
5.7 Nondimensional Correlations 167

CHAPTER 6. CONCLUSIONS 176
6.1 General Conclusions 176
6.2 Practical Implications 181
6.3 Future Work 182

References 184

Appendices 197

List of Tables

3.1 Circular and elliptic short nozzles (Type 1). 23

3.2 Circular and elliptic tube nozzles (Type 2). 25

List of Figures

3.1 Schematic diagram of the experimental set-up. 21
3.2 Nozzles with constant outer diameter. 24
3.3 Cross-section of the nozzle-tubes. 24
3.4(a) Schematic of the LDV optical system. 26
3.4(b) Schematic of the LDV data acquisition system. 27
3.5 Schematic of the cyclone aerosol generator. 29

4.2.1 The blowout limits of a methane jet diffusion flame as a function of the co-flowing stream velocity for different nozzle types and diameters. 36
4.2.2 A sketch of (a) attached and (b) lifted flames. 37

4.3.1 The flame blowout limits defined as (a) the jet volumetric flow rate and (b) the jet velocity as a function of the co-flowing stream velocity for two different discharge diameters. 39
4.3.2 The jet blowout velocity as a function of the co-flowing stream velocity for nozzles of different lip thicknesses. 40
4.3.3 The jet blowout velocity as a function of the co-flowing stream velocity for different aspect ratio nozzles of (a) Type 1 and (b) Type 2. 44
4.3.4 The blowout limits of a methane jet diffusion flame with (a) hydrogen and (b) carbon dioxide as additives issuing from elliptic nozzles of different aspect ratios. 45

4.4.1 The jet blowout velocity as a function of the co-flowing stream velocity for jets of different CH_4 - H_2 concentrations. 47
4.4.2 The jet blowout velocity as a function of the co-flowing stream velocity for different (a) carbon dioxide and (b) nitrogen concentrations in the methane jet. 48

4.5.1 The ratio of the blowout limits of a methane jet diffusion flame as a function of the type of auxiliary fuel and its concentration at (a) u_s = 1.0 m/s ($u_{j,b}$ = 12.5 m/s) and (b) u_s = 1.45 m/s ($u_{j,b}$ = 3.6 m/s). 54
4.5.2 The blowout limits as a function of the methane concentration in the co-flowing air stream for different aspect ratio nozzles. $C_{s,l}$ = 6.45 %. 55
4.5.3 The blowout limits as a function of the propane concentration in the co-flowing air stream for different aspect ratio nozzles. $C_{s,l}$ = 2.75 %. 56
4.5.4 The blowout limits as a function of the hydrogen concentration in the co-flowing air stream for different aspect ratio nozzles. $C_{s,l}$ = 9.50 %. 57
4.5.5 The blowout limits as a function of the methane concentration in the co-flowing air stream for different aspect ratio nozzles. $C_{s,l}$ = 6.80 %. 58
4.5.6 The blowout limits as a function of the propane concentration in the co-

flowing air stream for different aspect ratio nozzles. $C_{s,j}$ = 2.90 %. 59
4.5.7 The blowout limits as a function of the hydrogen concentration in the co-flowing air stream for different aspect ratio nozzles. $C_{s,j}$ = 9.60%. 60
4.5.8 The blowout limits as a function of the auxiliary fuel concentration in the co-flowing air stream for a nozzle with an aspect ratio of 1.32. 61
4.5.9 The blowout limits as a function of the auxiliary fuel concentration in the co-flowing air stream for a nozzle with an aspect ratio of 1.80. 62
4.5.10 The blowout limits as a function of the auxiliary fuel concentration in the co-flowing air stream for a nozzle with an aspect ratio of 2.72. 63
4.5.11 The blowout limits as a function of the methane concentration in the co-flowing air stream for different aspect ratio nozzles. $C_{s,j}$ = 6.45 %. 64
4.5.12 The blowout limits as a function of the methane concentration in the co-flowing air stream for different aspect ratio nozzles. $C_{s,j}$ = 6.61 %. 65
4.5.13 The blowout limits as a function of the methane concentration in the co-flowing air stream for different aspect ratio nozzles. $C_{s,j}$ = 6.80 %. 66
4.5.14 Radial temperature profiles in attached flames issuing into a co-flowing stream of air premixed with methane. 67

4.6.1 The limiting stream velocity of jet diffusion flames as a function of the discharge area. 69
4.6.2 The limiting stream velocity as a function of (a) the nozzle lip thickness and (b) the jet aspect ratio. 70
4.6.3 The limiting stream velocity as a function of (a) the jet additive concentration and (b) the maximum laminar burning velocity of the jet fuel. 71

4.7.1 The nondimensional limiting stream velocity as a function of the non-dimensional jet discharge diameter. 73
4.7.2 The nondimensional blowout limits of lifted diffusion flame for (a) larger diameter nozzles and (b) smaller diameter nozzles. 75
4.7.3 The nondimensional blowout limits of lifted flames for (a) larger diameter nozzles and (b) smaller diameter nozzles of different aspect ratios. 76
4.7.4 The nondimensional blowout limits of lifted flames showing the effect of different jet fuel compositions. 77
4.7.5 The nondimensional blowout limits of attached flames for nozzles of different discharge diameters and lip thickness. 77
4.7.6 The nondimensional blowout limits of attached flames as a function of the nozzle aspect ratio for (a) nozzles of Type 1 and (b) nozzles of Type 2. 78

5.1.1 Time-averaged axial velocity profiles within a cold circular jet for two different co-flowing stream velocities (R = 2.29 mm). 84
5.1.2 Time-averaged radial velocity profiles within a cold circular jet for two different co-flowing stream velocities (R = 2.29 mm). 85
5.1.3 Turbulence intensity level profiles within a cold circular jet for two different

co-flowing stream velocities (R = 2.29 mm). 86
5.1.4 Time-averaged axial velocity profiles within a lifted flame for two different co-flowing stream velocities (R = 2.29 mm). 87
5.1.5 Time-averaged radial velocity profiles within a lifted flame for two different co-flowing stream velocities (R = 2.29 mm). 88
5.1.6 Turbulence intensity level profiles within a lifted flame for two different co-flowing stream velocities (R = 2.29 mm). 89
5.1.7 A comparison of the axial distance where the fuel-air concentration equalled the lower flammability limit for (a) a cold jet and lifted flame and (b) lifted flames in co-flowing streams of different velocities. 90
5.1.8 A comparison of the time-averaged axial velocity profiles within cold jets and lifted flames (R = 2.29 mm). 91
5.1.9 A comparison of the time-averaged radial velocity profiles within cold jets and lifted flames (R = 2.29 mm). 92
5.1.10 A comparison of the turbulence intensity level profiles within cold jets and lifted flames (R = 2.29 mm). 93
5.1.11 Time-averaged axial velocity profiles within a cold circular jet for two different co-flowing stream velocities (R = 2.29 mm). 98
5.1.12 Time-averaged radial velocity profiles within a cold circular jet for two different co-flowing stream velocities (R = 2.29 mm). 99
5.1.13 A comparison of (a) the jet half-width and (b) the centerline velocity decay with downstream distance for cold jets in two different co-flowing stream velocities. 100
5.1.14 Time-averaged axial and radial velocity profiles for (a) and (c) cold jets, and for (b) and (d) attached flames issuing into a co-flowing stream of different velocities (R = 2.29 mm). 101
5.1.15 Velocity vectors of attached flames at the nozzle exit for different co-flowing stream velocities. 102
5.1.16 Time-averaged axial and radial velocity profiles for (a) and (c) cold jets, and for (b) and (d) attached flames issuing into a co-flowing stream of different velocities (R = 2.29 mm). 103
5.1.17 Time-averaged axial velocity profiles within attached flames for two different co-flowing stream velocities (R = 2.29 mm). 104
5.1.18 Time-averaged radial velocity profiles within attached flames for two different co-flowing stream velocities (R = 2.29 mm). 105
5.1.19 Turbulence intensity level profiles within attached flames for two different co-flowing stream velocities (R = 2.29 mm). 106

5.2.1 Time-averaged axial velocity profiles within attached flames with different jet discharge velocities (R = 2.29 mm). 110
5.2.2 Time-averaged axial velocity profiles within attached flames with different jet discharge velocities (R = 2.29 mm). 111
5.2.3 A comparison of the axial velocity gradients within (a) cold jets and (b)

attached flames with different jet discharge velocities (R = 2.29 mm). 112
5.2.4 Time-averaged radial velocity profiles within attached flames with different jet discharge velocities (R = 2.29 mm). 113
5.2.5 Time-averaged radial velocity profiles within attached flames with different jet discharge velocities (R = 2.29 mm). 114
5.2.6 Schlieren photographs showing the effect of varying jet velocities on the flow structure of attached flames in a co-flowing stream of velocity 0.65 m/s (d_j = 4.57 mm). 115
5.2.7 Turbulence intensity level profiles within attached flames with different jet discharge velocities (R = 2.29 mm). 116
5.2.8 Turbulence intensity level profiles within attached flames with different jet discharge velocities (R = 2.29 mm). 117
5.2.9 A comparison of (a) the jet half-width and (b) the centerline velocity decay with downstream distance in cold jets of different discharge velocities (R = 2.29 mm). 118
5.2.10 The axial distance where the fuel-air concentration equalled the lower flammability limit as a function of the jet discharge velocity for attached flames. 119

5.3.1 A comparison of (a) the jet half-width and (b) the centerline velocity decay with downstream distance for attached flames with different jet fuel compositions. 121
5.3.2 A comparison of the jet centerline velocity decay for cold jets of different fuel compositions. 122

5.4.1 Time-averaged axial velocity profiles within jets issuing into a co-flowing stream of air premixed with methane (R = 2.29 mm). 124
5.4.2 A comparison of (a) the jet half-width and (b) the centerline velocity with downstream distance in attached flames immersed in an air stream premixed with auxiliary methane (R = 2.29 mm). 125

5.5.1 Time-averaged axial velocity profiles within attached flames in a co-flowing stream of air premixed with carbon dioxide (R = 2.29 mm). 127
5.5.2 Turbulence intensity profiles within attached flames in a co-flowing stream of air premixed with carbon dioxide (R = 2.29 mm). 128

5.6.1 Time-averaged axial velocity profiles within a cold jet of aspect ratio 1.38 (R_{eq} = 2.15 mm). 132
5.6.2 Time-averaged axial velocity profiles within a cold jet of aspect ratio 1.60 (R_{eq} = 2.08 mm). 133
5.6.3 Time-averaged radial velocity profiles within a cold jet of aspect ratio 1.38 (R_{eq} = 2.15 mm). 134
5.6.4 Time-averaged radial velocity profiles within a cold jet of aspect ratio

1.60 (R_{eq} = 2.08 mm). 135
5.6.5 Turbulence intensity profiles within a cold jet of aspect ratio 1.38 (R_{eq} = 2.15 mm). 136
5.6.6 Turbulence intensity profiles within a cold jet of aspect ratio 1.60 (R_{eq} = 2.08 mm). 137
5.6.7 A comparison of the jet half-width of circular and elliptic jets with an aspect ratio of (a) 1.38 and (b) 1.60. 138
5.6.8 A comparison of the jet half-width within cold jets with an aspect ratio of (a) 1.0, (b) 1.38, and (c) 1.60 in a co-flowing stream of different velocities. 139
5.6.9 Time-averaged axial velocity profiles within cold jets of different aspect ratios with different discharge velocities. 140
5.6.10 A comparison of the jet half-width of elliptic jets with an aspect ratio of (a), (c) 1.38, and (b), (d) 1.60 with different discharge velocities. 141
5.6.11 Time-averaged axial velocity profiles within cold jets and attached flames with an aspect ratio of 1.38 (R_{eq} = 2.15 mm). 143
5.6.12 Time-averaged axial velocity profiles within cold jets and attached flames with an aspect ratio of 1.60 (R_{eq} = 2.08 mm). 144
5.6.13 Time-averaged radial velocity profiles within cold jets and attached flames with an aspect ratio of 1.38 (R_{eq} = 2.15 mm). 145
5.6.14 Time-averaged axial velocity profiles within cold jets and attached flames with an aspect ratio of 1.60 (R_{eq} = 2.08 mm). 146
5.6.15 Turbulence intensity profiles within cold jets and attached flames with an aspect ratio of 1.38 (R_{eq} = 2.15 mm). 147
5.6.16 Turbulence intensity profiles within cold jets and attached flames with an aspect ratio of 1.60 (R_{eq} = 2.08 mm). 148
5.6.17 A comparison of the jet half-width of (a) circular jets and elliptic jets with aspect ratios of (b) 1.38 and (c) 1.60. 149
5.6.18 A comparison of the velocity at the jet axis for (a) circular jets and elliptic jets with aspect ratios of (b) 1.38 and (c) 1.60. 150
5.6.19 Time-averaged axial velocity profiles within attached flames with an aspect ratio of 1.38 (R_{eq} = 2.15 mm). 154
5.6.20 Time-averaged axial velocity profiles within attached flames with an aspect ratio of 1.38 (R_{eq} = 2.15 mm). 155
5.6.21 Time-averaged axial velocity profiles within attached flames with an aspect ratio of 1.60 (R_{eq} = 2.08 mm). 156
5.6.22 Time-averaged axial velocity profiles within attached flames with an aspect ratio of 1.60 (R_{eq} = 2.08 mm). 157
5.6.23 Time-averaged radial velocity profiles within attached flames with an aspect ratio of 1.38 (R_{eq} = 2.15 mm). 158
5.6.24 Time-averaged radial velocity profiles within attached flames with an aspect ratio of 1.60 (R_{eq} = 2.08 mm). 159
5.6.25 A comparison of the jet half-width of attached flames issuing from elliptic

nozzles of aspect ratios (a) 1.38 and (b) 1.60. 160
5.6.26 The axial distance where the fuel-air concentration equalled the lower flammability limit as a function of the jet aspect ratio. 161
5.6.27 Time-averaged axial velocity profiles within attached flames with an aspect ratio of 1.38 in a co-flowing stream of air premixed with 2.0 % (by volume) methane (R_{eq} = 2.15 mm). 162
5.6.28 Time-averaged axial velocity profiles within attached flames with an aspect ratio of 1.38 in a co-flowing stream of air premixed with 2.0 % (by volume) methane (R_{eq} = 2.15 mm). 163
5.6.29 Time-averaged axial velocity profiles within attached flames with an aspect ratio of 1.60 in a co-flowing stream of air premixed with 2.0 % (by volume) methane (R_{eq} = 2.08 mm). 164
5.6.30 Time-averaged axial velocity profiles within attached flames with an aspect ratio of 1.60 in a co-flowing stream of air premixed with 2.0 % (by volume) methane (R_{eq} = 2.08 mm). 165
5.6.31 The variation of the jet half-width with dimensionless downstream distance for attached flames issuing from two different elliptic jets into a co-flowing air stream premixed with 2.0% (by volume) methane. 166

5.7.1 A comparison of dimensionless velocity profiles in the far-field region of a cold circular jet (d_j = 4.57 mm). 170
5.7.2 A comparison of dimensionless velocity profiles in the far-field region of a cold circular jet with (a) different jet discharge and co-flowing stream velocities and (b) different jet fuel compositions. 171
5.7.3 A comparison of dimensionless velocity profiles in the far-field region of lifted flames in a co-flowing stream of velocity (a) 0.65 m/s and (b) 0.70 m/s. 172
5.7.4 A comparison of dimensionless velocity profiles in the far-field region of cold jets and attached flames. 173
5.7.5 Dimensionless velocity profiles from nozzles of various aspect ratios in the near-field region of the jet. 174
5.7.6 Dimensionless velocity profiles from nozzles of various aspect ratios in the near-field region of the jet. 175
5.7.7 Dimensionless velocity profiles from nozzles of various aspect ratios in the near-field region of the jet. 175

A.1.1 Time-averaged axial and radial velocity profiles within a cold circular jet at a downstream distance of 79 mm for two different co-flowing stream velocities (R = 2.29 mm). 198
A.1.2 Time-averaged axial and radial velocity profiles within a lifted flame at a downstream distance of 79 mm for two different co-flowing stream velocities (R = 2.29 mm). 199
A.2.1 Time-averaged axial and radial velocity profiles within a cold circular jet

at a downstream distance of 1 mm for different jet discharge velocities (R = 2.29 mm). . . . 201
A.2.2. Time-averaged axial and radial velocity profiles within a cold circular jet at a downstream distance of 30 mm for different jet discharge velocities (R = 2.29 mm). . . . 202
A.2.3 Time-averaged axial and radial velocity profiles within a cold circular jet at a downstream distance of 45 mm for different jet discharge velocities (R = 2.29 mm). . . . 203
A.2.4 Time-averaged axial and radial velocity profiles within a cold circular jet at a downstream distance of 79 mm for different jet discharge velocities (R = 2.29 mm). . . . 204
A.2.5 A comparison of (a) the jet half-width and (b) the centerline velocity with downstream distance for cold jets with two different discharge velocities (R = 2.29 mm). . . . 205
A.2.6 Time-averaged axial and radial velocity profiles within a cold circular jet at a downstream distance of 1 mm with different jet discharge velocities (R = 2.29 mm). . . . 206
A.2.7 Time-averaged axial and radial velocity profiles within a cold circular jet at a downstream distance of 30 mm with different jet discharge velocities (R = 2.29 mm). . . . 207
A.2.8 Schlieren photographs showing the effect of varying jet velocities on the flow structure of cold jets in a co-flowing stream of velocity 1.21 m/s (d_j = 4.57 mm). . . . 208
A.3.1 Time-averaged axial velocity profiles within attached flames of different fuel compositions. . . . 210
A.3.2 Time-averaged radial velocity profiles within attached flames for different fuel compositions. . . . 211
A.3.3 Time-averaged axial and radial velocity profiles for jets of different fuel compositions. . . . 212
A.3.4 Time-averaged axial and radial velocity profiles within jets of different fuel compositions. . . . 213
A.3.5 Time-averaged axial and radial velocity profiles within jets of different fuel compositions. . . . 214
A.3.6 Time-averaged axial and radial velocity profiles within jets of different fuel compositions. . . . 215
A.4.1 Time-averaged axial velocity profiles within attached flames issuing into a co-flowing air stream premixed with CH_4. . . . 217
A.4.2 The variation of the axial velocity at the jet axis with downstream distance for attached flames issuing from two different elliptic jets into a co-flowing air stream premixed with 2.0 % (by volume) CH_4. . . . 218
A.5.1 Time-averaged axial velocity profiles of attached flames issuing into a co-flowing air stream premixed with CO_2. . . . 220
A.5.2 Turbulence intensity profiles within cold jets issuing into a co-flowing stream

of air premixed with CO_2. 221
A.6.1 Time-averaged axial velocity profiles for elliptic jets of aspect ratios (a) 1.38 and (b) 1.60. 223
A.6.2 Turbulence intensity profiles within cold elliptic jets of aspect ratios (a) 1.38 and (b) 1.60. 224
A.6.3 Time-averaged axial and radial velocity profiles within an attached flame discharging from an elliptic nozzle of aspect ratio 1.38. 225
A.6.4 Time-averaged axial and radial velocity profiles within an attached flame discharging from an elliptic nozzle of aspect ratio 1.60. 226
A.6.5 Time-averaged axial velocity profiles within a cold jet of aspect ratio 1.38 (R_{eq} = 2.15 mm). 227
A.6.6 Time-averaged axial velocity profiles within a cold jet of aspect ratio 1.60 (R_{eq} = 2.08 mm). 228

List of Symbols

A_j	jet discharge area (mm^2)
A_s	duct area (mm^2)
a	major axis half-width (mm)
a/b	major-to-minor axes ratio
b	minor axis half-width (mm)
C_s	volumetric concentration of auxiliary fuel in the air stream, % volume
$C_{s,l}$	volumetric concentration of auxiliary fuel in the air stream at flashback, % volume
d_j	jet diameter (mm)
d_q	quenching distance (mm)
Q	volumetric flow rate (m^3/h)
R	radius of a circular jet (mm)
Re	Reynolds number
R_{eq}	equivalent radius, $(a \cdot b)^{1/2}$ (mm)
r	radial distance (mm)
S_L	laminar burning velocity (m/s)
T	temperature (K)
u	local time-averaged axial velocity (m/s)
u_{cl}	time-averaged axial velocity at the jet axis (m/s)
u_j	mean discharge velocity (m/s)
$u_{j,b}$	mean discharge velocity at flame blowout in a co-flowing stream of air (m/s)

u_s co-flowing stream velocity (m/s)

u_{sJ} limiting co-flowing stream velocity (m/s)

u' rms value of the jet local velocity (m/s)

v local time-averaged radial velocity (m/s)

x axial downstream distance from the nozzle exit (mm)

Δ lip thickness of the nozzle (mm)

Δ_{ref} reference lip thickness (mm)

δ jet velocity-half radius (mm)

ρ density (kg/m^3)

Subscripts

b blowout

circ circular jet

cl jet axis

f fuel

j jet

m jet fuel mixture

LL lean flammability limit

o nozzle exit

ref reference

s co-flowing stream

sf auxiliary fuel in co-flowing air stream

CHAPTER 1

INTRODUCTION

1.1 General

Jet diffusion flames are employed in many combustion devices such as gas turbine combustors, industrial furnaces and petrochemical flares. Diffusion flames can be utilized in an unconfined quiescent atmosphere (known as free jet flames), but are often employed in a co-flowing stream of air. Introducing a co-flowing stream of air increases the efficiency of the process, reduces the flame length and, consequently, NO_x emissions [1]; however, this occurs at the expense of flame stability which can have serious safety and economical implications. Therefore, the efficient and stable operation of these devices should be maintained over a wide range of operating conditions.

Within the stability limits, two distinct operational regions can be identified as either *lifted* or *attached* flames, depending on the value of the jet and co-flowing stream velocity. In low co-flowing stream velocities, an increase in the jet velocity would result in the flame to lift off the nozzle rim and stabilize at some downstream distance from the jet exit. A further increase in the jet velocity would lead to the blowout of the lifted flame. At relatively higher co-flowing stream velocities, an increase in the jet velocity would lead to the sudden blowout of the attached flame and no lift-off would occur. The value of the co-flowing stream velocity that separates these two regions, i.e., lifted and attached flame blowout, is termed the *limiting stream velocity*. Limited information was available in the literature on the limiting stream velocity [2], and hence experimental data on the parameters

affecting the limiting stream velocity were required.

The stabilization of jet diffusion flames has been the focus of extensive theoretical and experimental efforts over the years. However, much of this attention was directed towards the stability of flames issuing into a quiescent medium. Numerous theories characterizing flame stability have emerged as a result but their respective assumptions identifying the physical mechanisms responsible for flame stabilization vary widely [3,4,5]. While these models yield a broad understanding of jet diffusion flames, they are restricted to *lifted* flame stabilization in a mostly quiescent environment. The presence of a co-flowing stream can significantly affect the blowout limits of the flame creating additional modelling difficulties to the already complex phenomenon of flame stabilization. Nevertheless, only a sparse number of studies have been conducted on jet flames in co-flowing streams despite the wide use of these systems in industry. Recent attempts have been made at predicting the blowout of *lifted* jet diffusion flames in co-flowing streams [6,7,8]; however, experimental data are lacking on the blowout limits of such flames to validate the models over a wider range of operating conditions. There is also relatively limited experimental information on the blowout limits of *attached* flames in a co-flowing oxidizing stream, and no adequate model is available to predict them.

At the same time, the improvement of the blowout limits is always beneficial as well as required. It is well recognized that the stability of jet diffusion flames is controlled by the mixing rate of the fuel and oxidizer as well as chemical reaction rates. An increase in the blowout limits can be realized when the entrainment rate is enhanced or when the chemical reaction rate is increased by employing more reactive fuels. An effective

technique to improve the blowout limits is the addition of a fuel into the surrounding air stream, commonly known as an "auxiliary fuel" [9,10,11]. Experimental data on the effect of employing this technique on the blowout limits of co-flowing jet flames have been sparse. It has also been suggested in previous cold flow studies that an elliptic nozzle with a small aspect ratio can be an effective device in enhancing the air entrainment rate near the nozzle exit [12,13]. However, the effect of these nozzles on the flame blowout limits have not been investigated.

Fuel quality and interchangeability are becoming increasingly important practical issues in the light of fuel reserves depletion and a wider use of poorer quality fuels. Low heating value fuels can be produced from a number of industrial and natural sources such as coal gasification, biomass processing and enhanced oil recovery by fire flooding to name a few and thus make it an attractive source of energy. However, a decrease in fuel quality with an increase in diluent concentration, commonly carbon dioxide and nitrogen, adversely affect not only the heating value of the fuel but also the flame stability, and thus necessitates the need to delineate the effect of the fuel composition on the blowout limits of diffusion flames. To enhance the combustion characteristics, the combustion of hydrogen-enriched fuels can be utilized. The effect of fuel quality on the blowout limits of jet diffusion flames was, therefore, investigated for a wide range of co-flowing stream velocities in the present study.

1.2 Objectives

The goal of the current research was to investigate the blowout limits of jet

diffusion flames for a range of co-flowing stream velocities and compositions, jet nozzle geometries (i.e., discharge diameter, lip thickness and ellipticity), and jet fuel additives. The flow structure of these flames issuing into a co-flowing oxidizing stream was investigated using laser Doppler velocimetry in an attempt to explain the experimentally observed behaviour of the blowout limits. Emphasis was placed on how a change in the operating conditions affected the flow characteristics of cold and ignited jets.

CHAPTER 2

LITERATURE REVIEW

2.1 General

There have been many experimental and theoretical investigations aimed at the understanding of the stability of jet diffusion flames. This chapter will summarize the experimental findings and postulated theories of various researchers for the lift-off and blowout behaviour of jet diffusion flames.

2.2 Experimental Studies of Flame Stability

Various experimental investigations have been conducted to assess the effect of different operational conditions (such as, for instance, the nozzle geometry and type of jet fuel) on the stability limits of jet diffusion flames and consequently the focus of this section is to review the experimental efforts of previous researchers on the parameters affecting the stability limits.

Effect of the Co-flowing Stream. The effects of many different parameters on flame stability have been investigated, however, much less effort has been directed to the study of the effect of the co-flowing stream velocity. The effects of an unconfined co-flowing air stream on the stability limits of jet diffusion flames have been studied experimentally [1,14-20]. Similar experiments were conducted on flames in a confined co-flowing stream [2,6,7,9,10,20-22]. Many of the studies described in the literature were limited to lifted flames in a relatively low range of stream velocities (up to 0.66 m/s) [10,22-24]. The flame

blowout limits for various jet fuels and small diameter nozzles in a co-flowing stream were reported by Wierzba et al. [11], Oladipo [25] and Karbassi [7]. Yoon et al. [20] conducted a study on the effect of a heated, supersonic co-flowing air stream on the blowout limits of attached flames for large diameter hydrogen jets. The experimental data showed that an increase in the co-flowing stream velocity significantly decreased the blowout limits of lifted flames, while their reattachment and lift-off limits were almost insensitive to the stream velocity. The blowout velocity of attached flames decreased slightly with increasing co-flowing stream velocity up to a certain stream velocity. With further increases in the stream velocity, the blowout limits of these flames dropped sharply. Despite many investigations on flame stability, the effect of the co-flowing stream velocity on the lift-off and blowout limits of lifted and attached flames has not been reported for a wide range of nozzle geometries and jet fuel compositions.

Effect of the Jet Fuel. The effect of the type of fuel on the stability limits of jet diffusion flames was studied experimentally. Kalghatgi [26] investigated the blowout limits of jet flames in still air for a variety of gaseous fuels and observed that the jet blowout velocity increased with the burning velocity of the jet fuel with the highest blowout limits observed with the hydrogen flame. The effect of the addition of inerts into an unconfined co-flowing hydrogen jet on the stability limits of lifted flames have been studied by Takahashi et al. [19]; they observed that the detrimental effect of the addition of nitrogen was stronger than that of argon or helium.

Investigations of unconfined and confined co-flowing streams have shown that the mode of stabilization was dependent on the type of fuel employed. For instance, methane

flames lifted off abruptly at a certain jet velocity while hydrogen flames exhibited a stable split flame in which there existed a small laminar flame near the nozzle rim and a turbulent lifted flame further downstream [14,18,25]. The phenomenon of a stable split flame in hydrogen flames was not observed in the studies of Karbassi [7], Takahashi et al. [19] and Oladipo [25].

Effect of Nozzle Geometry. More complex situations have been studied over the years aimed at improving flame stability: for example, some researchers examined the possibility of controlling flame stability with acoustic excitation [27], while others enhanced the flame stability by employing multistep nozzles [28] and swirlers [1,16,29]. However, merely a small change in the nozzle geometry, e.g., the nozzle lip thickness, discharge diameter, shape (whether the nozzle is contoured or a straight tube) and ellipticity, can generate very different flow fields which can significantly affect the mass entrainment rates near the nozzle exit and consequently the stability limits [14,15,30,31].

Discharge Diameter. Studies have shown that the lift-off and blowout velocities are highly dependent on the discharge diameter of the fuel jet. The effect of the discharge diameter on the blowout limits depends on whether the flame is lifted or attached at blowout. Extensive experimental investigations for the blowout velocities of lifted methane and propane jet flames in a quiescent surrounding was conducted for a variety of jet diameters [26,32,33]. The results indicated that an increase in the jet diameter increased the jet blowout velocity of lifted flames and had little effect on the lift-off height. Gollahalli et al. [34] reported that the lift-off velocities of free propane jet flames increased with a decrease in the jet diameter. The results obtained for attached unconfined co-flowing jet flames

indicated that the lift-off as well as blowout velocities increased with a decrease in the nozzle diameter [14]. Karbassi [7], who conducted studies on flame jets in a confined co-flowing stream, observed that the jet blowout velocity of *lifted* flames increased with the jet diameter while the lift-off and blowout velocities of *attached* flames showed a reverse trend. The study of Takahashi et al. [19] who worked with hydrogen/diluent jet flames in various oxidizing co-flowing streams showed that the blowout velocity of *lifted* flames tended to be constant with an increasing diameter (of greater than approximately 2 mm), but it increased drastically as the diameter approached zero.

Lip Thickness. The nozzle lip thickness was found to have a profound effect on the stability limits of diffusion flames. Studies conducted on attached unconfined co-flowing hydrogen-air and methane-air jet flames have shown that an increase in the nozzle lip thickness increased the lift-off and blowout velocities, and extended the co-flowing stream velocity in which a stable flame can exist [14,15,20].

Nozzle Shape. The effect of the ratio of the length to diameter of the nozzles and the shape of the velocity profiles at the nozzle exit on the stability limits of free and co-flowing flames were also examined [30,35]. An increase in this ratio resulted in an increase in both the lift-off and blowout velocities.

Ellipticity. Many experimental studies have been focussed on the flow structure of cold three-dimensional jets such as rectangular, triangular and elliptic jets [12,13,36-45]. For elliptic jets with small or moderate aspect ratios, the mass entrainment in the near-nozzle region was three to eight times (depending on the axial locations) higher than that in an axisymmetric jet. It was reported that the azimuthal deformations increased the interfacial

area in elliptic jets, engulfing more fluid from the surrounding air into the mixing layer compared with that of circular jets. Large entrainment of the elliptic jet was found to be mainly produced near the minor axis [13].

An interesting phenomenon of axis-switching was observed for rectangular and elliptic jets [12,13,36,37,45]. This axis-switching was caused by a much greater jet spread in the plane of the minor axis of the nozzle than in the plane of the major axis. Eventually, the jet became wider in the minor axis plane than in the major axis plane and the jet cross-section appeared to have switched at some distance downstream of the point of discharge. The distance from the nozzle to the cross-over location was found to increase linearly with the aspect ratio [37]. It was also reported that the switching of the axes in an initially turbulent jet occurred at a location farther downstream than that in an initially laminar jet [45]. From flow visualization experiments on large cold elliptic jets in a quiescent environment, it is known that the higher axial velocities in minor axis plane than in the major axis plane resulted in the distortion of the vortex ring that initially rolls up [12]. It is this distortion of the vortex ring that results in the improvement in the jet mass entrainment in elliptic jets. Since the axis-switching location follows the roll-up of the vortical structures and their subsequent deformation [45], it can be indicative of the amount of entrainment that follows. Further downstream, measurements conducted on cold rectangular jets of high aspect ratios (greater than 5:1) have shown that the entrainment rates were not much different from those of axisymmetric jets [36,37].

Furthermore, an off-axis peak (near the jet boundary) was observed in the axial velocity profile of the major axis plane in cold elliptic jets issuing into a quiescent

environments [13]. This saddle-shaped axial velocity profile was also documented for cold rectangular jets issuing from slots of aspect ratio 10 but not for those with an aspect ratio of 2 [38]. Quinn [38] suggested that the characteristic saddle-shaped mean streamwise velocity profiles in relatively high aspect ratios have steep gradients which, at sufficiently high values, can be detrimental to flame stability.

The results from these cold studies could not always be easily extrapolated to flames and hence necessitated the investigation of three-dimensional jet flames [31,46-52]. The majority of these studies were focussed on the velocity and temperature fields, and emission indices of ignited elliptic jets [31,46,47,50-52]. The velocity measurements in jet flames did not show an off-axis peak in ethylene-nitrogen jets issued from pipe injectors [47] but it was observed in propane-nitrogen jet flames [31]. Gollahalli et al. [31] attributed this to the difference in the geometry of the nozzle exit: the injector used in the study of Schadow et al. [47] was made be pressing a circular pipe and hence was more oval-shaped than elliptic shaped. Furthermore, elliptic nozzle flames were reported to have higher temperatures and concentrations of carbon dioxide and nitrogen oxide, but lower flame radiation and concentrations of soot and carbon monoxide than for circular flames.

The stability limits (i.e., the lift-off and reattachement velocity) of lifted flames issuing from elliptic nozzles (with a discharge area of 71 mm^2) into a low co-flowing stream velocity (of 0.66 m/s) were adversely affected by the ellipticity of the nozzle geometry [31,51]. The reduced stability for nozzles of higher aspect ratios (of greater than 2) was attributed to the development of the azimuthal deformations and higher turbulence levels that had a tendency to dilute the flame base region in lifted flames due to intense small-scale

fluctuations. However, Schadow et al. [47] who employed large elliptic nozzles in ducted rockets reported the existence of an optimum aspect ratio. They found that a jet with an aspect ratio of 3 yielded a greater jet spread and higher combustion efficiency than jets with aspect ratios of 2 and 3.5. This apparently contradictory behaviour may have been the result of the scaling [53]. There are no data in the literature on the stability limits of both lifted and attached flames issuing from nozzles of different aspect ratios for a wide range of co-flowing stream velocities.

2.2.1 Flow Structure

Velocity profiles can be a useful indication of the rate of mass entrainment of the surrounding stream into the jet flame. A change in the nozzle geometry or operating condition can significantly alter the flow structure of the jet and, consequently, the entrainment rate. The velocity profiles differ considerably in the far- and near-field regions of the jet and hence warrants the separate review of these velocities.

Far-field Region. The majority of the velocity profiles in cold co-flowing jets were studied experimentally in the far-field region of fully developed jets [54-63]. In general, two basic approaches have been developed for the correlation of the velocity profiles of a confined cold jet within a co-flowing air stream. The first approach utilized a similarity parameter to describe the turbulent mixing patterns in axisymmetrical constant density confined co-flowing jet flows [56]. This approach was modified to include the effects of different densities in the jet and surrounding air [60]. The second approach was based on the ratio of the co-flowing stream velocity to the velocity at the jet exit (i.e., $m = u_s / u_o$)

[54,55,59,61,62].

Three different equations were proposed to represent the velocity profile of a jet in a co-flowing stream. The semi-empirical equations developed by Forstall and Shapiro [61] were based on the cosine curve, and that of Abramovich [54] was expressed using the three-halves power curve. The error curve was the most commonly employed equation to yield the axial velocity profiles of the jet [3,55,56,59,60,62]. However, different researchers used different values of the coefficient and exponent in the error curve.

The correlations of Forstall and Shapiro [61], Antonia and Bilger [55] and Biringen [59] were applicable for flows with values of m (stream to jet discharge velocity ratio) greater than 0.1 while the non-dimensional velocity profiles of Becker et al. [56] and Steward and Guruz [60] were used for flows with values of m not greater than 0.034. It appears that the equations in the correlations of Forstall and Shapiro [61], Abramovich [54], Becker et al. [56] and Steward and Guruz [60] are more versatile in determining the velocity profiles than the restrictive flow characteristic curves of Antonia and Bilger [55,62] and Biringen [59]. Unfortunately, all of these correlations apply within a narrow range of values of the ratio, m, with the exception of the method of Abramovich [54]. However, at low m values, there is a significant deviation in the results obtained with the correlation of Abramovich [54] with that of Becker et al. [56].

Near-nozzle Region. The development of a non-dimensional correlation for the velocity profiles in the near-nozzle region of the jet has received considerably less attention in the past due to the difficulty in incorporating the effects of the initial conditions of the jet (e.g., nozzle geometry and whether the flow is initially laminar or turbulent) on the velocity

profiles [43,64-66]. A non-dimensional relation which correlates satisfactorily the velocity profiles in the near-field was developed for an initially laminar jet on the basis of experimental data collected from cold elliptic jets in still air [43].

Measurements in the near- and far-field regions of flames can be found in the literature although not as comprehensive as in cold jets and are limited to a narrow range of operating conditions [15,18,31,67,68]. To the best knowledge of the author, there are no correlations for the velocity profiles available in the literature for co-flowing jet flames.

2.2.2 Fuel/Diluent Premixed with the Co-flowing Air Stream

Previous research has shown that the blowout limits of a confined jet diffusion flame can be increased by premixing a fuel with the co-flowing air [9,10,11]. While this holds true at low co-flowing stream velocities and low auxiliary fuel concentrations in the co-flowing air stream, the combination of a higher co-flowing velocity and higher auxiliary fuel concentrations was found either to increase or decrease the blowout limit depending on the type of fuel used [11].

The presence of diluents - nitrogen, carbon dioxide and helium - in the surrounding stream has a detrimental effect on the stability limits of confined as well as unconfined flames [7,11,19]. The greatest decrease in the blowout limits were obtained with carbon dioxide, followed by nitrogen, helium and argon. Limited data are available in the literature related to the blowout limits of attached flames [11].

2.3 Theoretical Studies of Flame Stability

The development of models to predict the lift-off and blowout limits of jet diffusion flames has been the subject of many investigations in the past with much of the attention directed towards the modelling of lifted flames in a quiescent environment [3,4,5,26,32,69-73]. Only relatively recent models attempted to incorporate the blowout limits of a jet diffusion flame issuing into a confined co-flowing air stream; however, they are also limited to the blowout of lifted diffusion flames [6,7,74]. The models available attempted to yield an understanding of the underlying physical mechanisms responsible for the stability of jet diffusion flames. The models were based on widely varying concepts such as the critical velocity gradient, flame stretch, premixed flame base, laminar flamelet quenching, small-scale mixing and large-scale mixing.

Velocity Gradient and Flame Stretch Concept. The concept of the critical boundary velocity gradient proposed by Lewis and von Elbe [75] and Karlovitz et al. [76] was employed by some researchers in their blowout models (e.g., laminar diffusion flamelet models) [77,78]. According to this concept, the turbulence in the near-field of the jet contorted the flame surface thereby increasing the surface area and raising the consumption rate of the reactant mixture; however, the contorted flame surface was also accompanied by an increase in the velocity gradient. Interactions between the flow and the flame caused an excessive flame stretch that led to local flame extinction [76,79]. Near the nozzle rim the luminous reaction zone became thinner when the gas flow was increased, and at still higher flow velocities, holes appeared in the flame surface at the rim prior to the lifting

of the flame [76]. Flame extinction would occur if the velocity gradient at the jet boundary exceeded a critical value. Karlovitz et al. [76] formulated a dimensionless parameter, known as the Karlovitz flame-stretch factor, that included the critical velocity gradient as well as the velocity of the unburned gas and the flame front thickness.

Experimental studies have shown that the velocity gradients sustained by a lifted jet diffusion flame issuing into a co-flowing stream of low velocity remained relatively constant for a wide range of flame conditions tested [23,80]. The velocity gradient at the flame surface for methane and propane flames at the lift-off velocity was measured to be 450 to 500 s^{-1} [18,23,80].

Premixed Flame Base Model. The concept of a premixed flame base was employed by different researchers to explain the blowout limits of turbulent lifted diffusion flames [3,8,26,32,69,74,81]. Vanquickenbourne and van Tiggelen [3] first suggested that the doughnut-shaped base of the lifted flame consisted of a premixed fuel/air mixture and controlled the stability of the whole flame; the upper part of the flame was an ordinary diffusion flame in which the rest of the fuel burned with the entrained air. According to this concept, the flame will stabilize at some distance downstream from the nozzle tip where the fuel/air mixture is stoichiometric and the burning velocity equals the local jet velocity. The flame will blowout when the jet velocity exceeds the turbulent burning velocity. Extensive experimental measurements on the fuel composition, jet flow velocity and intensity of turbulence of methane jet flames in a quiescent atmosphere were conducted and confirmed the validity of this assumption [3].

Kalghatgi [26] used this flame stability model as well as dimensional analysis to develop a semi-empirical formula for the prediction of the blowout of lifted jet diffusion flames in still air. His semi-empirical model also includes the effect of the burner orientation to a surrounding air flow direction on the blowout limit. Kalghatgi [8,26,32,81] introduced also the concept of a stabilization height which was the last possible location for the existence of the lifted flame. Blowout would occur when, due to an increase in the jet velocity, the flame was forced downstream towards an axial distance that was greater than the stabilization height of the lifted flame. Flame stability could, therefore, be enhanced with an increase in the value of the stabilization height. In general, the empirical formula developed by Kalghatgi [26,32] for different flow conditions agree well with the experimental findings.

Recently, lifted flame stabilization was numerically simulated for methane jets flames in a co-flowing air stream of constant velocity [74]. The calculated lift-off heights compared well with the experimental data of Kalghatgi [32]. The simulations showed that the flame was stabilized at a height where the local axial velocity was approximately equal to the turbulent burning velocity. It also corroborated the other stabilization models (e.g., the laminar flamelet and mixing time theories) and suggested that the lift-off mechanism was the result of complex flame-flow interactions, only parts of which were incorporated in the simplified theories.

The use of the premixedness model to explain the lift-off and blowout phenomena have been questioned recently [72,78]. The assumption that the fuel and air are fully

premixed at the jet boundary of the flame was inconsistent with observations by other researchers who observed that the flame is located at the radial position where the flow is highly intermittent and that during a large fraction of the time only air is present at this position [72,78].

Laminar Flamelet Model. This model is based on the concept that the turbulent diffusion flame consisted of a collection of many laminar diffusion flamelets that were highly distorted and stretched by the turbulent flow [71,78,82]. In attached turbulent diffusion flames, the extinction of a large fraction of the laminar diffusion flamelets near the rim of the nozzle would lead to the lift-off of the flame. The flame would stabilize at a downstream distance where the strain rates were low enough to allow the ignition of a large proportion of the flamelets. The extinction of a large fraction of laminar flamelets in lifted flames at strain rates exceeding the critical value could result in the abrupt blowout of the flame. This concept satisfactorily predicted the lift-off heights reported by Kalghatgi [32] for methane jets in still air [83,84].

Numerical simulations of flame-vortex interactions were used to study the validity of the laminar flamelet assumption in diffusion flames [85]. Results showed that, in certain cases, the strain rate at which the flame gets quenched is much larger than the prediction of the laminar flamelet concept. Other researchers contended that this concept was valid as long as the mechanism of flame stabilization included the complex interactions between convection, turbulent mixing, heat release rates under strain and thermal expansion [83].

Mixing Time. Yet another very different mechanism for flame stabilization was proposed

to predict the stability limits of lifted jet diffusion flames in quiescent environments [4,5]. These models were based on the assumption that blowout occurred when the ratio of the time required for the physical mixing of the fuel and oxidant to form a combustible mixture was significantly lower than the characteristic chemical time. The value of this ratio could not be estimated from fundamental considerations and thus semi-empirical relations were derived. The authors, however, differed on the scaling of the mixing time. Byggstoyl and Magnussen [4] argued that the blowout characteristics were controlled by the molecular mixing rate while Broadwell et al. [5] claimed that large-scale mixing governed the blowout of jet diffusion flames. According to Byggstoyl and Magnussen [4], the lifted flame stabilized at the stoichiometric contour and at regions where the molecular mixing time equalled the chemical reaction time. However, Broadwell et al. [5,86] contended that experimental studies had shown that the large-scale structure dynamics dictated the entrainment, which in turn provided the environment for the subsequent turbulent cascade and mixing process. They proposed that the flame stability criterion should be evaluated for the last large coherent structure in the flame where the jet fuel concentration reached the stoichiometric value. An expression was derived for the jet blowout velocity that accurately predicted the experimental findings reported by Kalghatgi [26] for simple methane jet flames. A linear relationship between the lift-off height and jet exit velocity was also developed for a simple free jet flame of diluted and undiluted fuel mixtures [70]. Dahm and Mayman [87] and Dahm and Dibble [6] expanded this large-scale mixing model to include the blowout limits of lifted turbulent jet diffusion flames issuing into an unconfined and confined co-flowing air streams.

Karbassi [7] modified the model of Dahm and Dibble [6] by proposing a different time scale based on the Kolmogorov microscale of time. She also included the effects of different jet fuel compositions as well as of an auxiliary fuel premixed into the stream of air. The predictions of this model were experimentally verified for a range of surrounding stream velocities and compositions, jet fuel compositions and nozzle diameters.

CHAPTER 3

APPARATUS AND EXPERIMENTAL PROCEDURE

3.1 Experimental Set-up

A schematic diagram of the experimental set-up is presented in Fig. 3.1. The experimental apparatus consisted of a vertical combustion chamber, fuel and air supply systems, flow control valves, and a flow metering system. For simplicity, only two high pressure gaseous fuel/diluent feed lines are shown in Fig.3.1, although there were seven independent lines to supply fuel/diluents to the jet and co-flowing stream.

The tests were conducted in a 127 mm x 127 mm x 1300 mm stainless steel vertical combustion chamber, equipped with two opposing neo-ceramic windows for flame visualization studies. The fuel jet was discharged vertically in the centre of the chamber from nozzles with various diameters and shapes. Wall effects were insignificant at the operating conditions employed in this study.

A centrifugal blower supplied the co-flowing air, which could attain a maximum air stream velocity of 20 m/s. The co-flowing stream passed through a honeycomb straightener at the base of the combustor to produce a relatively uniform velocity distribution at the inlet of the combustor. The uniformity of the co-flowing stream was confirmed with hot-wire anemometry and laser Doppler velocimetry measurements.

Technical quality methane (≥98%) was employed as the primary jet fuel with hydrogen, nitrogen and carbon dioxide as additives to the methane jet. The co-flowing air

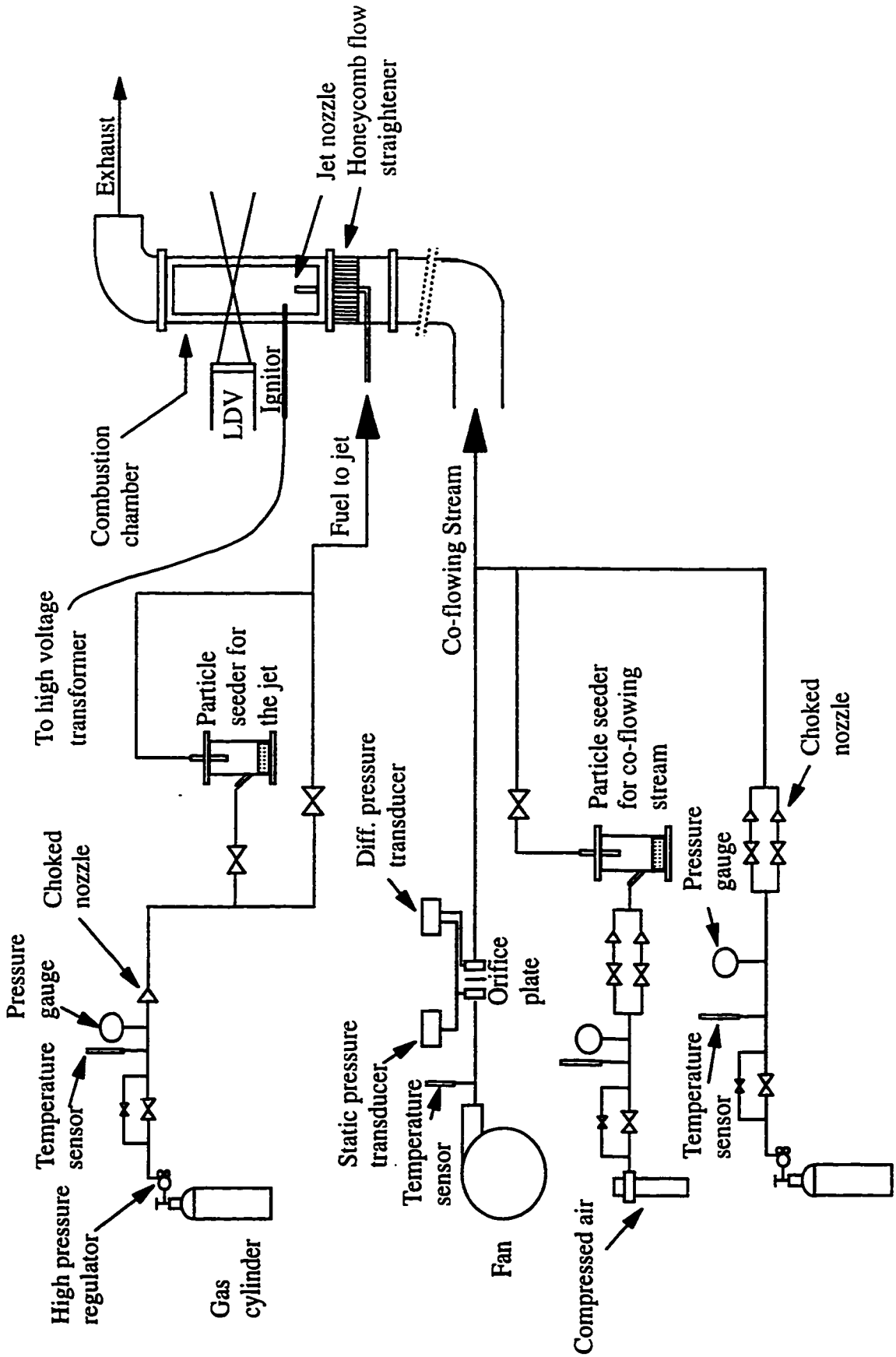

Fig. 3.1 Schematic diagram of the experimental set-up

stream could be premixed when necessary with the auxiliary fuels and diluents. These additional gases were introduced well upstream of the combustion chamber to ensure a homogeneous mixture of the co-flowing stream.

3.2 Flow Metering

The air flow rate was measured using sharp-edged orifice plates of various diameters for different ranges of flow rates. The flow rates of the compressed air, fuels and diluents were measured using calibrated choked nozzles. Eleven choked nozzles of different diameters were installed to provide measurements over a wide range of flow rates. The choke nozzles were calibrated using wet test meters. The calibration was mostly conducted with air as the working fluid and correction factors were applied to adapt the calibration for the different gases used in the experiments.

3.3 Jet Nozzles

Nozzles of two different shapes - short nozzles and tubes - were employed.

Short Nozzles. Circular brass nozzles of inner diameters 1.0, 1.5, 2.0 and 2.82 mm, and the elliptic equivalents of the 2.82 mm diameter jet were employed for many of the blowout limits experiments. A typical nozzle is shown in Fig. 3.2. The average length of the nozzles was 4 mm long and the outer diameter was held constant at approximately 5.6 mm. The discharge areas of the circular and elliptic nozzles remained unchanged (±5%), while the major-to minor axes ratio, a/b, varied from 1.3 to 2.7 (Table 3.1). The lip thickness of

the elliptic nozzles was not constant. The discharge areas were measured using a microscope. The equivalent radius, R_{eq} , was defined for the elliptic nozzles as $(a \cdot b)^{1/2}$ where a is the major axis half-width and b is the minor axis half-width [45].

Table 3.1 Circular and elliptic short nozzles (Type 1).

a/b	a (mm)	b (mm)	A_j (mm^2)	$R_{eq} = (a \cdot b)^{1/2}$
1.0	1.42	1.42	6.24	1.42
1.32	1.56	1.18	6.15	1.36
1.80	1.80	1.00	6.24	1.34
2.72	2.18	0.80	6.33	1.32

Tubes. Circular stainless steel fuel tubes with discharge areas of 16.4 mm^2 and 7.94 mm^2 and lip thicknesses ranging from 0.82 mm to 1.59 mm were employed. The elliptic injectors with major-to-minor axes ratios varying up to 1.60 were made by pressing a 4.6 mm inside diameter circular pipe (with a discharge area of 16.4 mm^2) into an oval shape (Fig. 3.3). Although the shape of the cross-section was not truly elliptic, it will be referred to as such for simplicity. The lip thickness of these nozzles was 0.89 mm. The shape and lip thickness of the tube nozzles were uniform over the length of the tubes providing a fully developed flow at the nozzle exit. The length of the nozzles was fifty times the diameter of the circular jet and fifty times the major axis of the elliptic jets.

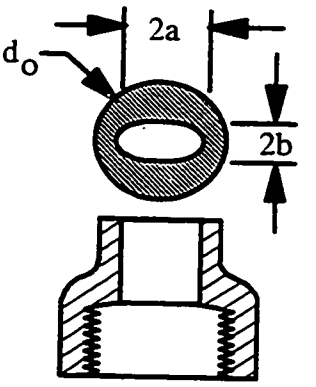

Fig. 3.2 Nozzles with constant outer diameter.

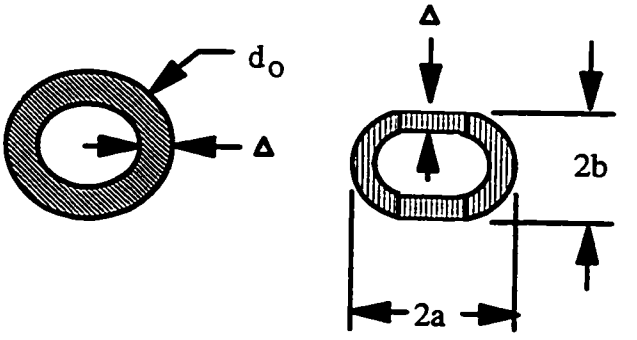

Fig. 3.3 Cross-section of the nozzle-tubes.

Table 3.2 Circular and elliptic tube nozzles (Type 2).

a/b	a (mm)	b (mm)	A_j (mm^2)	$R_{eq} = (a \cdot b)^{1/2}$
1.0	2.29	2.29	16.4	2.29
1.29	2.48	1.92	15.9	2.18
1.38	2.53	1.83	15.6	2.15
1.60	2.63	1.64	15.0	2.08

3.4 Laser-Doppler Velocimeter

Set-up. A schematic diagram of the laser Doppler velocimeter (LDV) that was assembled and utilized is shown in Figs. 3.4 (a) and (b). The system consisted of a 300 mW air-cooled argon ion laser (ILT Model 5500A), a two-colour LDV optical system (TSI 9100-8) and a frequency shift system (TSI Model 9180). The multi-line beam of the argon-ion laser was separated into the two colour lines of 514.5 nm and 488 nm wavelengths using a dichroic type colour separator. The assembly and especially the alignment of the system was labour intensive due to the high precision required in the procedure.

The instrument was operated in the backscatter mode with a beam separation of 9 mm and a transmitter lens with a focal distance of 121.4 mm. The control volume is determined by the type of optical unit and laser used. A resulting control size of 0.043 x 0.040 x 0.778 mm was obtained.

Data Acquisition System. The output signal from each photomultiplier tube was filtered, processed, and validated using two counter processors (TSI Model 1980B), one for each colour beam. Each counter processor module consisted of an Input Conditioner (Model

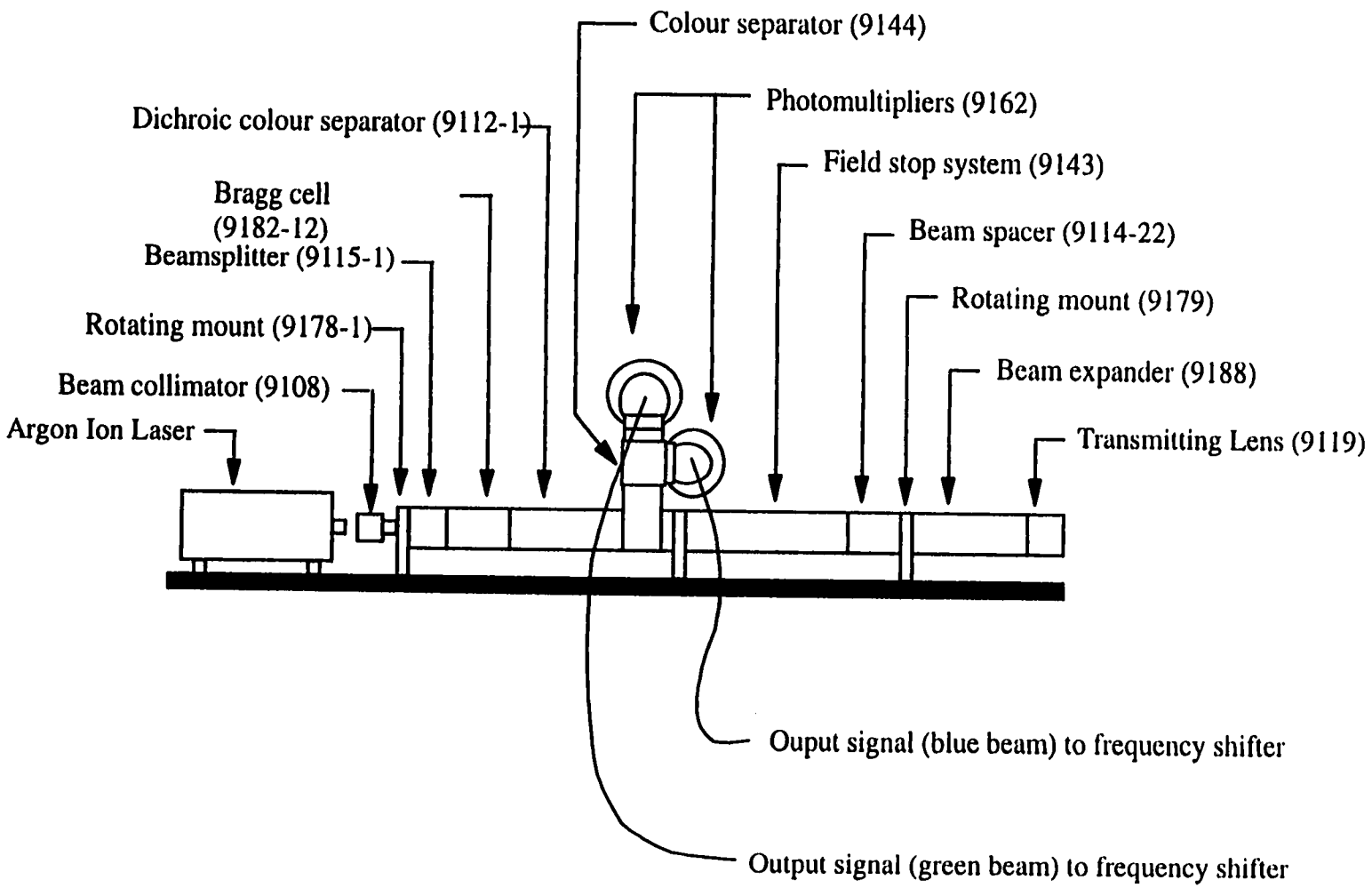

Fig. 3.4 (a) Schematic of the LDV optical system.

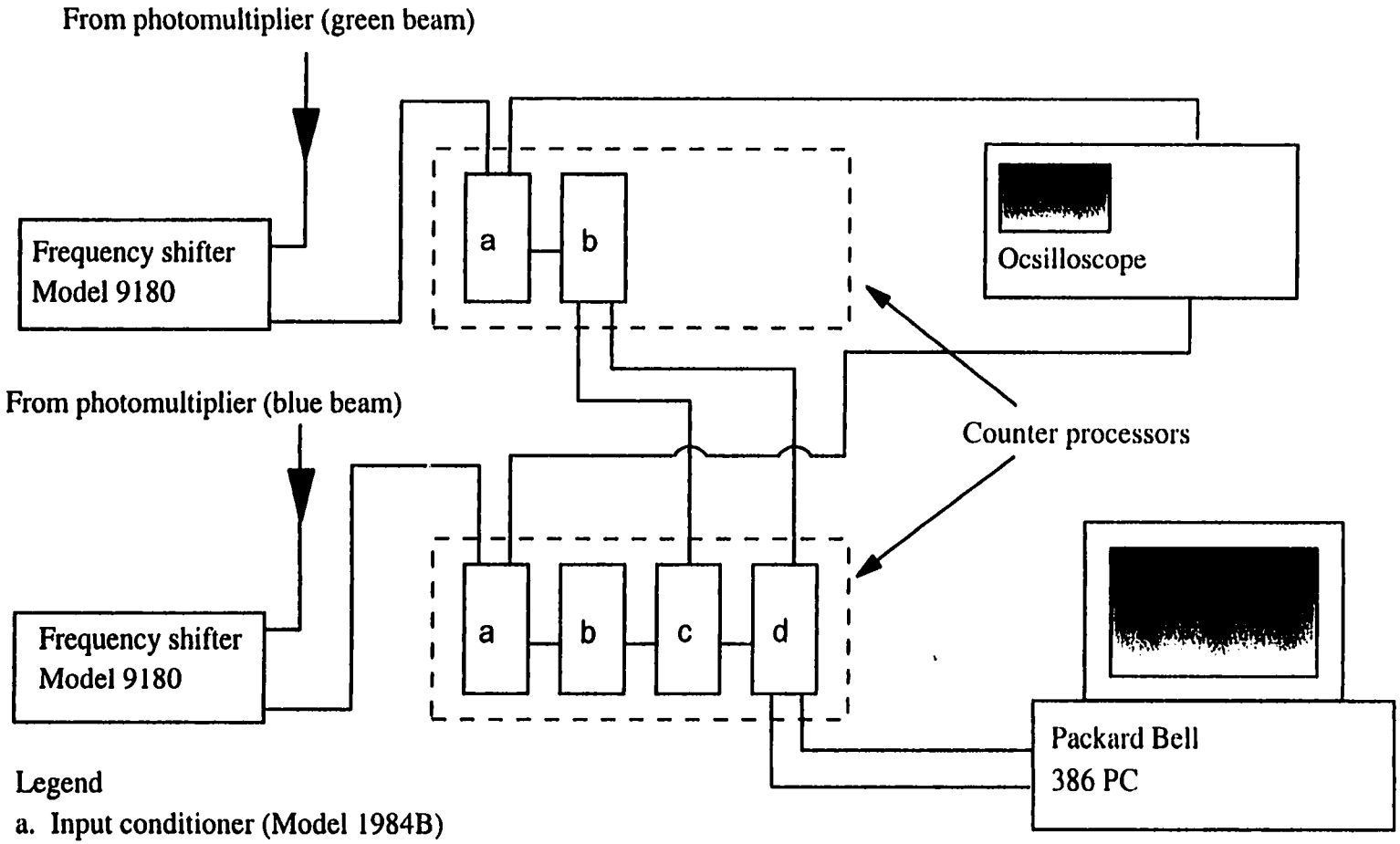

Legend

a. Input conditioner (Model 1984B)
b. Timer (Model 1985B)
c. Readout Panel (Model 1992)
d. Multichannel Interface (Model MI 990)

Fig. 3.4 (b) Schematic of the LDV data aquisition system.

1984B) and Timer (Model 1985B). The interconnection of the two counter processors enabled the common use of the Readout Panel (Model 1992) and Multichannel Interface (Model MI990) which were contained in the counter processor used for the blue beam. The counter processor modules determined the Doppler frequency transmitted from each of the photomultipliers by measuring the time it took a particle to travel a known number of interference fringes in the measuring volume. The measured time was then validated according to the desired accuracy and released through the computer interface in digital form. A microcomputer-based data acquisition and statistical analysis program, TSI's Flow Information Display (FIND) software, processed the output data of the LDV.

Flow Seeding. Laser Doppler velocimetry measurements required the gaseous flow under investigation to be uniformly and steadily seeded with micron-sized light scattering particles. The size and density of the seed particles was also of utmost importance. The seed particle must be small enough to follow the flow tested and yet be large enough to scatter sufficient light for the optimal operation of the LDV system. The density of the seed also had to be small and as close to the density of the gas tested as possible. The type of seed required depended on the flow situation and was determined by trial and error.

Alpha alumina particles of nominal size of 0.3 μm were found to seed satisfactorily the jet fuel and surrounding stream in the current study. Both the jet fuel and surrounding stream were independently seeded with a cyclone aerosol generator similar to that described by Glass and Kennedy [88]. Fig. 3.5 illustrates the particle seeding device. The seeder consisted of a plexiglass tube with a tangential gas inlet and a vertically upward

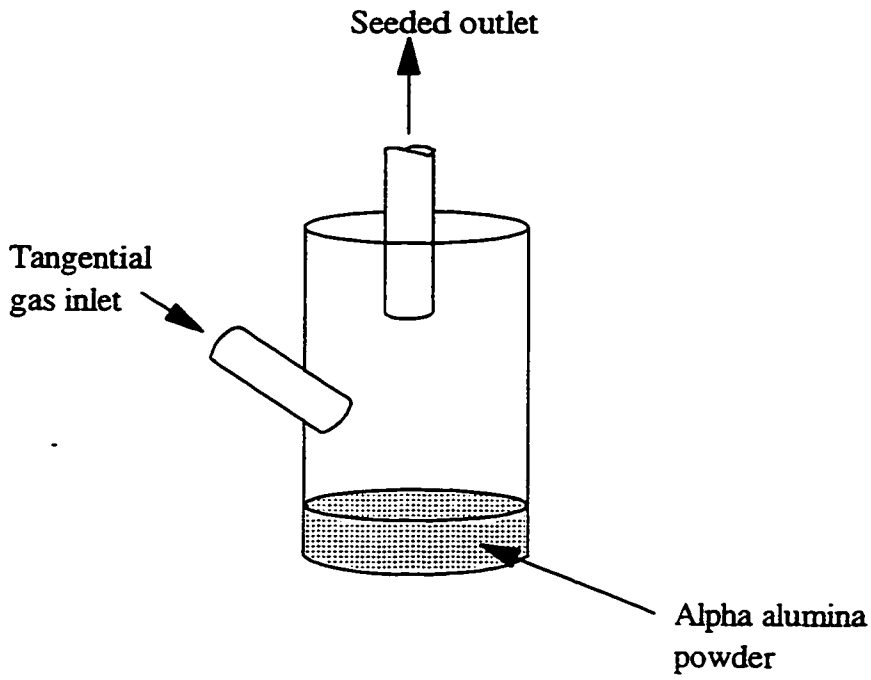

Fig. 3.5 Schematic diagram of the cyclone aerosol generator.

seeded outlet. In seeding the co-flowing air stream, compressed air was used to inject the seed into the co-flowing air stream. The particles were introduced well upstream of the combustion chamber to ensure that the flow was undisturbed in the test section.

Optical Window. In laser Doppler velocimetry, all windows and prisms must be of optical quality, i.e., of stringent surface flatness, to achieve the high precision obtainable by this measurement system. This is also true in schlieren photography. Although the neo-ceramic windows employed in the flame visualization studies were adequate for lift-off and blowout measurements, these tempered windows, like any tempered glass, significantly distorted images and hence could not be used for LDV measurements or schlieren imagery. Consequently, Vycor windows of optical quality were installed. Due to the high cost of these windows, windows of diameter 121 mm were purchased and modifications were made to the combustion chamber such that the location of the windows could be varied from the nozzle up to a downstream distance of approximately 250 mm.

3.5 Temperature Measurements

A number of ports were provided along the height of the combustor for inserting probes. The temperature field was probed with an uncoated platinum-platinum/13% rhodium thermocouple (type R) with a bead diameter of 0.25 mm and an outer sheath diameter of 1.6 mm. The readings were corrected for radiation and conduction losses following [89] and were accurate to ±15 °C. Since the thermocouple can act as a catalyst for the recombination of radicals and produce erroneous measurements, the thermocouple

was replaced frequently when a hysteresis in the temperature profile was apparent.

3.6 Schlieren System

A two-mirror Z arrangement schlieren system with a mercury vapour light source was used to visualize the flow structure in cold and flame jets. The mirrors had a diameter of 101.6 mm and a focal length of 1.22 m. Photographs were taken with a 35 mm TMAX 1600 ASA film.

3.7 Gas Analysis Measurements

Gas samples were withdrawn from cold and ignited jets through a stainless steel probe of tip diameter 3.1 mm. A water-jacket around the probe ensured that the samples were sufficiently cooled prior to entering the gas analyzers.

The samples were treated to remove particulates and moisture with a series of filters and chilled moisture traps. The concentrations of methane, carbon dioxide and carbon monoxide were analyzed with nondispersive infrared analyzers (Beckman Model 864) and were accurate to ±6%. The concentration of oxygen was analyzed with a paramagnetic analyzer (Beckman Model 755) and was accurate to ±1%.

3.8 Experimental Procedure

Lift-off and Blowout Measurements. The lift-off or blowout limits of jet diffusion flames were measured by first setting the co-flowing stream and jet velocity at a low value.

The jet was then ignited with an electrical spark. The igniter was then removed from the control volume. One of two procedures can then be followed to measure the lift-off and blowout limits. The first is by gradually increasing the jet discharge velocity while maintaining a constant co-flowing stream velocity. The second is by gradually increasing the co-flowing stream velocity while maintaining a constant jet discharge velocity. The difference in the procedures was within the experimental uncertainty of approximately ±5%. For convenience, the lift-off or blowout of a single component fuel jet was measured using the first procedure and that of a multi-component fuel jet using the second procedure. For the blowout limits of jets in still air, the windows from the combustion chamber were removed. The lift-off or blowout of the jet flames were observed visually. The measured volumetric flow rate or velocity of the jet at which the flame suddenly lifted off the nozzle rim or went out of the combustor entirely was deemed the lift-off or blowout limit, respectively. Some experiments were repeated to establish repeatability.

LDV Measurements. LDV measurements were conducted on both cold and ignited jets in different flow conditions. The origin of the Cartesian co-ordinate system (x,y,z) was located at the centre of the plane of the nozzle. Between 2000 to 5000 samples were taken per data point with a variable time window set at 10 μs.

It was required that for each data point, the maximum amplification be provided with a minimum amount of high and low frequency noise. This was achieved with the manual adjustment of the filters and gain amplifier on the counter processors. The frequency shift system, or bragg cell module, was employed to introduce a fixed frequency

shift between the two colour beams and produce a moving interference fringe. In doing so, accurate measurements could be obtained in highly turbulent flows where there was a recirculation zone and in flows of near-zero mean velocities. However, an optimum frequency shift was required such that it was high enough to measure these flows but not too high that the Doppler signal would be obscured by high frequency noise. The LDV measurements were accurate to ±7% and some experiments were repeated to establish repeatability.

CHAPTER 4

RESULTS AND DISCUSSION: BLOWOUT LIMITS

4.1 General

The effects of the co-flowing stream velocity, nozzle geometry, jet fuel additives, and auxiliary fuel composition in the co-flowing air stream on the flow structure and the blowout limits of methane jet diffusion flames were investigated experimentally. The initial temperature of the jet and co-flowing stream ranged from 18 to 22 °C for all of the experiments and the pressure in the combustor was about atmospheric.

The effect of the co-flowing stream velocity on the flame blowout limits is discussed in section 4.2, while the effect of changes in the jet nozzle geometry, i.e., nozzle diameter, shape and lip thickness, on the flame blowout limits is discussed in section 4.3 for a range of co-flowing air stream velocities together with discussions about some of the observed phenomena. The effect of additives to the jet fuel on the blowout limits is discussed in section 4.4. The effect of auxiliary fuel type and concentration in the co-flowing stream on the blowout limits of a methane jet is presented and discussed in section 4.5. The parameters affecting the limiting co-flowing stream velocity is discussed in section 4.6.

4.2 Effect of Co-flowing Stream Velocity

Generally, an increasing co-flowing stream velocity had a detrimental effect on the blowout limits of a jet flame. Figures 4.2.1 (a) and (b) show the blowout limit curves for

two different nozzles. At low co-flowing stream velocities, the blowout limits were reduced dramatically with a small increase in the co-flowing stream velocity, while its effect on the blowout limits was relatively smaller at higher co-flowing stream velocities. Experiments show that these regions are associated with the blowout of either a lifted or attached flame. At relatively low co-flowing air stream velocities, the flame was first attached to the burner rim (Fig. 4.2.2 (a)). As the jet flow rate was increased (at a constant co-flowing stream velocity), the flame lifted off the nozzle rim and stabilized at some distance downstream of the nozzle (Fig. 4.2.2 (b)). Further increases in the jet flow rate pushed the lifted flame further downstream until it eventually blew out of the combustor. Although the blowout limits decreased with an increase in the co-flowing stream velocity, the jet flame lift-off limit remained approximately constant (Figs. 4.2.1 (b)). The jet lift-off and blowout flow rates became equal at the limiting stream velocity, u_{sl}. At co-flowing stream velocities exceeding a certain value (i.e., u_{sl}), no lift-off of the flame was observed with an increase in the jet flow rate and the attached flame abruptly blew out. Therefore, the limiting co-flowing stream velocity separates the two distinct regions of flame stabilization mechanisms prior to the blowout condition, i.e., lifted and attached flames.

4.3 Effect of Nozzle Geometry

Discharge Diameter. Although the effect of the nozzle geometry on the diffusion flame stability limits have been the subject of many investigations in the past, there is no data available about this effect in the full range of possible co-flowing stream velocities for a

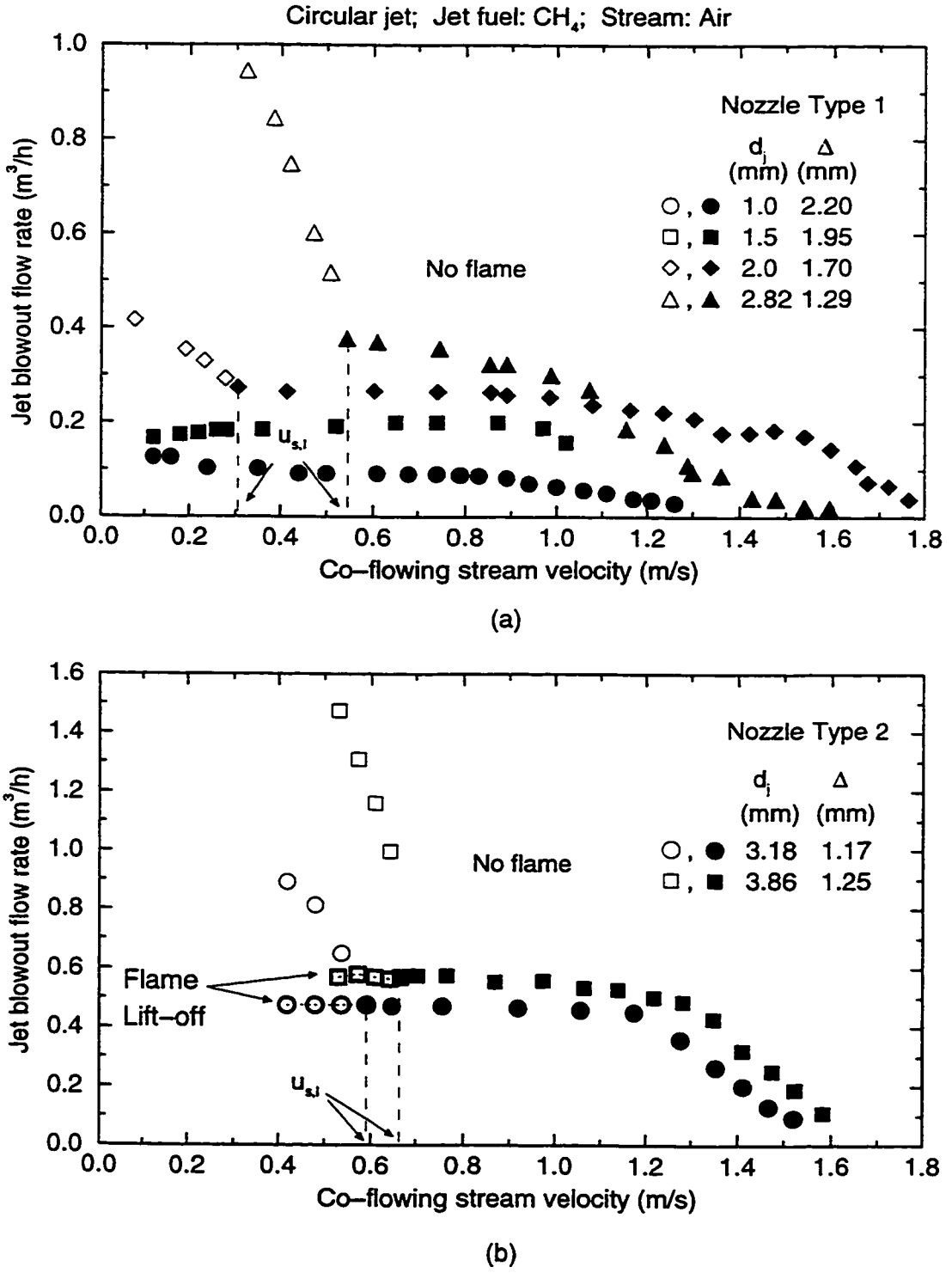

Fig. 4.2.1 The blowout limits of a methane jet diffusion flame as a function of the co–flowing stream velocity for different nozzle types and diameters. Solid symbols: attached flame blowout. Open symbol: lifted flame blowout.

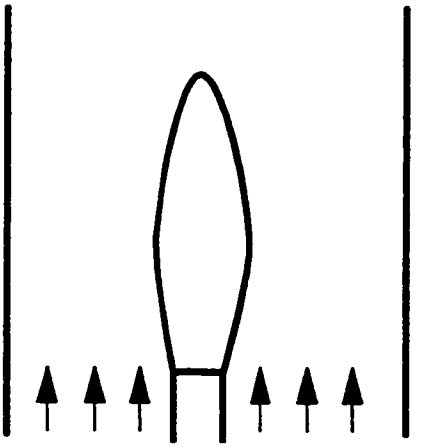

Attached Flame

(a)

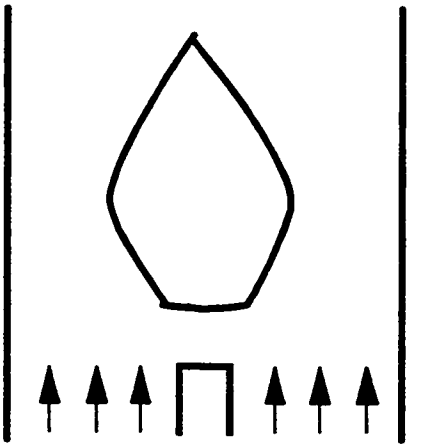

Lifted Flame

(b)

Fig. 4.2.2 A sketch of (a) attached and (b) lifted flames.

stable flame. The effect of the jet discharge diameter on the blowout limits were experimentally investigated on jets of Type 1 and 2. The jets of Type 2 were of approximately the same lip thickness while those of Type 1 had different lip thickness at approximately the same outer diameter of 5.6 mm. To eliminate the additional effect of various lip thicknesses, the effect of the discharge diameter on the blowout limits was shown for nozzles of Type 2. The flame blowout limits defined either as the jet volumetric flow rate or the jet discharge velocity at blowout are shown in Fig.4.3.1. It can be seen that the blowout limits increased substantially for lifted flames with an increase in the fuel jet discharge area. The rate of increase in the blowout limits can be very significant especially at very low co-flowing stream velocities. The rate of increase in the blowout limits of attached flames was not as significant.

Lip Thickness. The effect of lip thickness on the flame blowout limits was investigated for fuel jets discharged from stainless steel tubes of diameter 3.18 mm. The lip thickness was varied from 0.82 mm to 1.59 mm. The results are shown in Fig. 4.3.2. A variation in the lip thickness for the same discharge area did not have a considerable effect on the blowout limits of lifted flames. For the conditions employed, the flame stabilization region was far downstream of the jet rim and a small change in the nozzle lip thickness did not appear to exert a notable effect on the blowout limits of lifted flames.

In contrast, the effect of variations in the nozzle lip thickness on the blowout limits of attached flames was significant especially for higher co-flowing stream velocities in which the stability of the jet flame deteriorated very rapidly. For example, at a co-flowing

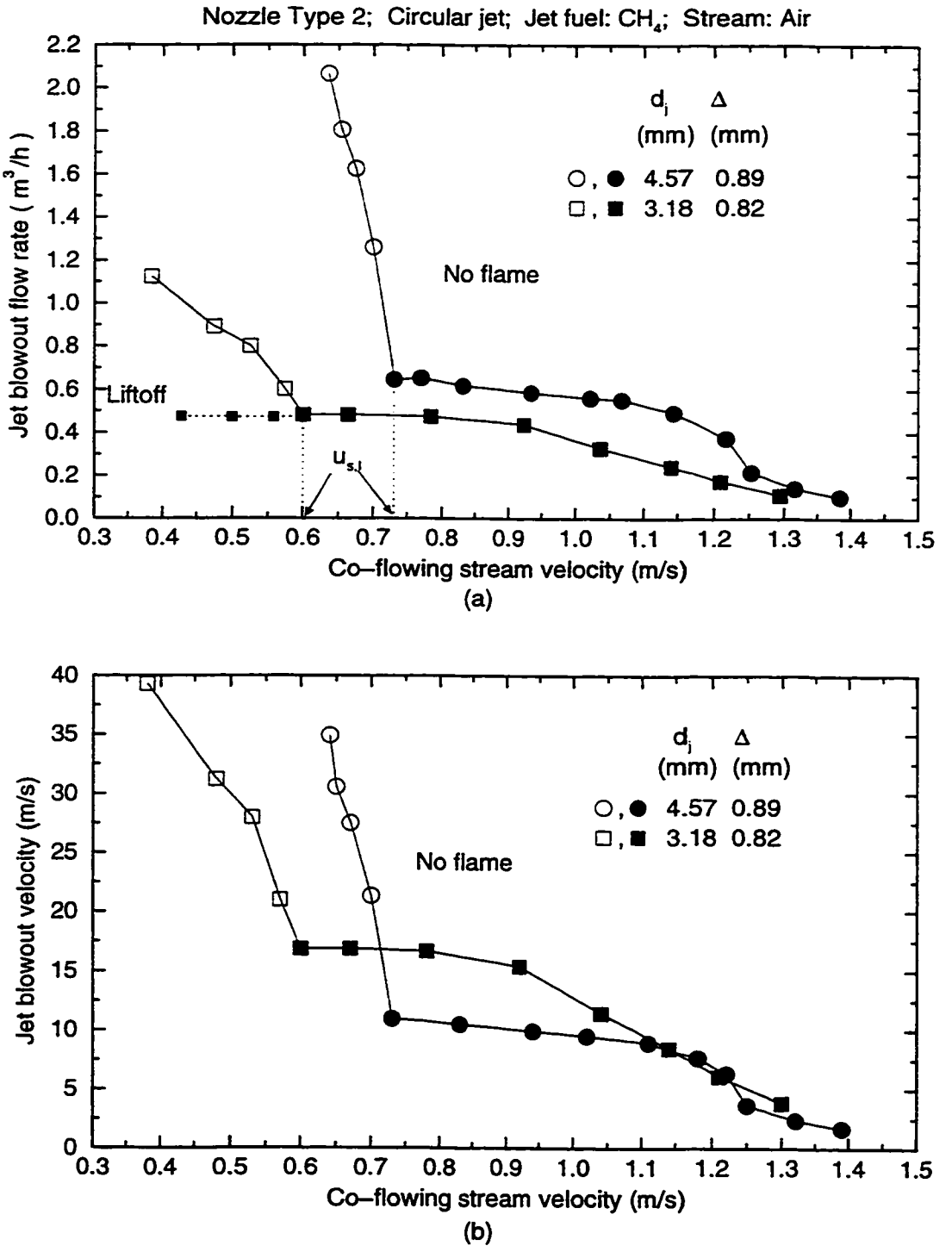

Fig. 4.3.1 The flame blowout limits defined as (a) the jet volumetric flow rate and (b) the jet velocity as a function of the co–flowing stream velocity for two different discharge diameters. Solid symbols: attached flame blowout. Open symbols: lifted flame blowout.

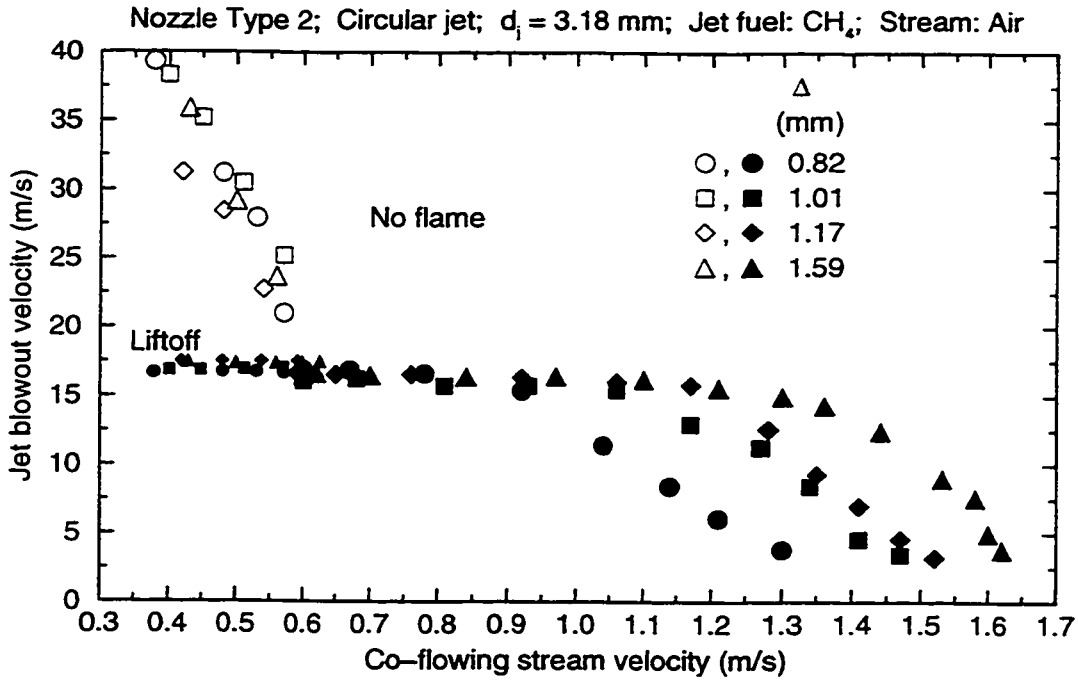

Fig. 4.3.2 The jet blowout velocity as a function of the co–flowing stream velocity for nozzles of different lip thicknesses. Solid symbols: attached flame blowout. Open symbols: lifted flame blowout.

stream velocity of 1.3 m/s, an increase in the lip thickness from 0.82 mm to 1.59 mm improved the blowout limit by more than 300%. Furthermore, the range of co-flowing stream velocities in which jet diffusion flames can be stabilized without additional external devices, was extended from 1.30 m/s to 1.62 m/s. This increased flame stability is due to the formation of a recirculation zone in the wake of the thick-walled fuel tube. In the recirculation zone, the fresh mixture is in contact with hot combustion products which increase the temperature of the fresh fuel-air mixture and the local burning velocity. Similar trends in the blowout of attached flames was observed by other researchers with unconfined co-flowing hydrogen jet flames [14,15]. It also can be seen that a change in the nozzle lip

thickness had very little effect on the lift-off velocity and limiting stream velocity when employing nozzle in the form of long tubes (Type 2). The former finding contradicts the observations of Takahashi and Schmoll [15] who found that for large diameter jets (i.e., d_j = 9.45 mm) the lip thickness has a profound affect on the lift-off velocity of methane-air co-flowing diffusion flames.

Elliptic Jets. In an attempt to improve the stability of attached flames, the effect of different nozzle geometries were investigated since cold flow studies conducted in still air on large elliptic jets had found that elliptic jets entrained several times more surrounding air than circular jets in the near-nozzle region [13]. The effect of the jet shape (i.e., elliptic jets of different aspect ratios) on the blowout limits was investigated with both types of nozzles.

The blowout limits for elliptic nozzles of Type 1 which had a non-uniform lip thickness are presented in Fig. 4.3.3 (a). It can be seen that the stability of lifted flames was not as greatly affected by varying the aspect ratio of fuel jets as that of attached flames. This might be expected since the stabilization of the lifted flame took place in the far-field region of the jet and studies of Ho and Gutmark [13] on cold free jets showed that the rates of entrainment for different elliptic jets were not much different from those for a circular jet at farther downstream distances.

The stability of attached flames, on the other hand, was governed by near-nozzle conditions and thus it was not unexpected that the shape of the nozzle influenced the blowout limits of attached flames. A small difference in the jet aspect ratio (from 1.32 to

1.80 in Nozzle Type 1) significantly affected the lift-off and blowout limits of attached flames. An apparent optimum aspect ratio with respect to the lift-off and blowout limit existed for attached flames. As can be seen, the lift-off and blowout velocities of a jet discharged from nozzles with an aspect ratio of 1.32 was much higher than those of the circular jet and elliptic jets with higher aspect ratios throughout the attached flame region. At a co-flowing stream velocity of 0.75 m/s, for instance, the blowout limit of an attached flame issuing from an elliptical nozzle of aspect ratio 1.32 was as much as 39% higher than that obtained with a circular nozzle, while the blowout limit of a nozzle with an aspect ratio of 2.72 decreased by as much as 28%. The difference in the blowout limits between the nozzles of various aspect ratios decreased as the co-flowing stream velocity increased. The existence of an optimum nozzle aspect ratio is probably the result of the combined effects of mixing rates, jet dynamic stability and flame-flow interactions. Although a relatively small increase in the jet aspect ratio has a stabilizing effect on the jet flame due to an enhanced entrainment rate, further increases in the jet aspect ratio produced greater jet dynamic instabilities that overshadowed the benefit of an increase in the entrainment rate. An elliptic jet with a small aspect ratio can, therefore, improve the blowout limits of attached flames especially at co-flowing stream velocities close to the limiting stream velocity.

The blowout limits for elliptic nozzles of Type 2 (with a uniform lip thickness and well developed flow at the nozzle exit) are shown in Fig. 4.3.3 (b). The trends in the behaviour of the blowout limits were similar to those of nozzles Type 1. The effect of the

nozzle ellipticity of these larger jets was not significant in the blowout limits of lifted flames as it was in those of attached flames. Substantial differences in the blowout limits of the circular and elliptic jets were observed at higher co-flowing stream velocities. The existence of an optimum aspect ratio in the blowout limits of attached flames was also apparent. The blowout velocity of a jet with an aspect ratio of 1.38 was much higher than the other aspect ratio jets employed especially at higher co-flowing stream velocities. The existence of an optimum aspect ratio with respect to jet spread and combustion efficiency was also reported by Schadow et al. [47] who employed large elliptic nozzles in ducted rockets. However, other studies conducted on the stability of flames issuing from an elliptic nozzle (a/b = 3) revealed that the lift-off and reattachment limit of the flame were reduced with an elliptic jet [31]. It is known for cold jets that for a given aspect ratio, vortical structures undergo more severe deformation in a smaller elliptic jet than in a larger one due to the greater curvature on the major-axis side, resulting in the earlier axis-switching and higher entrainment rates in the smaller elliptic jets [45]. It was also reported that axis-switching occurred farther downstream in an initially turbulent jet than in an initially laminar jet. Therefore, it is possible that the initially turbulent jet and the significantly larger jet discharge area and aspect ratio in the study of Gollahalli et al. [31] delayed the switching of the axes and reduced the entrainment of air while increasing the hydrodynamical instabilities, resulting in the lower lift-off limit.

It is interesting to note that the effect of the jet aspect ratio on the blowout limits was decreased when a small amount of hydrogen (15% by volume) was added to the

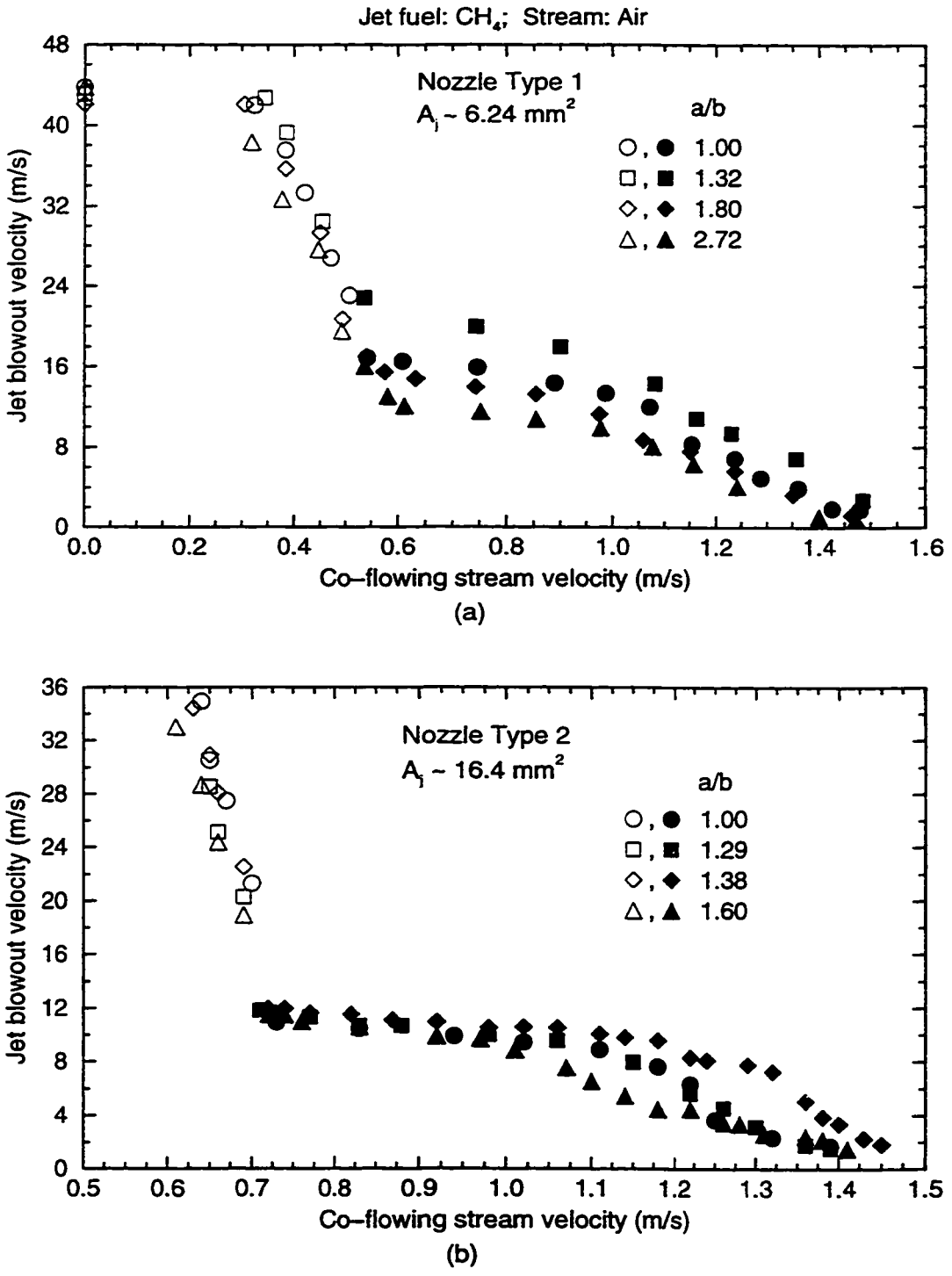

Fig. 4.3.3 The jet blowout velocity as a function of the co-flowing stream velocity for different aspect ratio nozzles of (a) Type 1 and (b) Type 2. Solid symbols: attached flame blowout. Open symbols: lifted flame blowout.

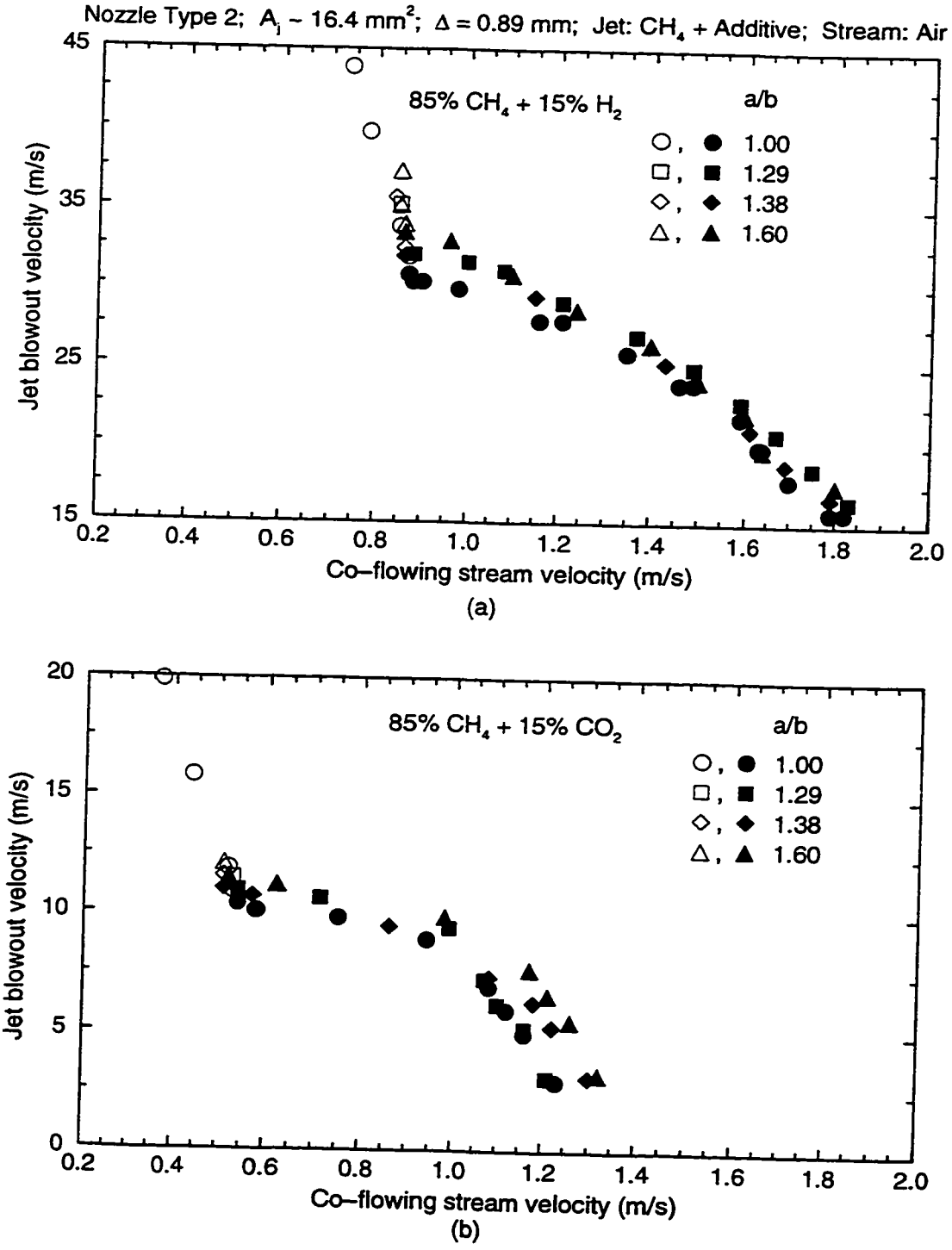

Fig. 4.3.4 The blowout limits of a methane jet diffusion flame with (a) hydrogen and (b) carbon dioxide as additives issuing from elliptic nozzles of different aspect ratios. Solid symbols: attached flame blowout. Open symbols: lifted flame blowout.

methane jet (Fig. 4.3.4 (a)). When carbon dioxide was added to the methane jet, the jet aspect ratio was observed to influence the blowout limits only at higher co-flowing stream velocities. The effect of the jet aspect ratio was different for this fuel mixture than for a pure methane jet, i.e., the blowout limits were increased with an increase in the jet aspect ratio. For instance, at a co-flowing stream velocity of 1.21 m/s, the blowout limit of an attached flame issuing from an elliptical nozzle of aspect ratio 1.60 was 100% higher than that obtained with the circular nozzle.

4.4 Effect of Jet Fuel Additives

The effect of the addition of hydrogen to methane on the flame blowout limits of a circular jet issuing from nozzles of Type 2 is shown in Fig. 4.4.1. It can be seen that adding a relatively small amount of hydrogen to the methane jet improved the blowout limits for all co-flowing stream velocities employed (i.e., for lifted as well as attached flames) by as much as 15 times those for a pure methane jet and also extended the range of co-flowing stream velocities at which a stable flame could exist. The addition of hydrogen substantially increased the maximum burning velocity of the fuel mixture which is very important to flame stabilization. It also increased the density difference between the two co-flowing streams promoting the mixing between the jet fuel and air stream [64,90].

The effect of the addition of diluents - carbon dioxide and nitrogen - to the jet fuel on the blowout limits is shown in Figs. 4.4.2 (a) and (b), respectively. It can be seen that the effect of diluents is much stronger for lifted flames than for attached flames. The

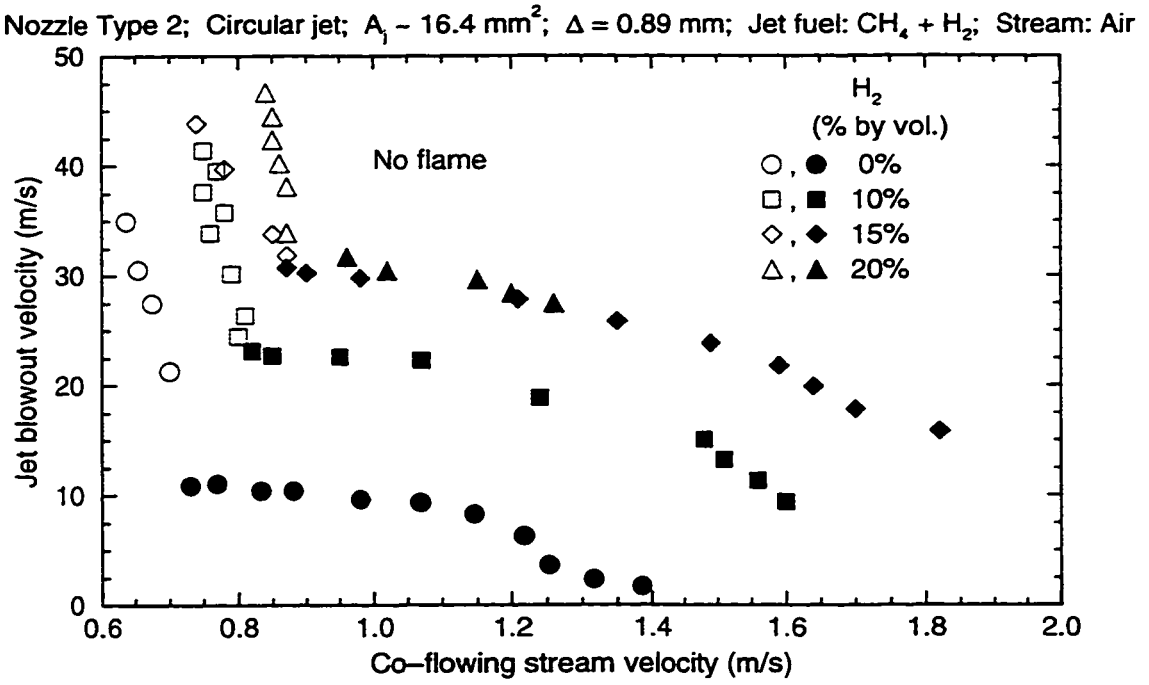

Fig. 4.4.1 The jet blowout velocity as a function of the co–flowing stream velocity for jets of different CH_4– H_2 concentrations. Solid symbols: attached flame blowout. Open symbols: lifted flame blowout.

stability of lifted flames deteriorated rapidly with the addition of diluents, while the blowout limits of attached flames were affected to a much lesser degree with the addition of carbon dioxide (up to 15% by volume) and the effect of adding nitrogen was almost negligible.

In lifted flames, the mixing of the jet and surrounding air is more significant and the addition of a diluent to the methane jet further diluted the fuel-air mixture. The addition of diluents also reduced the burning velocity of the fuel mixture which contributed to the decrease in the stability limits. A higher diluent concentration in the jet fuel resulted in a greater reduction in the burning velocity (up to 17% less for 15% CO_2). As expected, adding carbon dioxide to the jet fuel was more detrimental to the blowout limits than

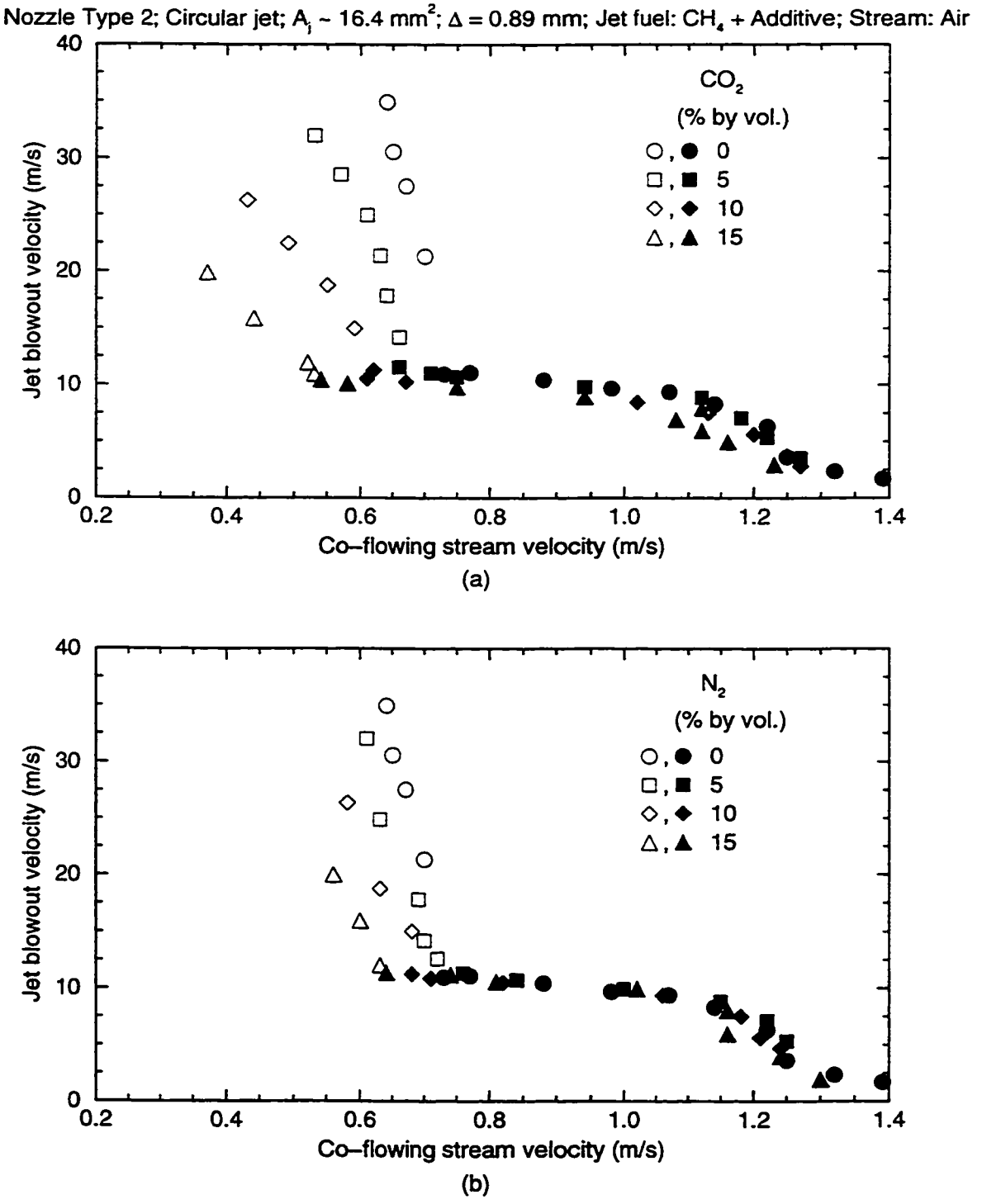

Fig. 4.4.2 The jet blowout velocity as a function of the co–flowing stream velocity for different (a) carbon dioxide and (b) nitrogen concentrations in the methane jet. Solid symbols: attached flame blowout. Open symbols: lifted flame blowout.

adding nitrogen due to the lower burning velocity and higher density of the carbon dioxide-methane mixture.

In *attached* flames, the amount of air entrained into the jet near the stabilization region (i.e., very close to the nozzle rim) is rather small. The addition of small concentrations of diluents such as carbon dioxide and nitrogen to the methane jet reduced the amount of fuel available; consequently, the local fuel-air ratio improved and may have offset the detrimental effect of the diluent on the burning velocity. When the co-flowing stream velocity was increased, the effect of the carbon dioxide on the blowout limits became more significant with an increase in its concentration.

4.5 Effect of Auxiliary Fuel in the Co-flowing Air Stream

The effect of an auxiliary fuel in the co-flowing stream on the blowout limits was investigated for attached flames with the intention of increasing their relatively low blowout limits. Methane, propane, ethylene and hydrogen were used as auxiliary fuels. Circular and non-circular nozzles of both types were employed. Changes in the blowout limits when a fuel was introduced into the surrounding stream ($u_{sf,b}$) were evaluated in terms of the ratio of these values to the corresponding blowout limit in a co-flowing pure air stream ($u_{j,b}$); therefore, a ratio greater than unity represented an improvement in the blowout limits with the addition of auxiliary fuel. To account for the effect of the type of auxiliary fuel introduced, the relative blowout limits, ($u_{sf,b}/u_{j,b}$), were plotted as a function of the ratio of the actual volumetric concentration of the auxiliary fuel in the co-flowing steam (C_s) to the

corresponding flashback limit concentration of the auxiliary fuel (C_{sJ}). The auxiliary fuel concentration at flashback represents the situation in which the fuel concentration in the co-flowing air reaches a sufficient level to support flame self-propagation in the co-flowing stream. The flashback limit concentrations for the fuels considered (C_{sJ}) are a function of the co-flowing stream velocity, and are shown in the corresponding figures.

Nozzle Type 1. For a circular jet of 2.82 mm in diameter, changes in the blowout limits of attached flames in an air stream of velocity 1.0 m/s with the addition of the auxiliary fuel are shown in Fig. 4.5.1 (a). The flames remained attached at blowout until the auxiliary fuel concentrations reached a certain value. For attached flames, there was a modest improvement in the blowout limits with increasing auxiliary fuel concentration to a maximum value of approximately 2.8 times those in pure air.

When the relative fuel concentration was increased beyond a certain value, which depended on the type of auxiliary fuel used, the flame lifted off. The presence of hydrogen, propane and methane in the surrounding co-flowing stream caused the flame to lift off at relative auxiliary fuel concentrations of 0.41, 0.64 and 0.75. A higher burning velocity auxiliary fuel required a smaller relative concentration in the air stream for the lift-off of the attached flame. For a lifted flame, even a small increase in the concentration of the auxiliary fuel dramatically improved the blowout limits, as shown by the broken lines in Fig. 4.5.1 (a). The greatest improvement in the blowout limits of methane jets was observed when the auxiliary fuel was hydrogen. This is probably due to its superior combustion properties.

Different trends were observed at a higher co-flowing stream velocity of 1.45 m/s as shown in Fig. 4.5.1 (b). The blowout limit of the methane jet at this stream velocity in a pure air stream was very small. When moderate auxiliary fuel concentrations were added to the air, the improvement in the blowout limits was much more significant at this co-flowing stream velocity than at a low velocity. The blowout limits were improved by as much as seven to nine times (depending on the type of auxiliary fuel) compared with those in an air only stream. A further increase in the auxiliary fuel concentration was either beneficial or detrimental to flame stability, depending on the type of fuel employed. For high burning velocity fuels such as hydrogen and ethylene at relative concentrations, C_s/C_{sJ}, higher than 0.59 and 0.74, respectively, the flame stability improved rapidly with a further small increase in fuel concentration as the formerly attached flame lifted off the burner rim. A higher co-flowing stream velocity required a higher concentration of hydrogen for the lift-off of the attached flame. On the other hand, an increase in the relative concentration (exceeding 0.7) of auxiliary fuels having relatively low burning velocities, such as methane and propane, did not cause the flame to lift off and the flame remained attached until blowout. The blowout limits of such flames deteriorated rapidly with further small increases in the auxiliary fuel concentration. The rapid changes in the blowout limits took place when the relative fuel concentration, C_s/C_{sJ}, was in the range of 0.6-0.7. At this concentration, the jet flame became engulfed in a premixed lean flame of the surrounding stream adjacent to the jet flame. This led to a further reduction in the oxygen available for entrainment into the jet and higher concentration of products of combustion in the region

of the jet flame. Since the mixing rates in attached flames are rather low at the nozzle rim where these flames stabilize and there is a deficiency in the oxygen concentration, the flame can either lift off the nozzle rim or blow out. The addition of high burning velocities fuels such as hydrogen and ethylene to the co-flowing air stream enabled the jet flame to lift off and stabilize at some downstream location where the local jet velocity equalled the burning velocity, while the addition of methane and propane to the air stream did not increase the burning velocity significantly enough to sustain a lifted flame and the attached flame blew out. Since the burning velocity of the methane jet in an air-hydrogen or -ethylene mixture is higher than that of a methane jet in air only stream, such high burning velocity flames can be stabilized at higher co-flowing stream velocities.

Effect of Nozzle Aspect Ratio. As can be seen in Figs. 4.5.2 to 4.5.7, the trends observed with elliptic nozzles of different aspect ratios are similar to those for a circular jet. At a low co-flowing stream velocity of 1.0 m/s, the attached flame lifted off at a certain auxiliary fuel concentration for all nozzles with different aspect ratios and for all of the different auxiliary fuels employed. At a higher co-flowing stream velocity of 1.45 m/s, flames issuing from elliptic nozzles lifted off only when hydrogen was used as the auxiliary fuel. At a co-flowing stream velocity of 1.0 m/s, the best improvement in the blowout limit was achieved with the larger aspect ratio nozzle of 1.80 and the lowest improvement was with the nozzle with an aspect ratio of 1.32 (i.e., the optimum ratio jet in air only). At a higher co-flowing stream velocity of 1.45 m/s, the best improvement in flame stability was recorded for the elliptical jet of aspect ratio 2.72 (although the blowout limit was the lowest for this aspect

ratio jet), followed by 1.80, 1.32 and then the circular jet. The addition of methane or propane at fuel concentrations approaching the flame flashback limit decreased the blowout limits regardless of the nozzle configuration. The addition of hydrogen at higher concentrations in the surrounding stream resulted in the lifting off of the attached flame for all of the nozzles employed. The blowout limits of a lifted jet flame increased significantly with a further small increase in hydrogen concentration and are represented by the broken lines.

Figures 4.5.8 to 4.5.10 (a) show that, for the same aspect ratio jet and a lower co-flowing stream velocity of 1.0 m/s, the blowout limits of attached flames in dimensionless form, $u_{sf,b}/u_{j,b}$, can be adequately correlated for different auxiliary fuels as a function of the relative concentration, $C_s / C_{s,l}$. However, this correlation does not include the lift-off of the flame and the effect of hydrogen at a higher co-flowing stream velocity of 1.45 m/s (Fig. 4.5.8 to 4.5.10 (b)).

Nozzle Type 2. The effect of methane as an auxiliary fuel in the co-flowing stream on the blowout limits was also investigated employing the larger and different type of circular and elliptic nozzles (Type 2). The results are shown in Figs. 4.5.11 to 4.5.13. At stream velocities of 1.0 and 1.45 m/s, the blowout limits of these jets have the same trends as those for nozzles of Type 1. In general, the addition of a small concentration of fuel in the air stream produced a more fuel-rich mixture at any radial location compared with when only air was present in the surrounding stream. The result was a shift of the combustion zone radially outward in the direction of smaller flow velocities, which would allow for flame

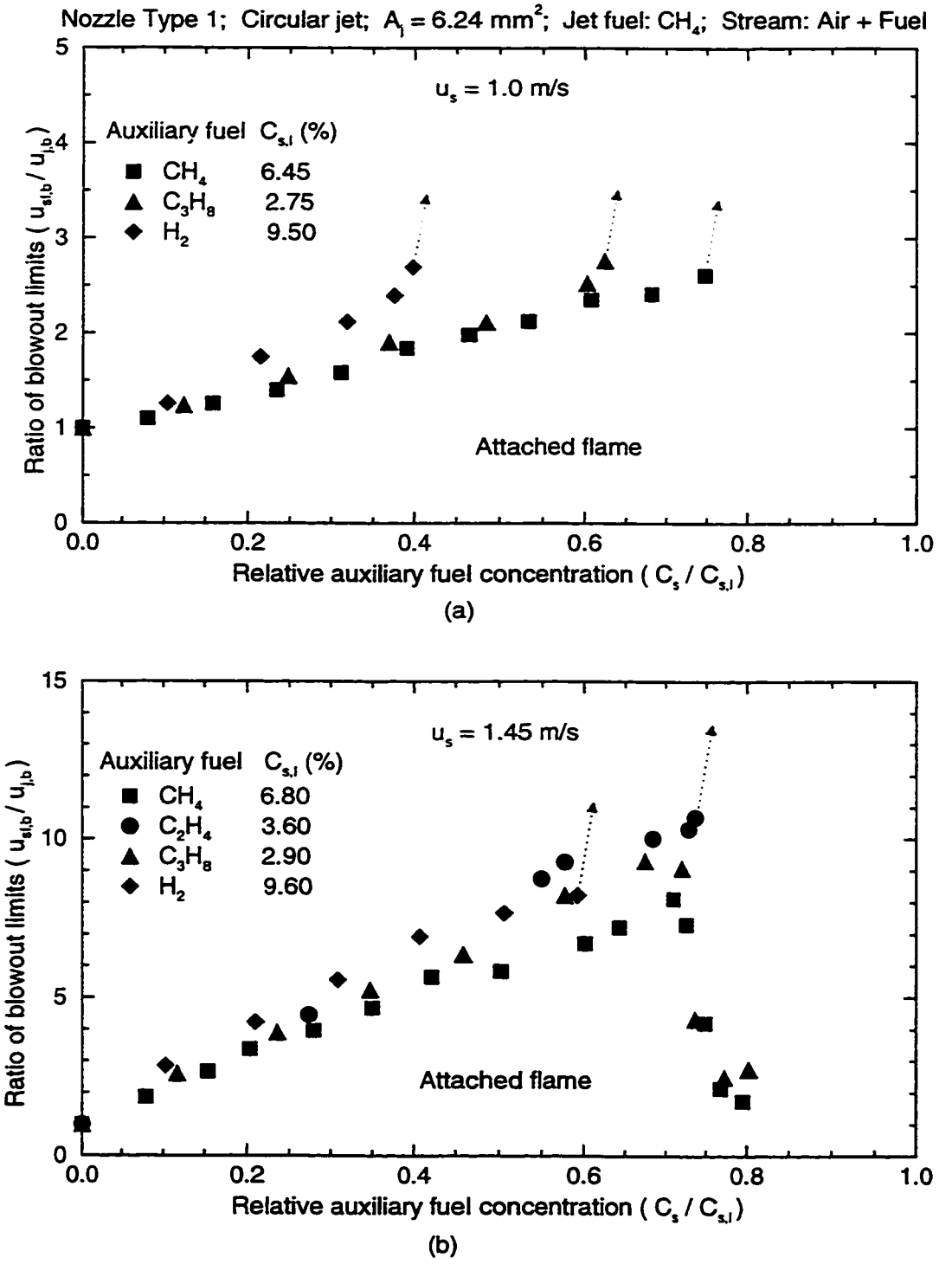

Fig. 4.5.1 The ratio of the blowout limits of a methane jet diffusion flame as a function of the type of auxiliary fuel and its concentration at (a) u_s = 1.0 m/s ($u_{j,b}$ = 12.5 m/s) and (b) u_s = 1.45 m/s ($u_{j,b}$= 3.6 m/s). Solid symbols: attached flame blowout. Arrows indicate lifted flame.

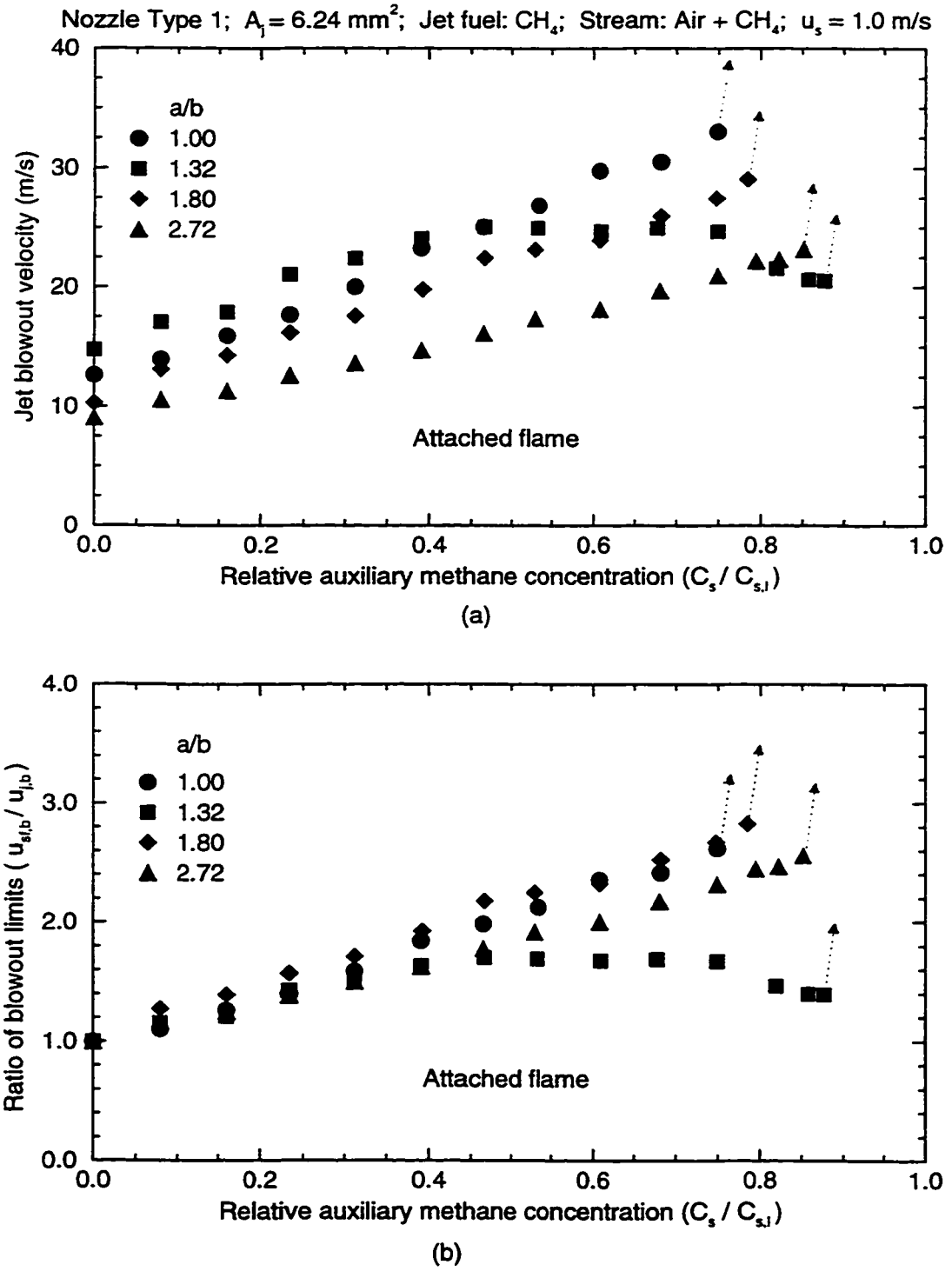

Fig. 4.5.2 The blowout limits as a function of the methane concentration in the co–flowing air stream for different aspect ratio nozzles. Solid symbols: attached flame blowout. Arrows indicate lifted flame. $C_{s,l}$ = 6.45 %.

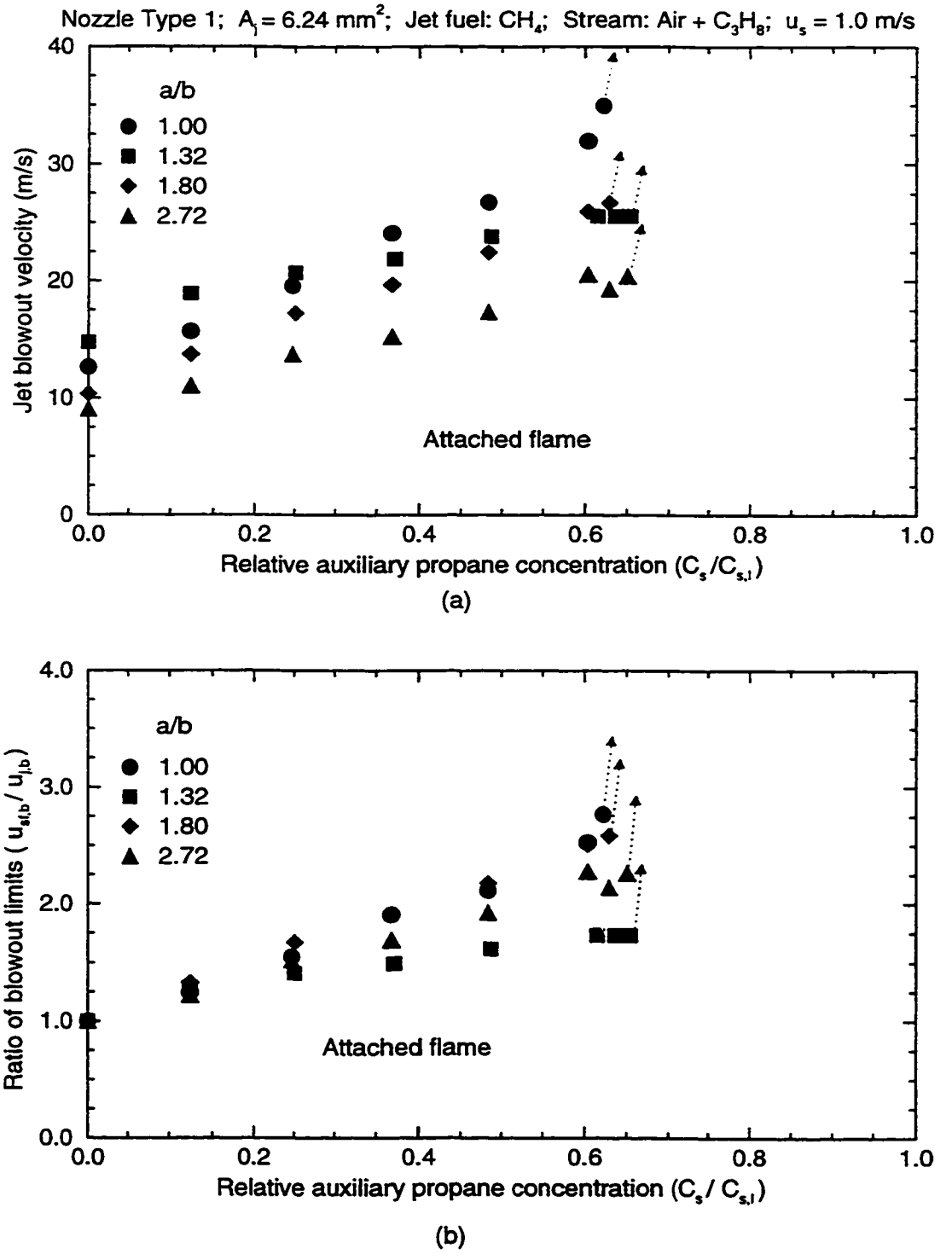

Fig. 4.5.3 The blowout limits as a function of the propane concentration in the co–flowing air stream for different aspect ratio nozzles. Solid symbols: attached flame blowout. Arrows indicate lifted flame. $C_{s,l}$ = 2.75 %.

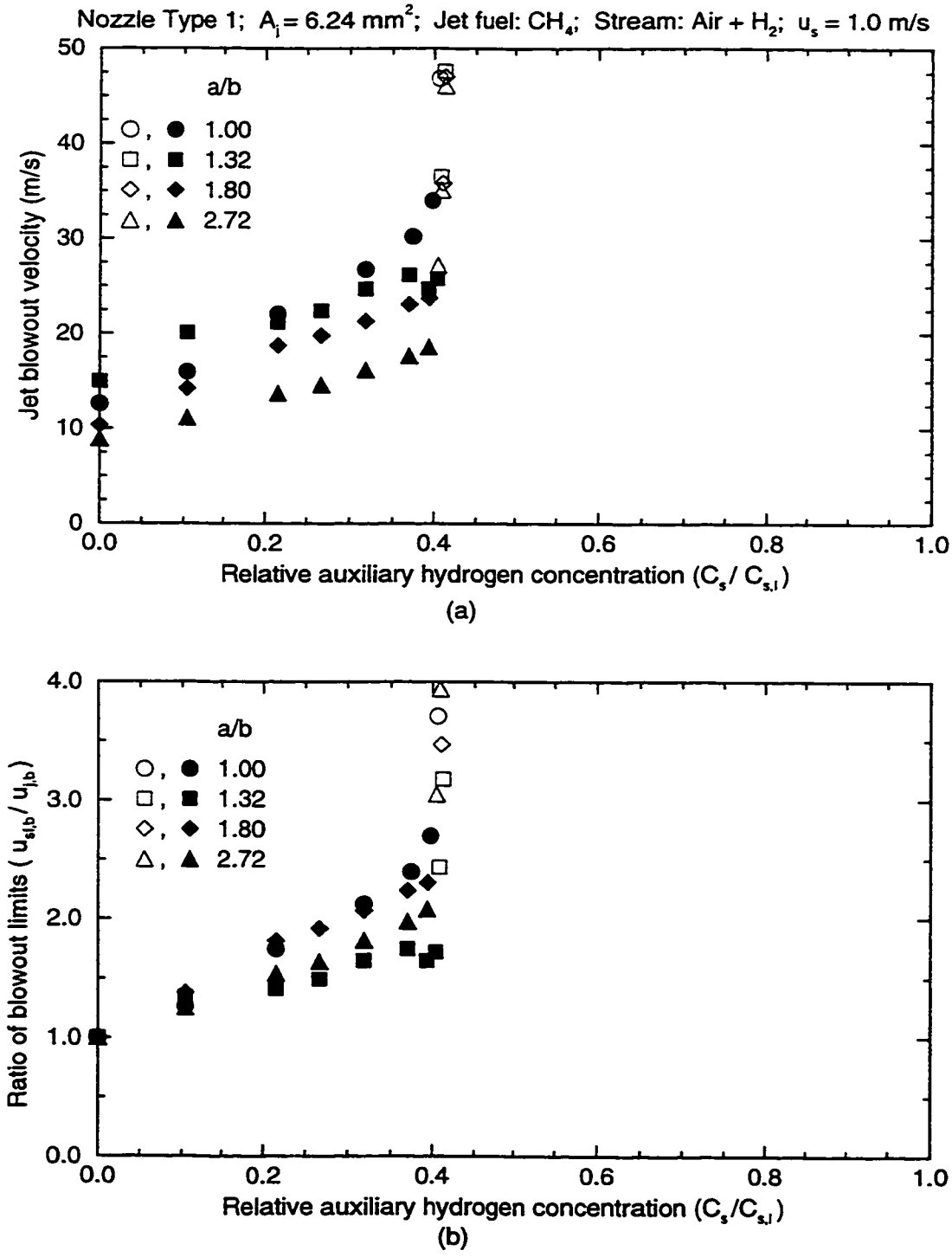

Fig. 4.5.4 The blowout limits as a function of the hydrogen concentration in the co–flowing air stream for different aspect ratio nozzles. Solid symbols: attached flame blowout. Open symbols: lifted flame blowout. $C_{s,l}$ = 9.50 %.

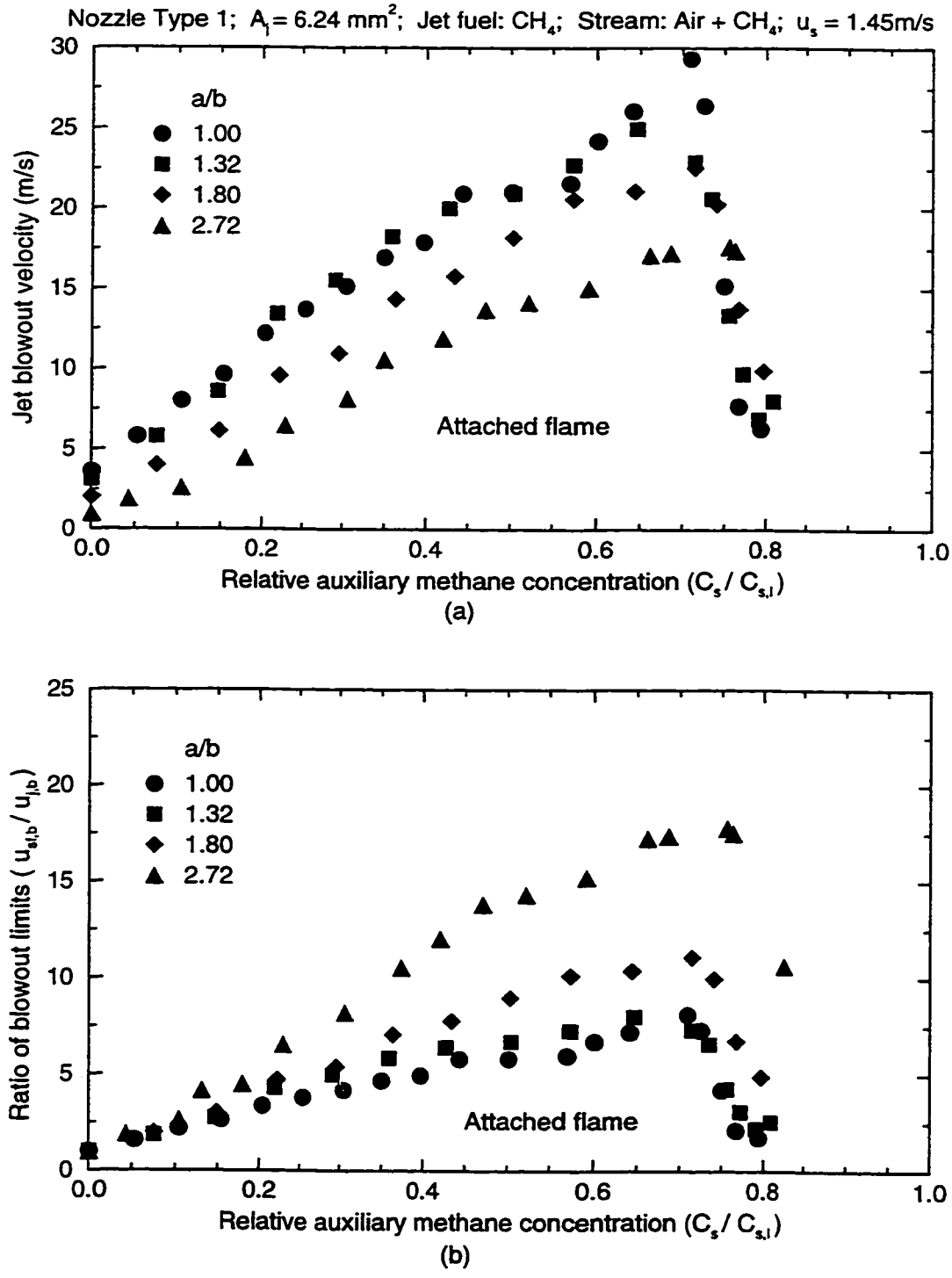

Fig. 4.5.5 The blowout limits as a function of the methane concentration in the co–flowing air stream for different aspect ratio nozzles. $C_{s,l}$ = 6.80 %.

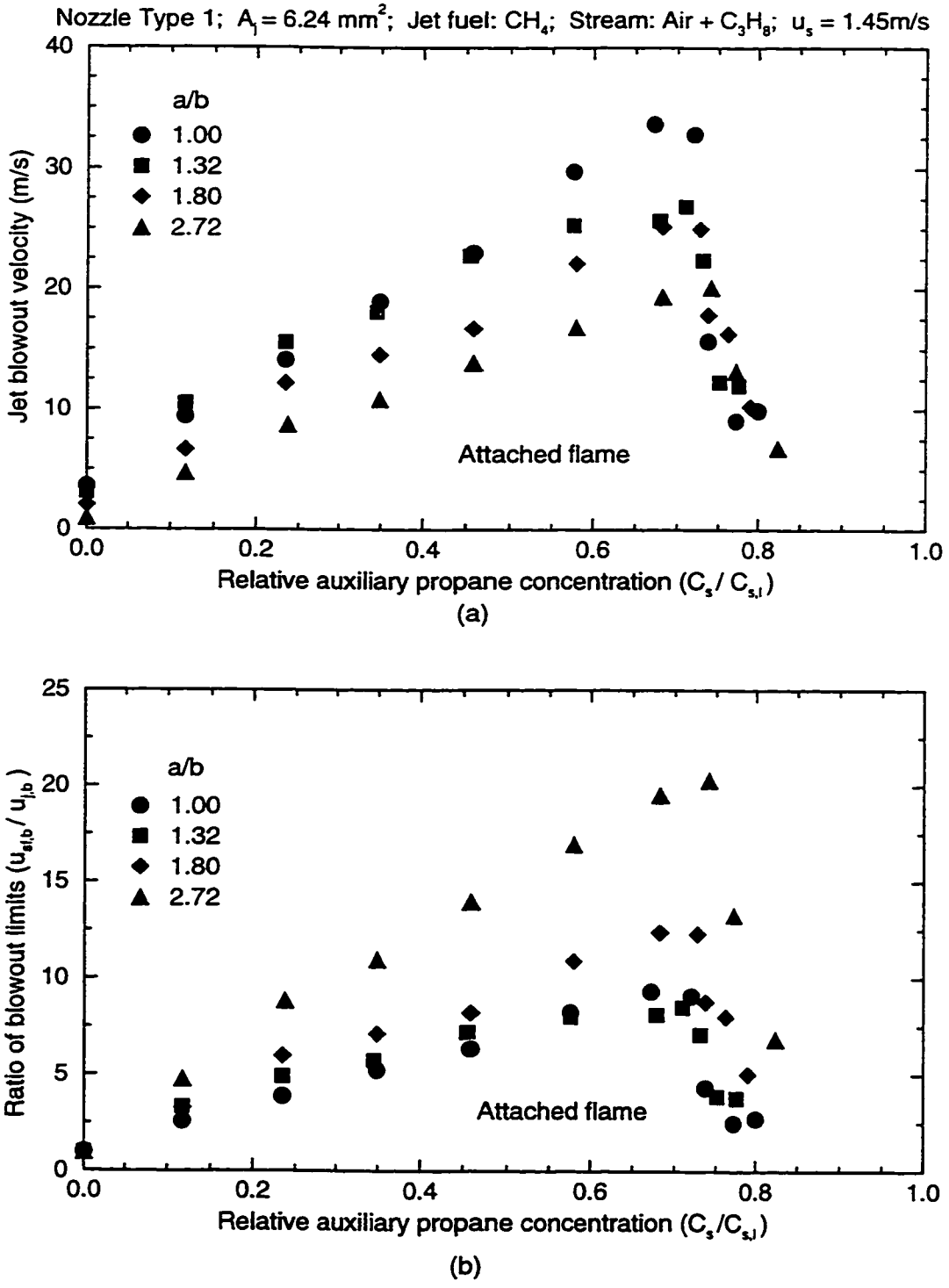

Fig. 4.5.6 The blowout limits as a function of the propane concentration in the co–flowing air stream for different aspect ratio nozzles. $C_{s,j}$ = 2.90 %.

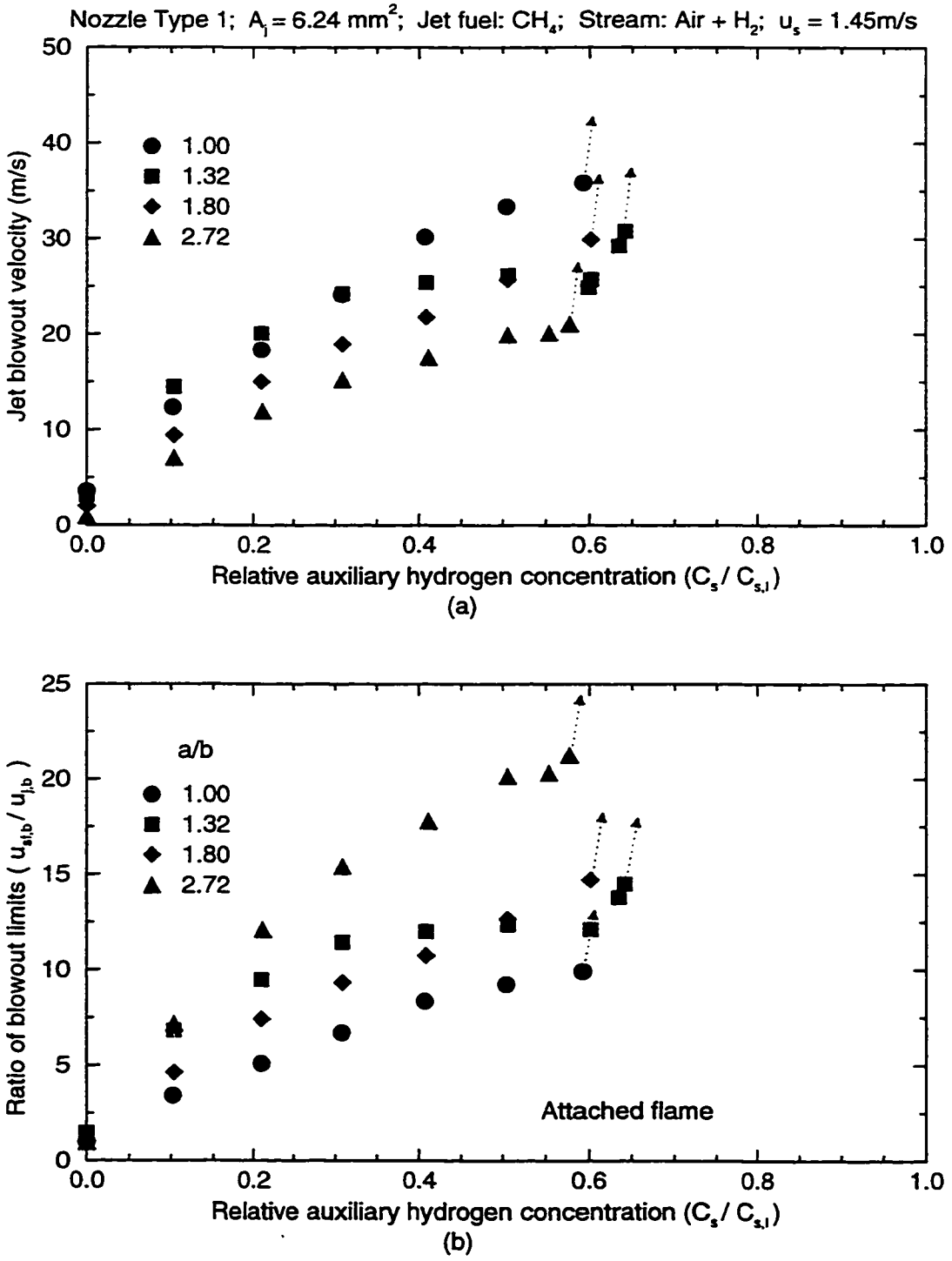

Fig. 4.5.7 The blowout limits as a function of the hydrogen concentration in the co–flowing air stream for different aspect ratio nozzles. Solid symbols: attached flame blowout. Arrows indicate lifted flame. $C_{s,l}$ = 9.60 %.

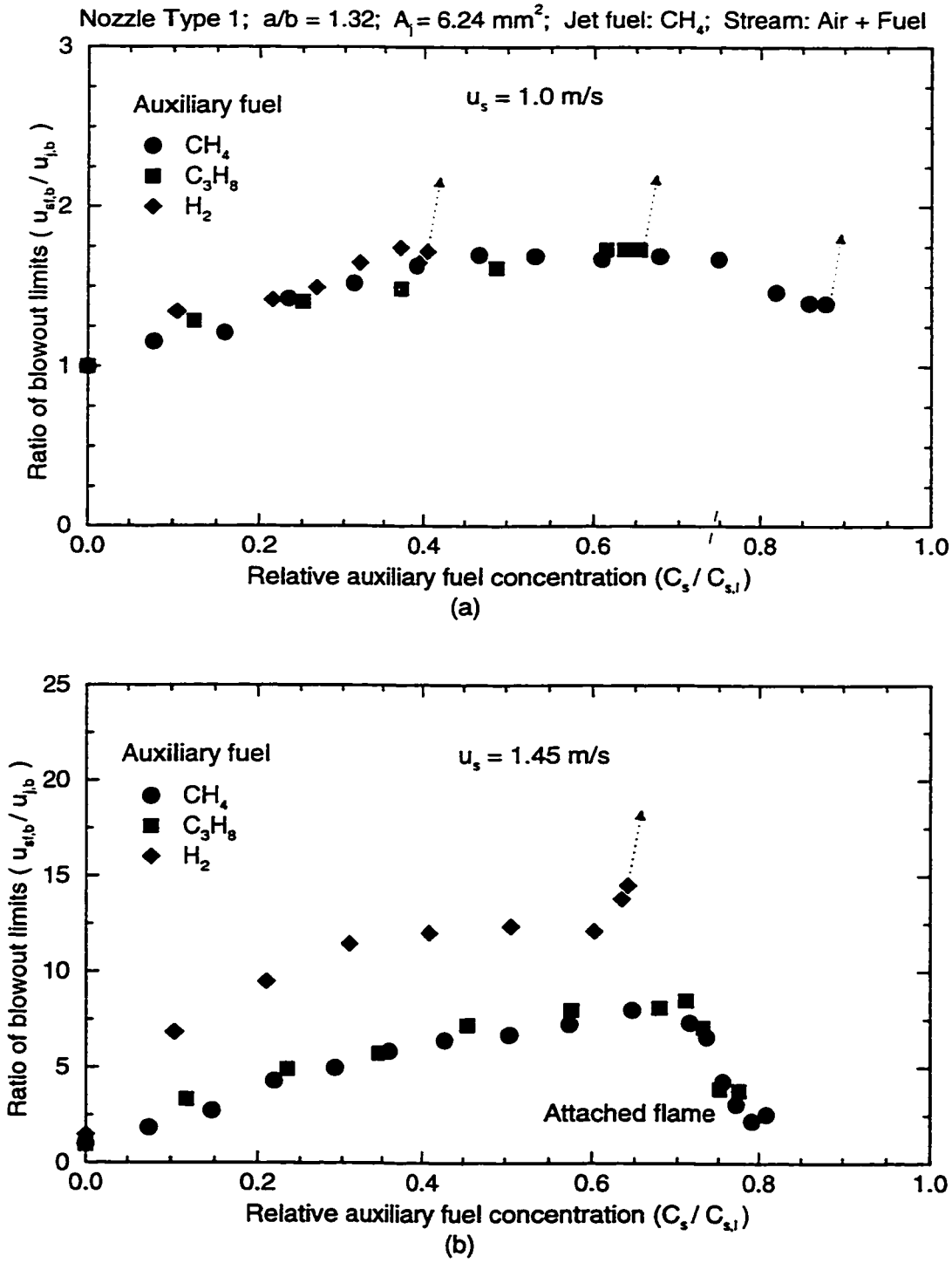

Fig. 4.5.8 The blowout limits as a function of the auxiliary fuel concentration in the co–flowing air stream for a nozzle with an aspect ratio of 1.32. Solid symbols: attached flame blowout. Arrows indicate lifted flame.

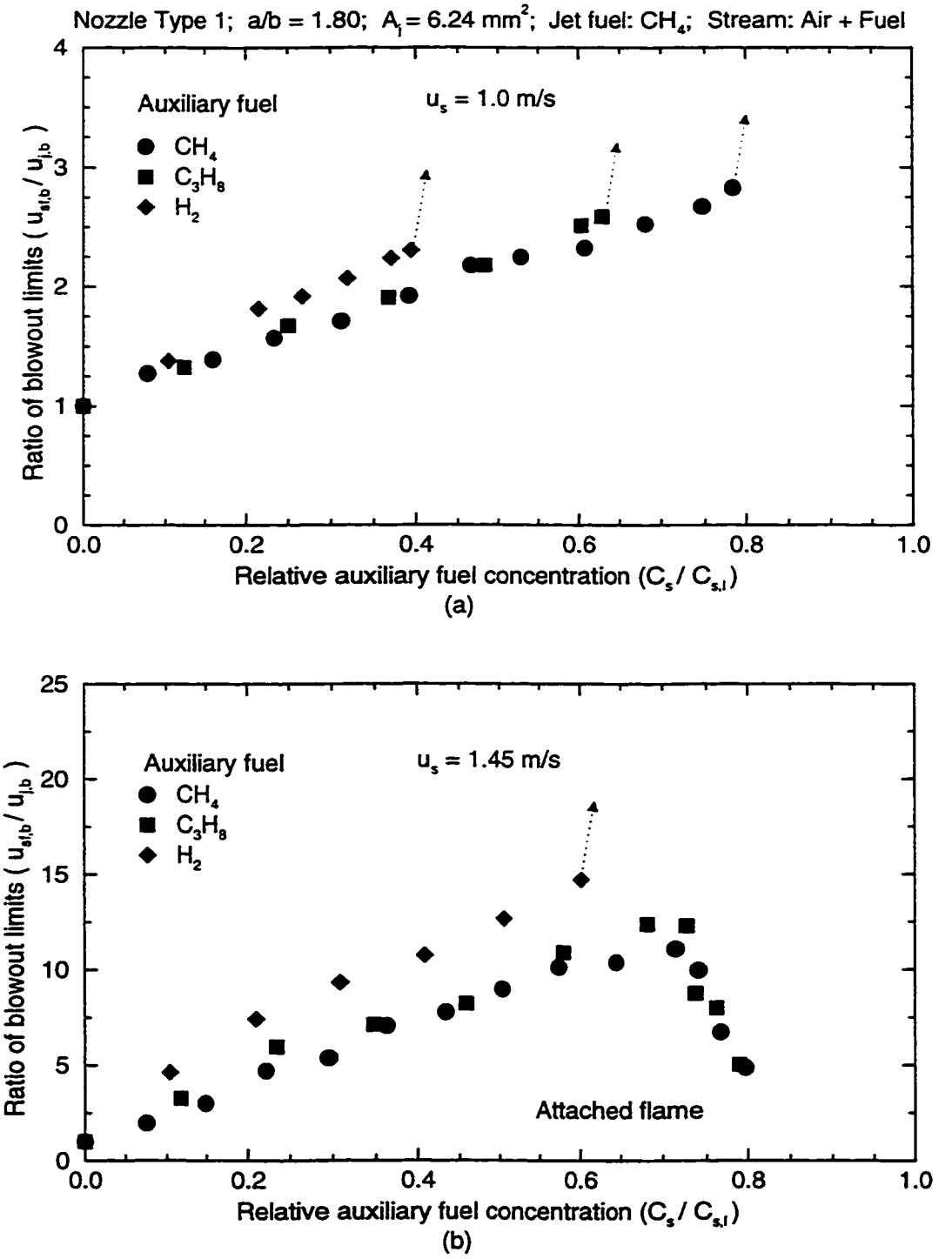

Fig. 4.5.9 The blowout limits as a function of the auxiliary fuel concentration in the co–flowing air stream for a nozzle with an aspect ratio of 1.80. Solid symbols: attached flame blowout. Arrows indicate lifted flame.

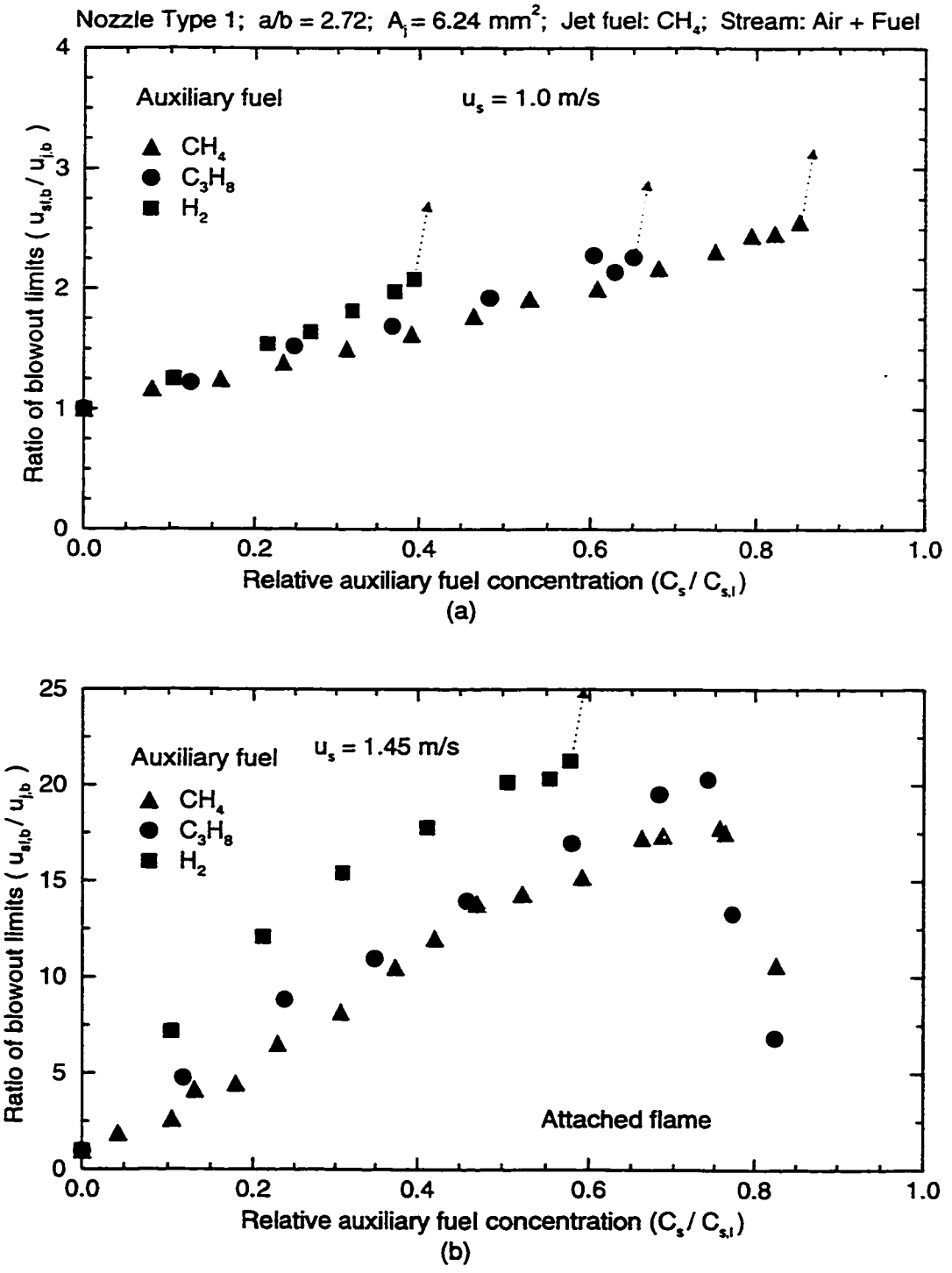

Fig. 4.5.10 The blowout limits as a function of the auxiliary fuel concentration in the co–flowing air stream for a nozzle with an aspect ratio of 2.72. Solid symbols: attached flame blowout. Arrows indicate lifted flame.

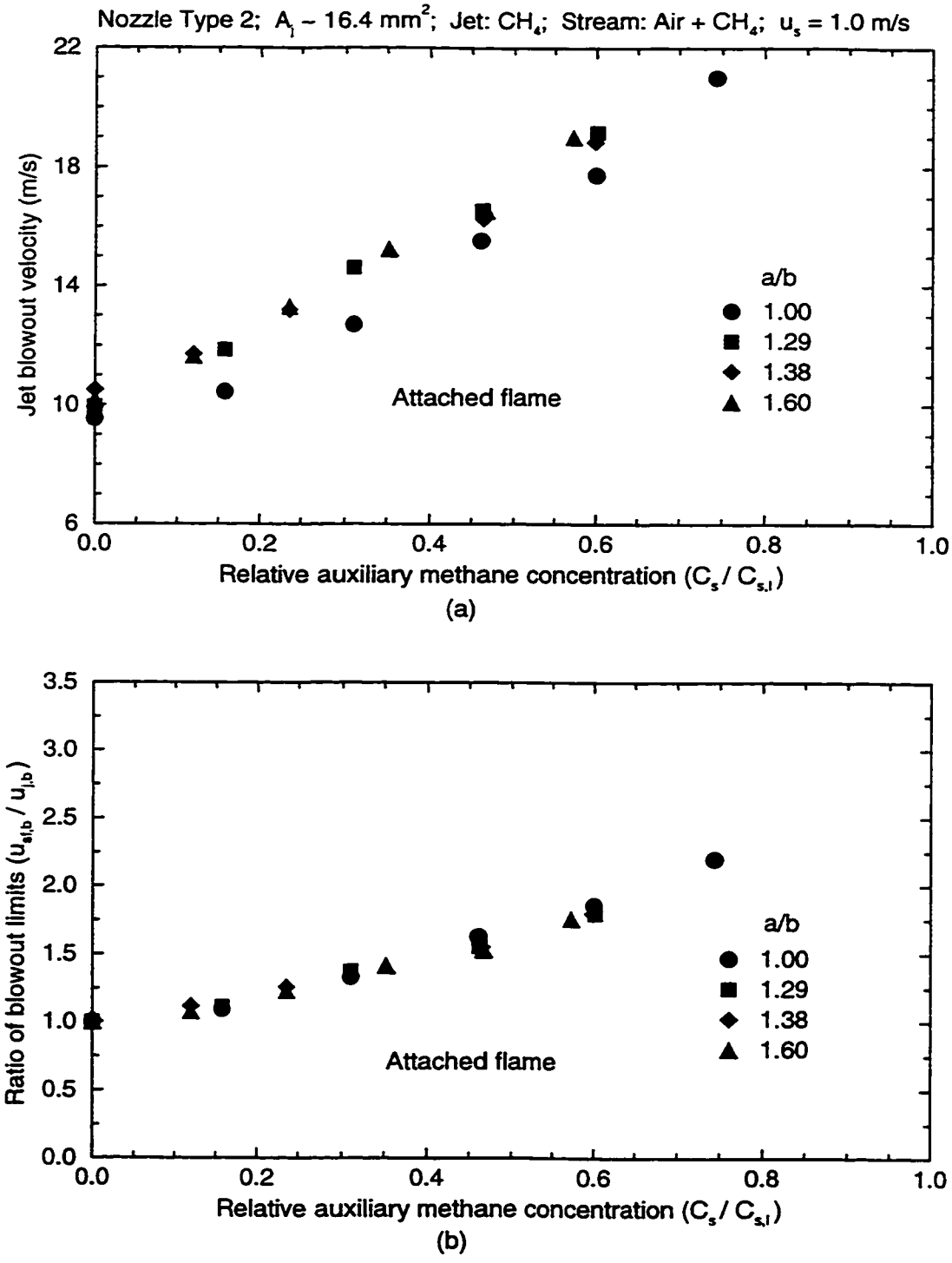

Fig. 4.5.11 The blowout limits as a function of the methane concentration in the co–flowing air stream for different aspect ratio nozzles. $C_{s,l}$ = 6.45 %.

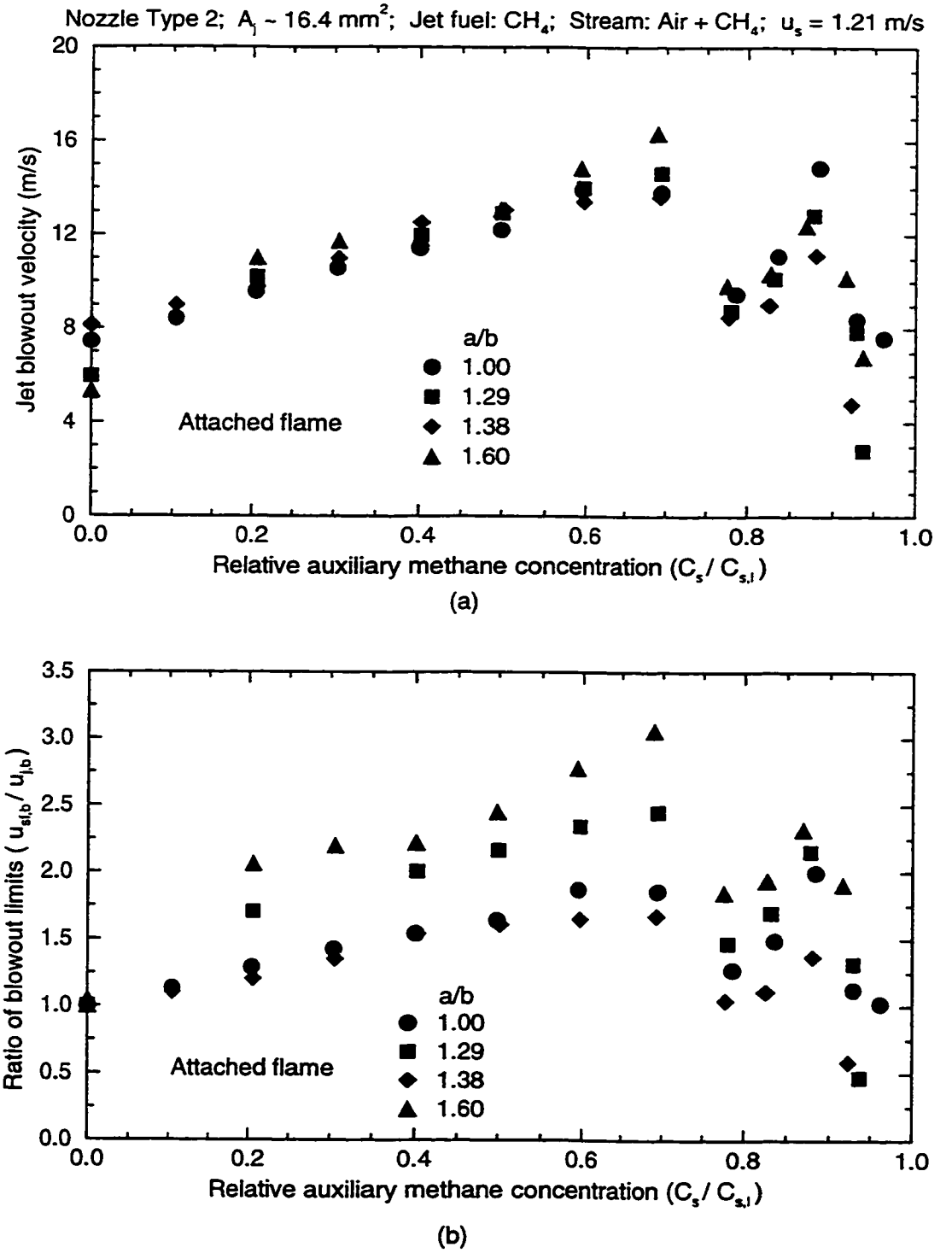

Fig. 4.5.12 The blowout limits as a function of the methane concentration in the co–flowing air stream for different aspect ratio nozzles. $C_{s,l}$ = 6.61 %.

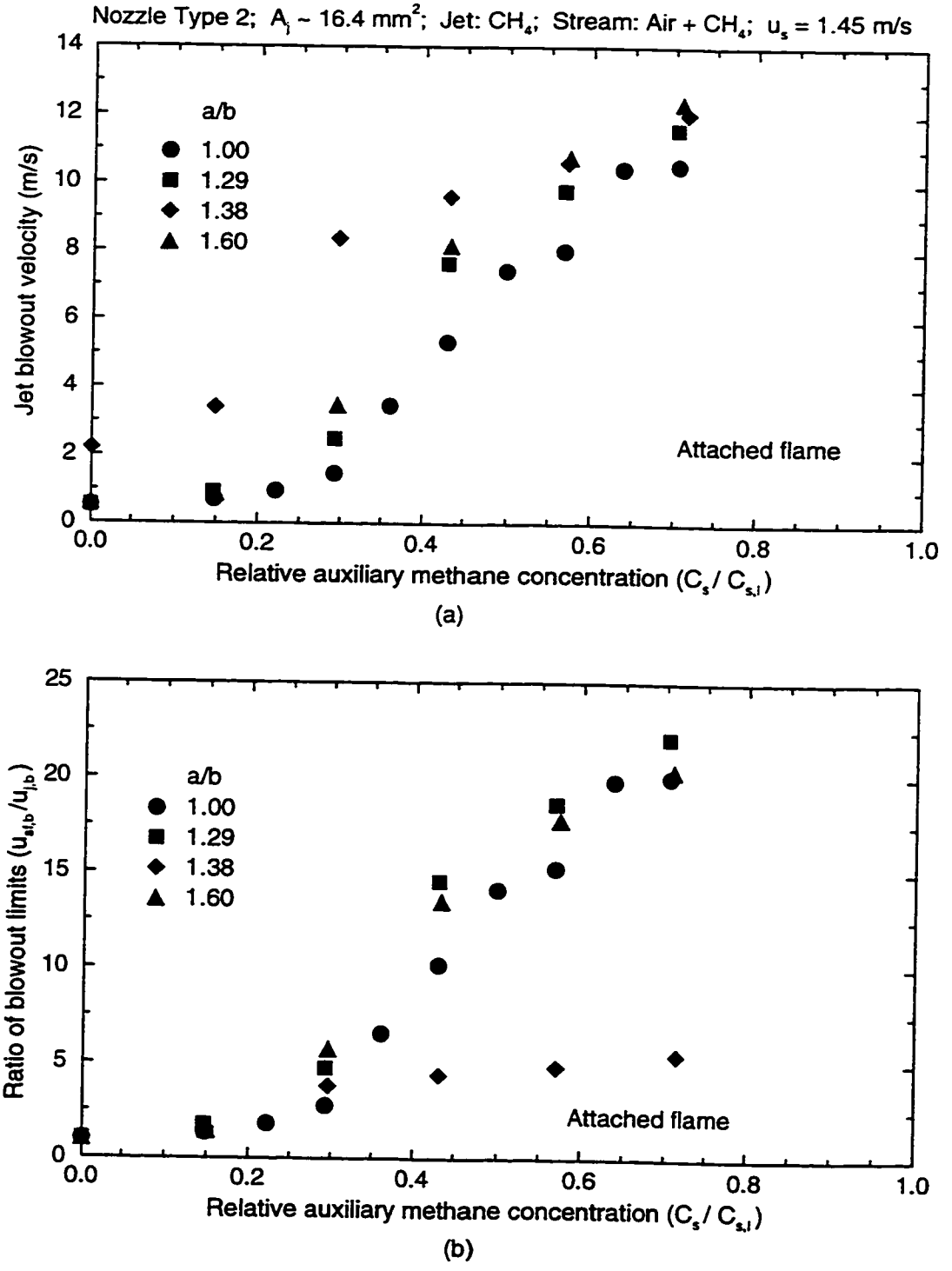

Fig. 4.5.13 The blowout limits as a function of the methane concentration in the co–flowing air stream for different aspect ratio nozzles. $C_{s,l}$ = 6.80 %.

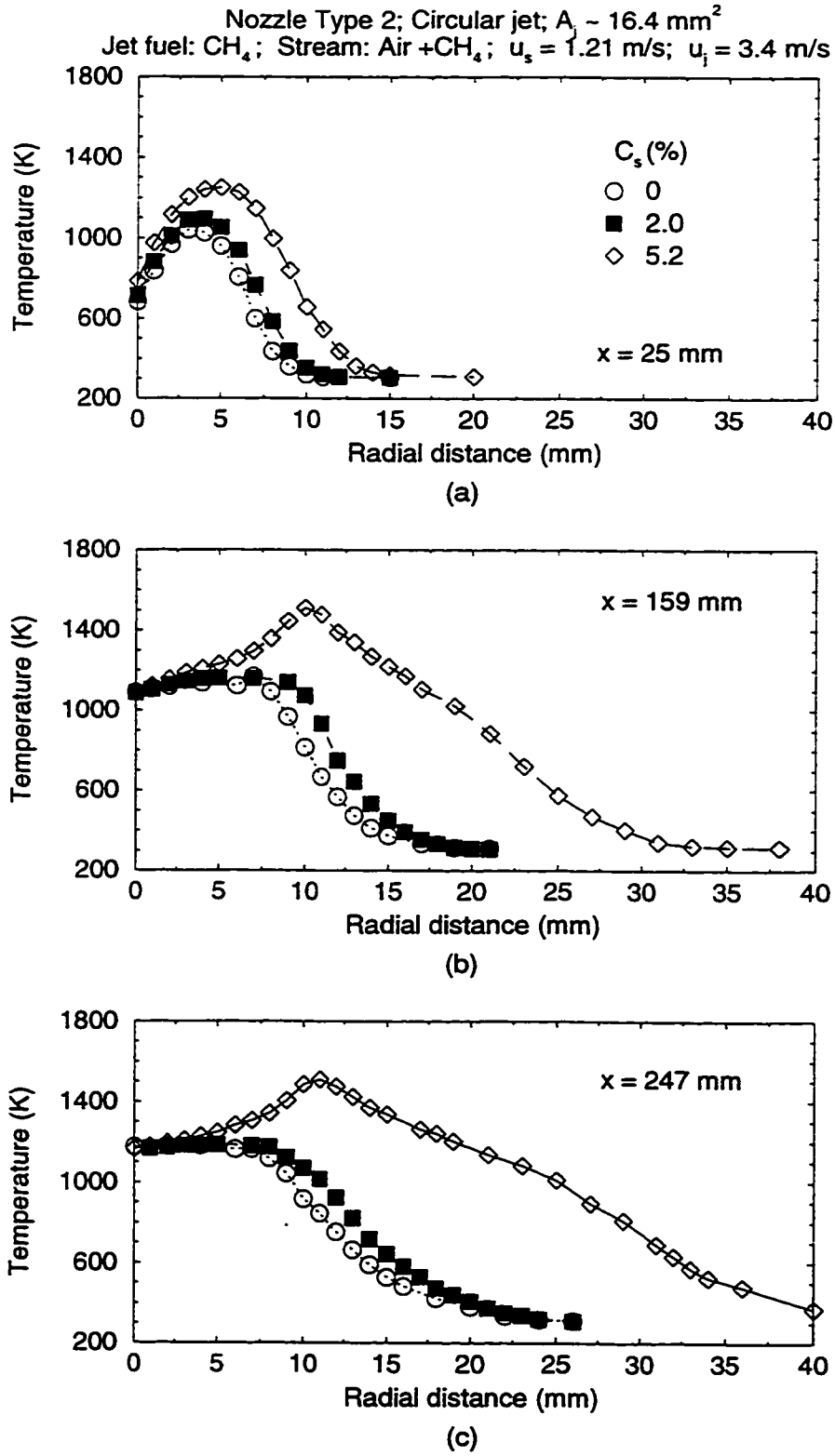

Fig. 4.5.14 Radial temperature profiles in attached flames issuing into a co–flowing stream of air premixed with methane.

stabilization to occur at higher mean jet discharge velocities. The greater the concentration of the fuel in the stream, the greater was such a shift in the combustion zone. This was confirmed with temperature measurements at three different axial distances of 25, 159 and 247 mm as shown in Fig. 4.5.14 (Nozzle Type 2). The effect of ellipticity seems to be smaller for this type of nozzle than for nozzles of Type 1. Unexpected trends for the blowout limits, however, were observed at a stream velocity of 1.21 m/s and at higher auxiliary methane concentrations. There existed a "hump" in the stability curves for all of the jets as the blowout limits increased and then decreased again at auxiliary methane concentrations ranging from 0.78 to 0.90. Since the hump was also observed for the circular nozzle, this behaviour was probably not related to the nozzle shape.

4.6 Limiting Stream Velocity

The limiting co-flowing stream velocity, separating the regions of lifted flame blowout from the region of attached flame blowout, was highly dependent on the jet discharge diameter and the type of jet fuel. The limiting stream velocities for circular methane jets are shown in Fig. 4.6.1 for various diameter nozzles of both types. It can be seen that the limiting velocity increases with the discharge diameter. The experimental results also show that variations in the jet lip thickness and ellipticity did not affect the value of the limiting stream velocity for a jet of approximately constant discharge area (Fig. 4.6.2 (a) and (b)). This was valid for jets issued from both types of nozzles.

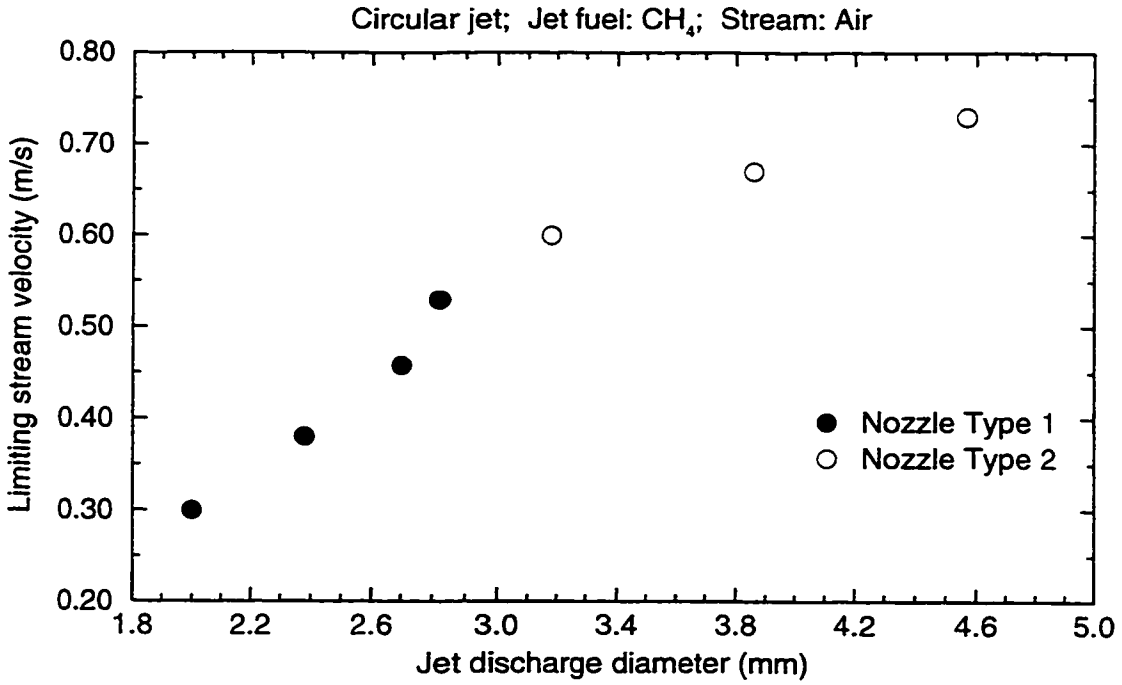

Fig. 4.6.1 The limiting stream velocity of jet diffusion flames as a function of the discharge area.

The inclusion of additives to the methane jet substantially influenced the limiting stream velocity which appeared to increase proportionally with the concentration of hydrogen added to the methane jet and decrease when nitrogen or carbon dioxide were added to the methane (Fig. 4.6.3 (a)). It seems that there is a linear relationship between the limiting stream velocity and the maximum laminar burning velocity of the jet fuel mixture, S_L, as shown in Fig. 4.6.3 (b). The maximum laminar burning velocity, S_L, for the methane-hydrogen mixtures was taken from the experimental results of Haniff et al. [91] and for the methane-diluent mixtures from the results of Reed et al. [92].

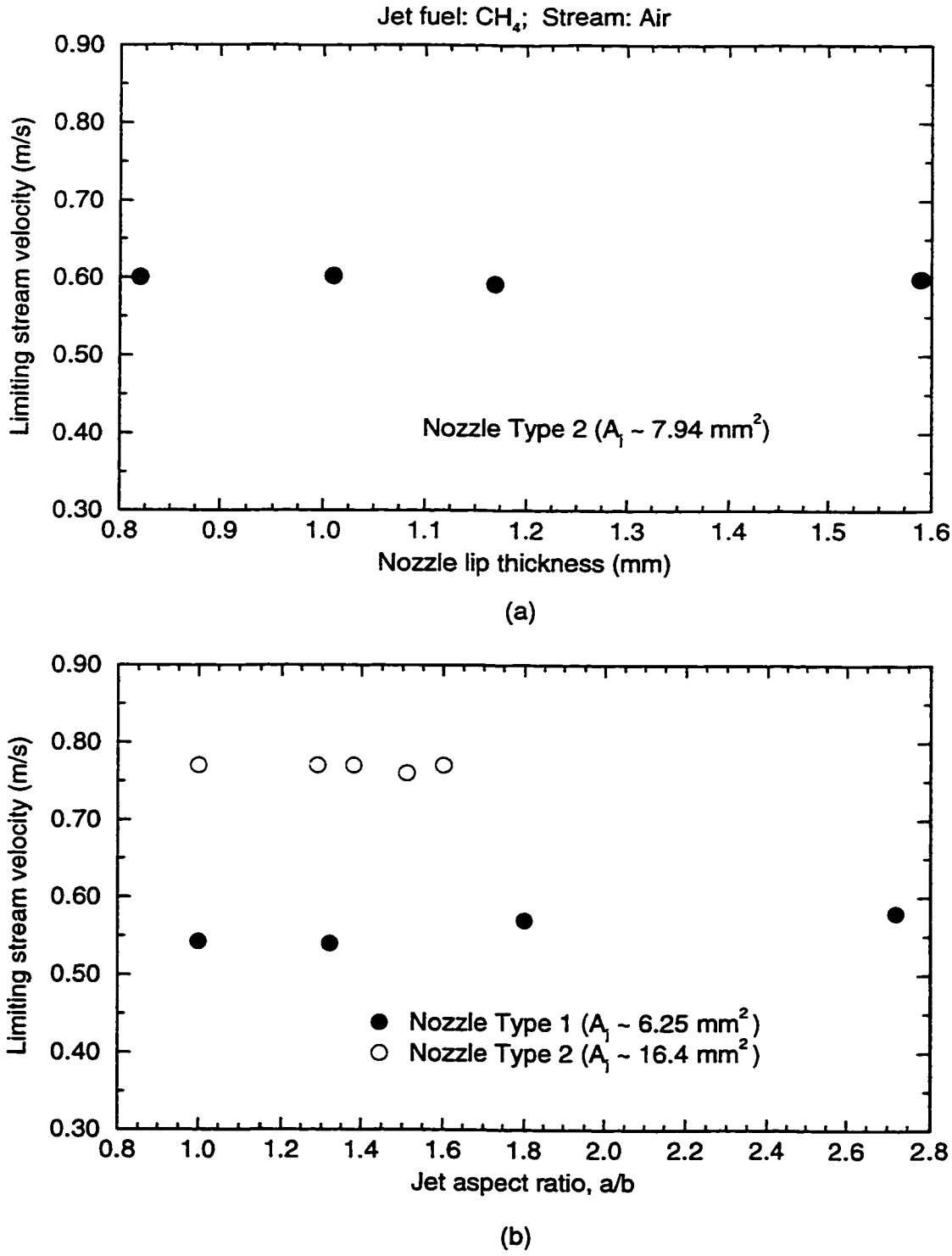

Fig. 4.6.2 The limiting stream velocity as a function of (a) the nozzle lip thickness and (b) the jet aspect ratio.

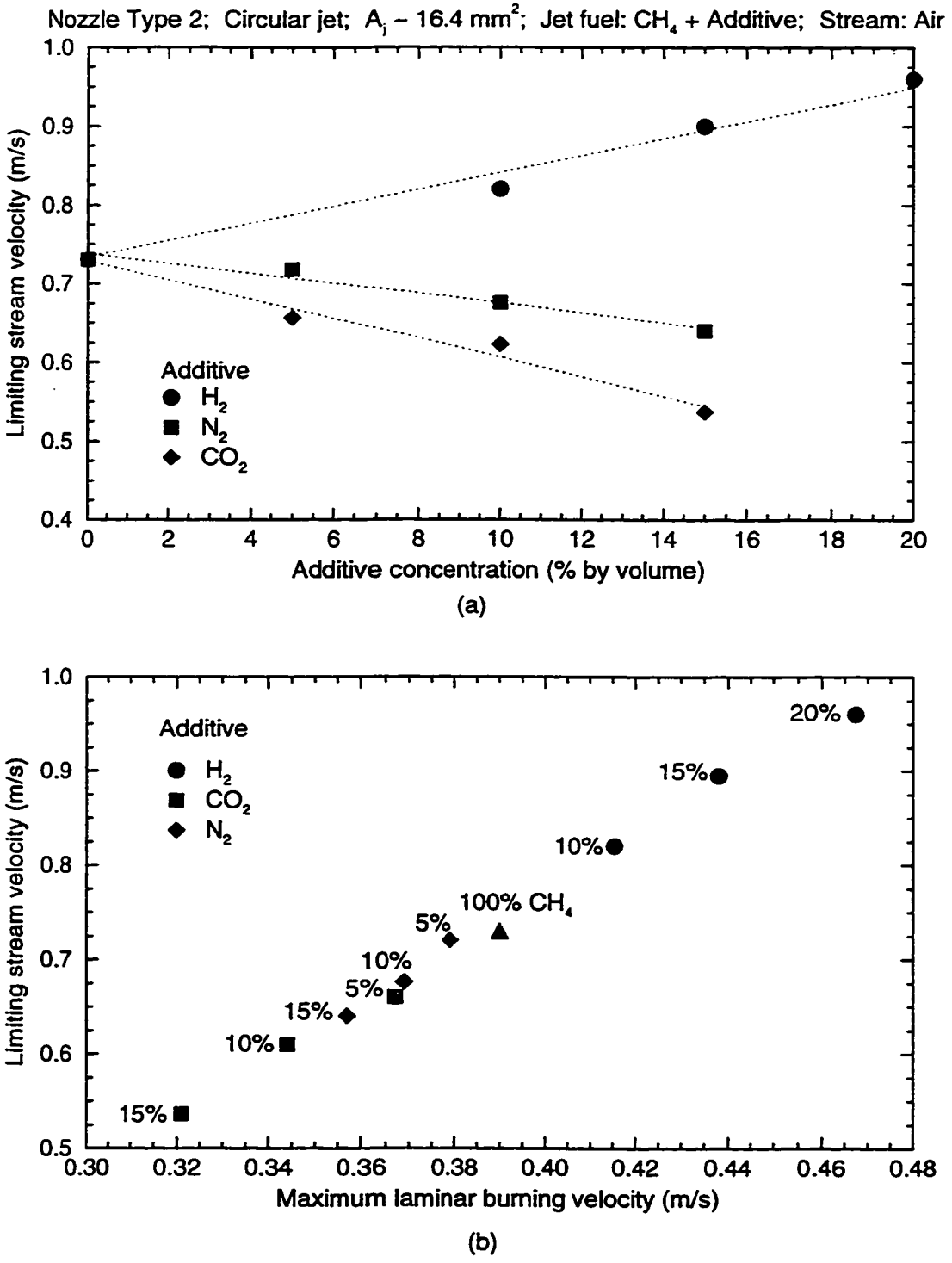

Fig. 4.6.3 The limiting stream velocity as a function of (a) the jet additive concentration and (b) the maximum laminar burning velocity of the jet fuel.

4.7 Nondimensional Correlations

An attempt was made to correlate the experimentally established blowout limits of lifted and attached flames for nozzles of varying diameters. However, the blowout limits of lifted and attached flames had to be correlated separately due to their different flame stabilization mechanism.

The limiting stream velocities separating these two regions of flame blowout can be correlated well for different nozzle diameters and different jet fuels in terms of the velocity ratio, $u_{s,l}/S_L$, as a function of the diameter ratio, d_j/d_q where $u_{s,l}$ is the limiting stream velocity, S_L is the maximum laminar burning velocity, d_j is the jet diameter, and d_q is the quenching distance of the fuel. The correlation is shown in Fig. 4.7.1.

Lifted Flame. The blowout limits of lifted flames obtained for different jet fuels on nozzles of discharge diameters greater than 2.0 mm can be well correlated in terms of the momentum ratio, $(u_{j,b}/u_s)\ (\rho_j/\rho_s)^{1/2}$, as a function of the ratio of the co-flowing stream velocity to limiting stream velocity (Fig. 4.7.2). For comparison, data taken from Oladipo [25] and Kar [97], who employed small nozzles with a configuration different from that employed in the present study are also shown in the figure. Since scaling effects play a role in the blowout limits, two correlations were developed - one for small diameter jets and the other for large diameter jets. This is consistent with measurements of Takahashi et al. [19] who found that the blowout limits of lifted flames were not as significantly affected by a change in the discharge diameter of large diameter jets as they were with small diameter jets. For smaller nozzles of diameters of 2.82 mm and less, the correlation can be improved

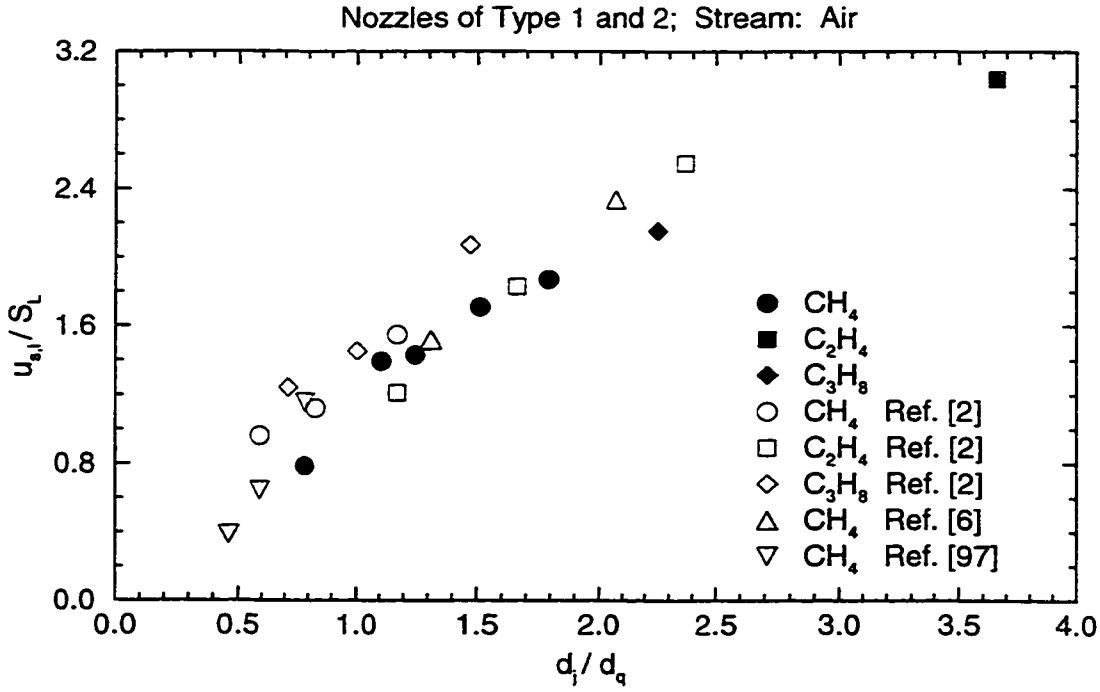

Fig. 4.7.1 The nondimensional limiting stream velocity as a function of the nondimensional jet discharge diameter. Solid symbols: present study. Open symbols: data in literature.

by including a non-dimensional diameter ratio (Fig. 4.7.2 (b)).

Since it was shown earlier that the blowout limits of lifted flames are not affected by the ellipticity of the nozzle, the same correlations will be valid for these jets depending on the area of discharge. For smaller jets, the diameter ratio required previously is replaced with the square root of the discharge area, A_j. A_{ref} is taken as 3.14 mm^2. The correlations are shown in Fig. 4.7.3 for lifted flames issuing from nozzles with different aspect ratios.

The effect of additives to the fuel jet can be correlated adequately by introducing

the ratio of the burning velocity as shown in Fig. 4.7.4. This correlation is sensitive to the value of $S_{L,m}$ and the accuracy of the available data in literature to estimate $S_{L,m}$ is very important for this correlation. It seems that the effect of hydrogen is well correlated while that of the diluents were not as good. The empirical values of the laminar burning velocities in the literature for stoichiometric mixtures of methane and a diluent (i.e., carbon dioxide or nitrogen) deviate substantially amongst the various authors and could account for the scatter in the data [91-94].

Attached flame. The blowout limits of attached flames are highly dependent on the nozzle geometry, such as the nozzle lip thickness and ellipticity; therefore, the effects of these parameters are correlated separately. The correlation for the blowout limits of jets discharged from circular nozzles of different diameters and lip thicknesses is shown in Fig. 4.7.5 (Δ_{ref} was taken as 1.0 mm).

The correlation for the blowout limits of attached flames issuing from elliptic nozzles of Type 1 and 2 is shown in Figs. 4.7.6 (a) and (b) where A_s is the area of the surrounding stream and was used as the reference area, R_{eq} is the equivalent radius defined as $(a \cdot b)^{1/2}$ and R_{ref} is taken as 1.0 mm. It was not possible to find a convenient and simple correlation with respect to the jet aspect ratio since the effect of the jet ellipticity was very complex as is evident with the existence of an apparent optimum aspect ratio. Clearly, the correlation oversimplifies the otherwise complex nature of the flame-flow interactions associated with an increase in the aspect ratio.

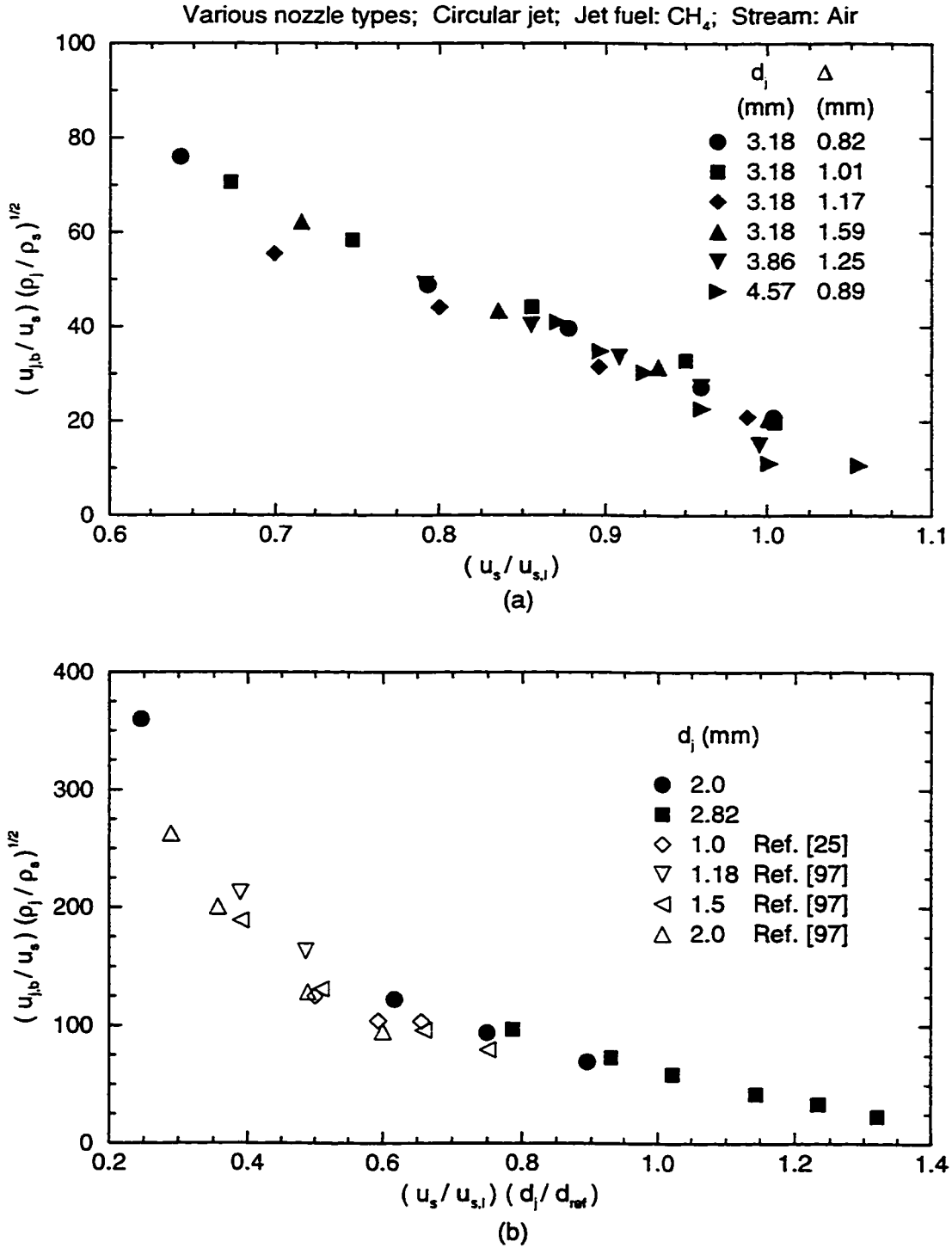

Fig. 4.7.2 The nondimensional blowout limits of lifted diffusion flame for (a) larger diameter nozzles and (b) smaller diameter nozzles. Solid symbols: present study. Open symbols: data in literature.

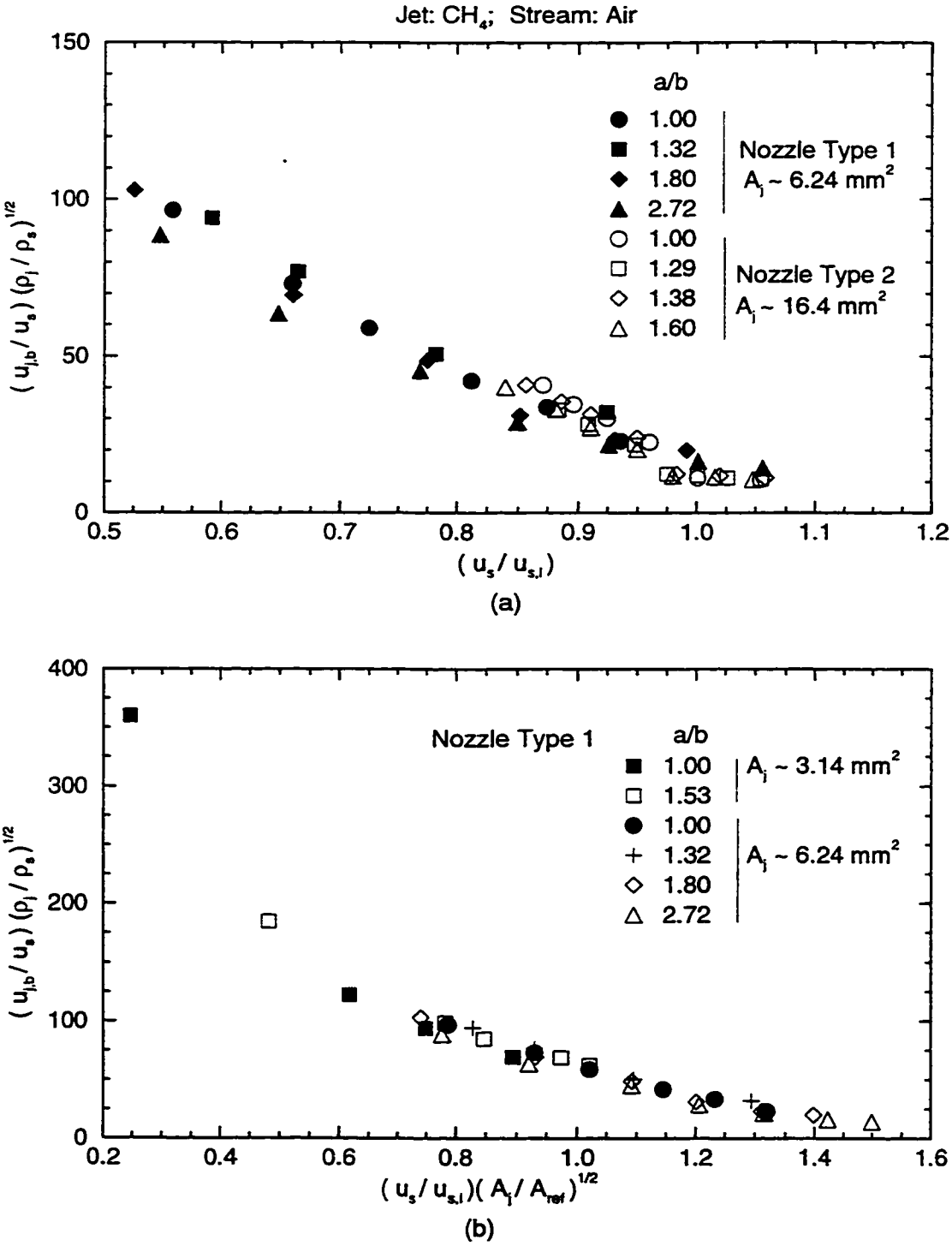

Fig. 4.7.3 The nondimensional blowout limits of lifted flames for (a) larger diameter nozzles and (b) smaller diameter nozzles of different aspect ratios.

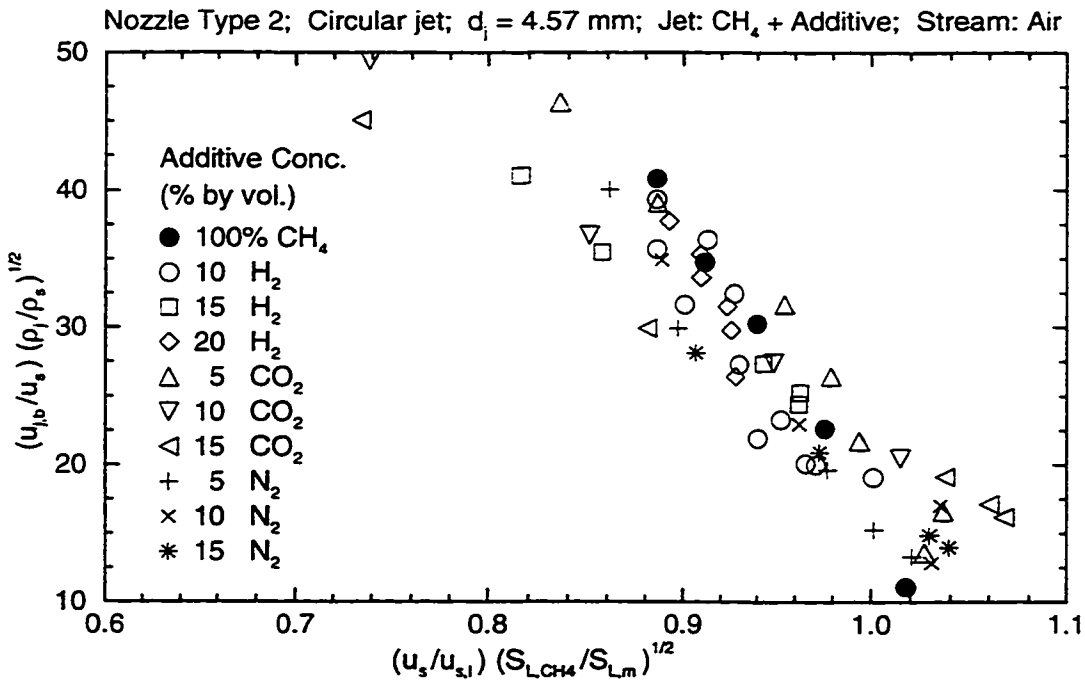

Fig. 4.7.4 The non–dimensional blowout limits of lifted flames showing the effect of different jet fuel compositions.

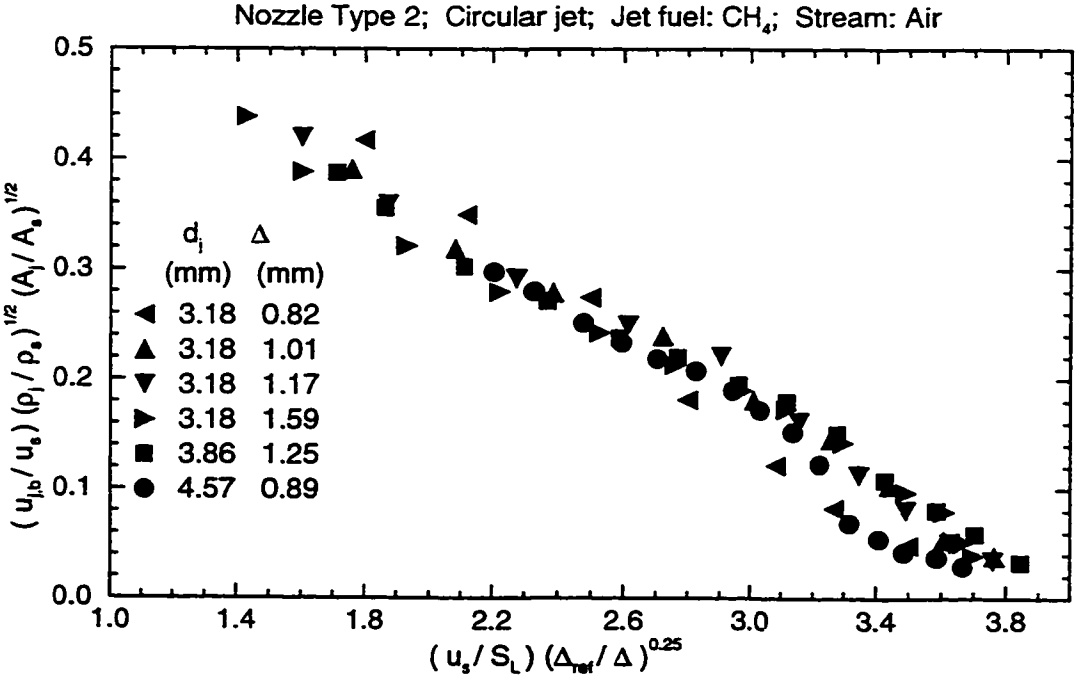

Fig. 4.7.5 The non–dimensional blowout limits of attached flames for nozzles of different discharge diameters and lip thicknesses.

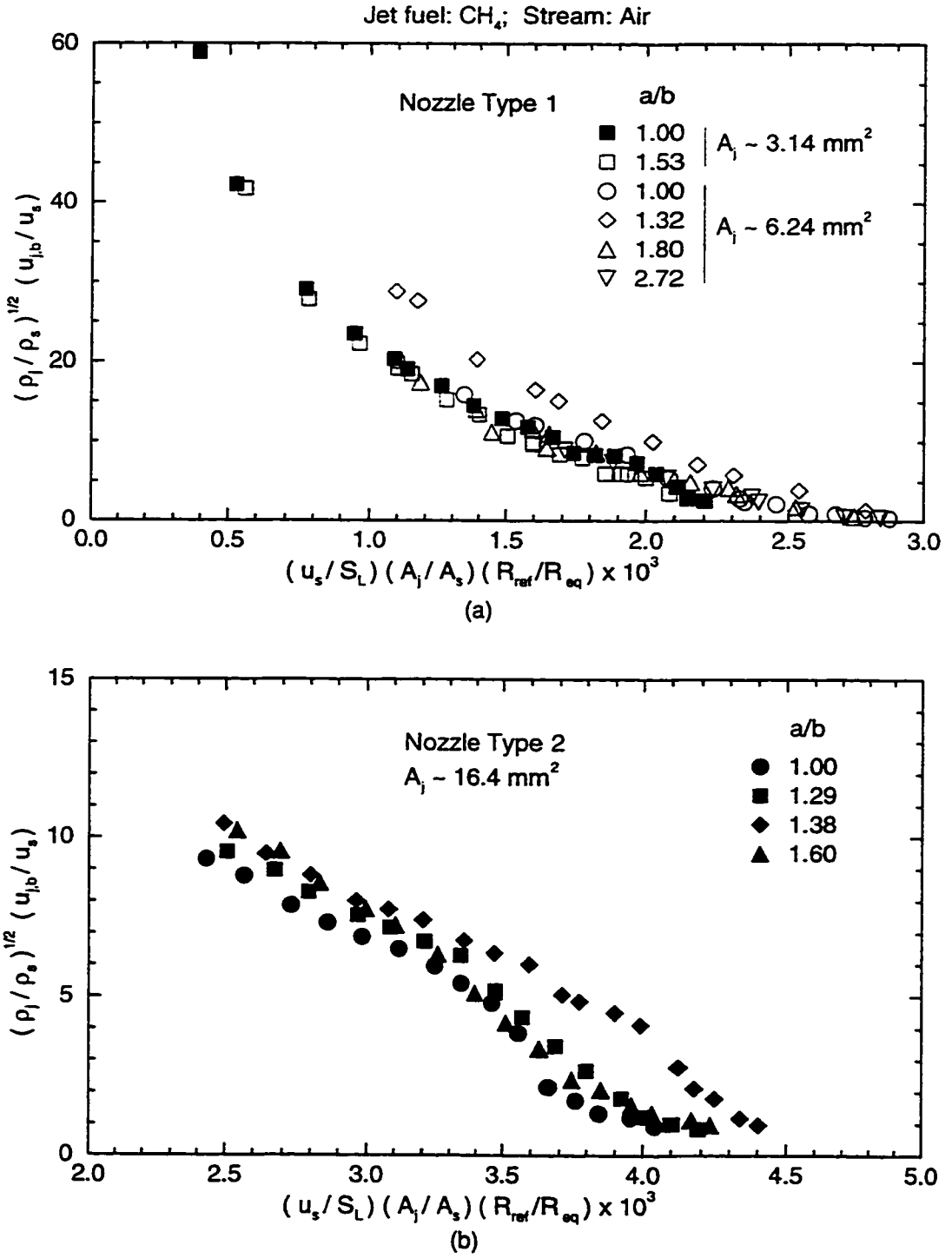

Fig. 4.7.6 The nondimensional blowout limits of attached flames as a function of the nozzle aspect ratio for (a) nozzles of Type 1 and (b) nozzles of Type 2.

CHAPTER 5

RESULTS AND DISCUSSION: VELOCITY FIELD MEASUREMENTS

In the previous chapter, it was shown that the nozzle shape (i.e., a/b ratio) influenced significantly the blowout limits of attached flames. There existed an optimum aspect ratio in which the blowout limits were higher than those of jets with higher or lower aspect ratios. To explain this phenomenon, an investigation on the flow structure of such jets was carried out using laser Doppler velocimetry. The emphasis was on how changes in the co-flowing stream velocity, jet velocity, nozzle ellipticity, jet fuel composition and the concentration of auxiliary fuels or diluent in the co-flowing air stream affect the flow characteristics of the jet flame. To decrease the effect of additional factors (e.g., non-uniform lip thickness and transitional flow at the nozzle exit), the experiments were conducted on the larger area, long tube nozzles with a uniform lip thickness of 0.89 mm. Circular and elliptic nozzles with aspect ratios of 1.38 and 1.60 were used. The axial and radial velocity as well as turbulence intensity profiles were generally shown at four different axial distances and measurements taken at other distances are presented in the appendix.

5.1 Effect of Co-flowing Stream Velocity

It was shown previously (Fig. 4.2.1) that an increase in the co-flowing stream velocity had a detrimental effect on the blowout limits with the rate of decrease greater for

lifted flames than for attached flames. This section presents the results of the study on the effect of the co-flowing stream velocity on the flow structure. Cold jets, lifted flames and attached flames were examined.

Cold Jets. A comparison of the profiles of the time-averaged axial and radial velocity of cold jets at two different co-flowing stream velocities (u_s = 0.65 and 0.70 m/s) is shown in Figs. 5.1.1 and 5.1.2 for different downstream distances up to 225 mm from the nozzle rim. The jet mean exit velocity was held constant at 11.5 m/s (Re = 2770). The stream velocities of 0.65 and 0.70 m/s were chosen because these velocities were within the region of lifted flame blowout and such a small change in the stream velocity brought about a dramatic decrease in the blowout limits of lifted flames. The axial and radial velocities were presented as a function of the dimensionless radial distance, r / R , where r is the radial distance from the jet axis and R is the radius of the nozzle. The data show that the radial velocities were very small for both of the co-flowing air stream velocities at all axial distances investigated. There was little effect of an increase in the co-flowing stream velocity from 0.65 m/s to 0.70 m/s on the axial velocity of cold jets at a downstream distance of 60 mm. A small difference in the axial velocity profiles was apparent at downstream distances of 122, 172 and 225 mm. The local axial velocity became higher due to a modest increase in the co-flowing stream velocity (of 8%) which would cause a lifted flame to move further downstream probably to where the local gas velocity at the flame base equalled the local turbulent burning velocity.

A comparison of the corresponding turbulence intensity profiles is shown in Fig.

5.1.3. The turbulence intensity in these figures is defined as a percentage of u'/u, where u' is the local rms value and u is the local time-averaged axial velocity. There is very little difference in the turbulence level between the two jets until a downstream distance of 172 mm was reached. At this and the further downstream distance of 225 mm, the turbulence intensity within the jet issuing into the 0.65 m/s stream is greater than that issuing into the 0.70 m/s jet at radial distances of $8 \leq r/R \leq 13$ at x = 172 mm and $3.5 \leq r/R \leq 12$ at x = 225 mm.

Lifted Flames. The time-averaged axial and radial velocities were also measured in the presence of lifted flames at two different co-flowing stream velocities (u_s = 0.65 and 0.70 m/s) and a jet mean velocity of 11.5 m/s (Figs. 5.1.4 and 5.1.5). At these conditions, the flame stabilized at distances of approximately 135 mm and 160 mm for jets in a co-flowing stream with velocities of 0.65 m/s and 0.70 m/s, respectively. In the cold region of the jet, i.e., x < 122 mm, the axial velocity profiles are very similar; however, at x = 122 mm, the radial velocity profile of the jet issuing into the lower stream velocity of 0.65 m/s is significantly higher than that of the jet in the stream velocity of 0.70 m/s. This higher radial velocity for u_s = 0.65 m/s is on account of the closer proximity of the lifted flame. At a further downstream distance of 172 mm, the jet issuing into the lower co-flowing stream velocity (u_s = 0.65 m/s) is well within the region of the lifted flame, while this downstream distance is just above the base of the lifted flame issuing into the higher stream velocity (u_s = 0.70 m/s). The radial velocity profile at this distance is substantially higher for the jet issuing into the stream with a velocity of 0.70 m/s. This outward radial flow in the vicinity of the flame base ultimately resulted in a significant radial expansion of the jet which, in

turn, resulted in significantly lower axial velocities. The fluctuations in the axial velocity profile within the jet in the higher co-flowing stream (u_s = 0.70 m/s) are on account of the nearby flame base. At a further downstream distance of 225 mm, the radial velocities are very small for both conditions; however, the jet issuing into a stream with a velocity of 0.70 m/s had higher axial velocities than those issuing into a stream with a velocity of 0.65 m/s for radial distances where the flame is approximately located (i.e., $8 < r/R < 13$).

The corresponding turbulence intensity level profiles within lifted flames are shown in Fig. 5.1.6. It can be seen that the turbulence intensity increased significantly near the flame base in both cases. The intensity of turbulence of the jet in the co-flowing stream velocity of 0.65 m/s at a distance of 122 mm (close to the flame base) was higher than that for the jet in a stream velocity of 0.70 m/s. At a higher distance of 172 mm, close to the flame base in a stream velocity of 0.70 m/s, the trend was reversed.

An indirect indication of the entrainment rate was obtained by measuring the concentration of methane at the axis (centerline) at different distances. The fuel concentration within the jet is maximum at the jet axis and hence it can be assumed that the last possible location, x_{LL}, for flame stabilization is located at the centerline where the fuel concentration is equal to the lean flammability limit. A low value of x_{LL}, would signify an enhanced mixing rate. Gas analysis measurements were conducted on cold jets and lifted flames for the same jet discharge velocity of 11.5 m/s. It was observed that for cold jets even a substantial increase in the co-flowing stream velocity from 0.65 to 1.21 m/s did not change the entrainment rate by any significant margin as indicated by the approximately

constant value of x_{LL} of 427 mm. A comparison of a cold jet and a lifted flame are shown in Fig. 5.1.7 (a) for a co-flowing stream velocity of 0.65 m/s. The presence of a lifted flame increased the value of x_{LL}. The mixing process was inhibited due to the decreased density and increased viscosity of the jet gases (mostly combustion products). These results are consistent with studies conducted on the development of eddies, which is crucial to the mixing process, within cold and ignited jets in still air [95].

The effect of the co-flowing stream velocity on the downstream position, x_{LL}, for lifted flames is shown in Fig. 5.1.7 (b). The co-flowing stream velocity was varied from 0.30 to 0.65 m/s. It can be seen that a small increase in the stream velocity from 0.3 to 0.52 m/s resulted in a much lower value of x_{LL} and the lean flammability limit was obtained closer to the jet exit. An increase in the co-flowing stream velocity resulted in a higher lift-off height which, in turn, led to a leaner fuel-air mixture at the flame base. Therefore, the cold region of the lifted flame is the region of enhanced entrainment of air and thus an increase in the lift-off height was beneficial to the entrainment rate for the entire flame.

Therefore, the decrease in the blowout limits of lifted flames due to an even modest increase in the co-flowing stream velocity is the combined result of two factors. An increase in the local axial velocities increased the entrainment rate, diluting the mixture beyond the flammability limit much closer to the nozzle rim in the region of higher local velocities. If the burning velocity can be assumed to be approximately the same, the jet blowout velocity should decrease in order to achieve the balance between the burning velocity and the jet local jet velocity.

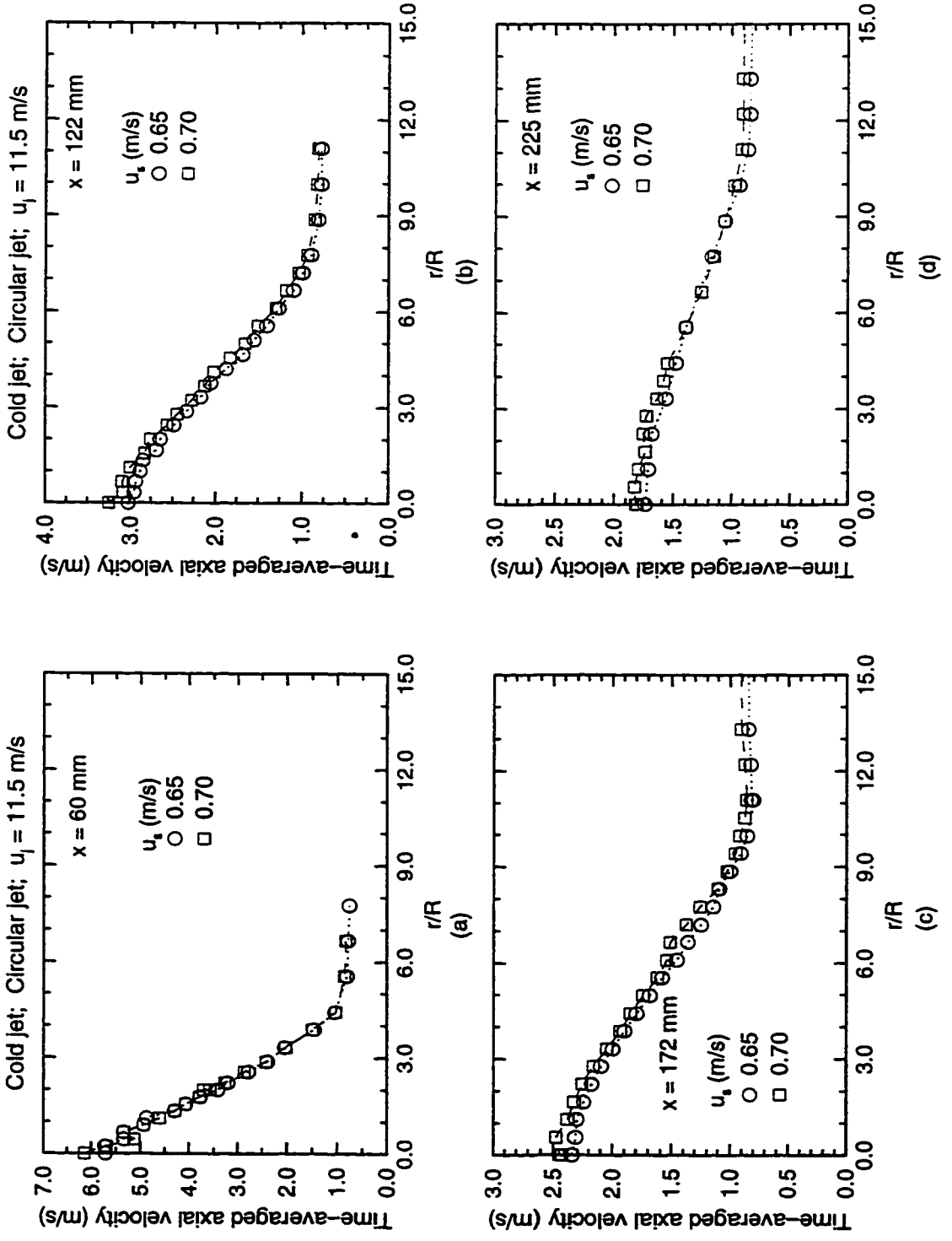

Fig. 5.1.1 Time-averaged axial velocity profiles within a cold circular jet for two different co-flowing stream velocities (R = 2.29 mm).

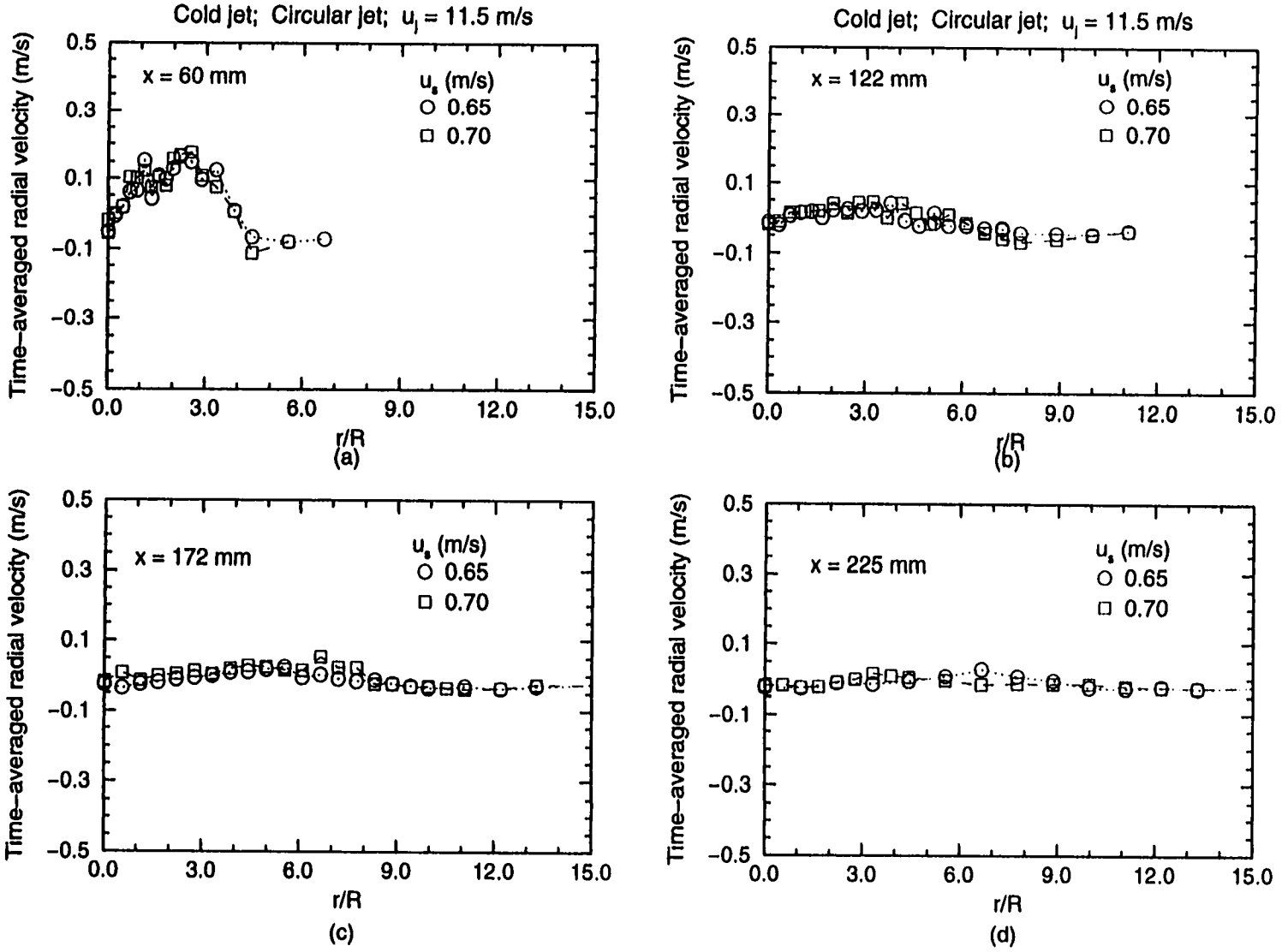

Fig. 5.1.2 Time–averaged radial velocity profiles within a cold circular jet for two different co–flowing stream velocities (R = 2.29 mm).

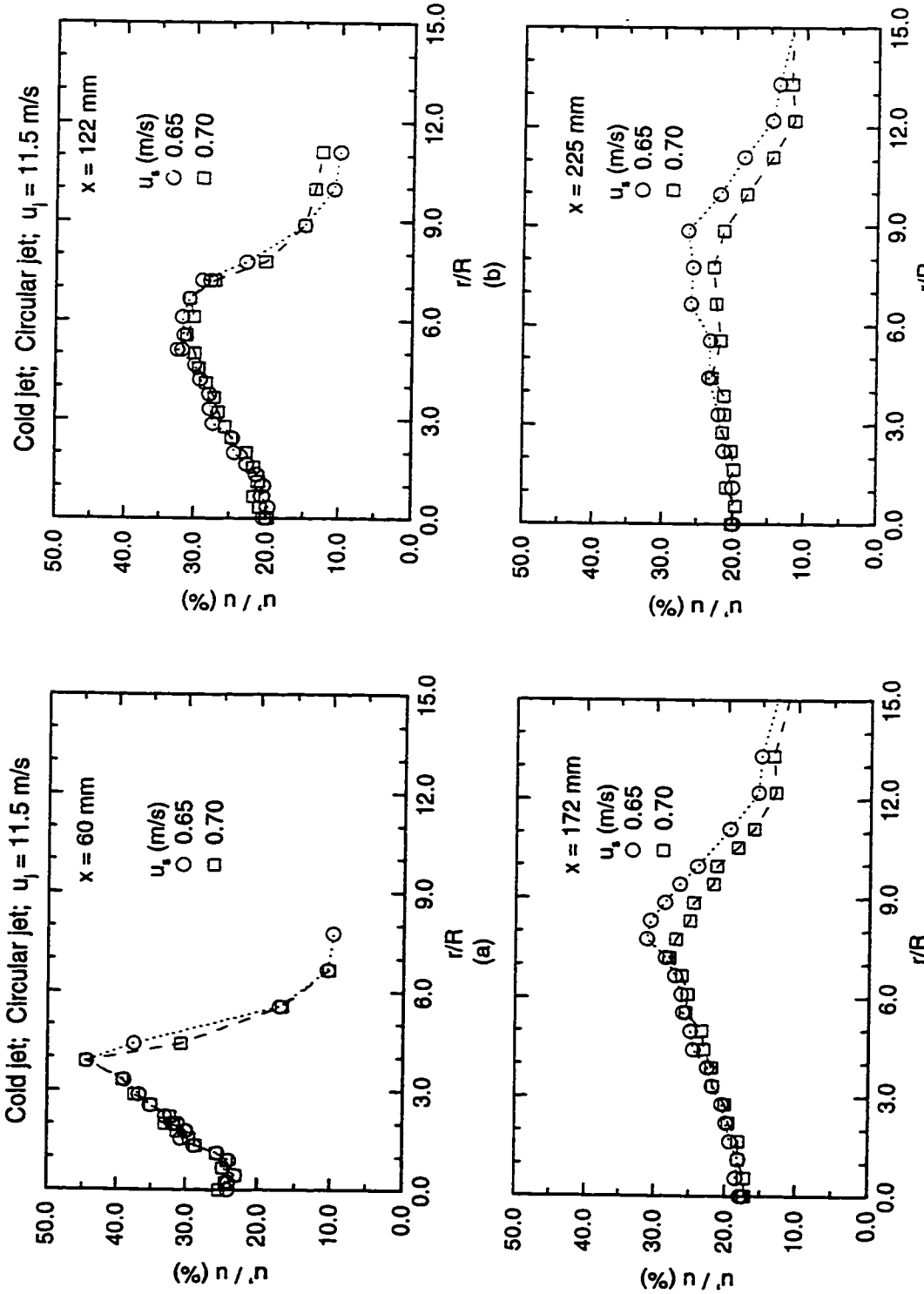

Fig. 5.1.3 Turbulence intensity level profiles within a cold circular jet for two different co-flowing stream velocities (R = 2.29 mm).

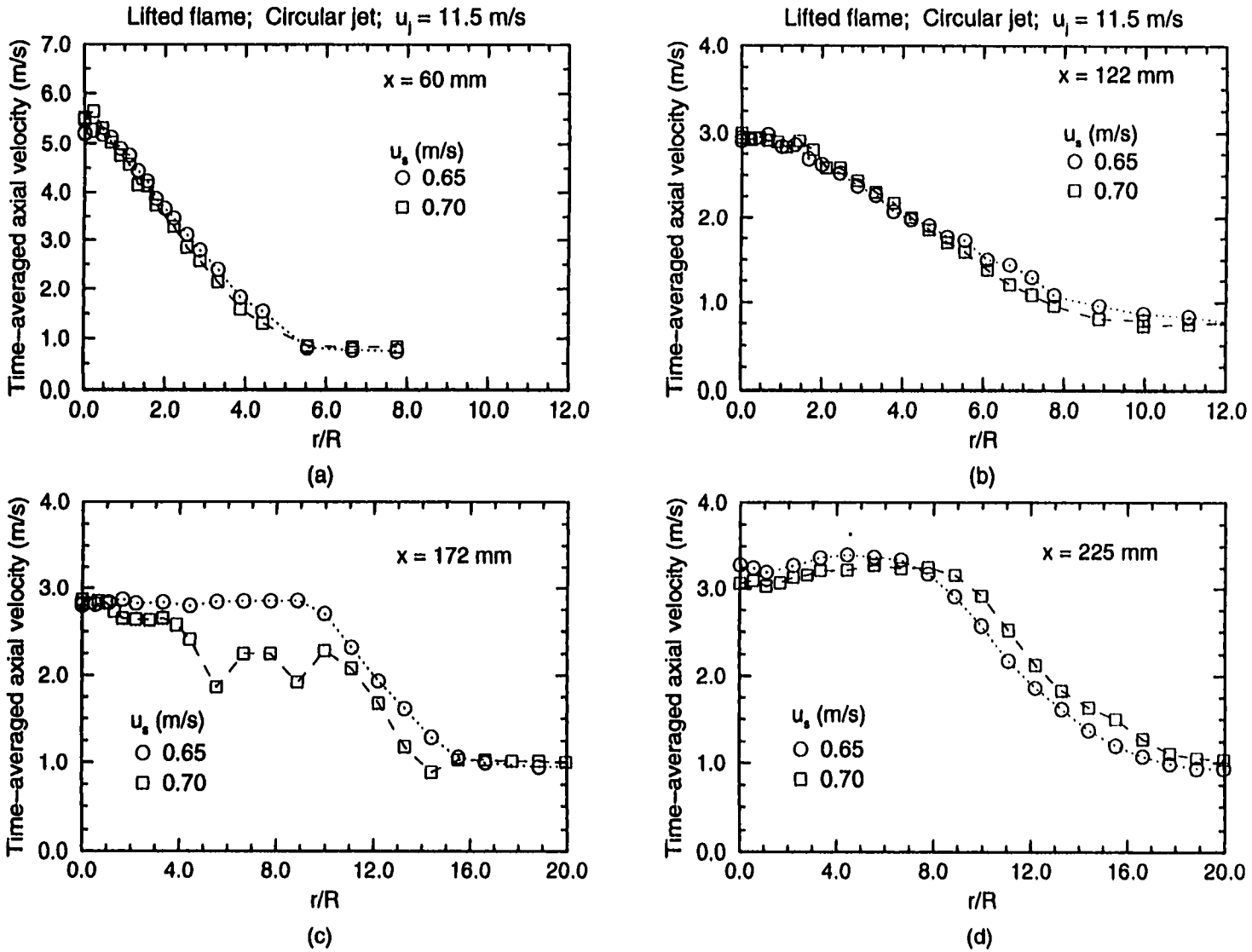

Fig. 5.1.4 Time–averaged axial velocity profiles within a lifted flame for two different co–flowing stream velocities (R = 2.29 mm).

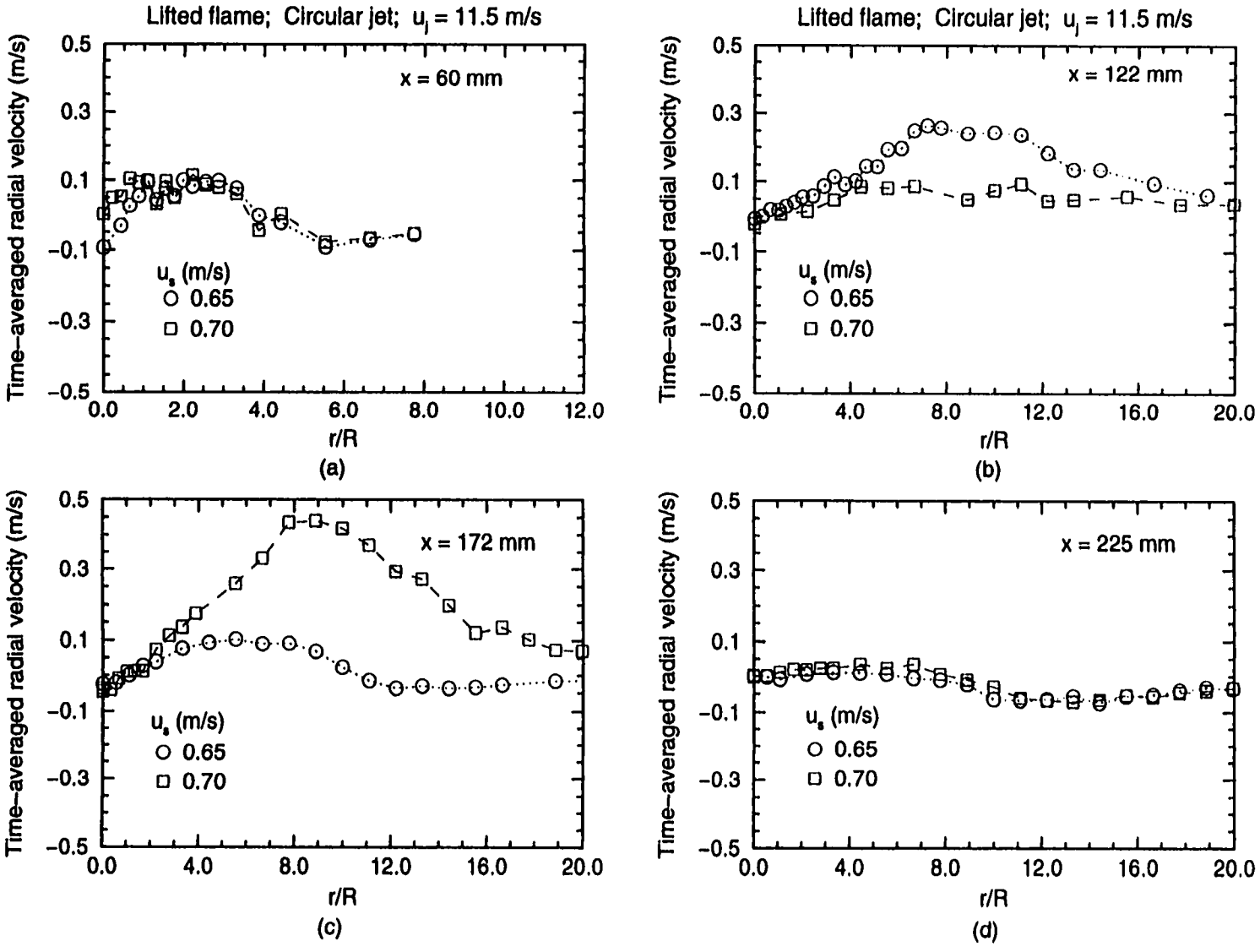

Fig. 5.1.5 Time–averaged radial velocity profiles within a lifted flame for two different co–flowing stream velocities (R = 2.29 mm).

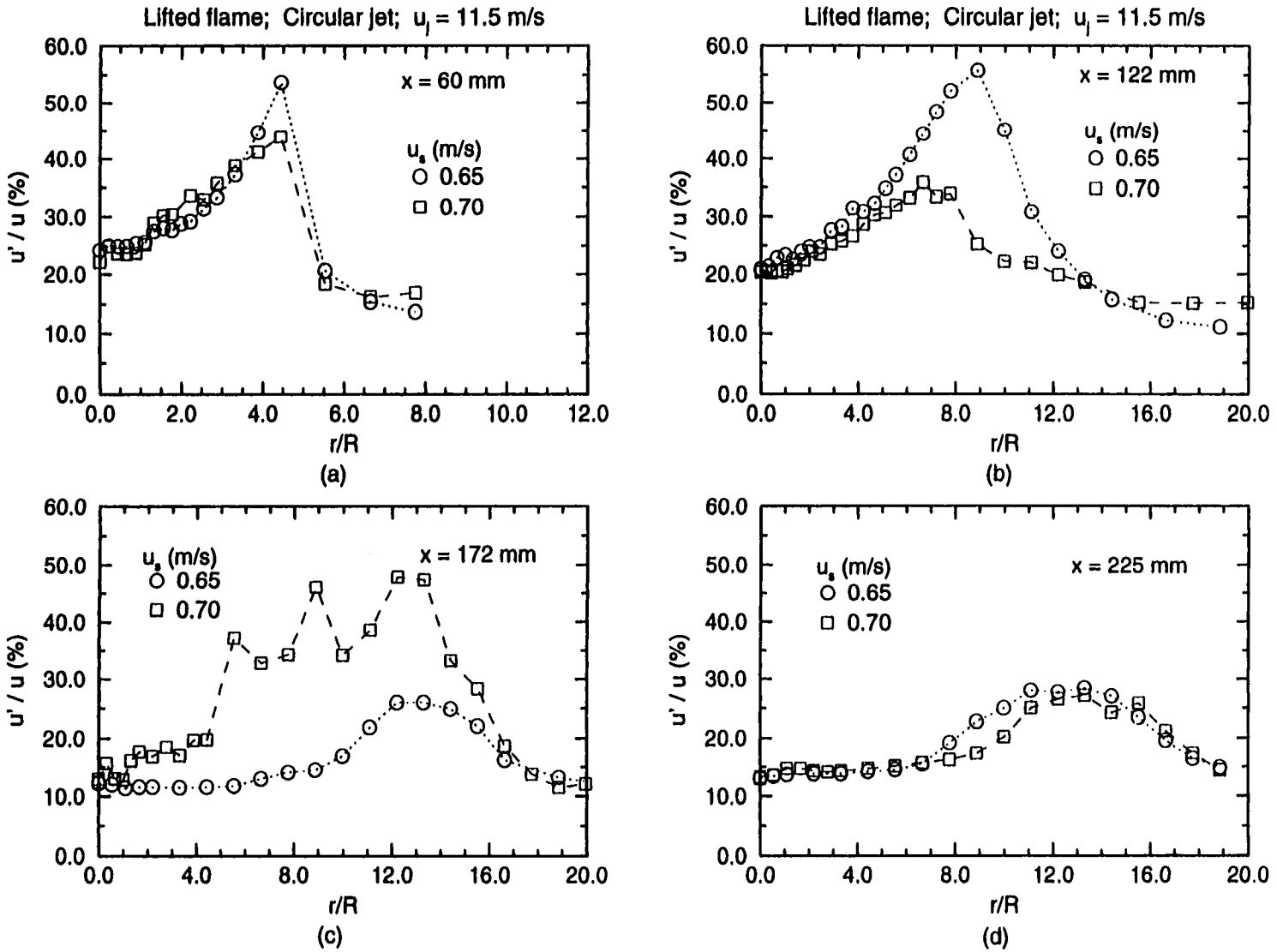

Fig. 5.1.6 Turbulence intensity level profile within a lifted flame for two different co–flowing stream velocities (R = 2.29 mm).

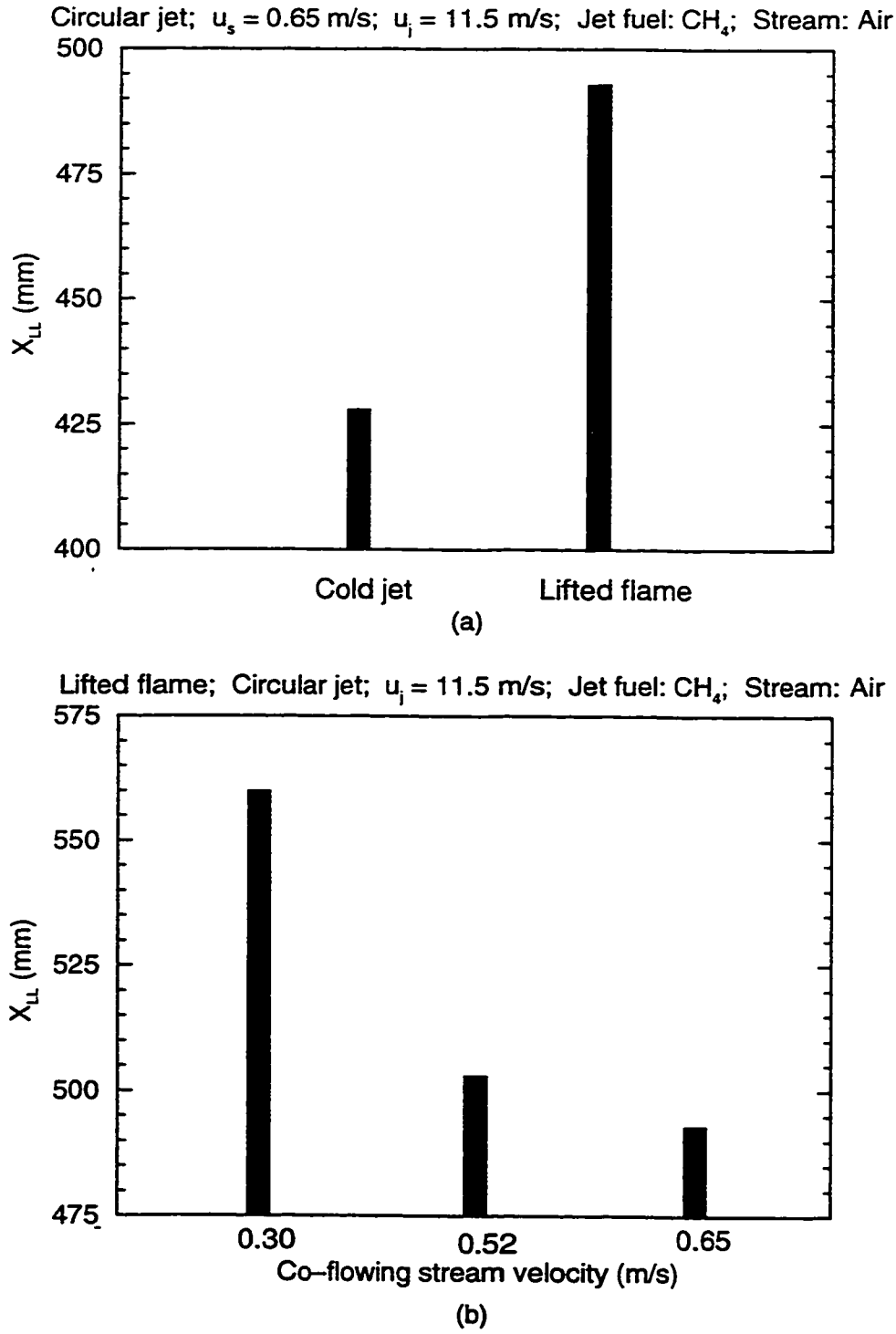

Fig. 5.1.7 A comparison of the axial distance where the fuel–air concentration equalled the lower flammability limit for (a) a cold jet and lifted flame and (b) lifted flames in co–flowing streams of different velocities.

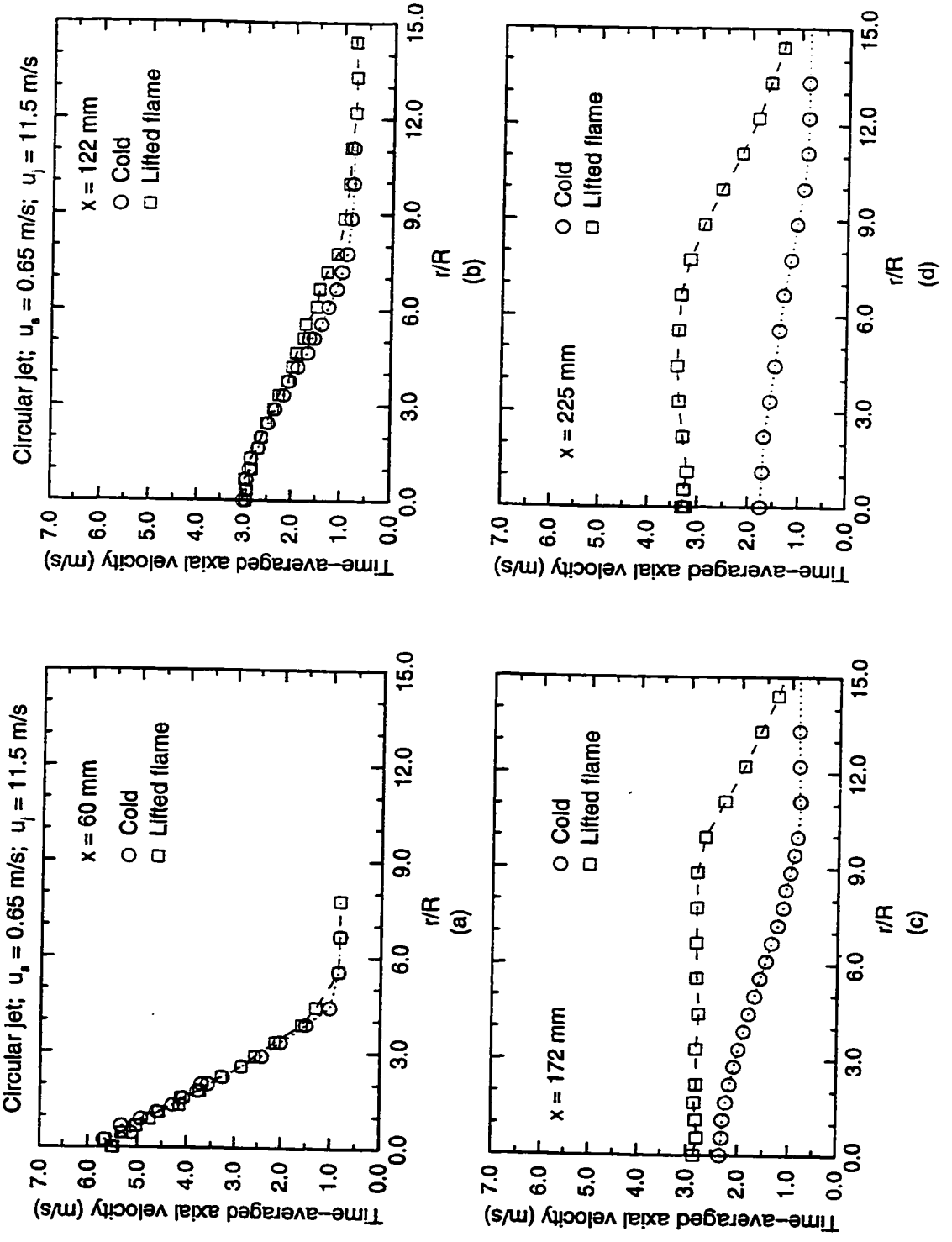

Fig. 5.1.8 A comparison of the time-averaged axial velocity profiles within cold jets and lifted flames (R = 2.29 mm).

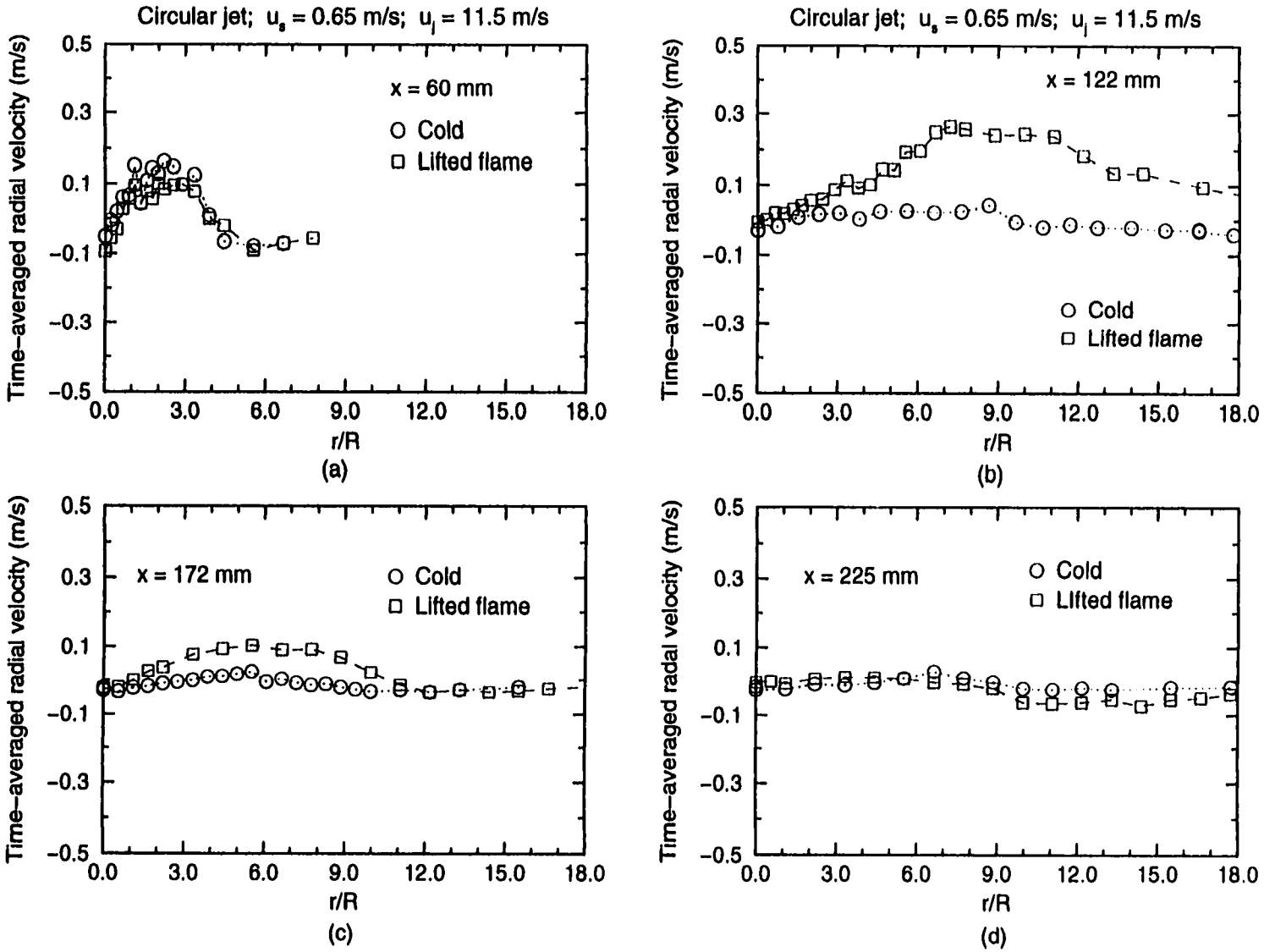

Fig. 5.1.9 A comparison of the time–averaged radial velocity profiles within cold jets and lifted flames (R = 2.29 mm).

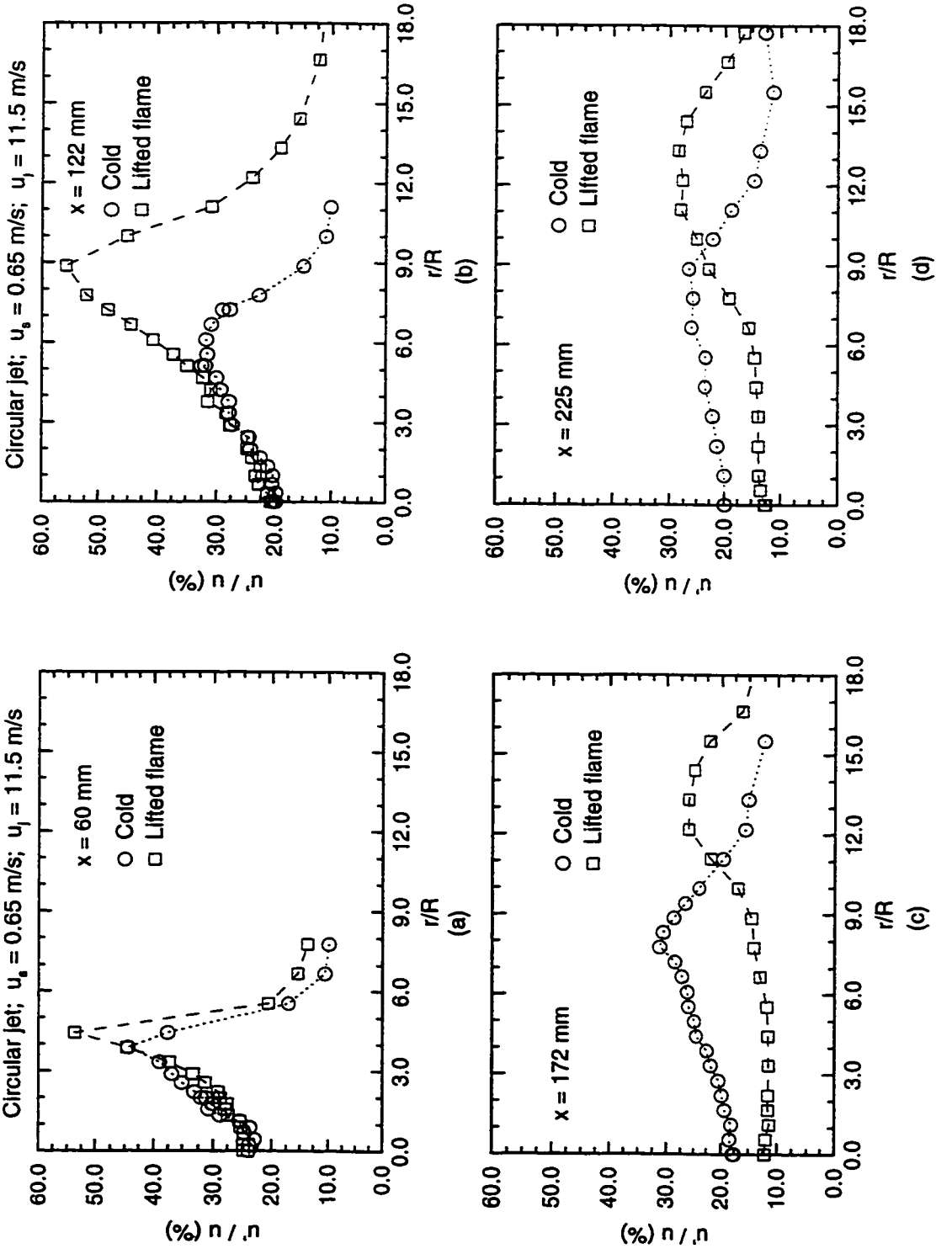

Fig. 5.1.10 A comparison of the turbulence intensity profiles within cold jets and lifted flames (R = 2.29 mm).

A comparison of the velocity and turbulence intensity profiles of cold jets and lifted flames for a co-flowing stream velocity of 0.65 m/s and a jet discharge velocity of 11.5 m/s are shown in Figs. 5.1.8 to 5.1.10. It can be seen that the flow structure in the cold region of the lifted flame is comparable with that in the cold jet until a downstream distance of 122 mm is reached. At this downstream distance, the effect of the flame was apparent as the radial velocities and turbulence intensity levels in the lifted flame were significantly higher than in cold jets. The axial velocities were approximately the same. Further downstream at x = 172 and 225 mm, the axial velocities were increased considerably and the peak turbulence intensity level occurred more radially outward in the lifted flame than in cold jets. The turbulence intensity towards the jet axis were significantly lower within the lifted flame than in cold jets. It can be seen that measurements in the cold region of the lifted flame, well away from the flame base, can also be obtained with cold jets without the loss of accuracy. This is desirable since measurements in cold jets eliminate many of the experimental difficulties encountered when a flame is present.

Attached Flame. A co-flowing stream velocity of 0.73 m/s or greater corresponded to the region of attached flame blowout. Since the stability of attached flames is governed by near-nozzle conditions, measurements were conducted at downstream distances up to 79 mm from the nozzle exit. At a co-flowing stream velocity of 1.21 m/s, the largest difference between the blowout limits of the nozzle with an aspect ratio of 1.38 compared with the other nozzles was observed and only the jet flame issued from the nozzle with an

aspect ratio of 1.38 was stable at a jet velocity of 7.2 m/s. Therefore, the velocity profiles of cold jets were determined for a jet velocity of 7.2 m/s and a co-flowing stream velocity of 1.21 m/s for different nozzles. The effect of an increase in the co-flowing stream velocity from 0.65 m/s to 1.21 m/s on the axial and radial velocity profiles of a circular jet is shown in Figs. 5.1.11 and 5.1.12. The radial velocity profile shows that the local radial velocities of jets in a co-flowing stream velocity of 0.65 m/s were, in general, greater than for jets in a stream velocity of 1.21 m/s. However, the jet issuing into the 1.21 m/s stream had higher axial velocities in the far-field region especially at $x \geq 60$ mm than of that issuing into a 0.65 m/s stream.

The jet half-width, i.e., the radial distance from the jet axis to the location where the time-averaged axial velocity attained half of its maximum value, δ, is usually used to illustrate jet growth [31,36,37,54]. Its variation with the dimensionless downstream distance, x/R, is compared in Fig. 5.1.13 (a) for a circular cold jet with a mean discharge velocity of 7.2 m/s issuing into two different co-flowing stream velocities of 0.65 m/s and 1.21 m/s. The corresponding decay of the centerline (maximum) jet velocity, u_{cl} , with downstream distance is also shown (Fig. 5.1.13 (b)). A greater jet spread and centerline velocity decay was observed in the cold jet discharging into the co-flowing stream of velocity 0.65 m/s. Intuitively, a lesser jet spread and centerline velocity decay due to a increase in the stream velocity from 0.65 to 1.21 m/s would be associated with a decrease in the mixing rate of the fuel and air; however, the phenomenon became more complicated for jets issuing into a co-flowing stream since the stream also added its momentum to the

primary jet. Therefore, the effect of the co-flowing stream velocity on the mixing of the fuel and surrounding air was better established with gas analysis measurements as shown earlier.

The effect of the co-flowing stream velocity on the flow structure of attached flames was investigated at a co-flowing stream velocity of 1.21 m/s and a jet velocity of 3.4 m/s (Re = 816). At this condition, a stable attached flame from all of the circular and elliptic jets employed could be sustained (up to u_s = 1.21 m/s). To understand better the flame-flow interactions, measurements were conducted with cold jets and flames at the same operational conditions.

A comparison of the profiles of the mean axial and radial velocities within cold jets and attached flames at downstream distances of 1 mm are shown in Fig. 5.1.14 for three different co-flowing stream velocities. At this very small distance from the nozzle, there is no significant effect of the co-flowing stream velocity on the velocity profiles within cold jets as well as attached flames. The radial velocities within the cold jets were rather small and unaffected by the co-flowing stream velocity. However, measurements for attached flames showed a region of significant inward radial velocities especially at lower co-flowing stream velocities, indicating the entrainment of air into the jet. It can be seen more clearly in Fig. 5.1.15 which shows velocity vectors at this distance for three different co-flowing stream velocities. The higher entrainment rates would contribute to higher reaction rates and jet expansion which can be seen in Fig. 5.1.14. A decrease in the entrained air velocity due to an increase in the co-flowing stream velocity could be responsible for the decrease

in the blowout limits of attached flames.

The velocity profiles at an axial distance of 30 mm from the nozzle are shown in Fig.5.1.16 for cold jets and attached flames. As expected, the jet expansion was more significant in the presence of a flame. The effect of the co-flowing stream velocity on the velocity profiles diminished especially within the inner regions of the jet flame and was not apparent until r/R > 1.2. At distances further downstream from the nozzle (x = 45, 60 and 79 mm), the local axial velocities within attached flames were higher for the higher co-flowing stream velocity of 1.21 m/s in the vicinity of the flame front, i.e., r/R = 3.8 (Fig. 5.1.17). The radial velocities, however, were small and their profiles were very similar for different co-flowing stream velocities (Fig. 5.1.18).

The effect of the co-flowing stream velocity on the turbulence level within an attached flame can be seen in Fig. 5.1.19. A significant difference in the turbulence level due to an increase in the co-flowing stream velocity is apparent only at the nozzle exit (Fig. 5.1.19 (a)). The significant increase in the turbulence level at a co-flowing stream velocity of 1.21 m/s did not appear to contribute to an increase in the entrainment rate, however such strong velocity fluctuations would have contributed to a decrease in the jet stability (the blowout limit for a circular jet at u_s = 1.21 m/s was almost twice less than that at u_s = 0.73 m/s). Generally, the turbulence intensity decreased with axial distance from the nozzle exit.

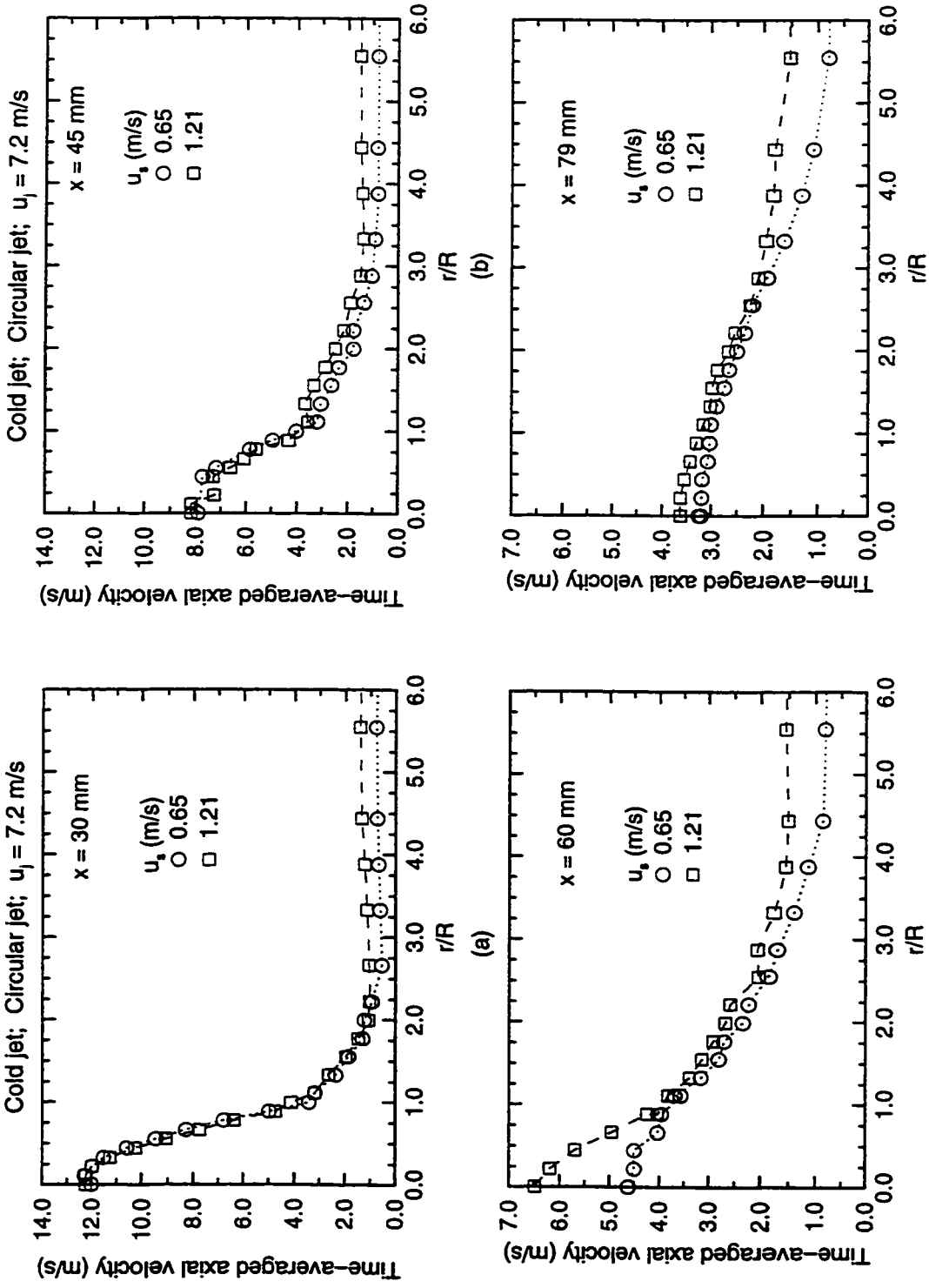

Fig. 5.1.11 Time–averaged axial velocity profiles within cold jets for two different co–flowing stream velocities (R = 2.29 mm).

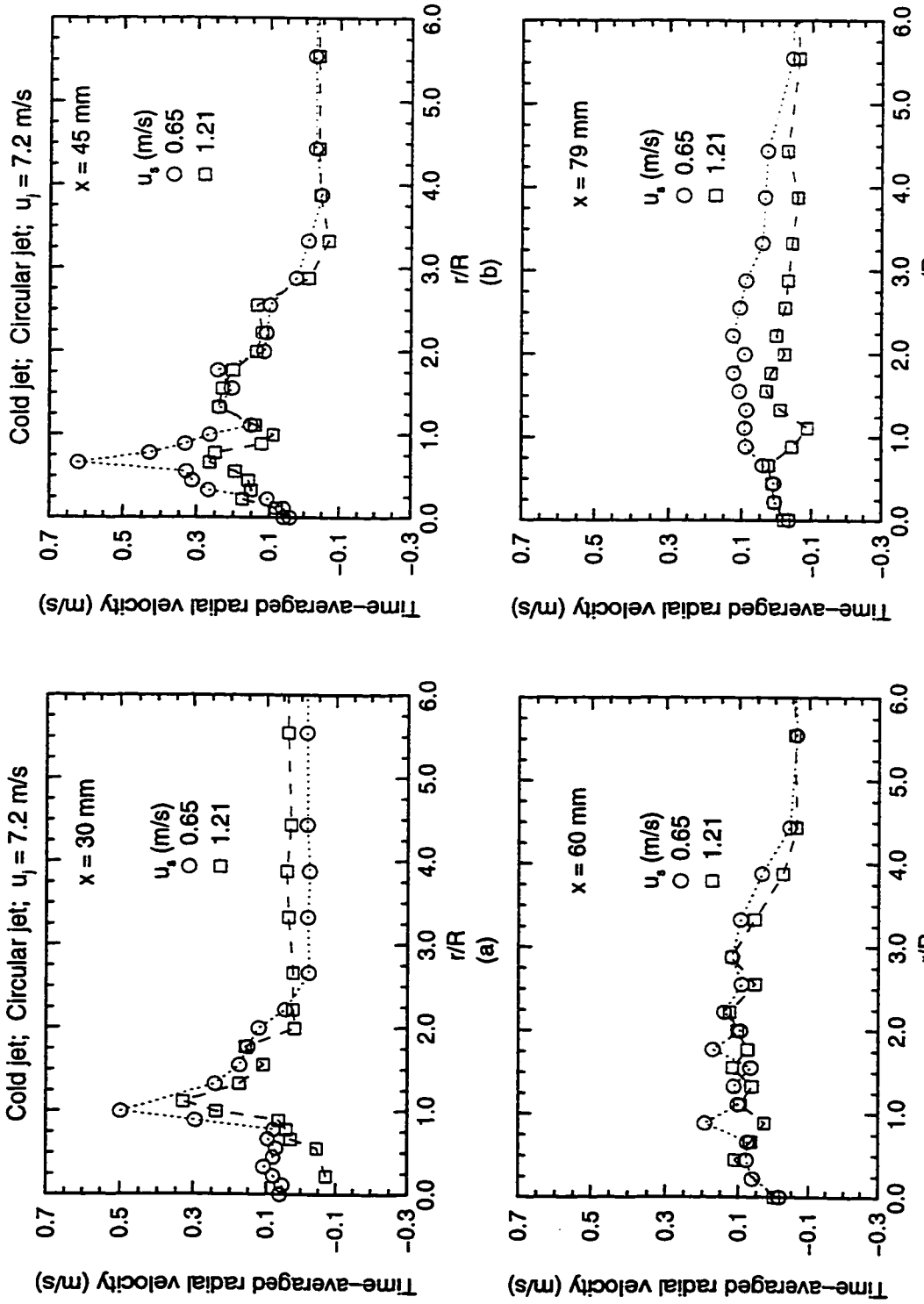

Fig. 5.1.12 Time–averaged radial velocity profiles within cold jets for two different co–flowing stream velocities (R = 2.29 mm).

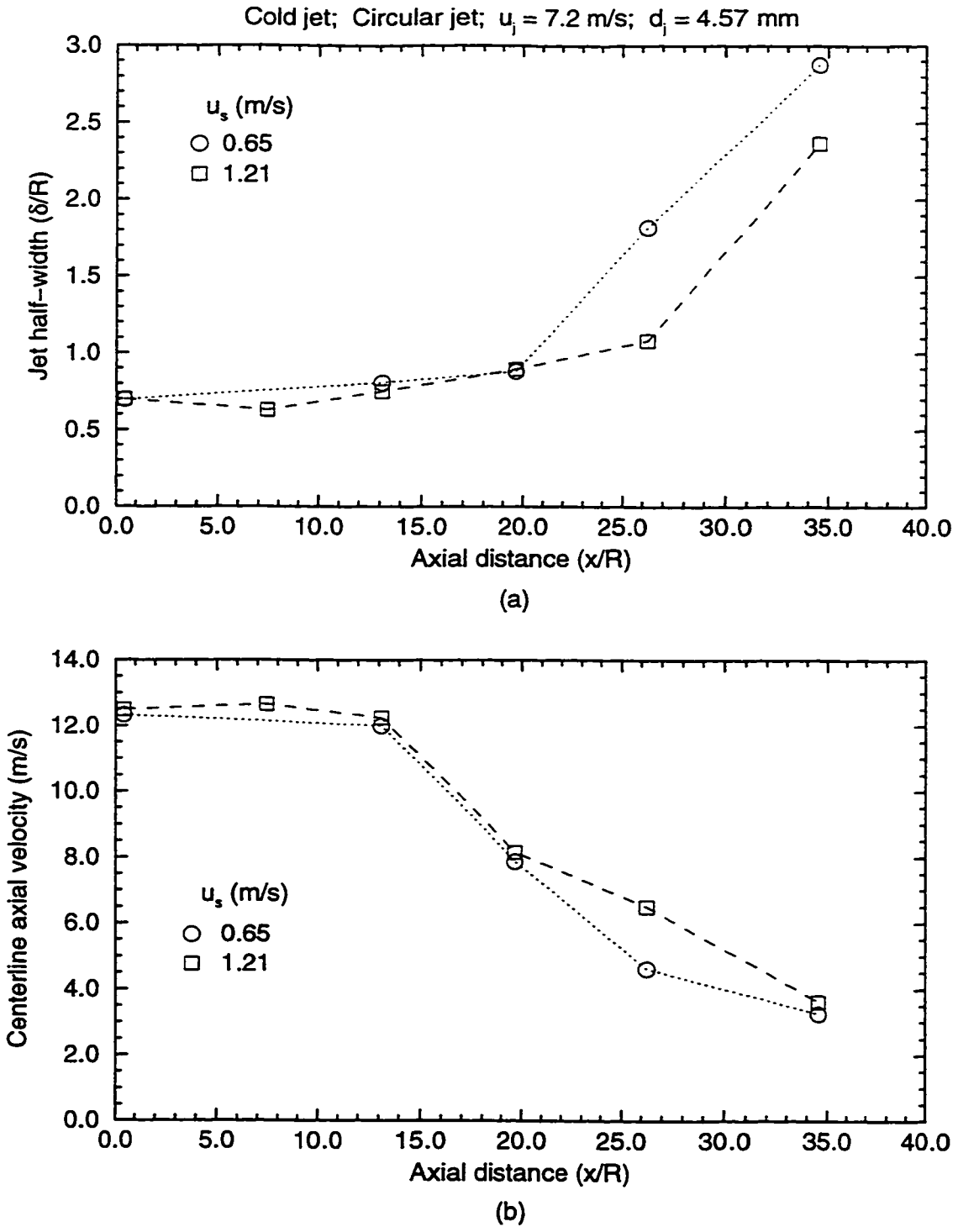

Fig. 5.1.13 A comparison of (a) the jet half–width and (b) the centerline velocity decay with the downstream distance for cold jets in two different co–flowing stream velocities.

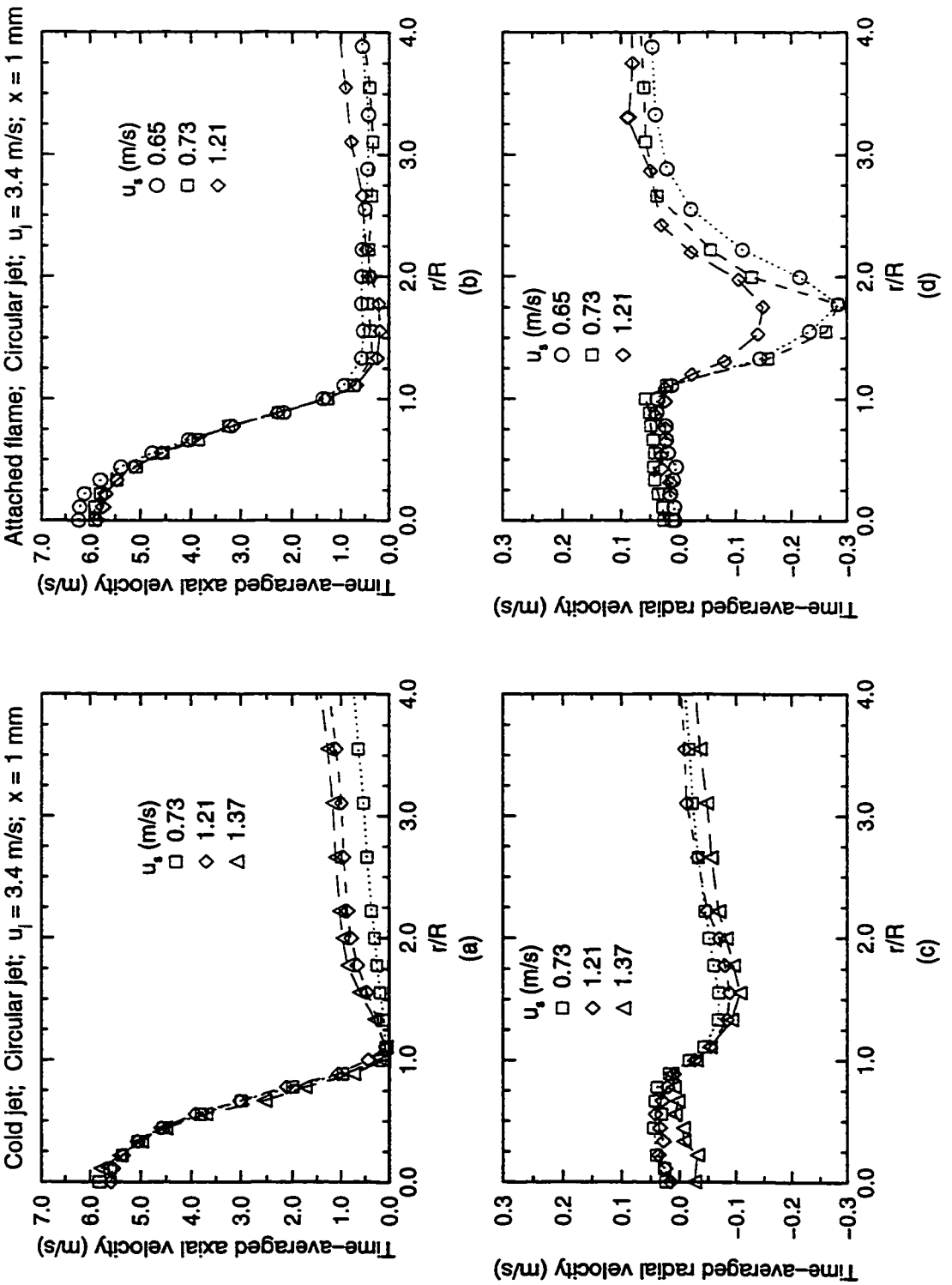

Fig. 5.1.14 Time–averaged axial and radial velocity profiles for (a) and (c) cold jets, and for (b) and (d) attached flames issuing into a co–flowing stream of different velocities (R = 2.29 mm).

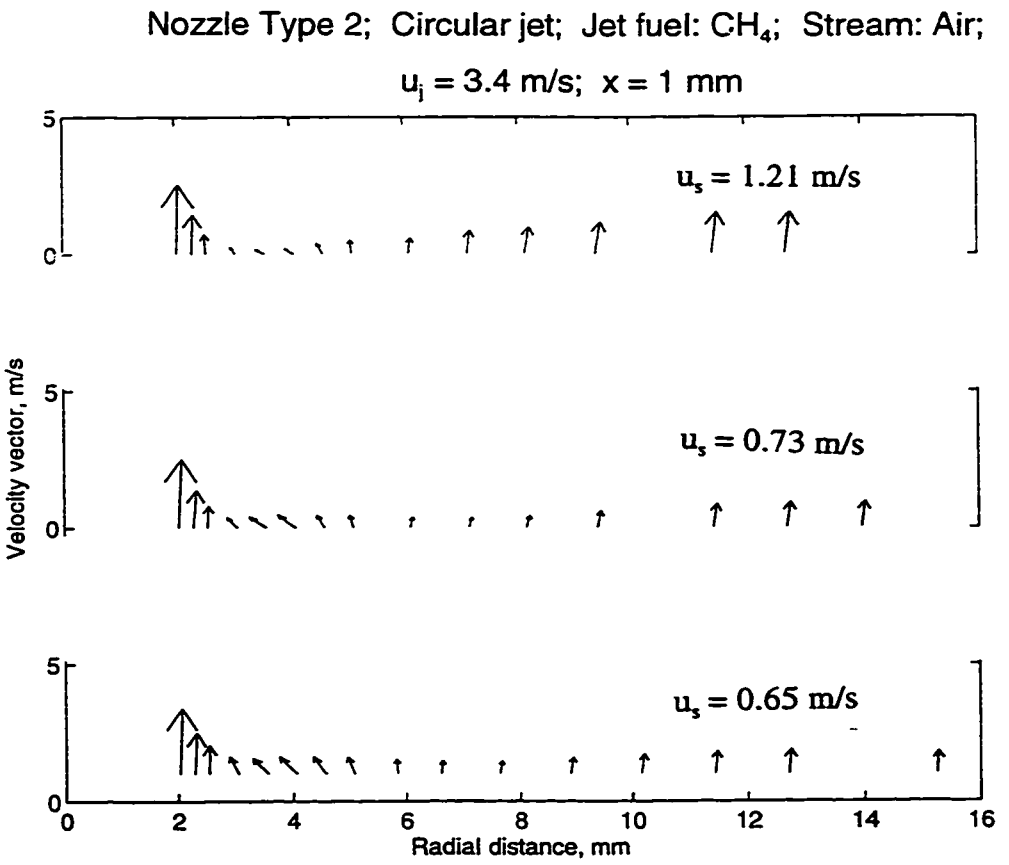

5.1.15 Velocity vectors of attached flames at the nozzle exit for different co-flowing stream velocities.

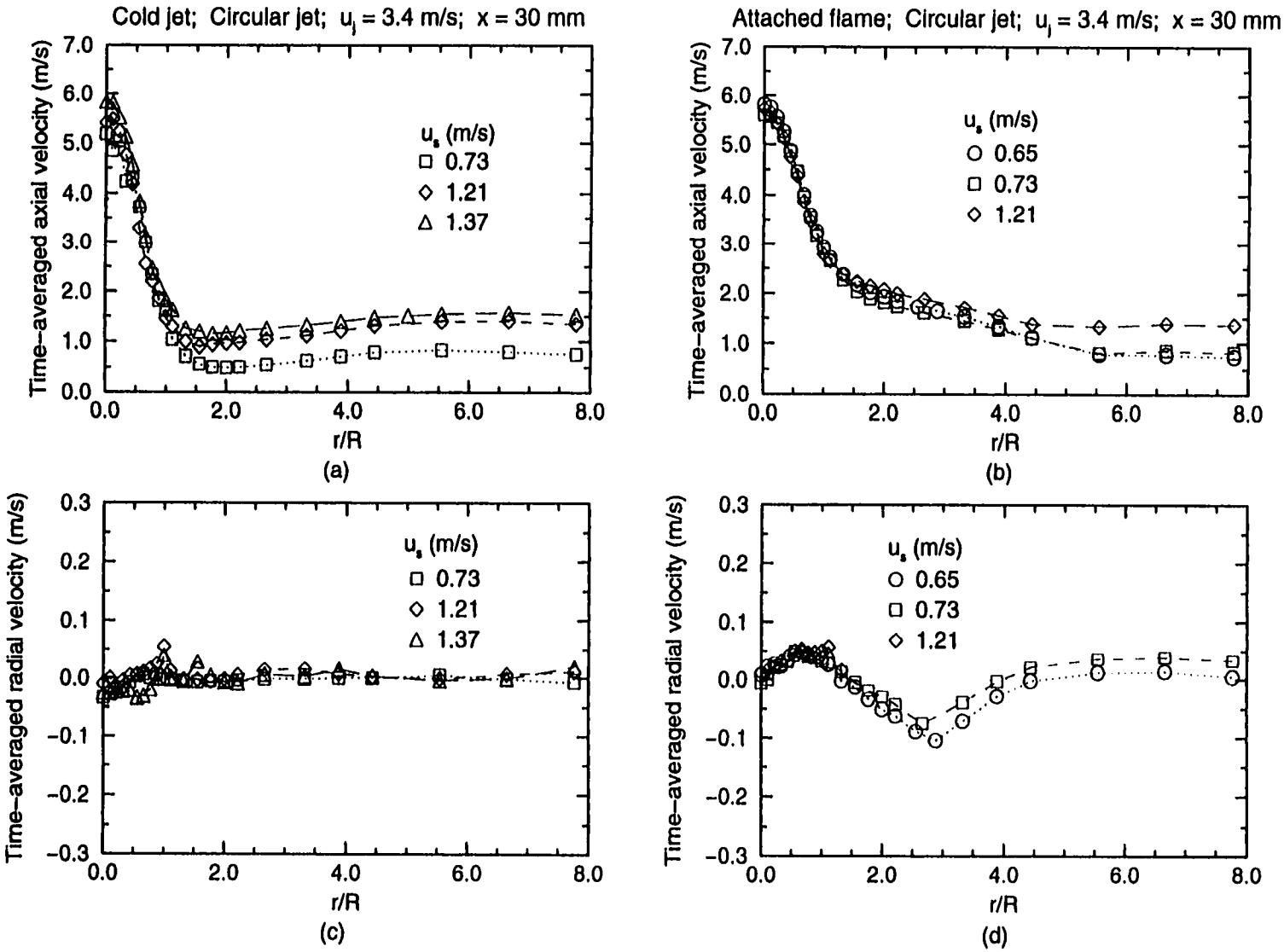

Fig. 5.1.16 Time-averaged axial and radial velocity profiles for (a) and (c) cold jets, and for (b) and (d) attached flames issuing into a co-flowing stream of different velocities (R = 2.29 mm).

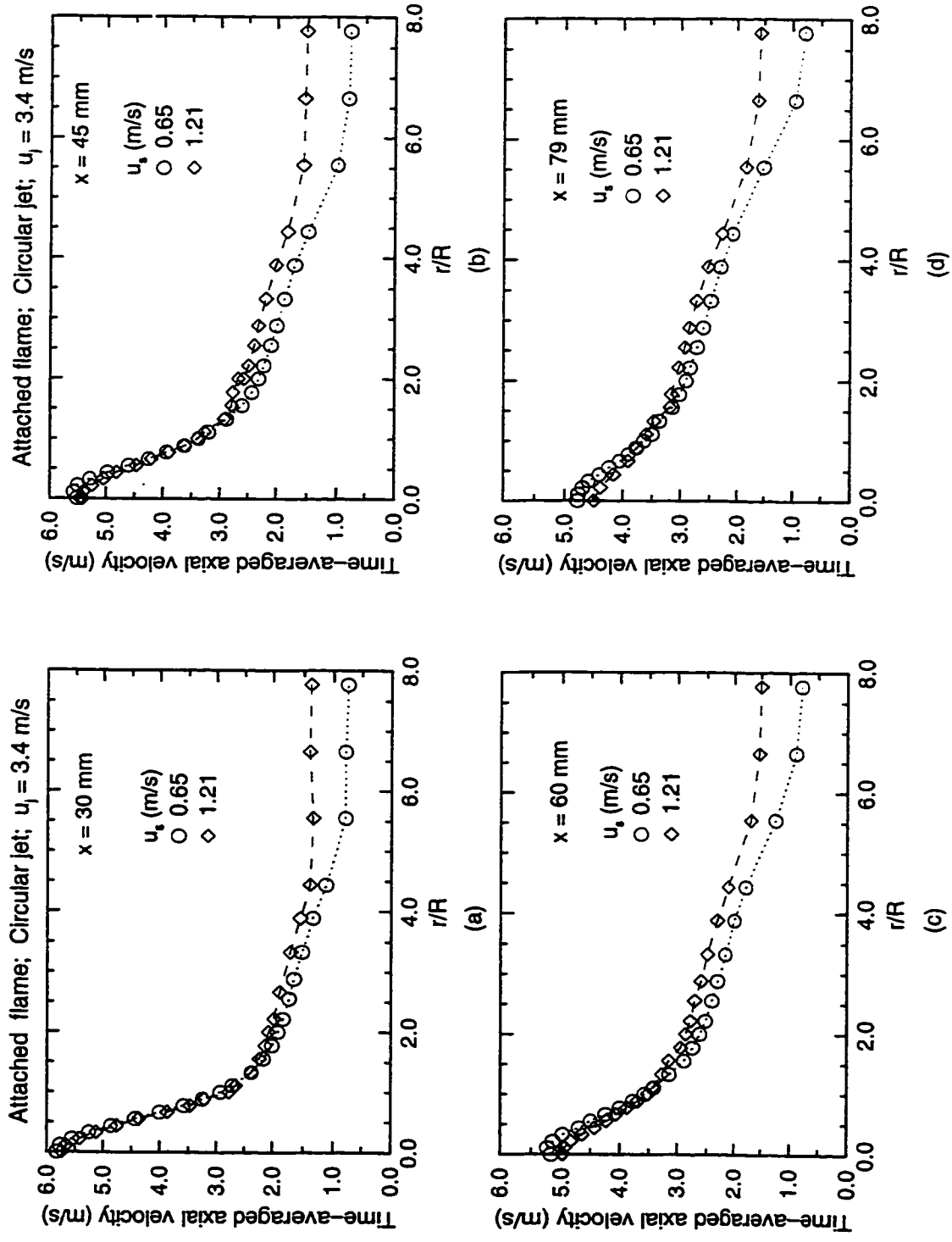

Fig. 5.1.17 Time–averaged axial velocity profiles within attached flames for two different co–flowing stream velocities (R = 2.29 mm).

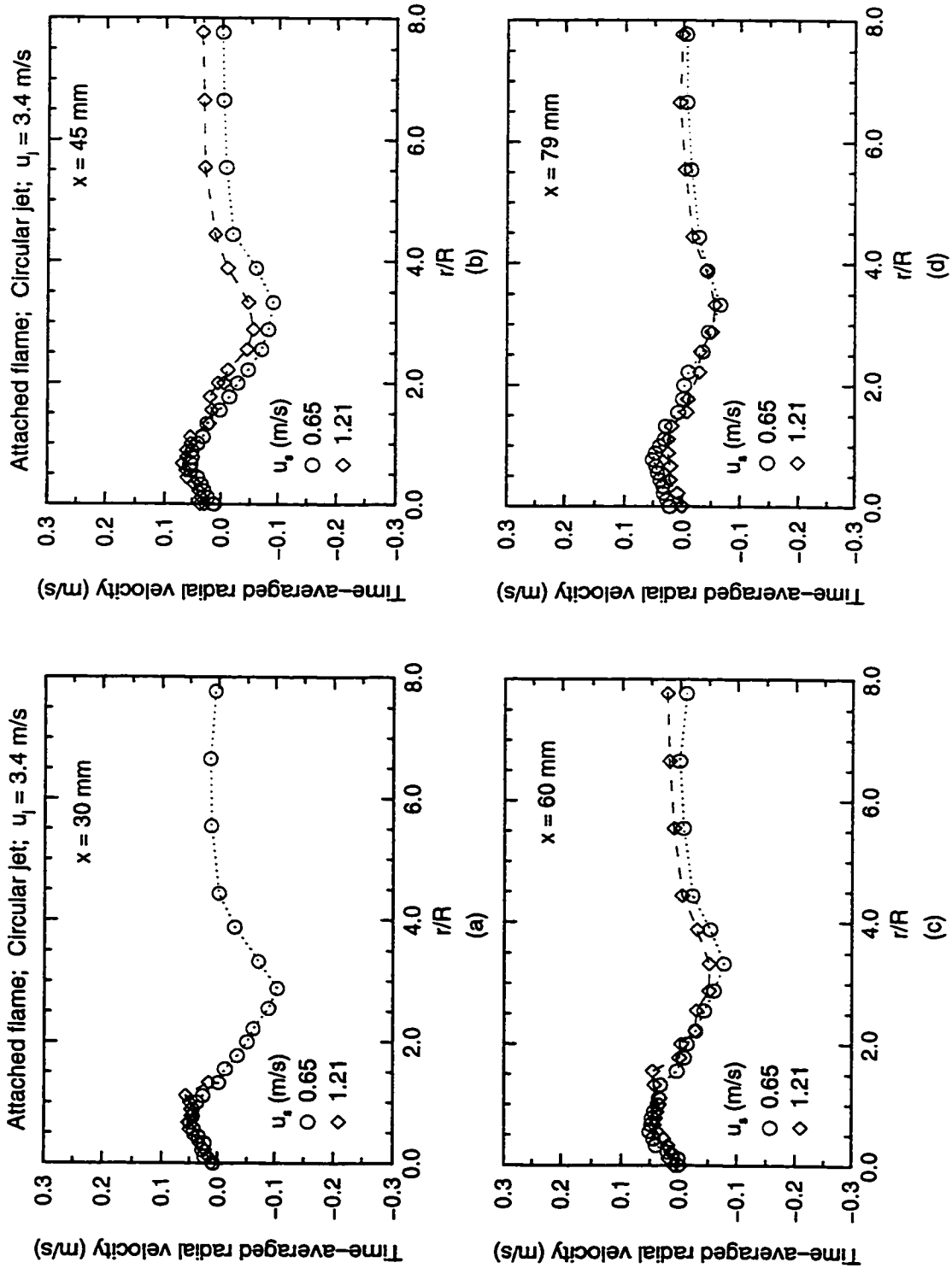

Fig. 5.1.18 Time–averaged radial velocity profiles within attached flames for two different co–flowing stream velocities (R = 2.29 mm).

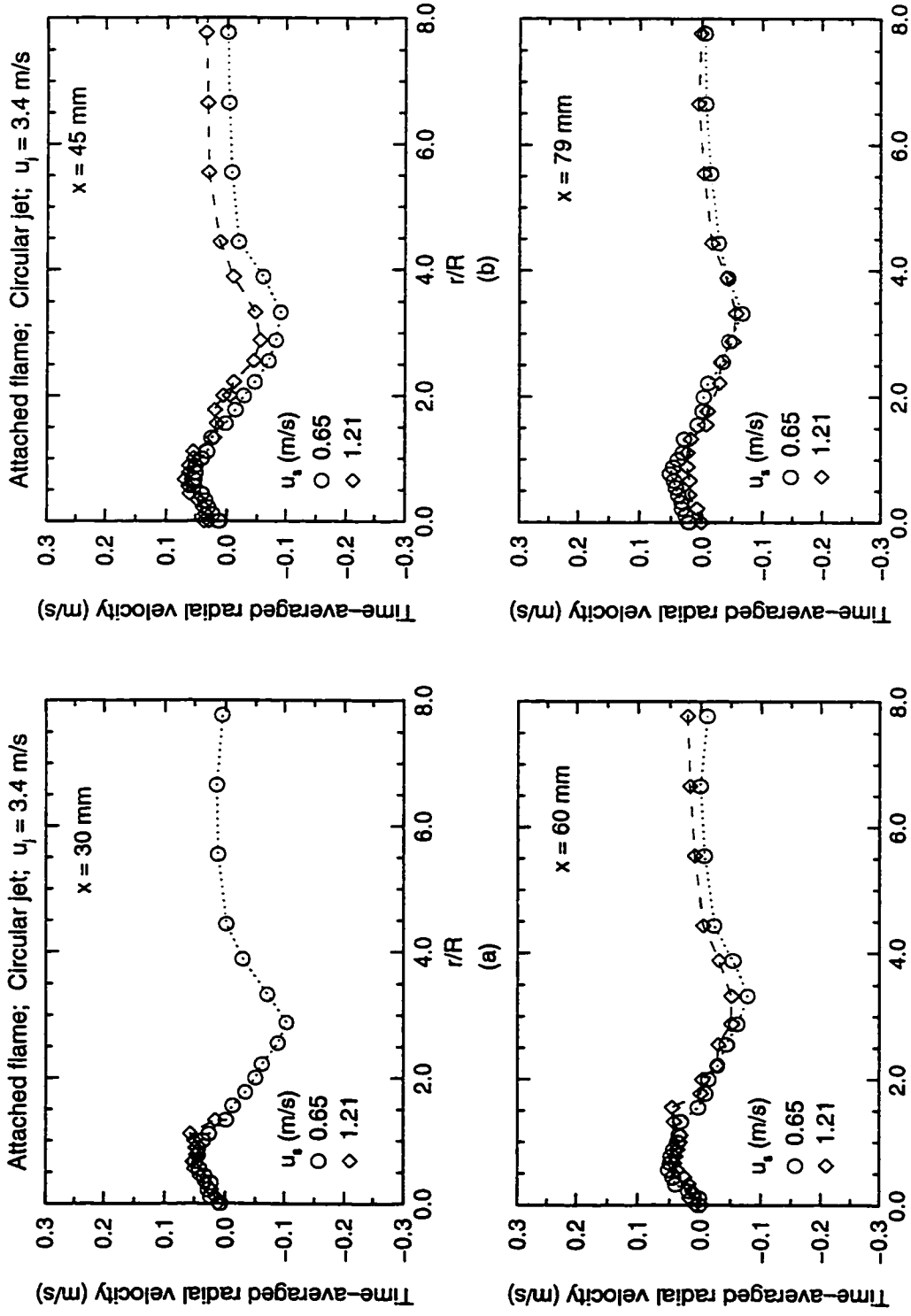

Fig. 5.1.19 Turbulence intensity level profiles within attached flames for different co–flowing stream velocities (R = 2.29 mm).

5.2 Effect of Jet Discharge Velocity

The effect of the jet discharge velocity on the flow characteristics was investigated for attached flames at a co-flowing stream velocity of 0.65 m/s. This velocity was chosen since, at a stream velocity of 1.21 m/s, the flame blowout limit was very low ($u_{j,b}$ = 6.3 m/s). Profiles of the time-averaged axial velocity at downstream distances of 1.0 to 79 mm are shown in Figs. 5.2.1 and 5.2.2. The jet discharge velocities were varied from 3.4 to 11 m/s (Re = 816 - 2630). It can be seen that at x = 1.0 mm (in the stabilization region of attached flames), the velocity gradients near the jet border are steep in jets with a discharge velocity of 11 m/s and may be close to the critical value (the lift-off velocity is 11.2 m/s at this stream velocity). Figure 5.2.3 shows the profiles of the axial velocity gradients at a downstream distance of 1 mm. An increase in the jet discharge velocity increased the velocity gradients, and the strain rate sustained by the flame surface at the near lift-off condition (i.e., u_j = 11 m/s) was measured to be approximately 500 s^{-1} , which is consistent with that of other researchers who had employed different operating conditions [23,80]. With a further increase in the jet velocity, the highly strained flame would lift off the nozzle rim and find a stable downstream region. In the region of attached flame blowout, a steep velocity gradient due to an increase in the jet velocity combined with a lower entrained air velocity due to a higher co-flowing stream velocity (Section 5.1) would result in the blowout of the flame at jet velocities of 6.3 m/s and higher (at u_s = 1.21 m/s).

Figures 5.2.1 and 5.2.2 also show that further downstream (x = 30 to 79 mm), an increase in the jet velocity reduced the potential core as the jet spread outward and decayed

faster. For instance, the jet with a velocity of 11 m/s had a significant jet spread and reduced centerline axial velocity at x = 30 while those of 7.2 and 3.4 m/s experienced very little centerline axial velocity decay. The radial velocity profiles in Figs. 5.2.4 and 5.2.5 show that the radial velocity of the jet with a discharge velocity of 11 m/s fluctuated significantly from the inward to outward direction at x = 17 mm and to a lesser degree at x = 30 mm, indicating the presence of vorticities which were not present at the lower jet velocities of 3.4 and 7.2 m/s. The 11 m/s jet then experienced a significant outward flow at a downstream distances of 30 mm and greater. The 7.2 m/s jet was observed to have increased values of the radial velocity at a downstream distance of 79 mm.

Schlieren photographs in Fig. 5.2.6 confirm that the known phenomenon of the break-point location, i.e., the downstream region where the laminar flow became turbulent, is located closer to the jet exit as the jet velocity is increased. A significant jet spread was observed in the turbulent region of the jet. The break-point location of jets with a velocity of 11 and 7.2 m/s occurred at approximately x = 12 and 65 mm, respectively; consequently, from LDV measurements, an increase in the radial velocities and the decay of the centerline axial velocity were observed at x = 17 mm and other distances for the 11 m/s jet and at only x = 79 mm for the 7.2 m/s jet. The 3.4 m/s jet did not show any signs of turbulent flow throughout the field observed in the schlieren photograph (i.e., up to x = 95 mm) and, hence, the radial flow outward of the 3.4 m/s jet was not observed in the LDV measurements at the specified distances.

The corresponding effect of the jet velocity on the turbulence level within jet flames

is shown in Figs. 5.2.7 and 5.2.8. At the jet exit, the turbulence level was higher for the 7.2 and 11 m/s jet than for the 3.4 m/s jet. Further downstream until x = 60 mm, a significantly elevated turbulence intensity was observed only within the 11 m/s jet. The turbulence intensity in the 7.2 m/s jet became significant again at x = 60 and 79 mm. The jet with a velocity of 3.4 m/s did not experience turbulence in the measurement field, i.e., up to x = 79 mm. Schlieren images confirm these findings.

Figs. 5.2.9 (a) and (b) show the effect of the jet discharge velocity on the jet half-width and maximum jet velocity decay of jets in the presence of a flame. The centerline jet velocity decay is presented in the dimensionless form $(u_{cl} - u_s) / (u_{cl,o} - u_s) = f(r / R)$, where u_{cl} is the axial velocity at the jet axis, $u_{cl,o}$ is the axial velocity at the jet axis at x = 1 mm, and u_s is the mean co-flowing stream velocity. The jet spread and maximum velocity decay was the greatest for the jet with a velocity of 11 m/s, followed by the 3.4 m/s and then by the 7.2 m/s jet. This unexpected trend may be explained as follows. From the schlieren photographs, the 3.4 m/s jet was laminar throughout the measurement field and the 7.2 m/s jet was laminar until a downstream distance of approximately 65 mm from the nozzle exit. For laminar jet flames, the mixing rates between the fuel and oxidant is relatively small and an increase in the jet velocity from 3.4 m/s to 7.2 m/s reduced the mixing process; consequently, the jet spread and centerline axial velocity decay was not greater for the 7.2 m/s jet than the 3.4 m/s jet and it remained unchanged for a significant downstream distance. With a further increase in the discharge velocity to 11 m/s, turbulence began to set in much closer to the jet exit (at approximately x = 12 mm) and the mixing process was

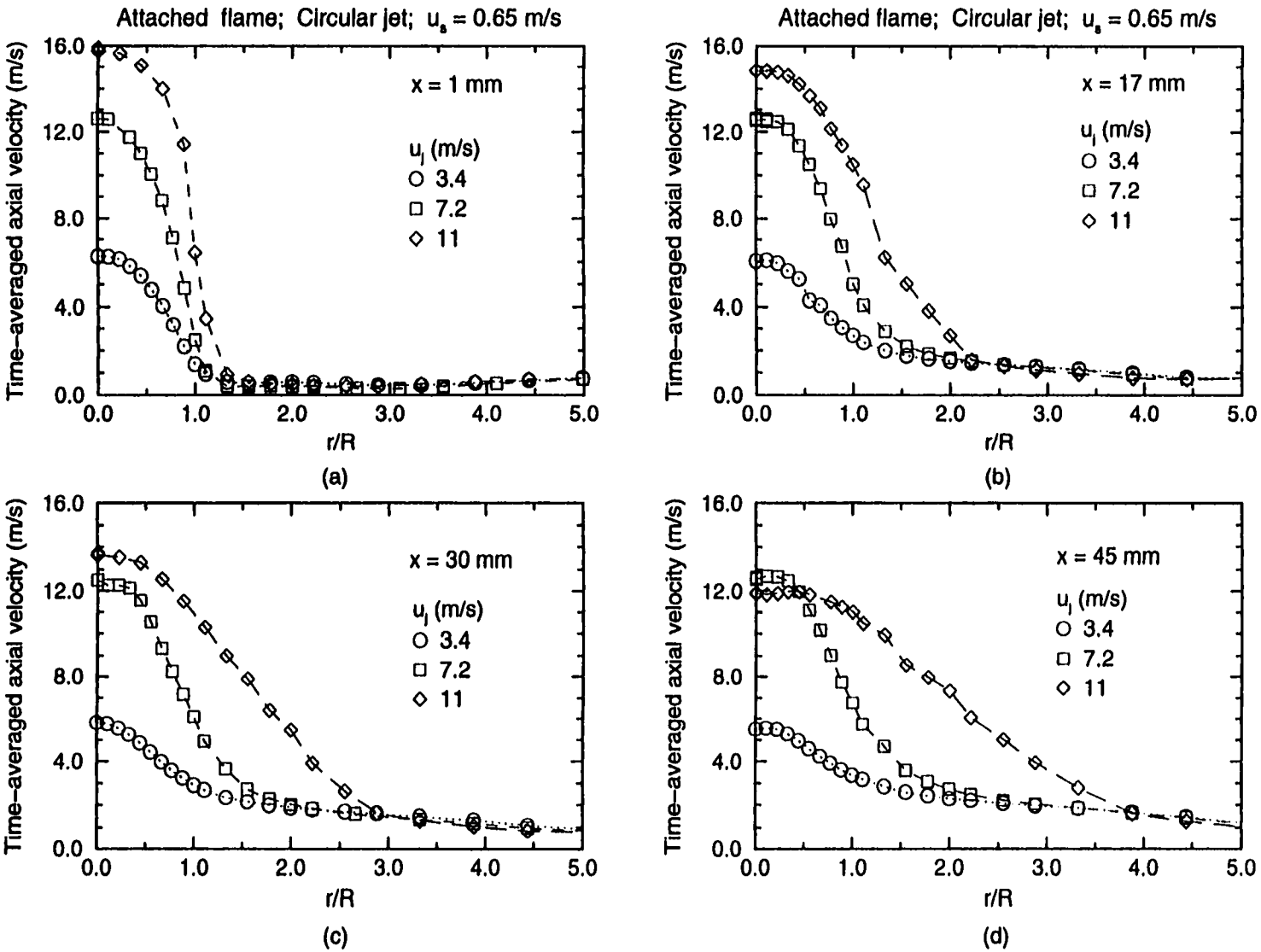

Fig. 5.2.1 Time-averaged axial velocity profiles within attached flames with different jet discharge velocities (R = 2.29 mm).

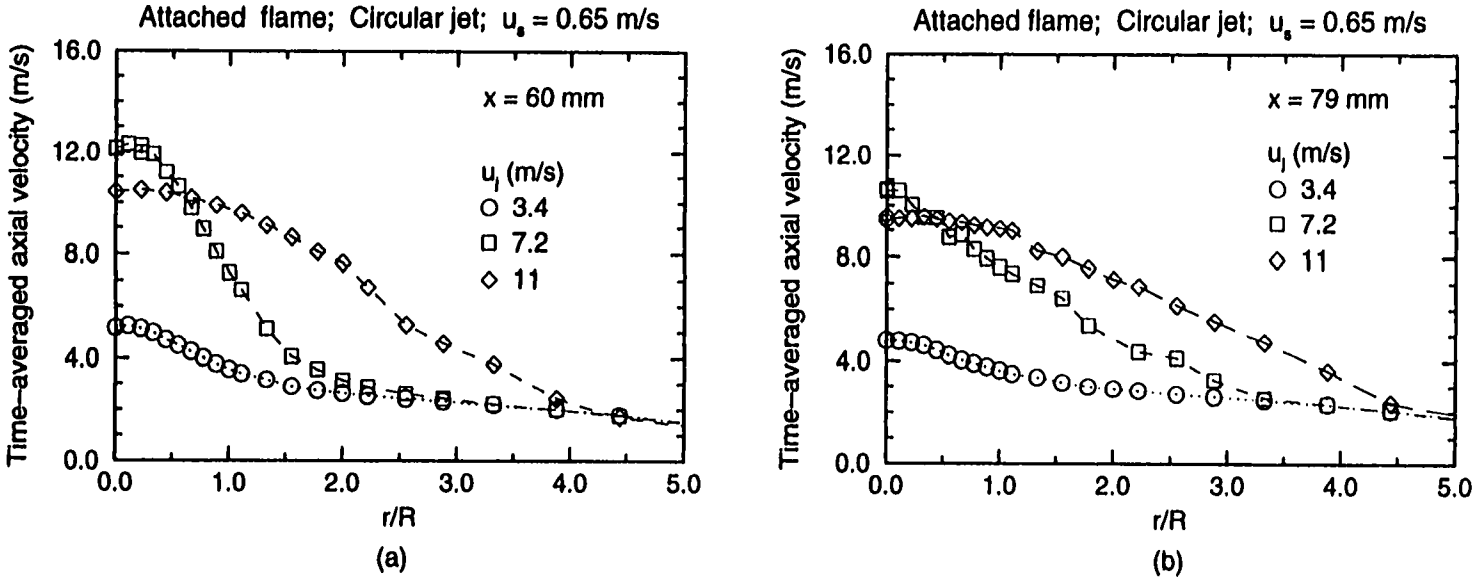

Fig. 5.2.2 Time-averaged axial velocity profiles within attached flames with different jet discharge velocities (R = 2.29 mm).

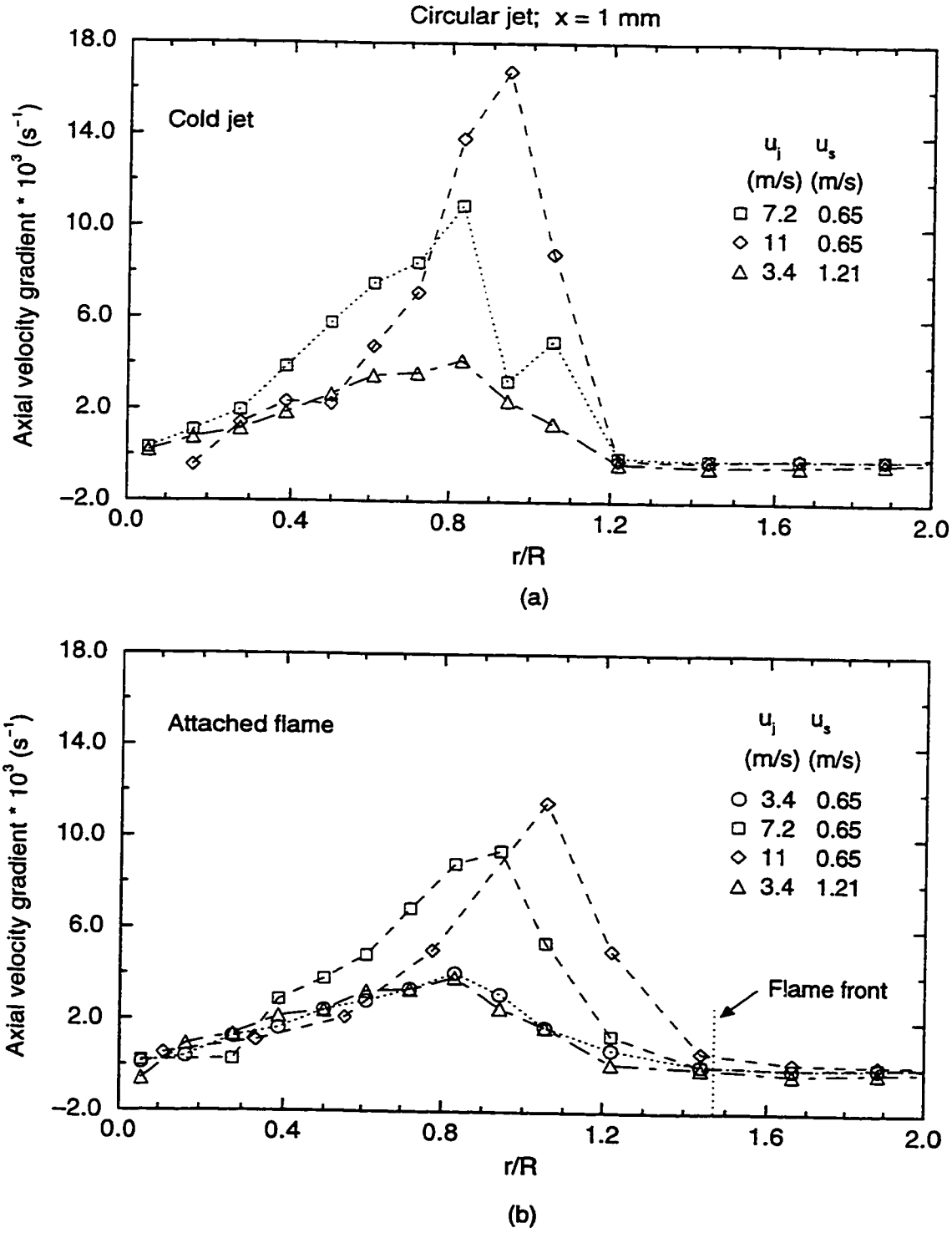

Fig. 5.2.3 A comparison of the axial velocity gradients within (a) cold jets and (b) attached flames with different jet discharge velocities (R = 2.29 mm).

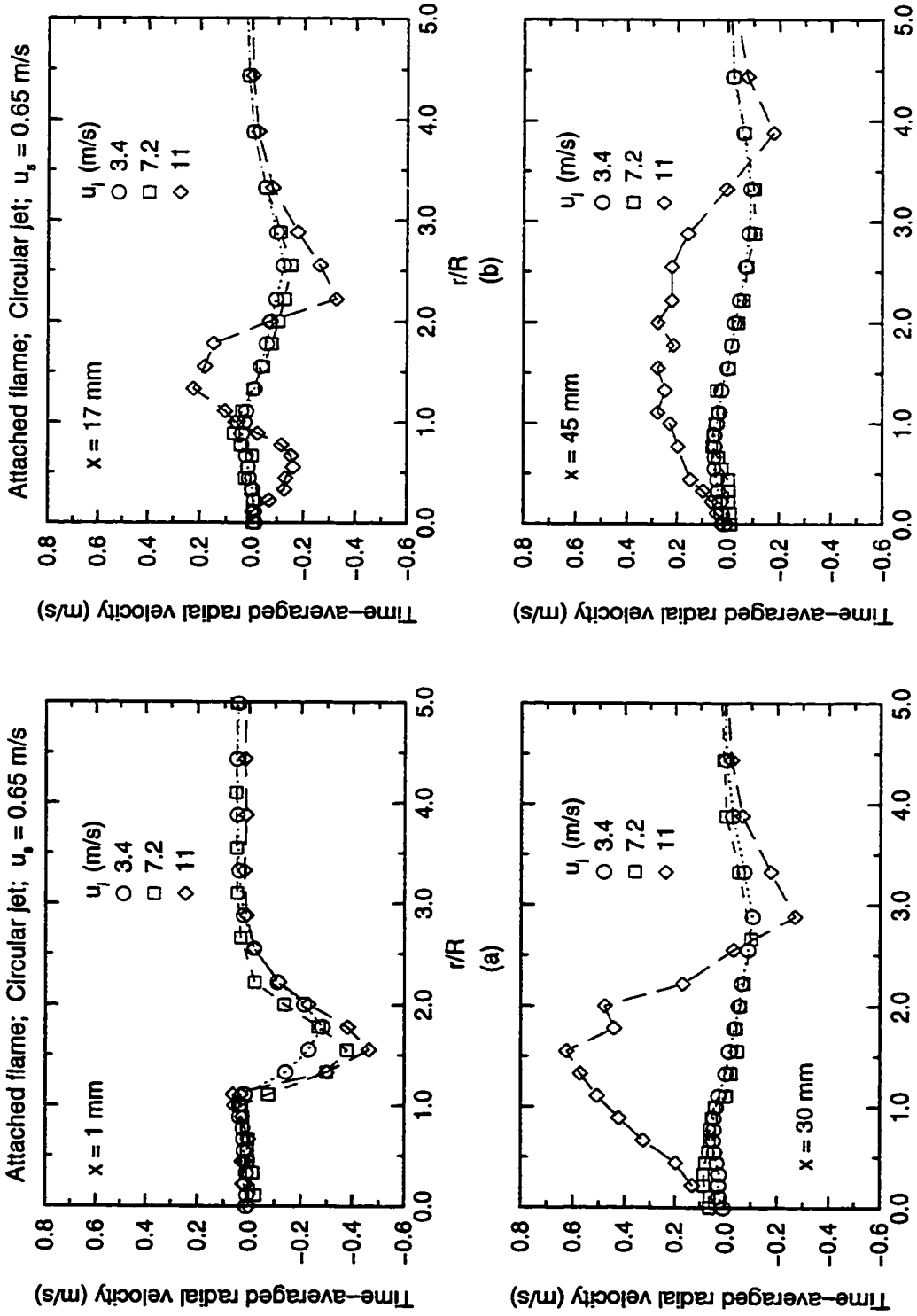

Fig. 5.2.4 Time–averaged radial velocity profiles within attached flames with different discharge velocities (R = 2.29 mm).

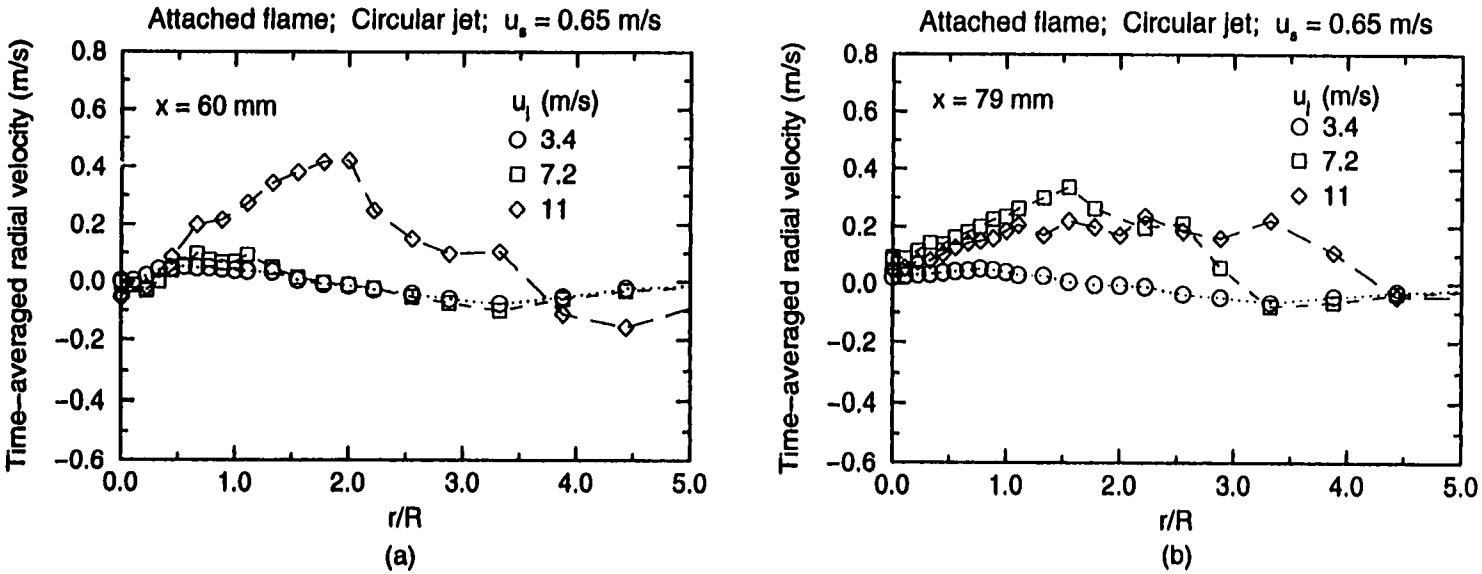

Fig. 5.2.5 Time–averaged radial velocity profiles within attached flames with different discharge velocities (R = 2.29 mm).

Attached flame; Circular jet; u_s = 0.65 m/s

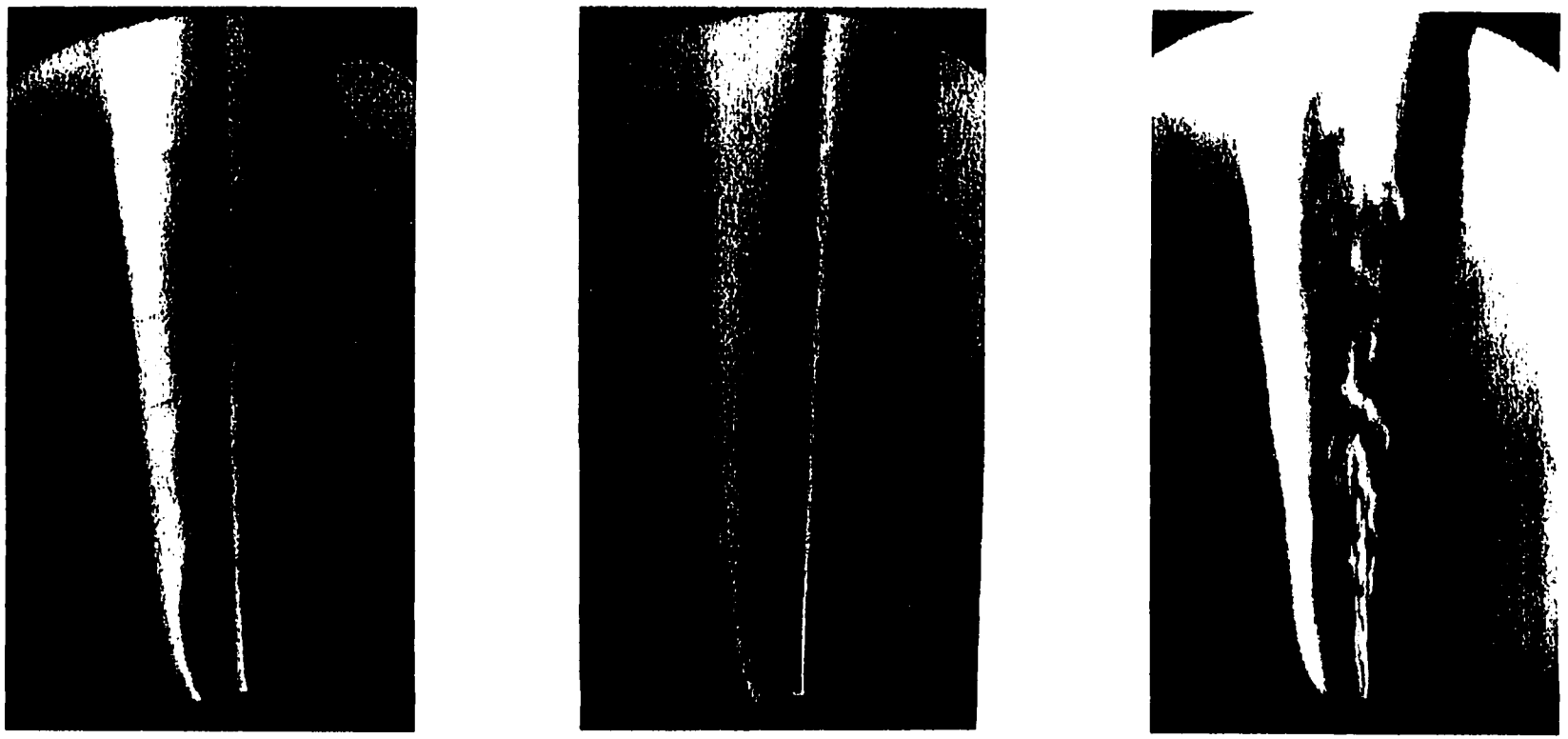

(a)
u_j = 3.4 m/s (Re_j = 816)

(b)
u_j = 7.2 m/s (Re_j = 1722)

(c)
u_j = 11 m/s (Re_j = 2630)

Scale: 1 cm

Fig. 5.2.6 Schlieren photographs showing the effect of varying jet velocities on the flow structure of attached flames in a co-flowing stream of velocity 0.65 m/s (d_j = 4.57 mm).

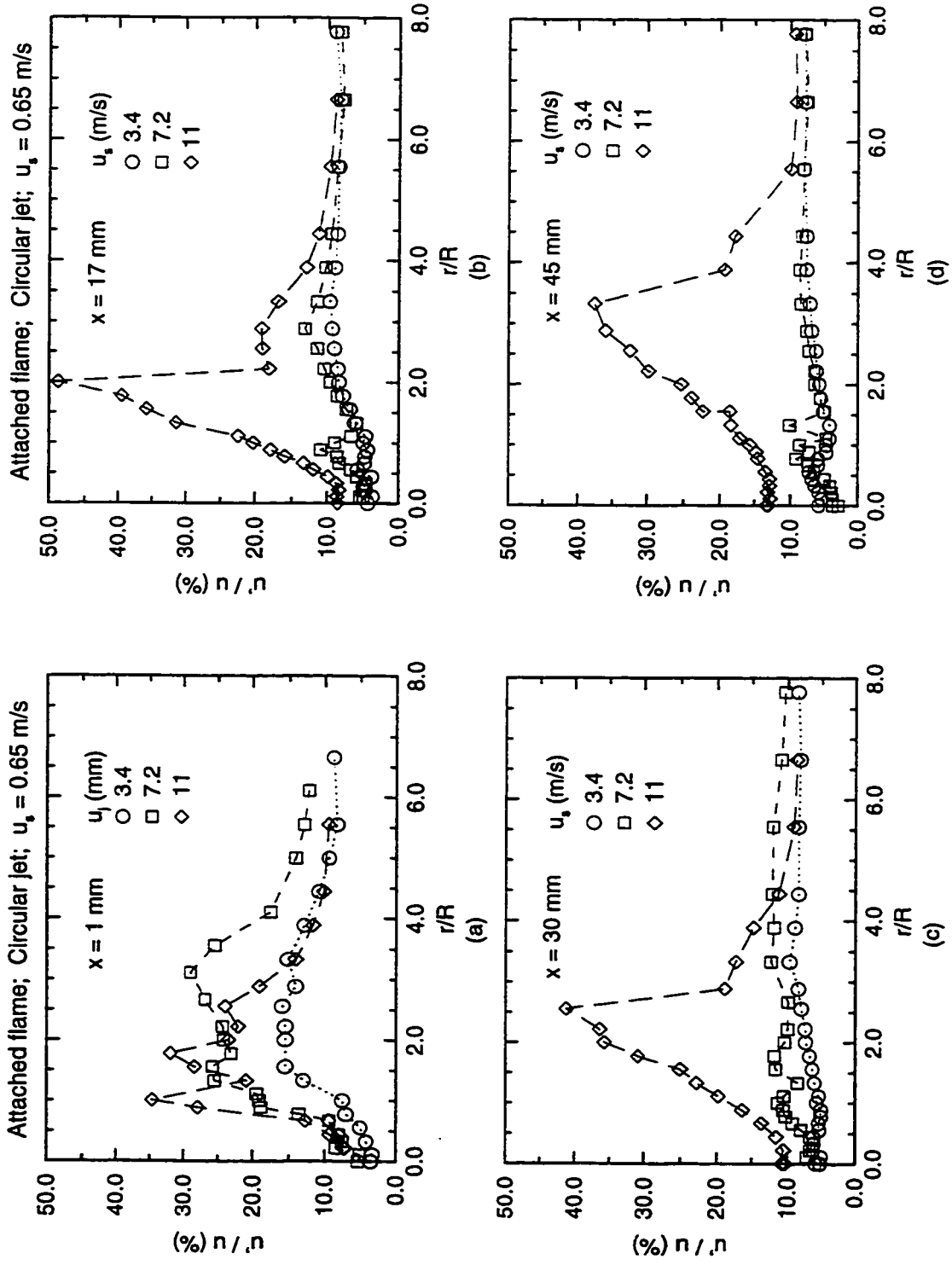

Fig. 5.2.7 Turbulence intensity level profiles within attached flames with different jet discharge velocities (R = 2.29 mm).

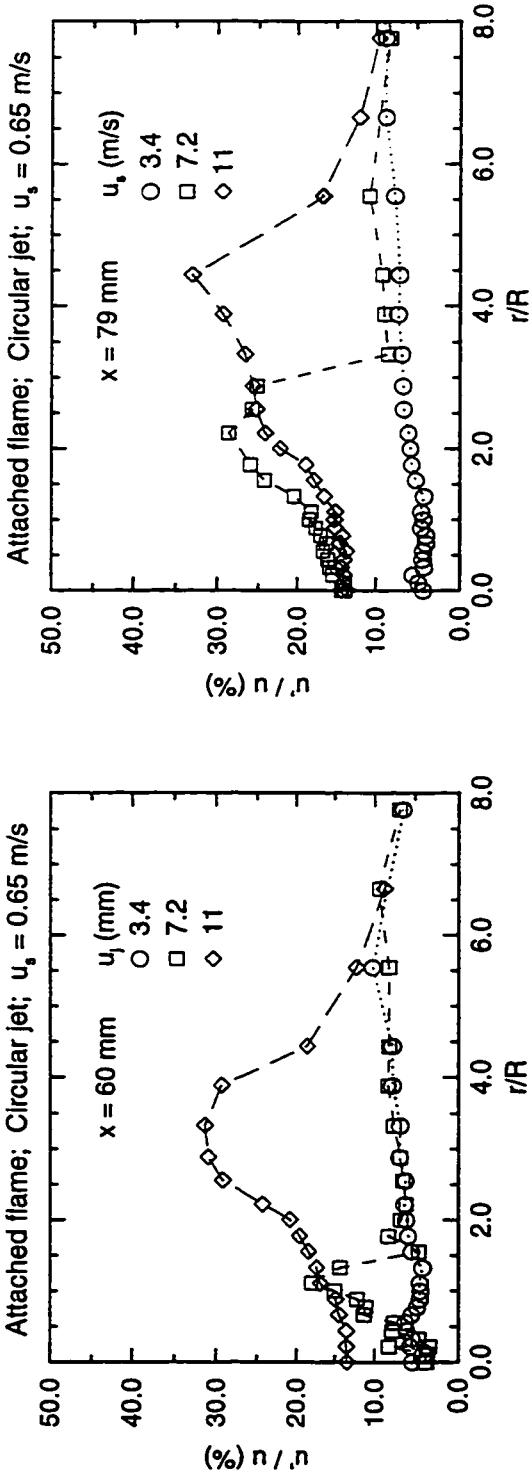

Fig. 5.2.8 Turbulence intensity level profiles within attached flames with different jet discharge velocities (R = 2.29 mm).

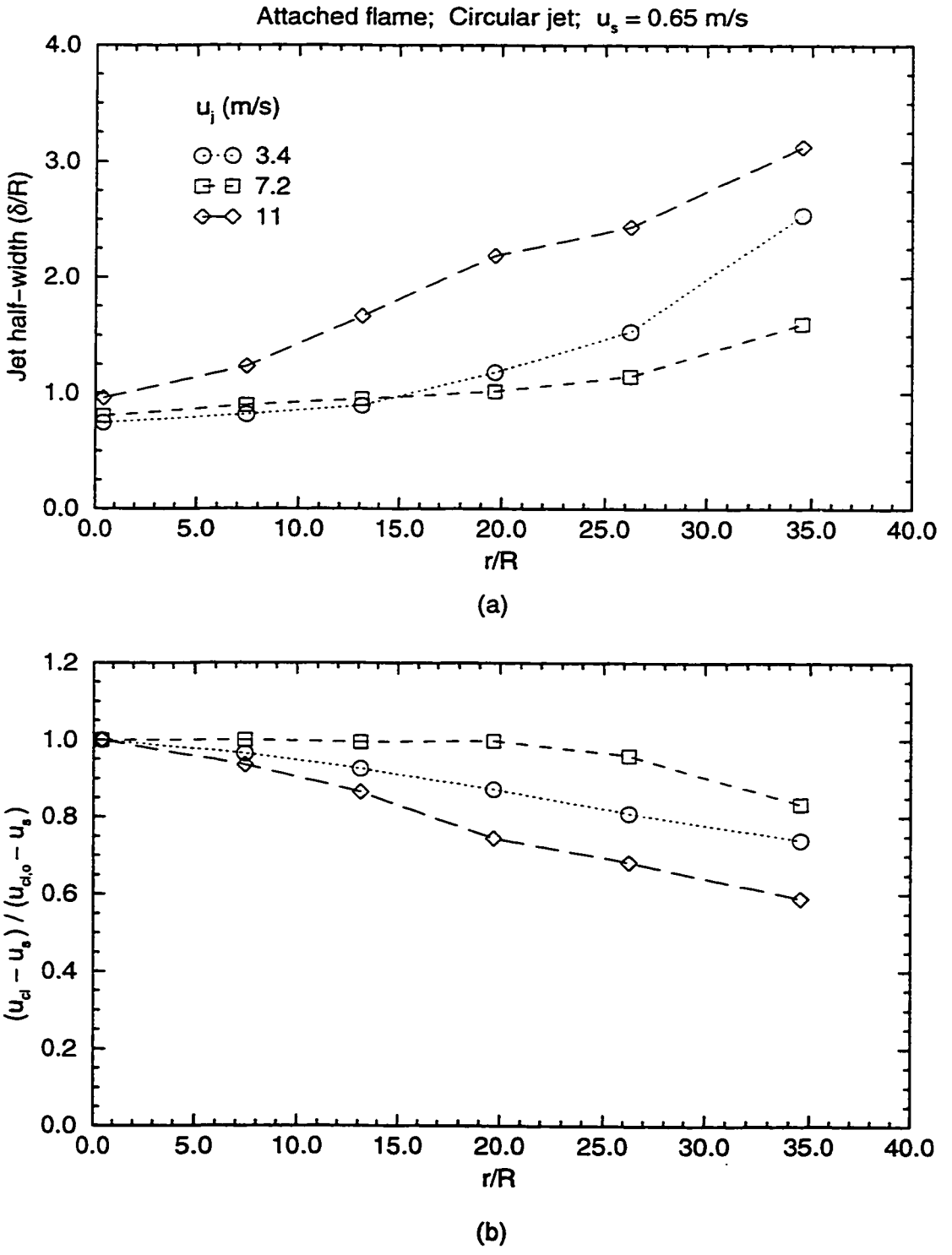

Fig. 5.2.9 A comparison of (a) the jet half–width and (b) the centerline velocity decay with downstream distance in cold jets of different discharge velocities (R = 2.29 mm).

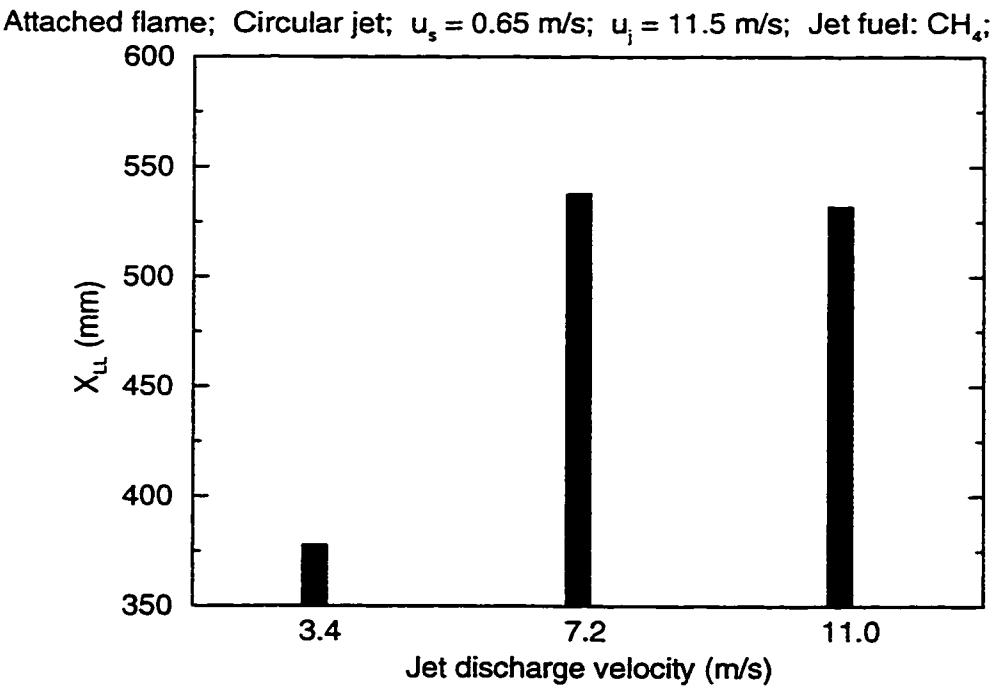

Fig. 5.2.10 The axial distance where the fuel–air concentration equalled the lower flammability limit as a function of the jet discharge velocity for attached flames.

promoted through turbulent air entrainment. A greater jet spread and centerline axial velocity decay was therefore observed for this turbulent jet than for the laminar jets. This is in agreement with the results of gas analysis measurements. The axial position where the fuel concentration at the jet axis is equal to the lean flammability limit, x_{LL}, is shown in Fig. 5.2.10 for attached flames issuing into a co-flowing stream of velocity 0.65 m/s. An increase in the jet velocity from 3.4 m/s to 7.2 m/s increased the axial distance, x_{LL} which is expected since increasing the jet velocity increases the volume of fuel to be mixed with air. However, increasing the jet velocity from 7.2 m/s to 11 m/s marginally decreased x_{LL}, despite the increased volume of fuel discharged, and thus the entrainment of air had increased.

5.3 Effect of Hydrogen Addition

It was discussed previously in Chapter 4 that adding hydrogen to the methane jet improved considerably the blowout limits compared with a pure methane jet (Fig. 4.4.1). The effect of hydrogen addition on the flow structure was investigated for a circular methane flame jet containing 40% by volume hydrogen. A comparison of the jet growth and centerline axial velocity decay for the two different jet fuels is shown in Figs. 5.3.1 (a) and (b). The jet discharge velocity and co-flowing stream velocity were held constant at 3.4 m/s and 1.21 m/s, respectively. A greater jet spread and a faster decay of the centerline axial velocity with downstream distance was observed in the methane-hydrogen jet than in the purely methane jet. The addition of hydrogen substantially increased the density

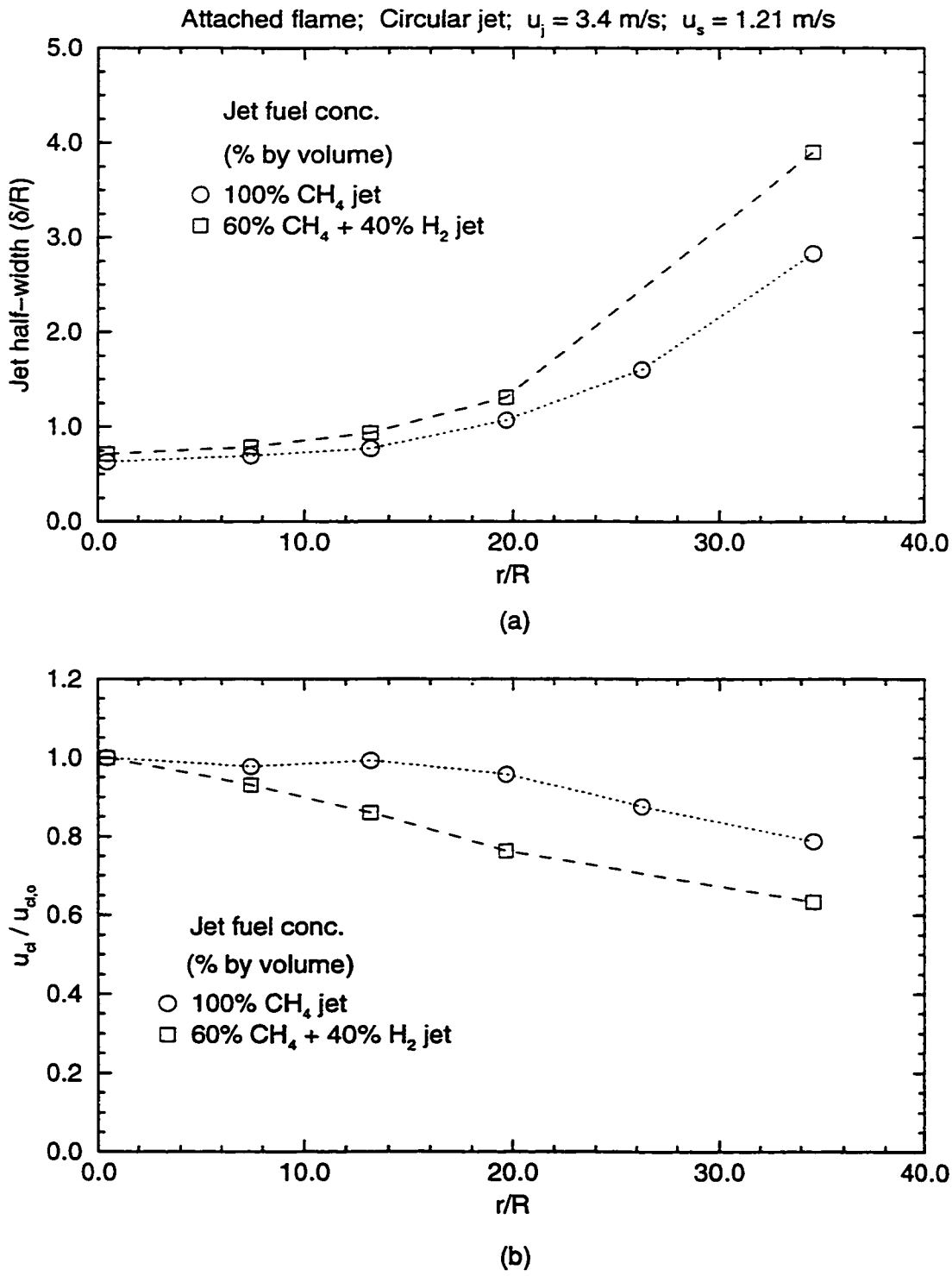

Fig. 5.3.1 A comparison of (a) the jet half–width and (b) the centerline velocity decay with downstream distance for attached flames with different jet fuel compositions.

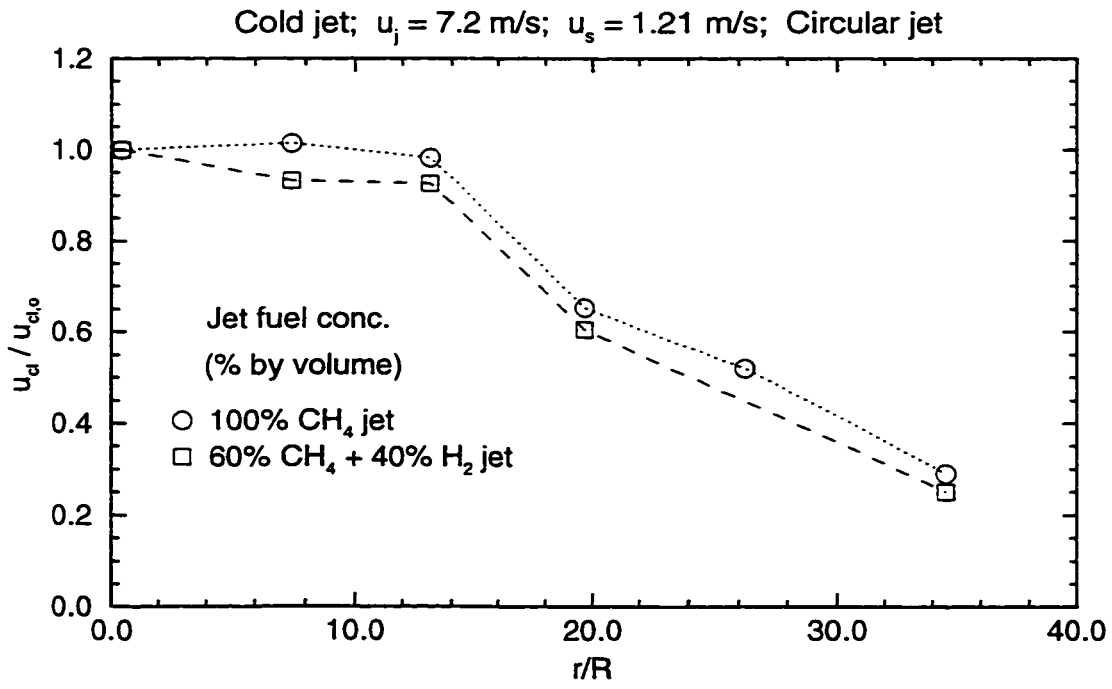

Fig. 5.3.2 A comparison of the jet centerline velocity decay for cold jets of different fuel compositions.

difference (by 37%) between the two co-flowing streams and it was expected that the mixing of the reactants would be promoted. These findings are consistent with those of [64] who conducted experiments on co-flowing cold jets of different densities. The differences in the centerline velocity decay is much less evident for these jets in the absence of a flame (Fig. 5.3.2). The corresponding time-averaged axial and radial velocity profiles from which the data were obtained are attached in Appendix III.

5.4 Effect of Auxiliary Methane in the Co-flowing Air Stream

It was discussed earlier (Chapter 4) that an addition of a fuel to the air stream affects significantly the blowout limits of jet diffusion flames; therefore, the effect of an addition of methane to the co-flowing stream on the flow structure within a flame was investigated for a circular jet flame using laser Doppler velocimetry measurements. To avoid the occurrence of flashback in the co-flowing stream, the auxiliary methane was employed at relatively small concentrations (up to 5.2 % by volume). The axial velocity profiles of a methane flame in a co-flowing stream of air premixed with methane of concentrations of 2 and 5.2% by volume are shown in Fig. 5.4.1. The jet and co-flowing stream velocities were 3.4 and 1.21 m/s, respectively. A higher concentration of methane in the co-flowing air resulted in higher axial velocities within the jets especially at higher r/R ratios. Moreover, the jet spread and centerline velocity were higher in a co-flowing stream with higher auxiliary fuel concentrations as shown in Figs. 5.4.2 (a) and (b). However, the significantly greater shift in the flammability envelopes radially outward in the direction of smaller flow velocities (as discussed in Chapter 4) offsets the detrimental effect of an increase in the axial velocities on the stability of diffusion flames and allows for flame stabilization to occur at higher mean jet discharge velocities.

5.5 Effect of a Diluent in the Co-flowing Air Stream

The effect of the introduction of a diluent - carbon dioxide - into the surrounding air stream on the flow structure of attached flames was investigated. A methane-hydrogen

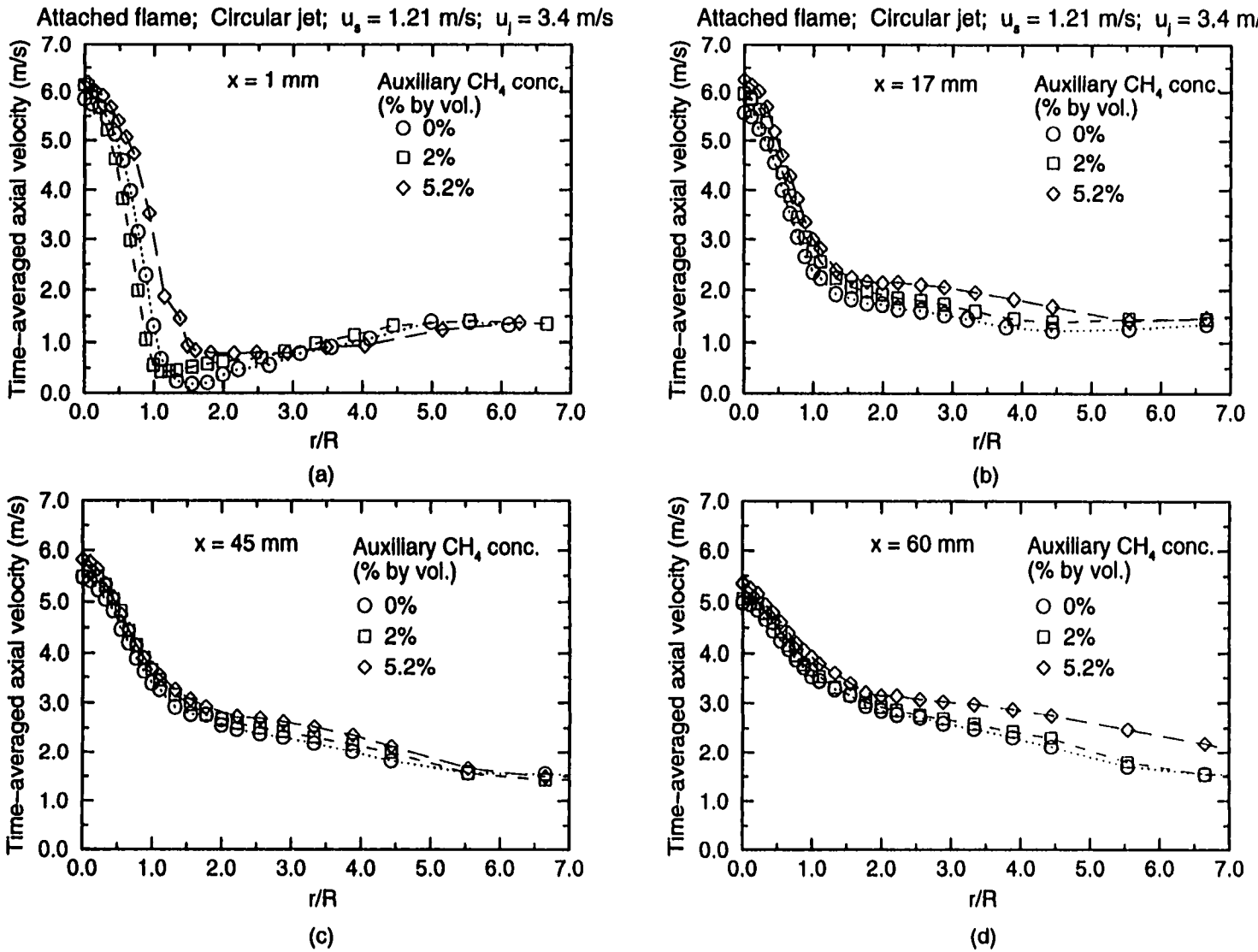

Fig. 5.4.1 Time-averaged axial velocity profiles within jets issuing into a co-flowing stream of air premixed with methane (R = 2.29 mm).

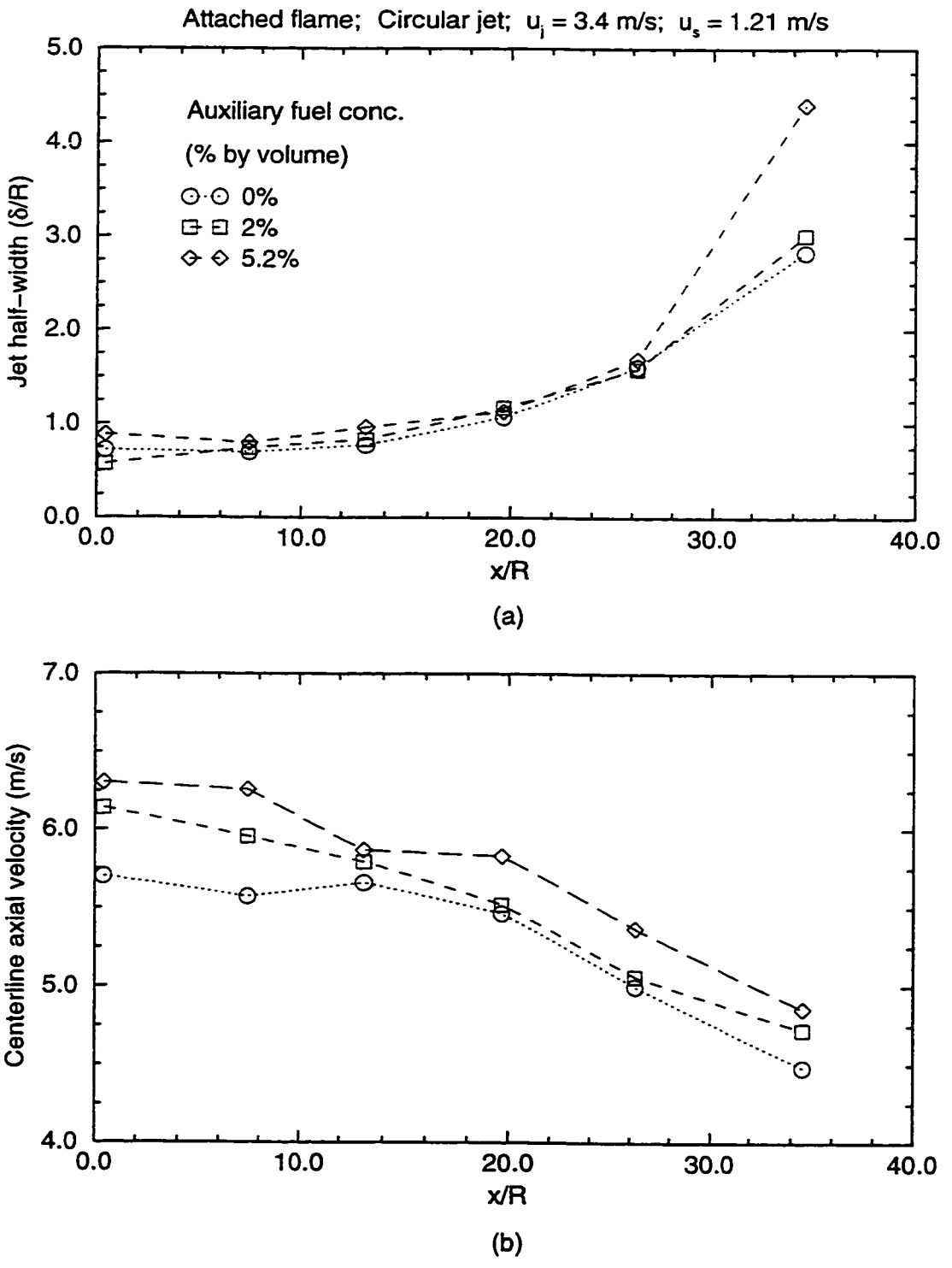

Fig. 5.4.2 A comparison of (a) the jet half–width and (b) the centerline velocity with downstream distance in attached flames immersed in an air stream premixed with auxiliary methane (R = 2.29 mm).

mixture (60% CH_4 + 40% H_2 by volume) was used as a jet fluid. The jet discharge velocity and co-flowing stream velocity were held constant at 7.2 and 1.21 m/s, respectively, and the concentration of CO_2 in the co-flowing air stream was 3% (by volume). A comparison of the axial velocity profiles at downstream distances of $x \leq 79$ mm for an attached flame issuing into a pure air stream and an air-CO_2 mixture stream is shown in Fig. 5.5.1. It can be seen that there is very little difference in the two profiles throughout the measurement range despite the slightly increased density difference between the jet and surrounding stream. This holds true also for the turbulence intensity profiles as seen in Fig. 5.5.2. The significant reduction in the blowout limits for a fuel jet in an air-CO_2 stream observed in the study of Wierzba et al. [11] is, therefore, most likely the primary result of the reduction of oxygen entrained into the jet as well as the decrease in the burning velocity and flammability limits of the fuel-air-diluent mixture within the jet.

5.6 Effect of Jet Nozzle Ellipticity

As discussed earlier, a small change in the ellipticity of the jet (from a/b = 1.38 to 1.60) resulted in significant changes in the blowout limits of attached flames; therefore, tests were conducted on cold and ignited jets to investigate the effect of the jet aspect ratio on the jet flow structure in an attempt to explain the observed trends for the blowout limits.

5.6.1 Cold jet

LDV measurements reveal that, in general, the effect of the nozzle geometry on the

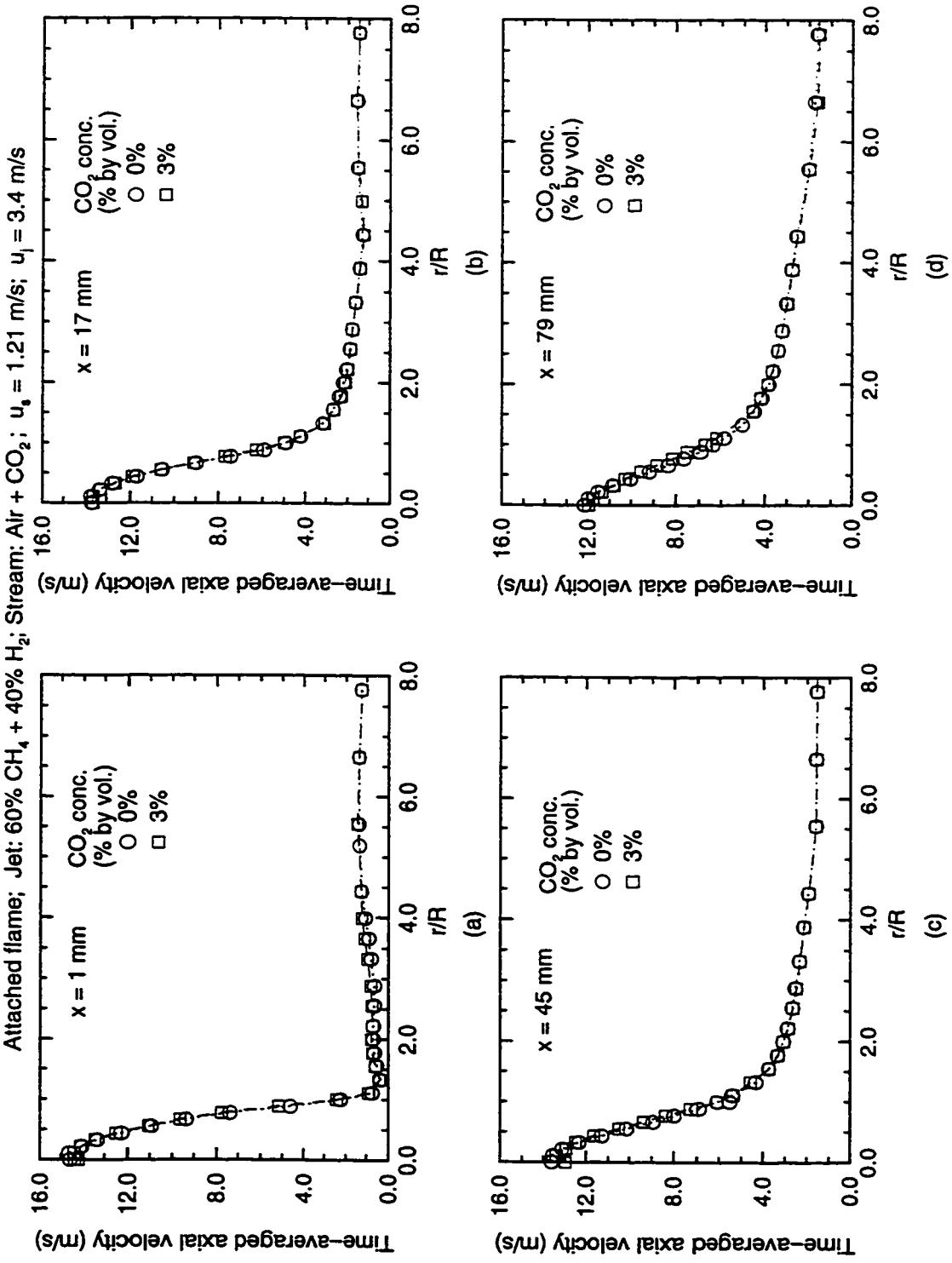

Fig. 5.5.1 Time–averaged axial velocity profiles within attached flames in a co–flowing stream of air premixed with carbon dioxide (R = 2.29 mm).

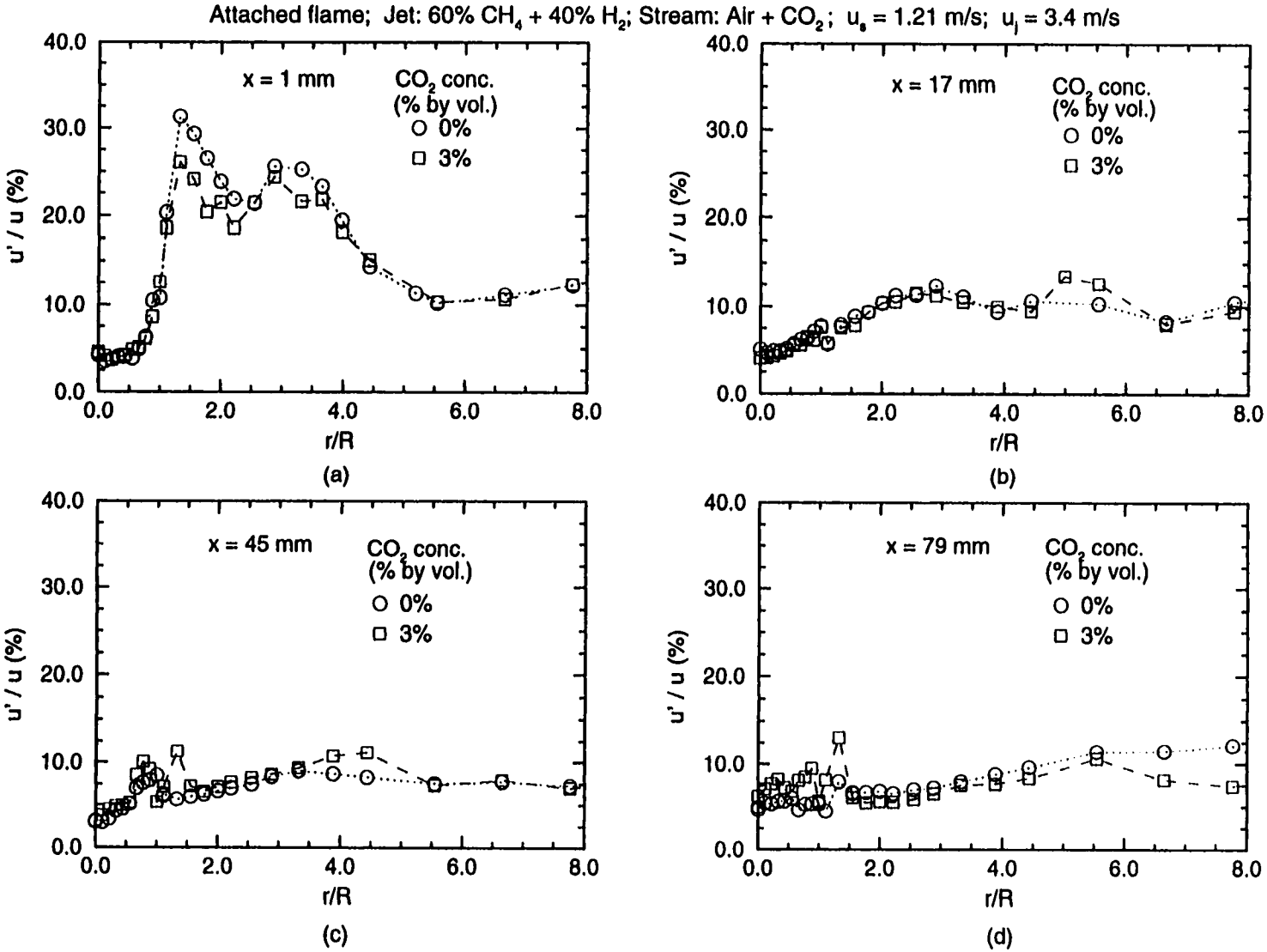

Fig. 5.5.2 Turbulence intensity profiles within attached flames in a co-flowing stream of air premixed with carbon dioxide (R = 2.29 mm).

flow structure within a cold jet occurred primarily in the region relatively close to the nozzle. The time-averaged axial and radial velocity profiles established at different downstream distances for jets with two different aspect ratios, a/b, of 1.38 and 1.50 are shown in Figs. 5.6.1 and 5.6.2. A co-flowing stream velocity, u_s, of 0.65 m/s corresponded to the region of lifted flame blowout and the jet discharge velocity, u_j , was 7.2 m/s. R_{eq} is the equivalent radius, defined as $(a \cdot b)^{1/2}$ where a is the major axis half-width and b is the minor axis half-width. It can be seen that at greater downstream distances ($x > 30$ mm), the jet width did not increase as significantly in the major axis as it did in the minor axis. This was also indicated by the small, and frequently negative, radial velocities in the major axis plane while the radial velocities in the minor axis plane were always positive and several times higher than those in the major plane (Figs. 5.6.3 and 5.6.4). As a result, the jet expanded faster and eventually became wider in the minor plane than in the major plane at a certain downstream distance from the nozzle and the jet appeared to have switched the orientation of its cross-section, i.e., axis-switching had occurred. At a distance of 60 mm, the axial velocity profiles were almost identical for the jets of two different aspect ratios.

The corresponding turbulence intensity level profiles for these elliptic jets are shown in Figs. 5.6.5 and 5.6.6. In general, a higher peak turbulence intensity level was observed in the minor axis plane than in the major axis plane. At axial distances up to 45 mm, the turbulence level profiles of the 1.38 and 1.60 aspect ratio jets were very different. At a further downstream distance of 60 mm, the turbulence intensity profiles in both of the elliptic jets became similar. The time-averaged jet axial and radial velocity profiles and jet

growth were also very similar at this downstream distance. Therefore, a change in the nozzle aspect ratio did not seem to have a considerable effect on the flow field at these downstream distances. Since at this co-flowing stream velocity, the flame (just before blowout) stabilized at a considerable distance from the nozzle for all of the different nozzles employed, changes in the nozzle geometry would not affect significantly the blowout limits of lifted flames as was established experimentally.

The axis-switching phenomenon in these elliptic jets can also be seen in Fig. 5.6.7 in which the jet half-width is plotted as a function of the dimensionless downstream distance, x/R_{eq}. The jet growth of the circular jet is also shown for comparison. In general, the growth of the elliptic jet in the minor axis was faster than the growth of the circular jet, which, in turn, was greater than that in the major axis of the elliptic jet. In both the 1.38 and 1.60 aspect ratio jets, axis-switching occurred at a downstream distance, x/R_{eq} , between 15 and 21.

Effect of the Co-flowing Stream Velocity. An increase in the co-flowing stream velocity from 0.65 m/s to 1.21 m/s for the same discharge velocity of 7.2 m/s had a mitigating effect on the rate of jet spread especially at greater downstream distances for the nozzles employed as shown in Fig. 5.6.8. The effect of the co-flowing stream velocity on the jet half-width of the circular jet is also included for comparison. The corresponding axial velocity profiles from which the data were obtained for a co-flowing stream velocity of 1.21 m/s are attached in Appendix VI. At the stream velocity of 1.21 m/s, the rate of jet spread in the major axis of the elliptic jets was approximately the same as that in the circular jet.

Effect of the Jet Discharge Velocity. The effect of the jet discharge velocity on the axial velocity profiles within elliptic jets at a co-flowing stream velocity of 0.65 m/s are shown in Fig. 5.6.9 at downstream distances of 1.0 and 30 mm for jet discharge velocities of 7.2 and 11 m/s. The profiles in the plane of the minor axis of elliptic jets were parabolic in nature (like those for the circular jet) while those along the major axis were more of a "top-hat" profile especially for higher values of jet aspect ratios and jet velocities (e.g., a/b = 1.60 at u_j = 11 m/s). At a discharge velocity of 11 m/s, the maximum axial velocities occurred near the boundary of the jet (and not at the jet axis) in the major axis plane of both jets. Although this off-axis peak resulted in a significant increase in the velocity gradient, it did not appear to affect the lift-off velocity of these nozzles (Fig. 4.3.3) (In comparison, the lift-off velocities of the nozzles of Type 1 were significantly affected by the nozzle aspect ratio). The initially larger differences in the velocity profiles in the major and minor axis planes at x = 1 mm became very similar at a distance of 30 mm especially for the higher jet discharge velocity.

The effect of the jet discharge velocity is compared for 3.4 and 7.2 m/s at a higher co-flowing stream velocity of 1.21 m/s (Fig. 5.6.10). The jet spread of the minor axis was substantially decreased and the onset of axis-switching was delayed for the jet with an aspect ratio of 1.60.

The presence of a flame can significantly change the flow characteristics of elliptic jets as in the case for circular jets. The axial and radial velocity profiles for cold and

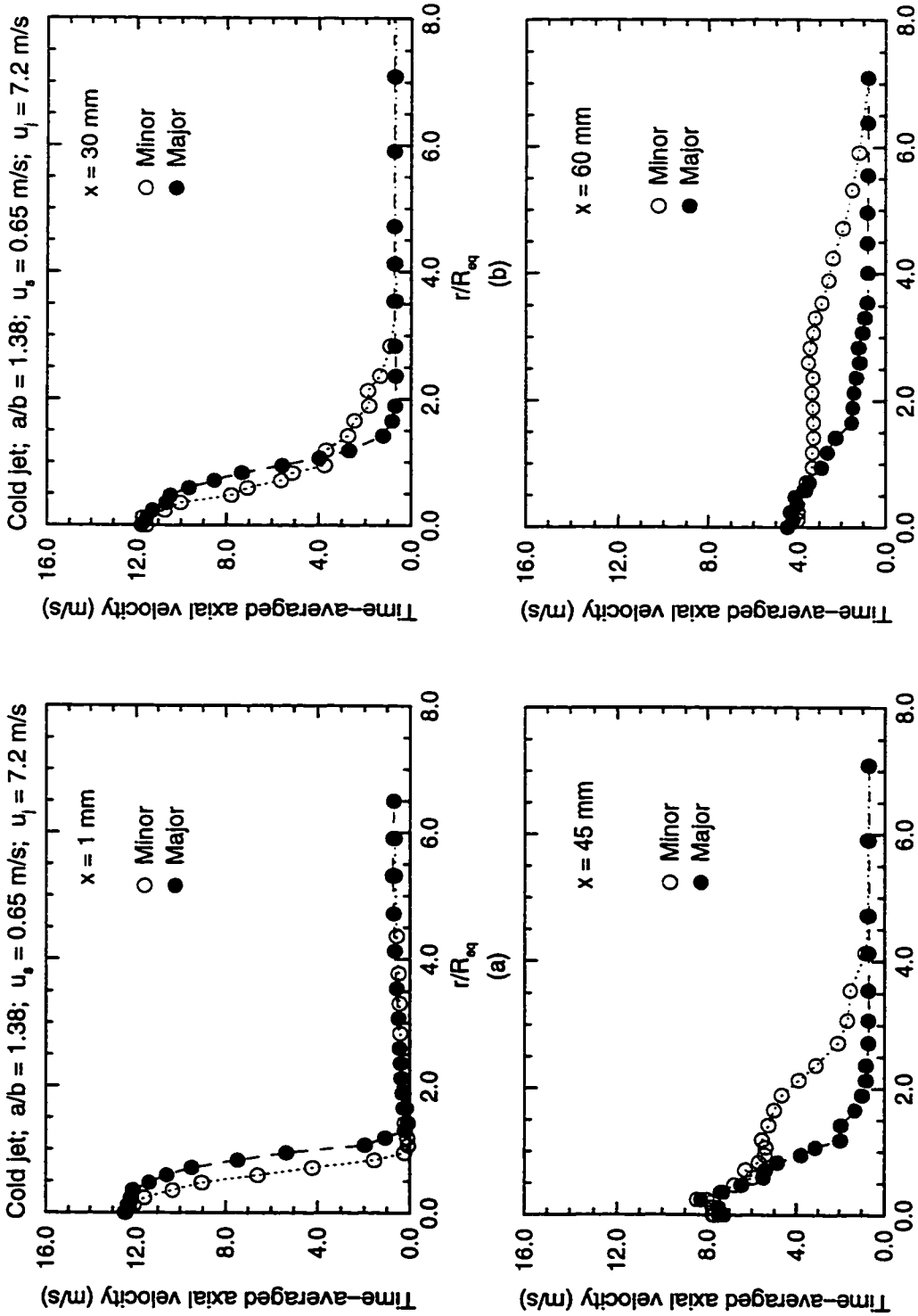

Fig. 5.6.1 Time–averaged axial velocity profiles within a cold jet of aspect ratio 1.38 (R_{eq} = 2.15 mm).

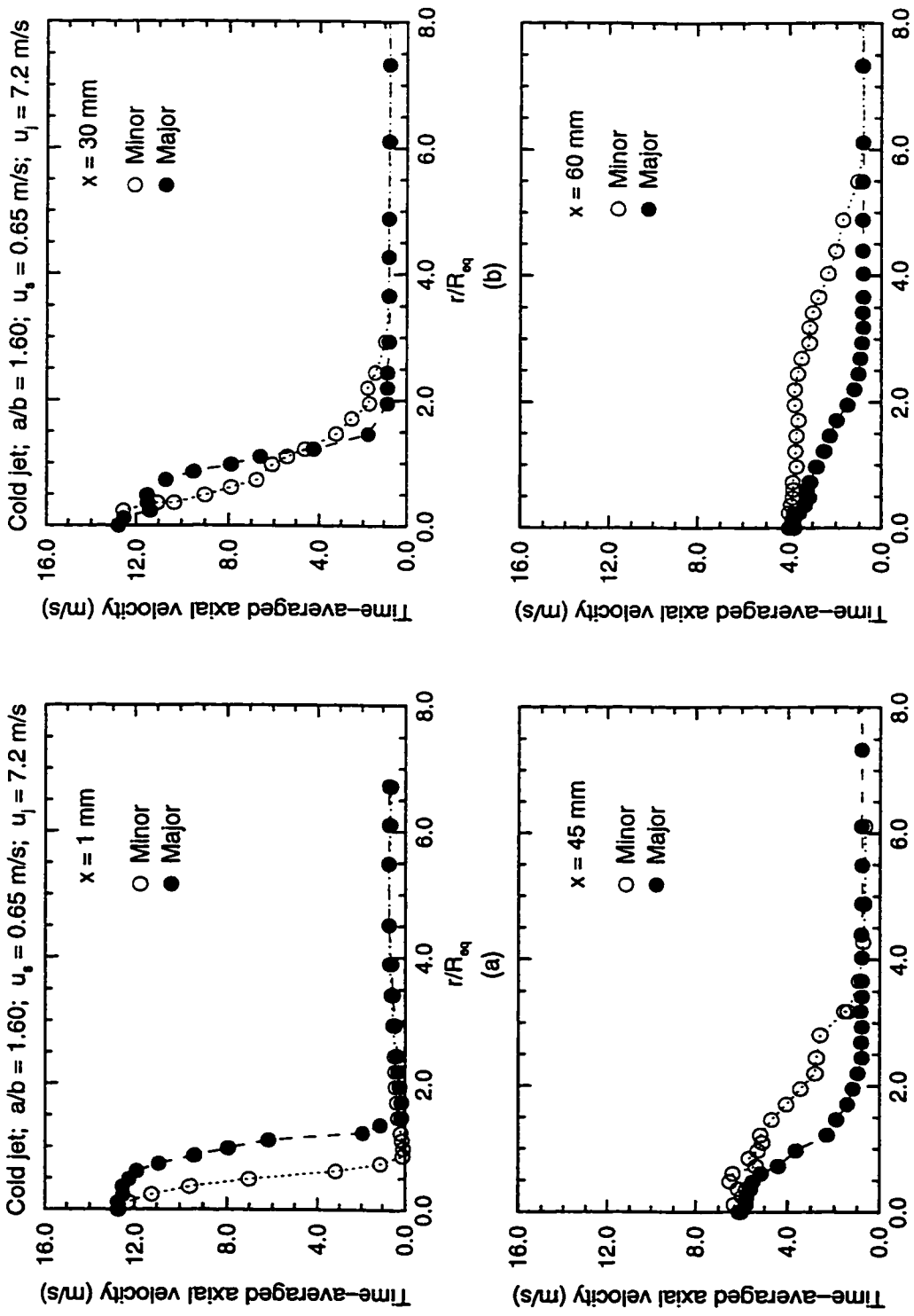

Fig. 5.6.2 Time–averaged axial velocity profiles within a cold jet of aspect ratio 1.60 (R_{eq} = 2.08 mm).

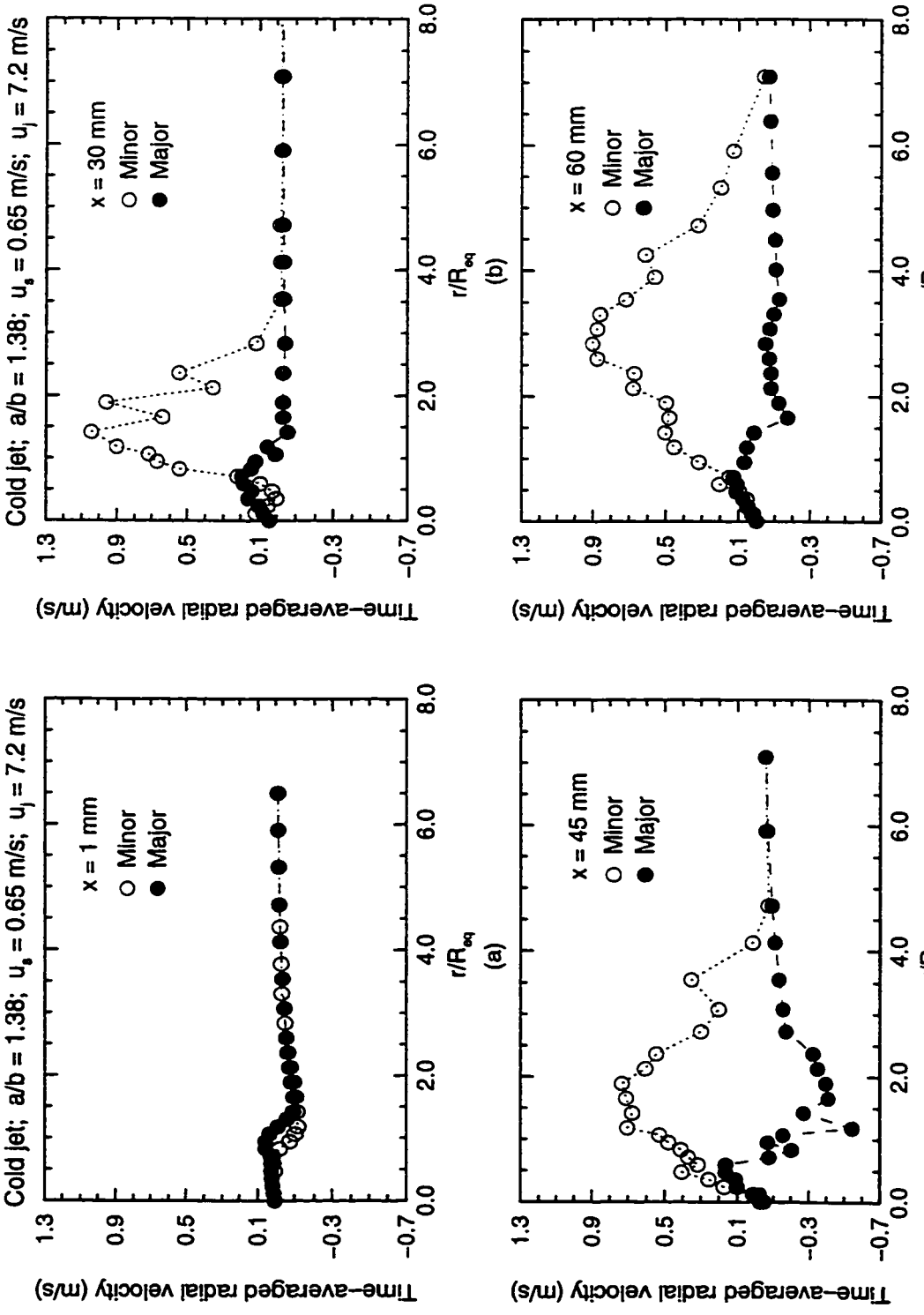

Fig. 5.6.3 Time–averaged radial velocity profiles within a cold jet of aspect ratio 1.38 (R_{eq} = 2.15 mm).

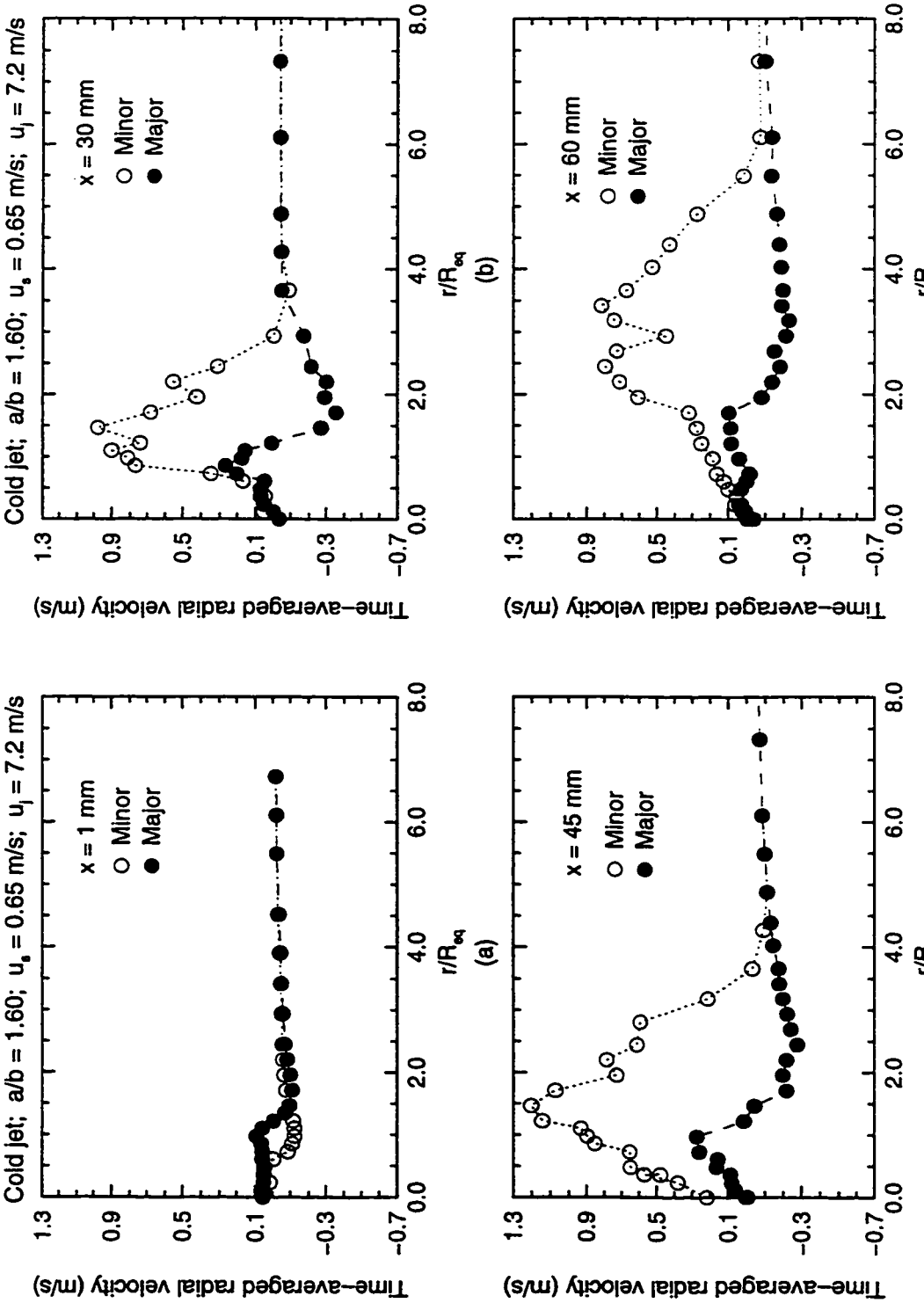

Fig. 5.6.4 Time–averaged radial velocity profiles within a cold jet of aspect ratio 1.60 (R = 2.08 mm).

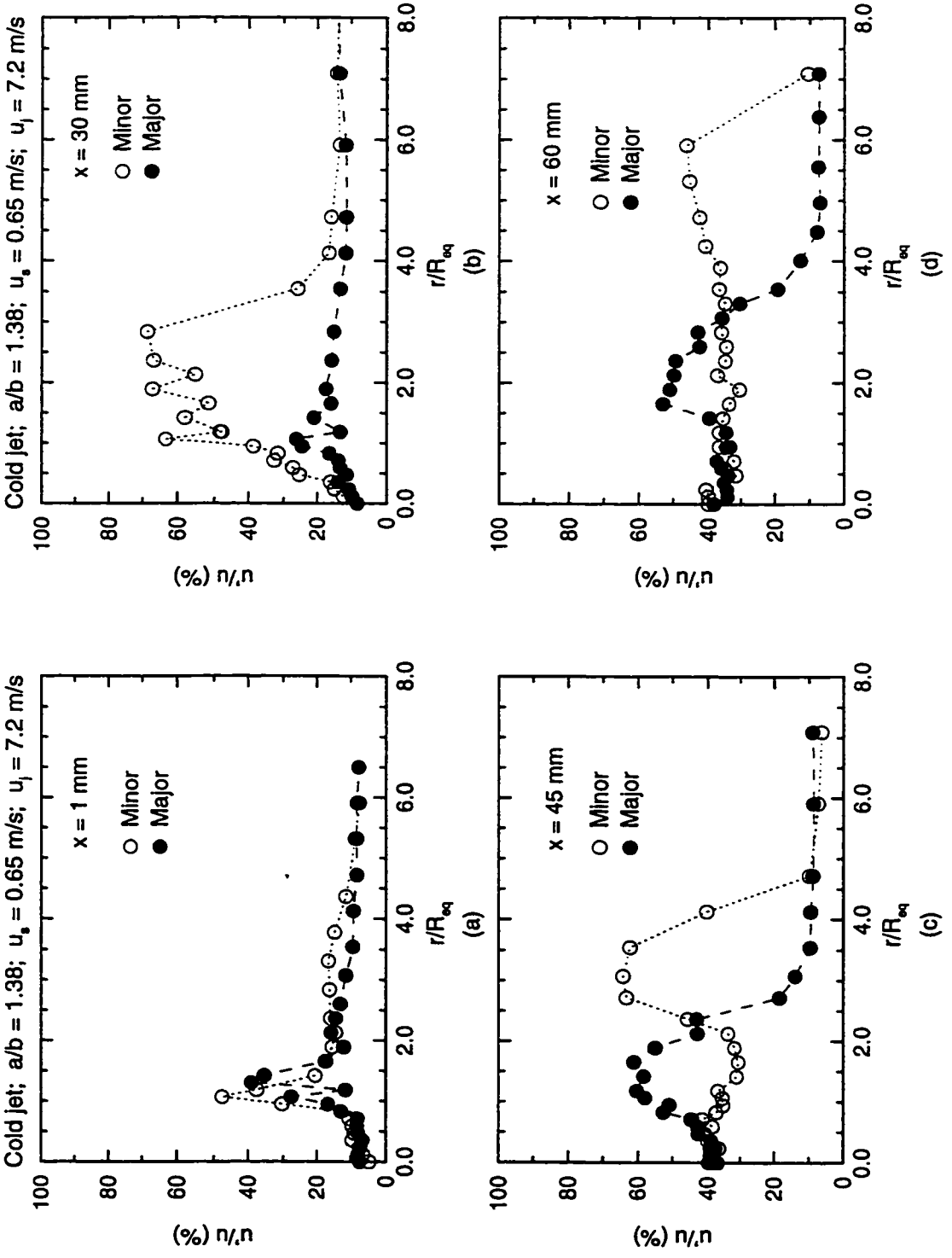

Fig. 5.6.5 Turbulence intensity profiles within a cold jet of aspect ratio 1.38 (R_{eq} = 2.15 mm).

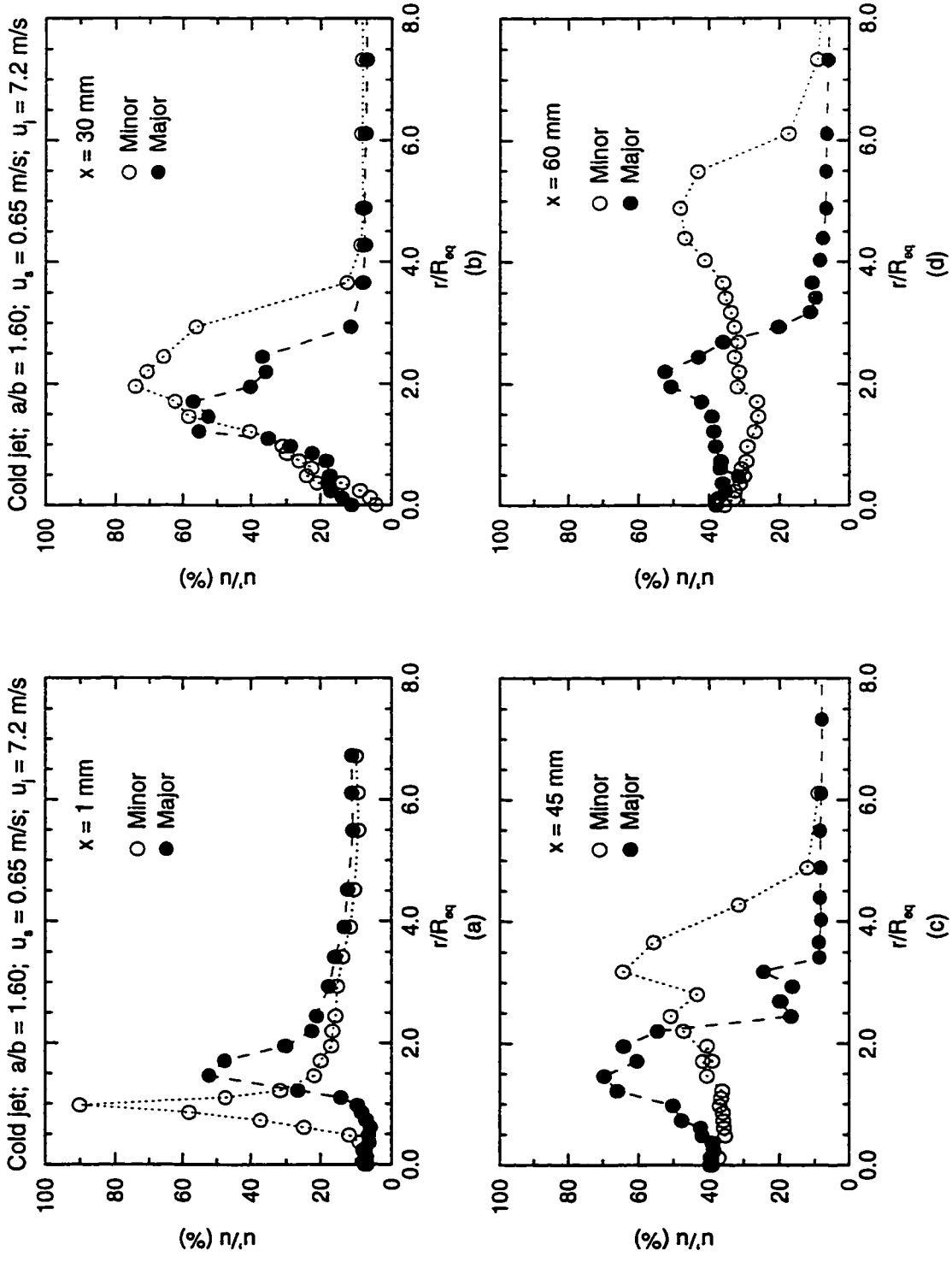

Fig. 5.6.6 Turbulence intensity profiles within a cold jet of aspect ratio 1.60 (R_{eq} = 2.08 mm).

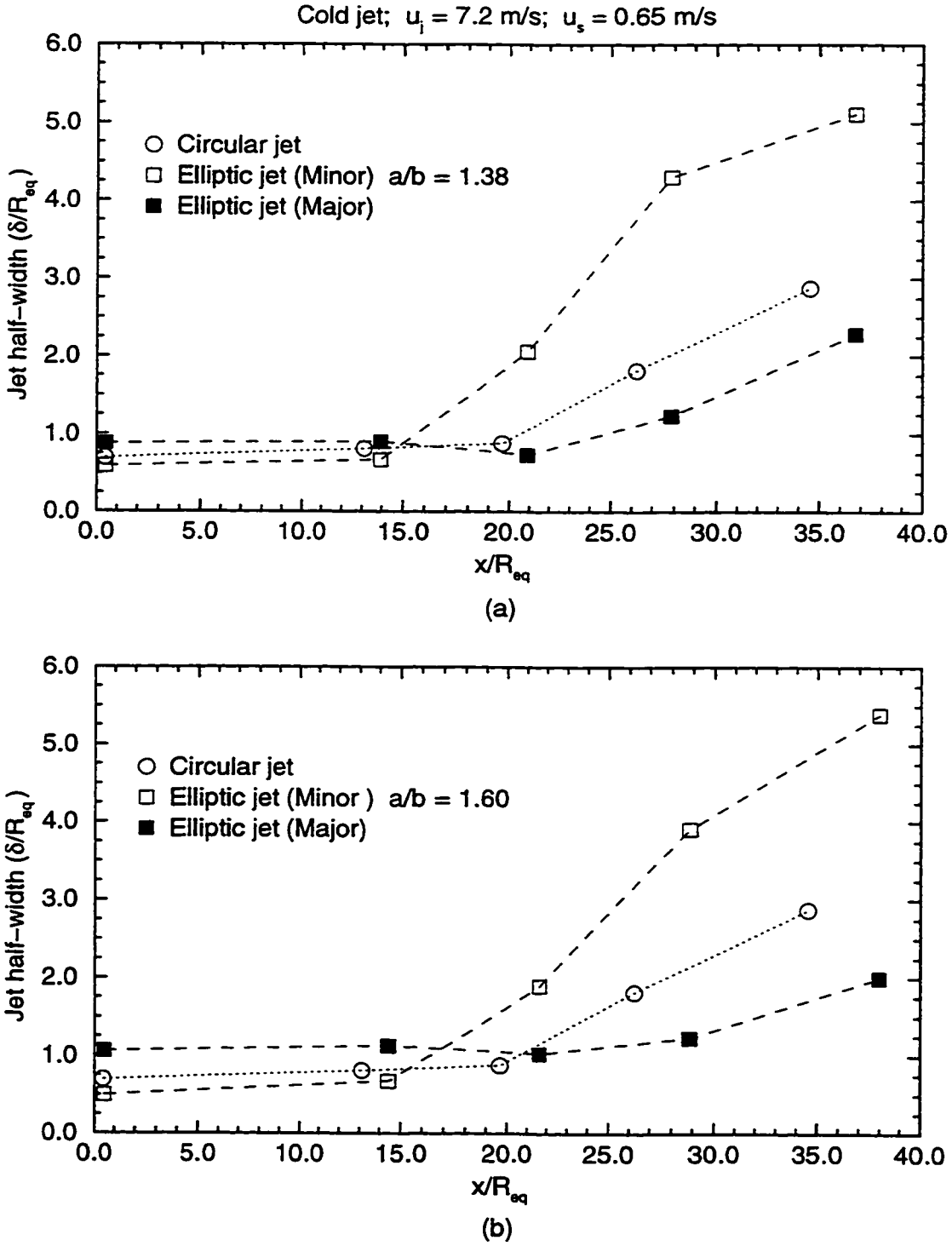

Fig. 5.6.7 A comparison of the jet half–width of circular and elliptic jets with an aspect ratio of (a) 1.38 and (b) 1.60.

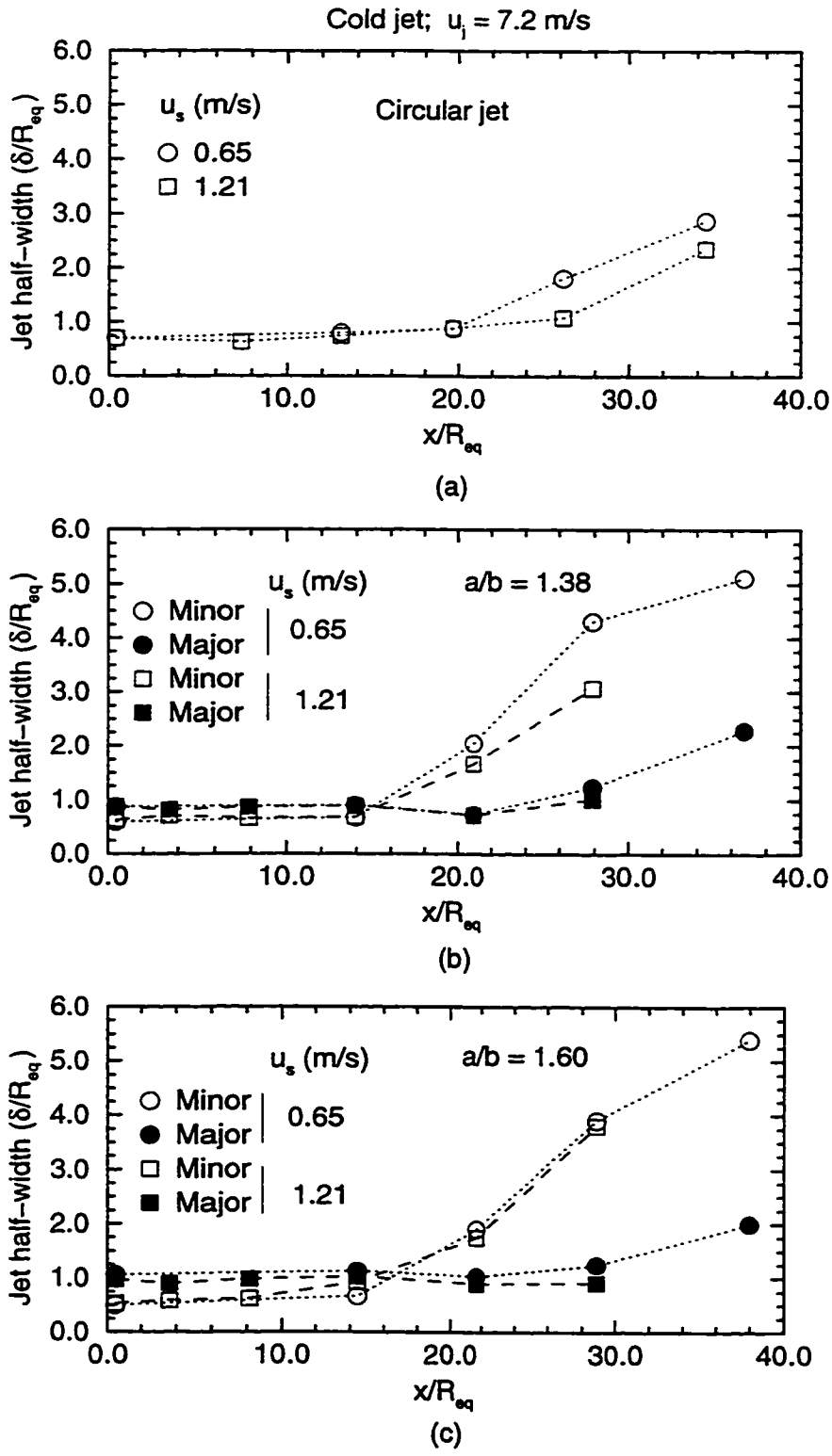

Fig. 5.6.8 A comparison of the jet half–width within cold jets with an aspect ratio of (a) 1.0, (b) 1.38, and (c) 1.60 in a co–flowing stream of different velocities.

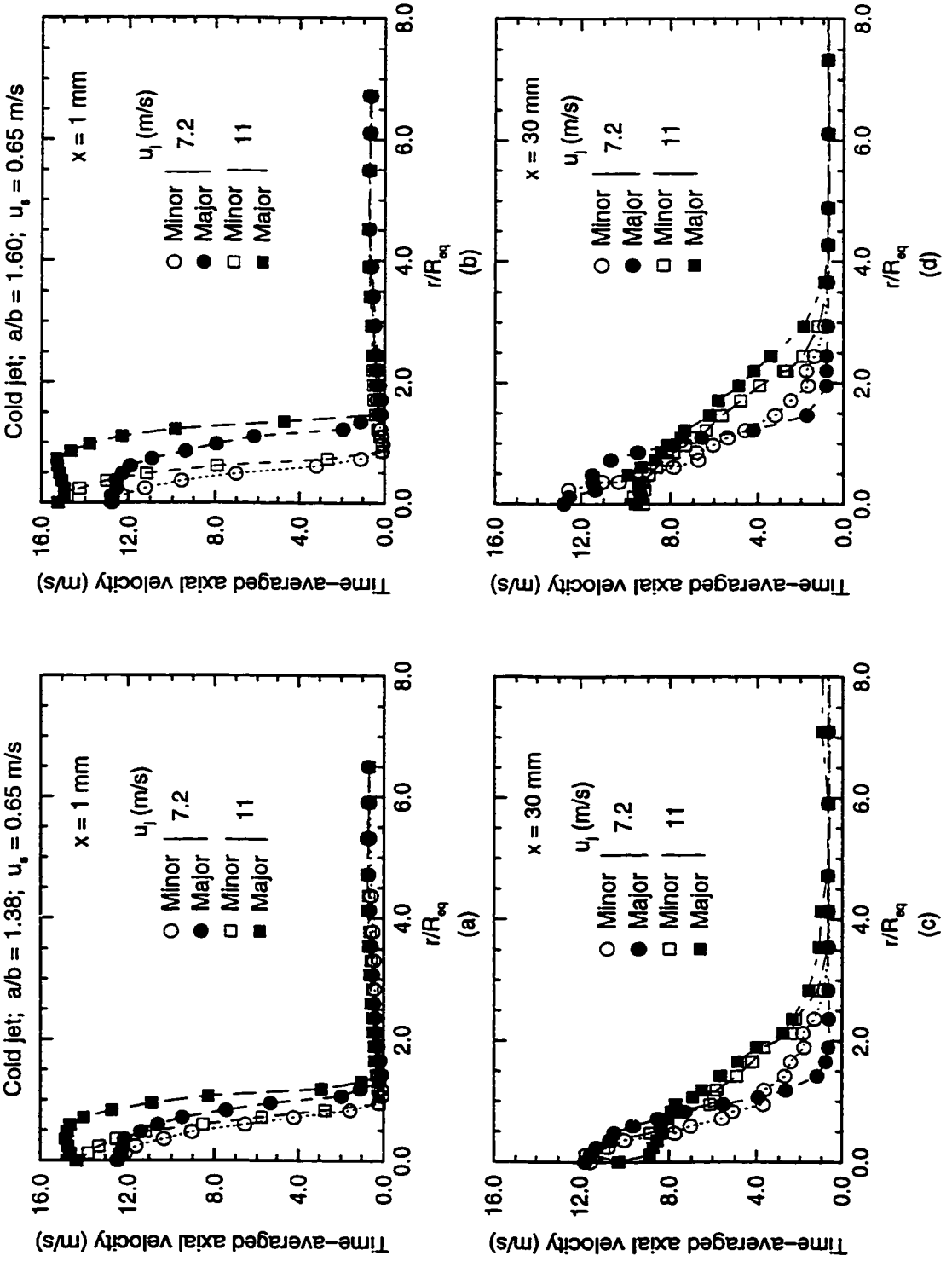

Fig. 5.6.9 Time–averaged axial velocity profiles within cold jets of different aspect ratios with different discharge velocities.

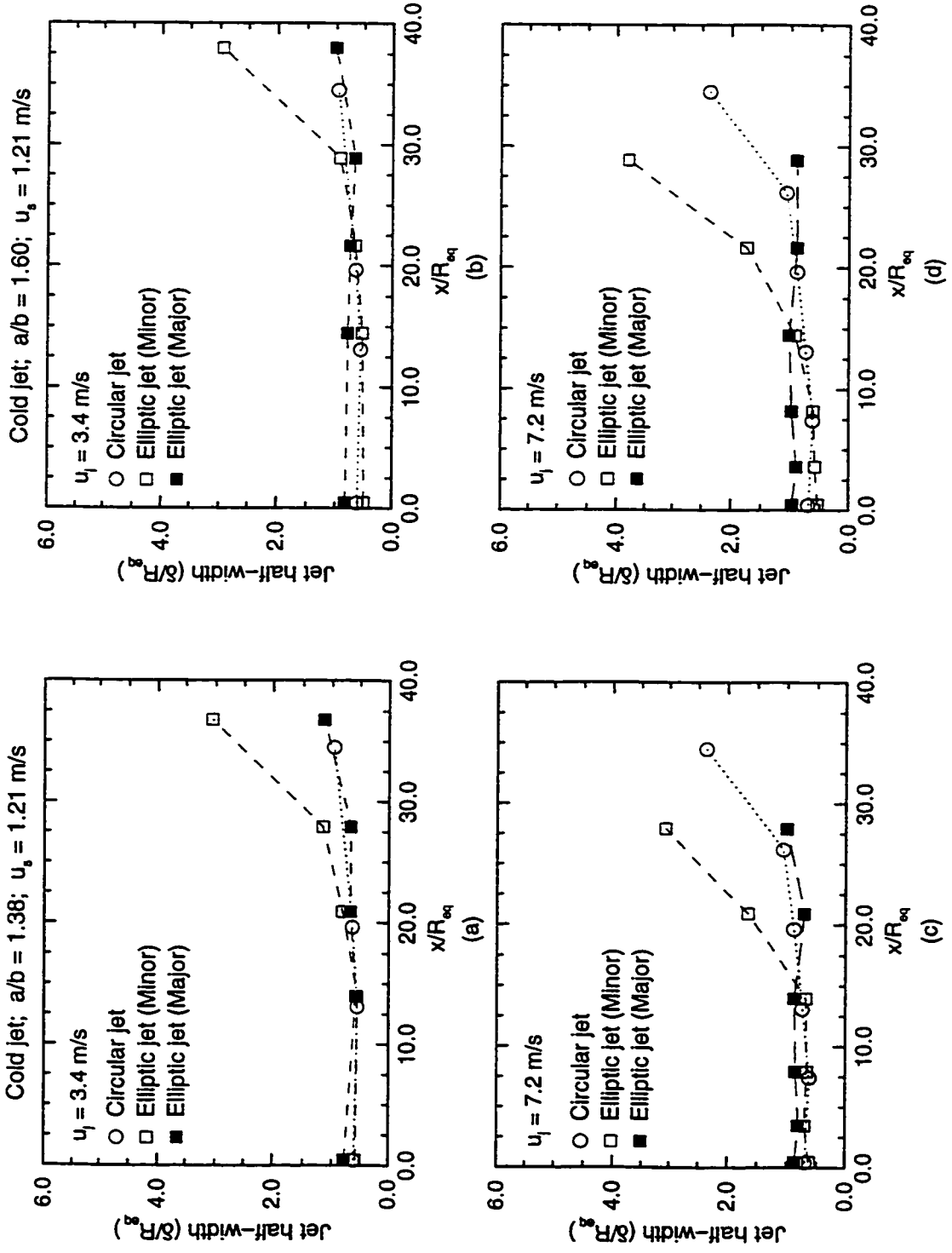

Fig. 5.6.10 A comparison of the jet half-width of elliptic jets with an aspect ratio of (a), (c) 1.38, and (b), (d) 1.60 with different discharge velocities.

ignited jets with a discharge velocity of 7.2 m/s in a co-flowing stream of velocity 0.65 m/s are shown in Figs. 5.6.11 to 5.6.14. The effect of the presence of the flame on the axial velocity values was relatively small at downstream distances of 1 and 30 mm. At higher distances, i.e., x = 45 and 60 mm, the axial velocities in the inner region of the flame were several times higher than those for cold jets. The radial profiles for the cold jet and in the presence of a flame differed significantly especially at larger downstream distances with, generally smaller radial velocities in the ignited jets. The radial velocities for an ignited jet of 1.38 aspect ratio were approximately the same and very low in both the major and minor planes. These profiles differed significantly from those for the jet of aspect ratio 1.60 especially with respect to the radial velocities in the minor axis plane, which were much higher.

The turbulence intensity level profiles for both elliptic jets are compared in Figs. 5.6.15 and 5.6.16. The turbulence intensity profiles were very similar for jets of both aspect ratios except at a downstream distance of 30 mm, where approximately axis-switching for the 1.38 aspect ratio jets was taking place. As in the case for circular jets, the intensity of turbulence in the direction of both the minor and major axes planes was lower within flames than that in cold jets. For example, the maximum turbulence intensity decreased from 63% in a cold flow to 22% in a reacting flow for a jet with aspect ratio 1.38 as shown in Fig. 5.6.18 (c) (x = 45 mm). This is in agreement with observations reported in literature on large jets in a quiescent environment. Browand and Ho [96] reported that a large part of the fluctuating velocity was contributed by the large coherent structures

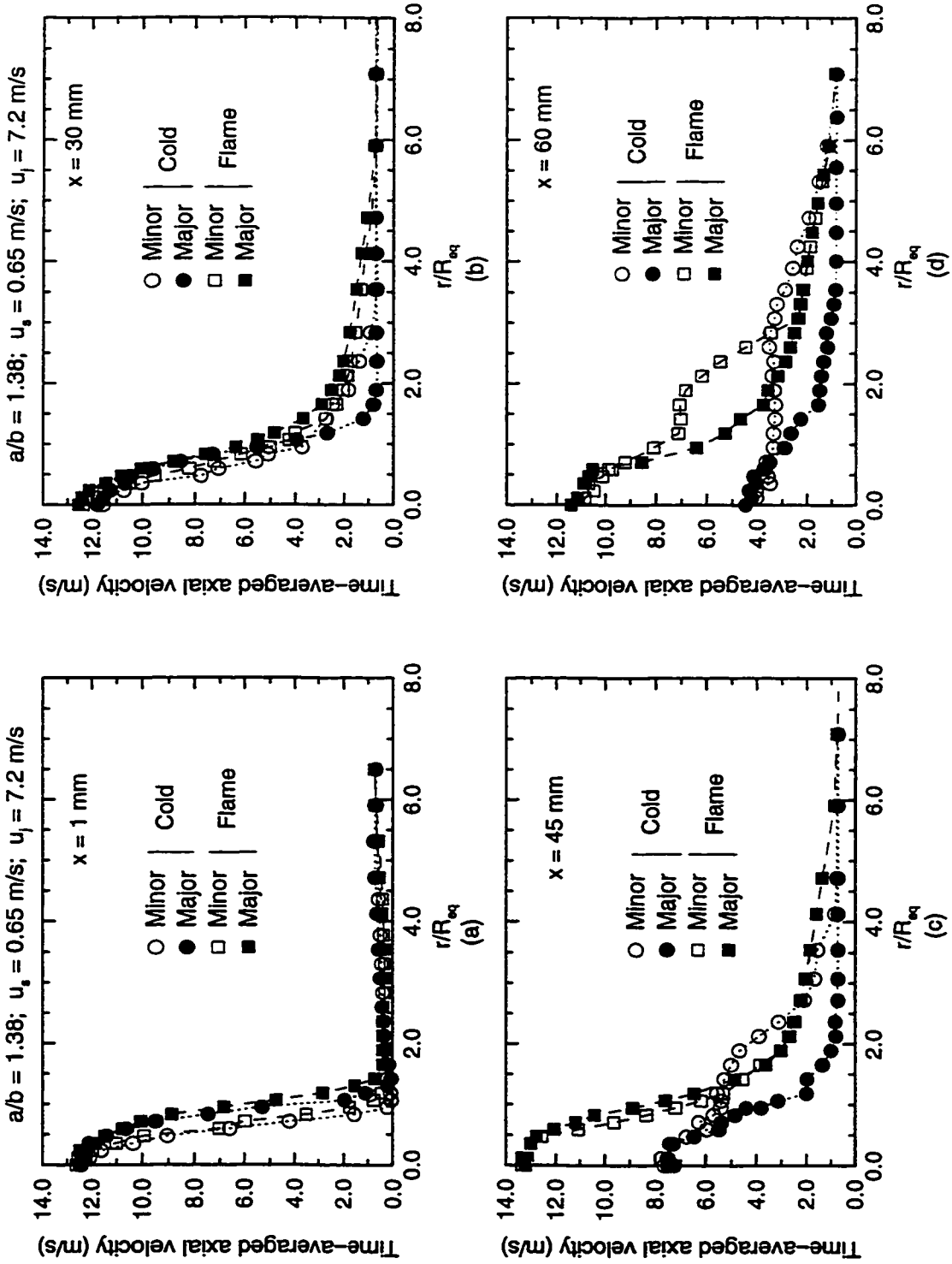

Fig. 5.6.11 Time-averaged axial velocity profiles within cold jets and attached flames with an aspect ratio of 1.38 (R_{eq} = 2.15 mm).

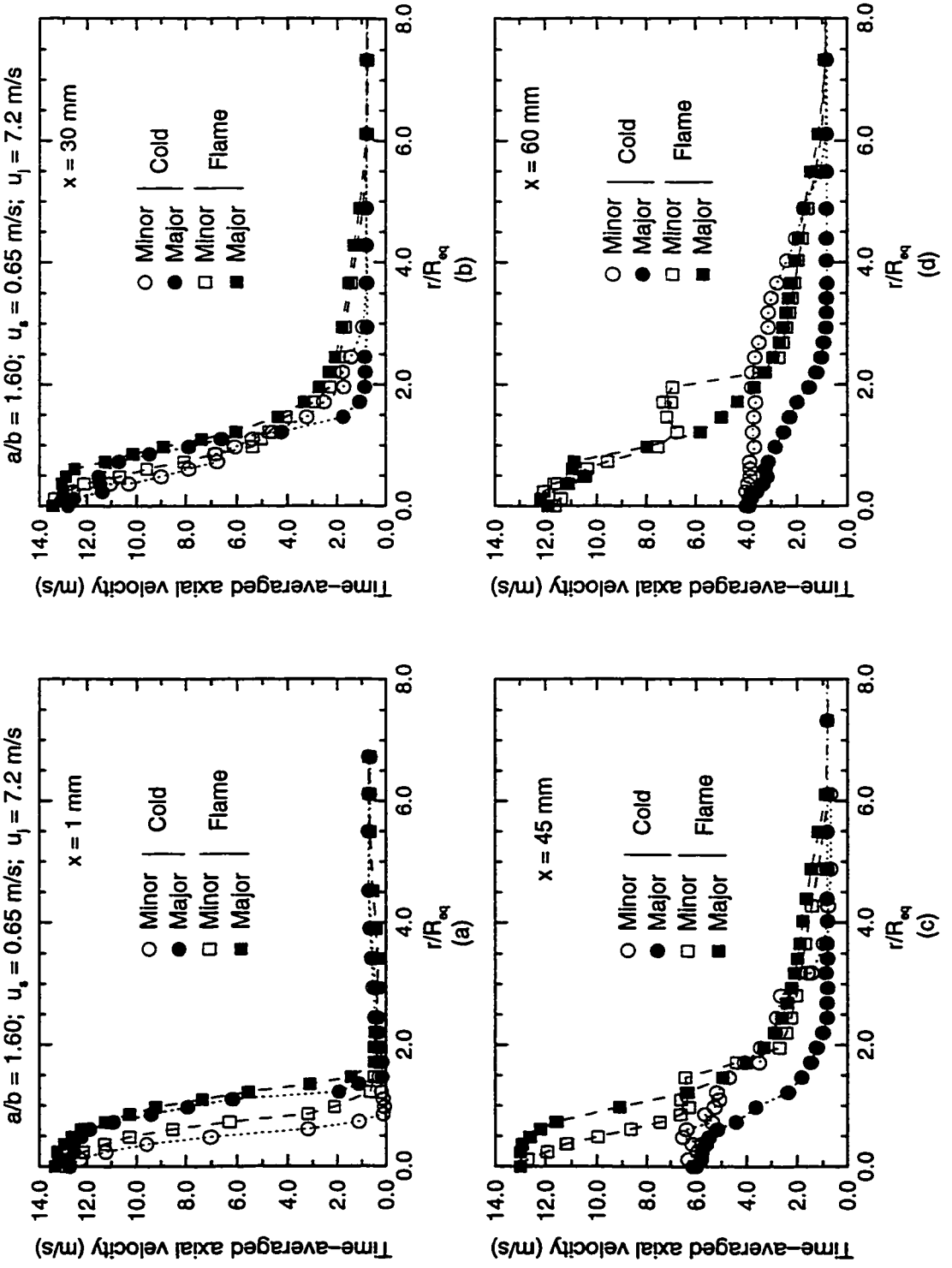

Fig. 5.6.12 Time-averaged axial velocity profiles within cold jets and attached flames with an aspect ratio of 1.60 (R_{eq} = 2.08 mm).

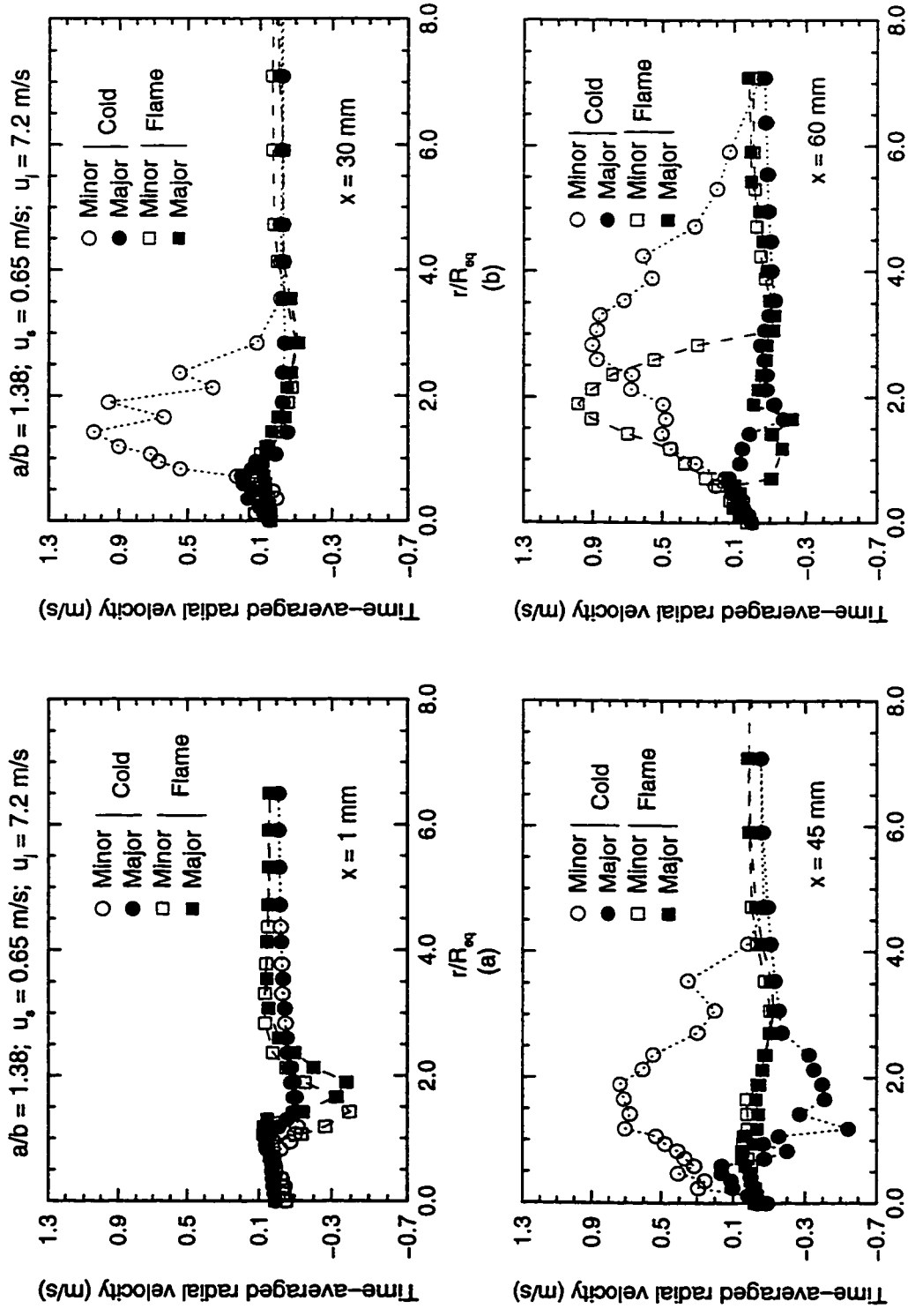

Fig. 5.6.13 Time–averaged radial velocity profiles within cold jets and attached flames with an aspect ratio of 1.38 (R_{eq} = 2.15 mm).

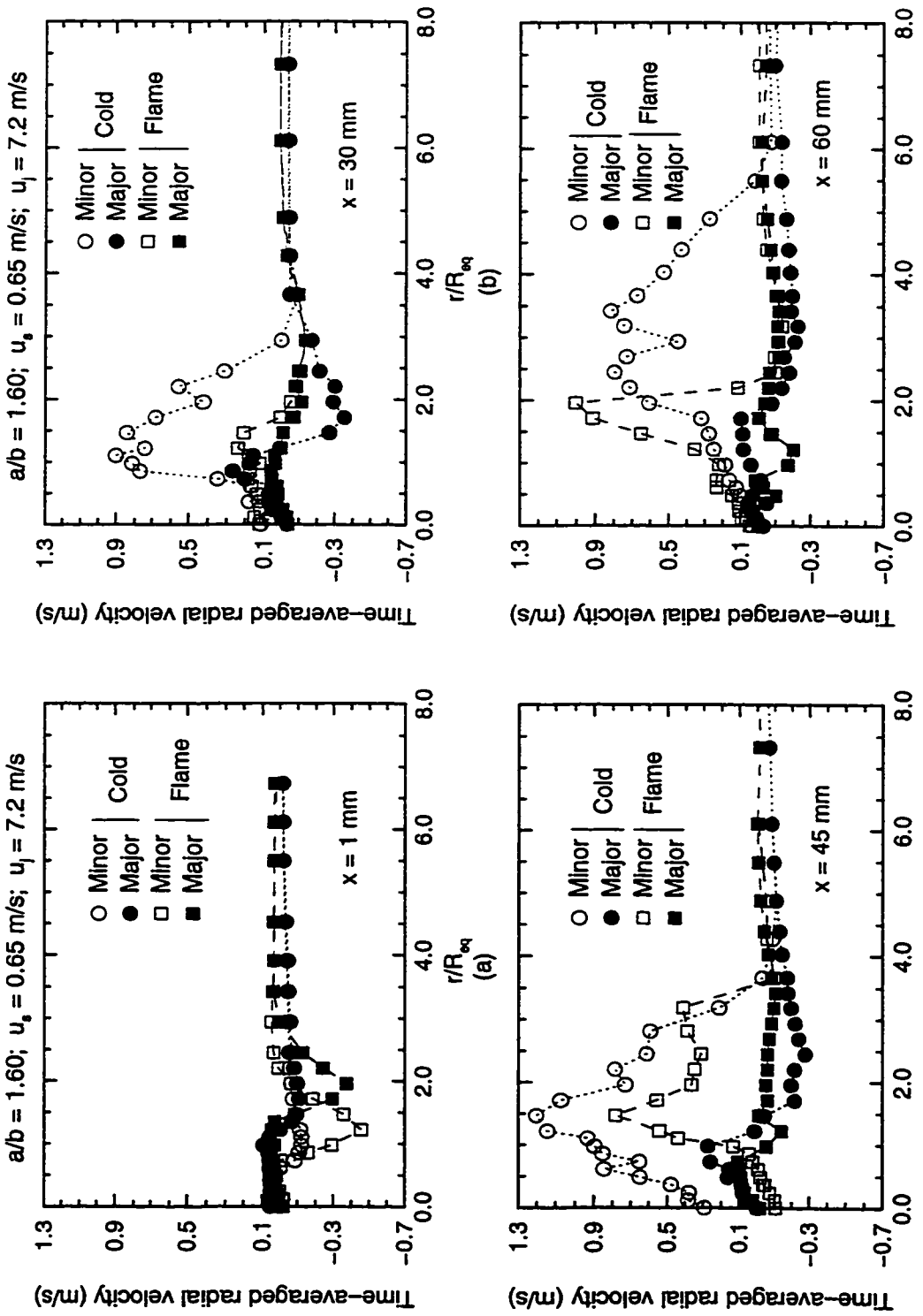

Fig. 5.6.14 Time–averaged radial velocity profiles within cold jets and attached flames with an aspect ratio of 1.60 (R_{eq} = 2.08 mm).

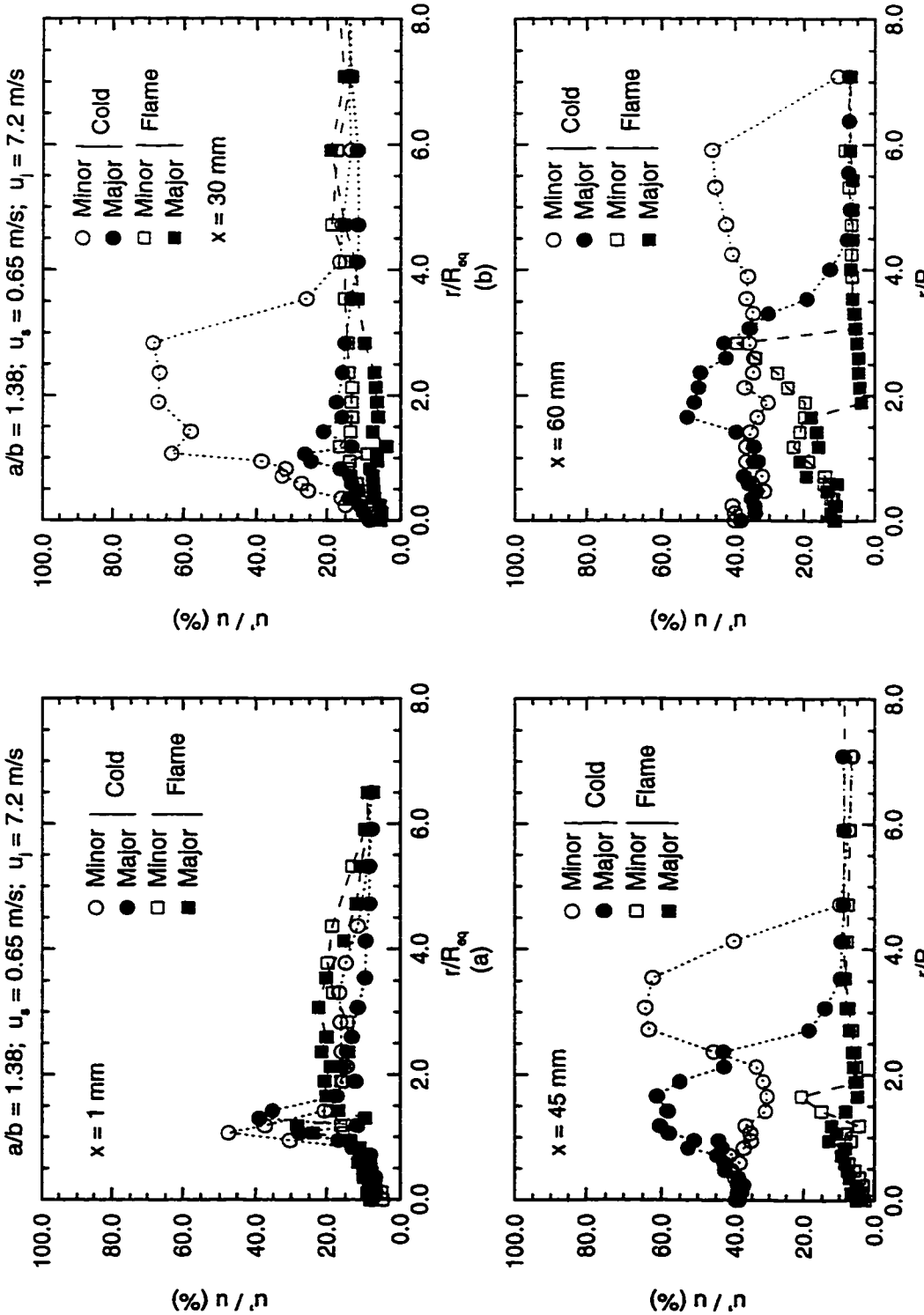

Fig. 5.6.15 Turbulence intensity profiles within cold jets and attached flames with an aspect ratio of 1.38 (R_{eq} = 2.15 mm).

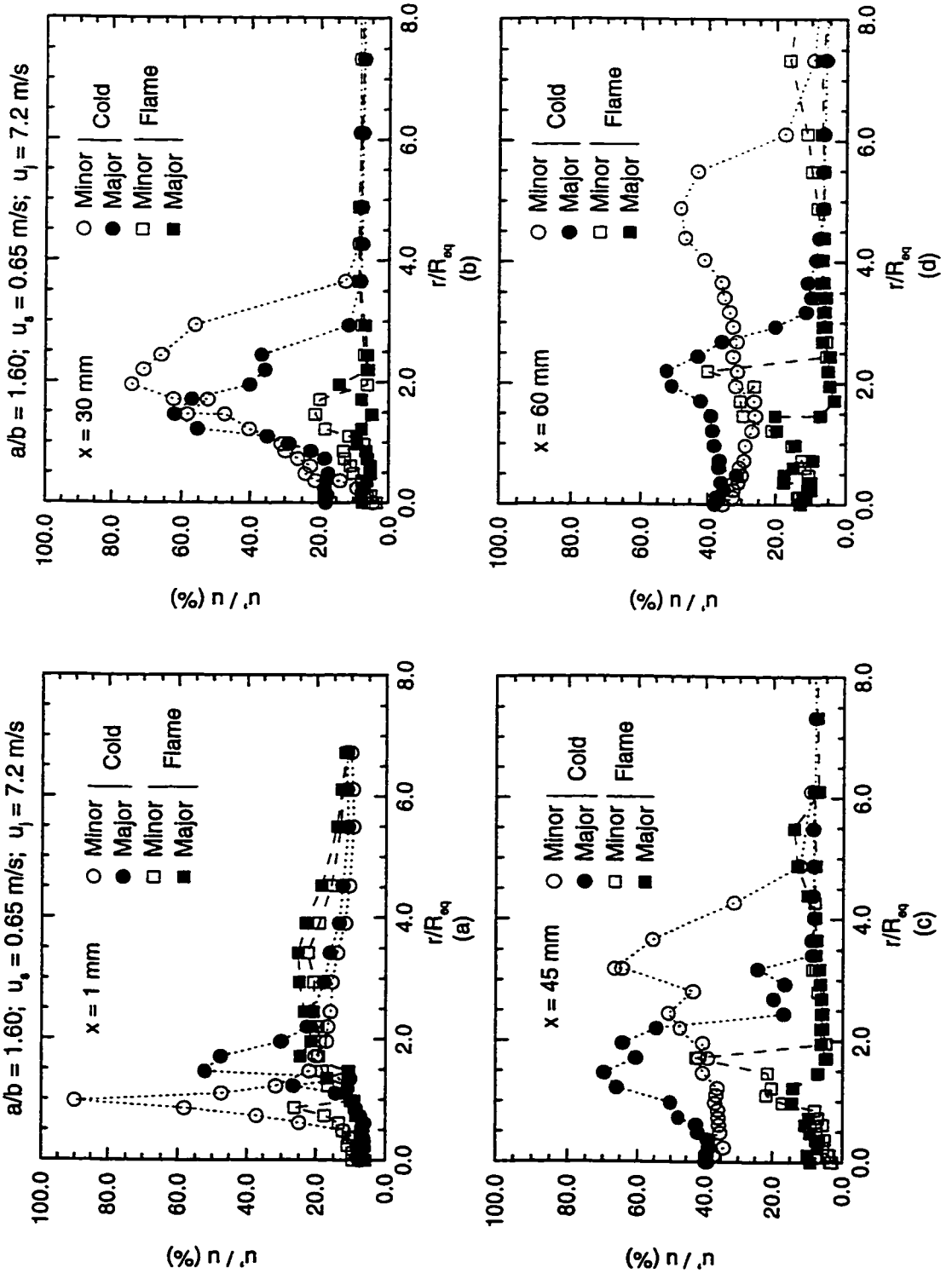

Fig. 5.6.16 Turbulence intensity profiles within cold jets and attached flames with an aspect ratio of 1.60 (R_{eq} = 2.08 mm).

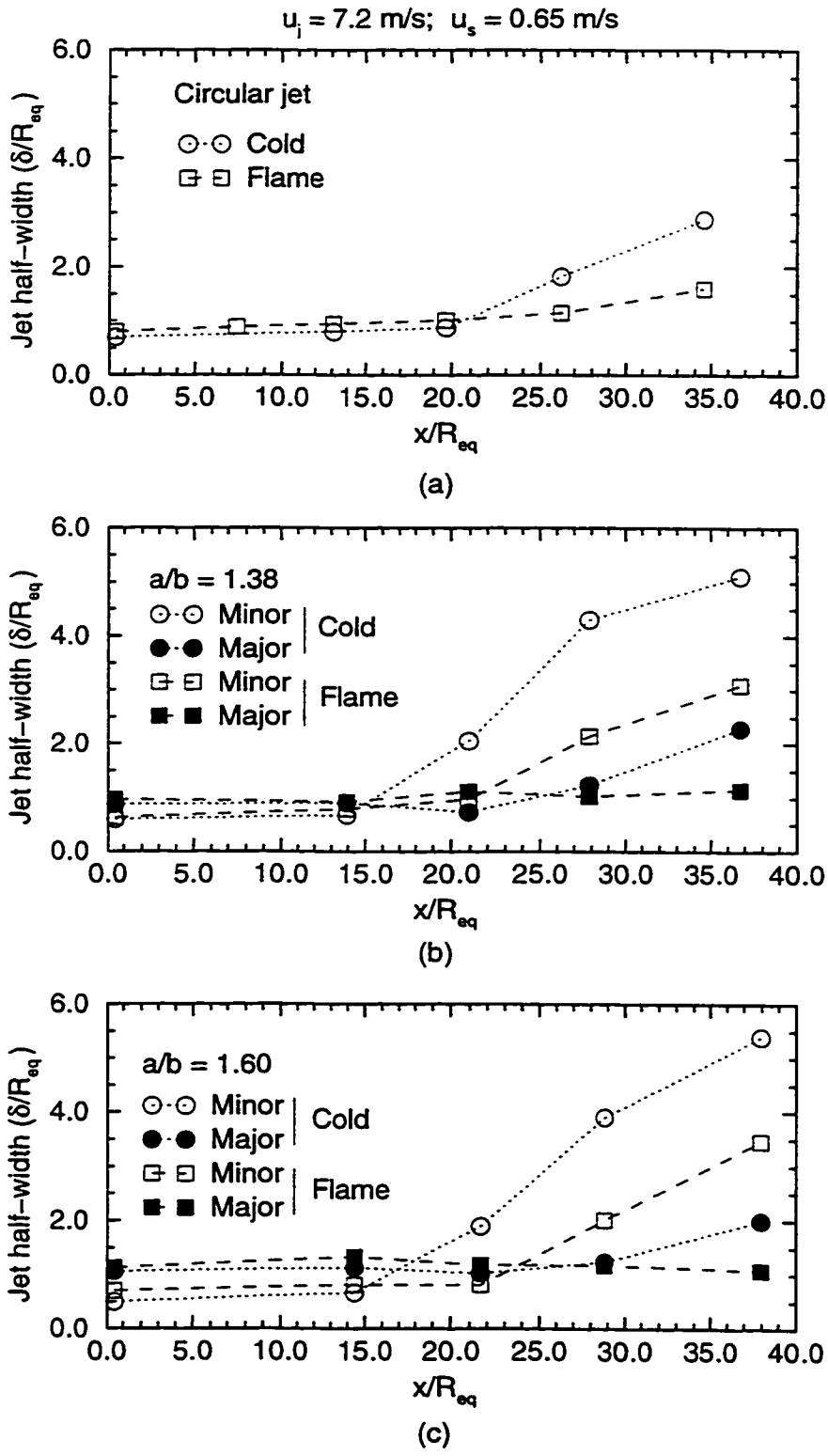

Fig. 5.6.17 A comparison of the jet half–width of (a) circular jets and elliptic jets with aspect ratios of (b) 1.38 and (c) 1.60.

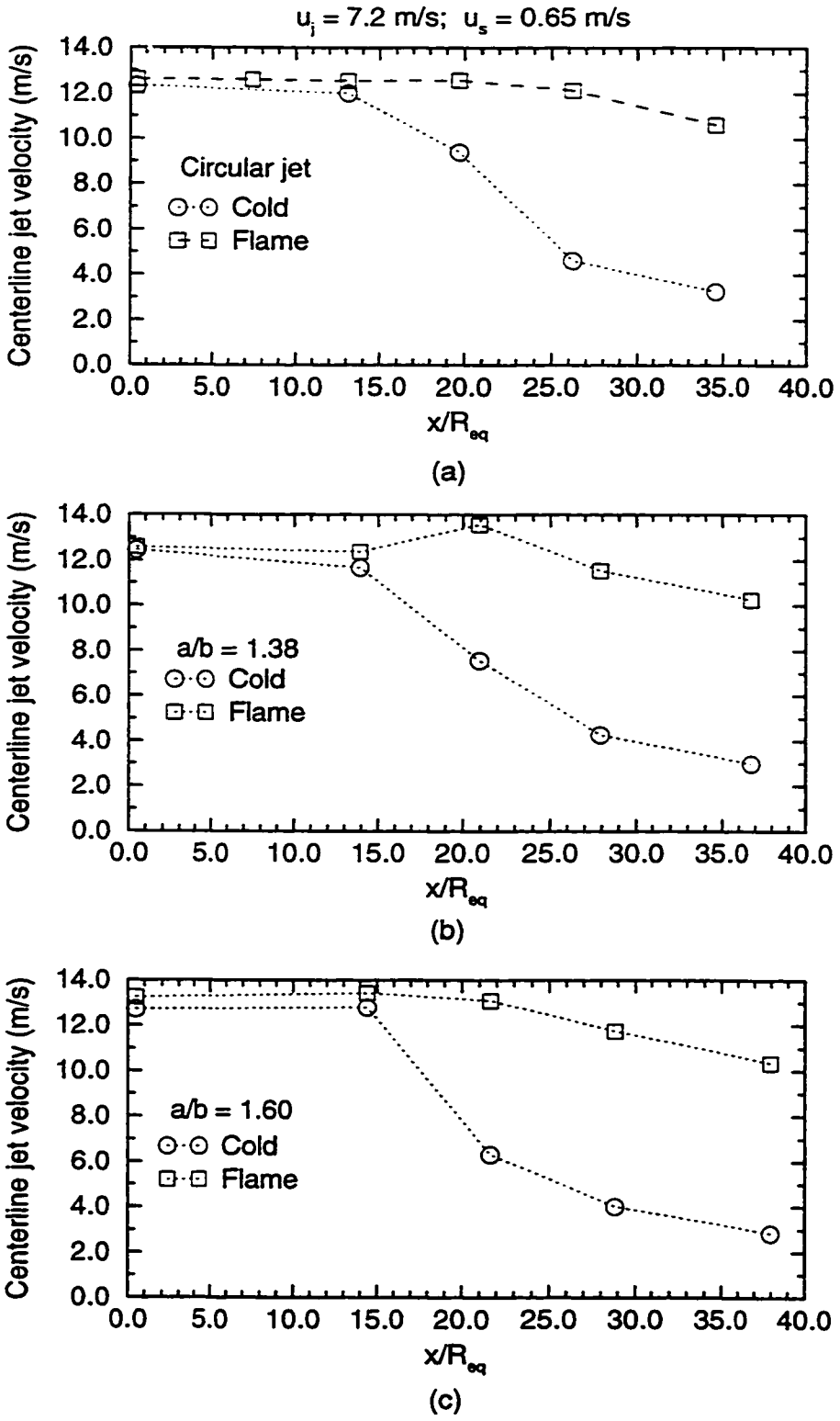

Fig. 5.6.18 A comparison of the velocity at the jet axis for (a) circular jets and elliptic jets of aspect ratios (b) 1.38 and (c) 1.60.

developed in the jet, and Savas and Gollahalli [95] showed that the growth of these structures in the near-nozzle region of an attached flame was retarded in the presence of a flame.

The corresponding variations of the jet half-width and centerline velocity decay, u_{cl}, with dimensionless downstream distance, x/R_{eq}, are compared in Figs. 5.6.17 and 5.6.18. The jet spread and centerline velocity decay, are mitigated in the presence of a flame. The heat released from the flame delayed the occurrence of axis-switching in elliptic jets further downstream by suppressing the flow instabilities that were responsible for axis-switching and the consequent higher mass entrainments in elliptic jets.

5.6.2 Attached Flames

The flow structure of flames in the region of attached flame blowout was investigated for a co-flowing stream velocity of 1.21 m/s, since a large difference in the blowout limits of various aspect ratio jets was recorded at this condition. The experiments were conducted at a jet velocity of 3.4 m/s. The time-averaged axial and radial velocity profiles are shown in Figs. 5.6.19 to 5.6.24 for elliptic jets with an aspect ratio of 1.38 and 1.60. From these figures, it can be seen that the velocity profiles of the jet with an aspect ratio of 1.38 are very similar soon after the nozzle exit (at x = 7.5 mm) in the major and minor axes planes. However, for jets issuing from the nozzle with an aspect ratio of 1.60, differences in the velocity profiles in the major and minor axes planes are still very significant until a downstream distance of x = 45 mm. The relatively greater jet spread in

the minor axis than in the major axis of the 1.38 aspect ratio jet near the nozzle exit, where attached flames stabilize, is indicative of a greater entrainment rate for this jet compared with the higher aspect ratio jet of 1.60. Within the jet of aspect ratio 1.60, the similar jet spread in both planes in the near nozzle region would cause axis-switching to occur further downstream.

The corresponding jet half-width variation with the dimensionless downstream distance for these two jets are compared in Fig. 5.6.25. For comparison, the corresponding data for the circular jet are also shown. Axis-switching appears to have occurred twice along the downstream distance, the first at some downstream distance, x/R_{eq} , between 14 and 21 (or x = 30 and 45 mm) and then again between 21 and 28 (or x = 45 and 60 mm) for flame jets issuing from 1.38 aspect ratio jets. The differences between the jet-half width in both planes are rather small compared to those for a jet discharge velocity of 7.2 m/s at a co-flowing stream velocity of 0.65 m/s (Fig. 5.6.7). The 1.60 aspect ratio jet, however, approached circularity at a downstream distance of $x/R_{eq} = 38$. Although the axis-switching phenomenon occurred further downstream than the location where attached flames stabilize (i.e., in the vicinity of the nozzle exit), its relative location is indicative of the flow structure development near the nozzle exit. Therefore, the enhanced mixing near the nozzle for the jet of aspect ratio 1.38 (in comparison with the jet of aspect ratio of 1.60) could be the reason for its higher blowout limit. These observed trends are consistent with gas analysis measurements. The effect of the jet aspect ratio on the values of distances where, at the jet axis, the fuel concentration is equal to the lean flammability limit (x_{LI}) is shown in Fig.

5.6.26. They were calculated on the basis of gas analysis. The values of x_{LL} for cold jets are also shown for comparison. Changes in the position of the lean flammability limit (at the jet centerline) when elliptic jets were employed were evaluated in terms of the ratio of this value to the corresponding value of x_{LL} for a circular jet. A ratio less than one represented an improvement in the mixing intensity of the fuel and air. It can be seen that, for both cold and ignited jets, the lean flammability limit concentration at the jet axis was reached much closer to the jet exit and consequently the air entrainment rate was appreciably enhanced when the jet nozzle was elliptic than when it was circular. The presence of a flame mitigated the effect of the jet aspect ratio on the value of x_{LL}. In the presence of a flame, the lowest value of x_{LL} was observed for the jet with an aspect ratio of 1.38 followed by the 1.60 aspect ratio jet. These results signify a more rapid mixing between the fuel and air within the 1.38 aspect ratio jet than within the other two jets and coincide with the experimental blowout limits. The trend, however, was quite different for cold jets with the lowest value of x_{LL} obtained by the nozzle with the larger aspect ratio of 1.60. In previous cold flow studies on large jets in a quiescent environment, it was also observed that elliptic jets enhanced the entrainment of air into the mixing layer and that an increase in air entrainment could be obtained with a small increase in the jet aspect ratio [13,45]. This would indicate the existence of complex flame-flow interactions.

Effect of Auxiliary Methane. An addition of 2% (by volume) of methane into a co-flowing stream of air had a significant effect on the flow within the jet as can be seen in Figs. 5.6.27 to 5.6.31. The trend in the variation of the jet half-width in a methane-air stream is

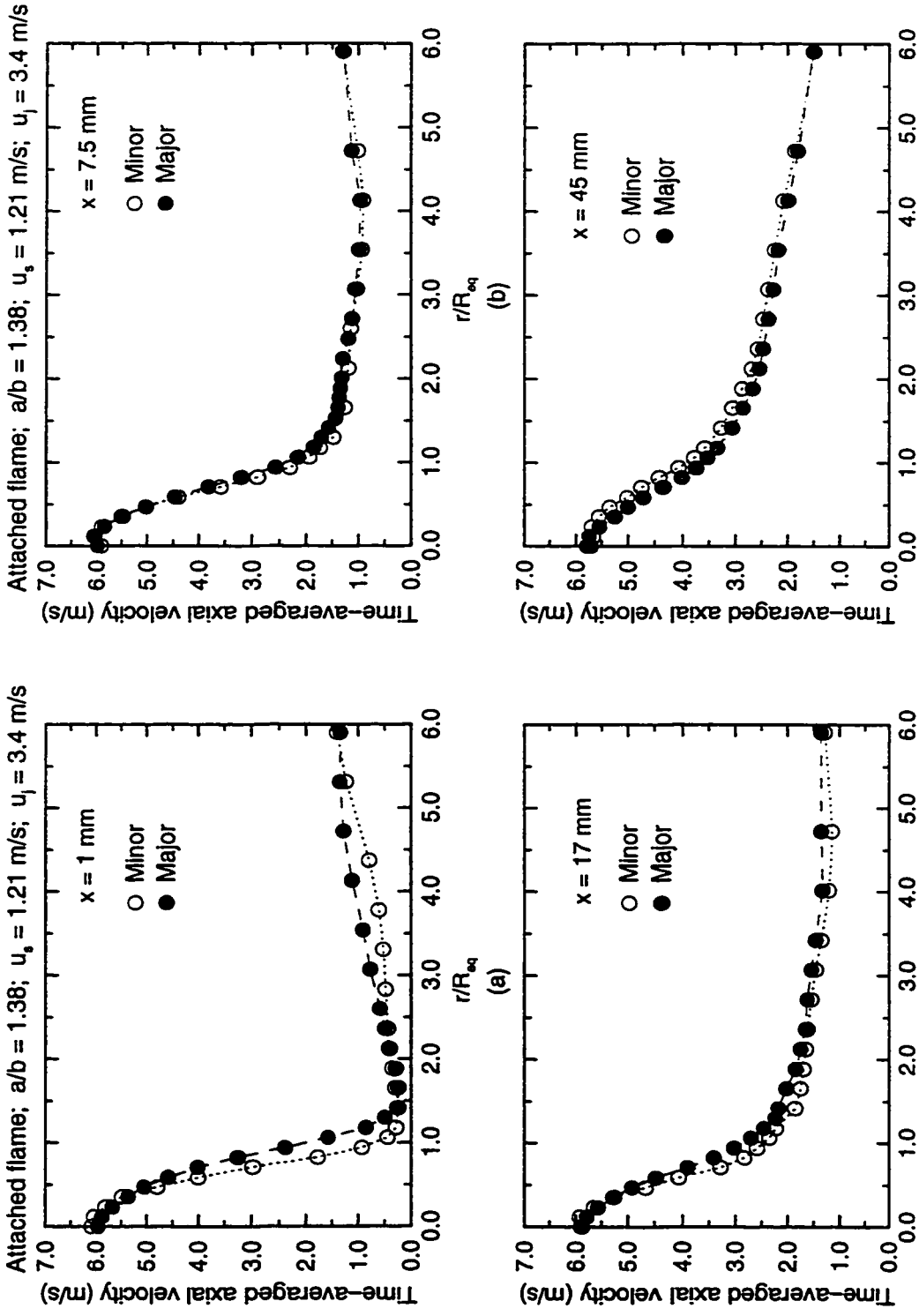

Fig. 5.6.19 Time-averaged axial velocity profiles within attached flames with an aspect ratio of 1.38 (R_{eq} = 2.15 mm).

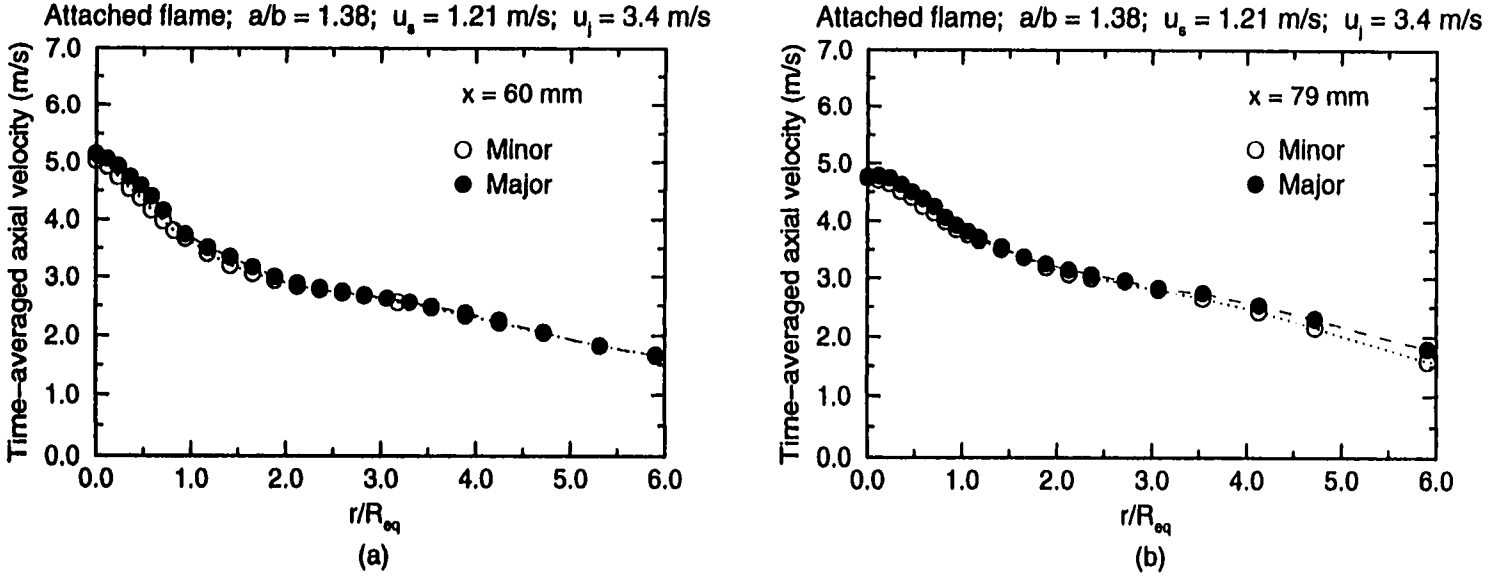

Fig. 5.6.20 Time–averaged axial velocity profiles within attached flames with an aspect ratio of 1.38 (R_{eq} = 2.15 mm).

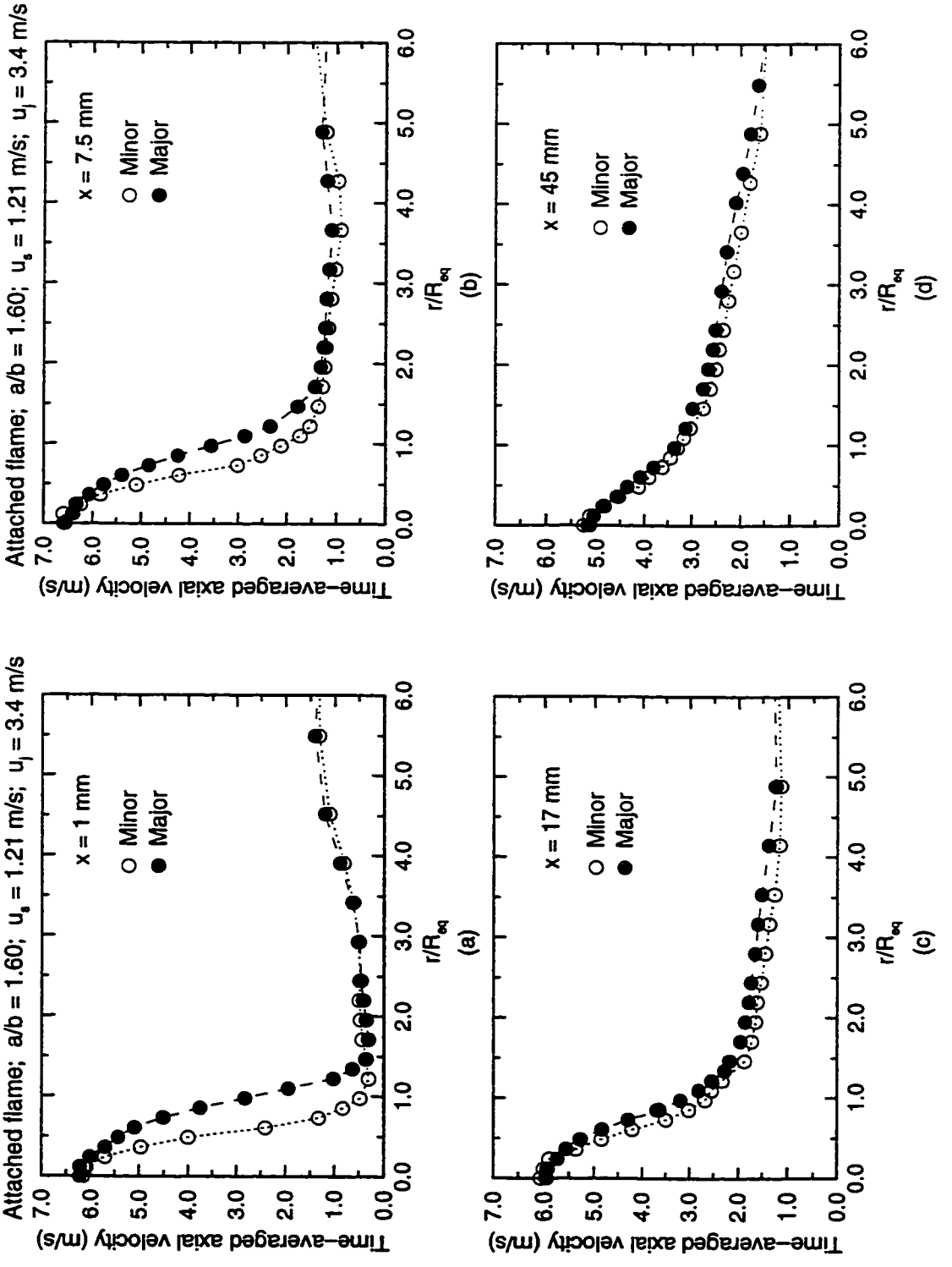

Fig. 5.6.21 Time–averaged axial velocity profiles within attached flames with an aspect ratio of 1.60 (R_{eq} = 2.08 mm).

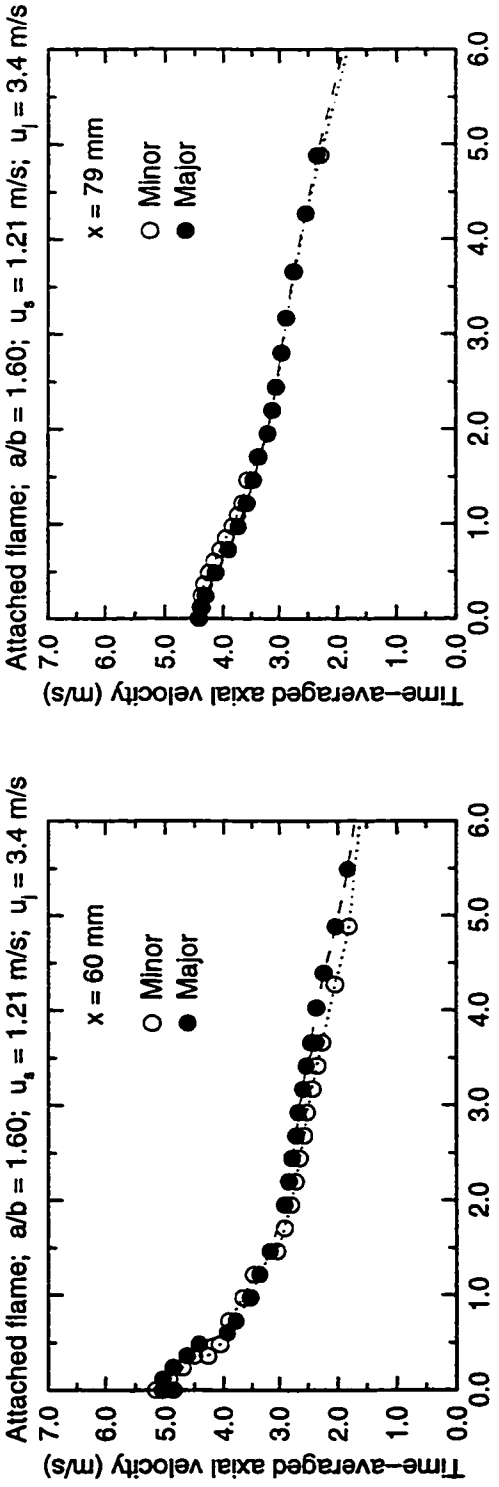

Fig. 5.6.22 Time–averaged axial velocity profiles within attached flames with an aspect ratio of 1.60 (R_{eq} = 2.08 mm).

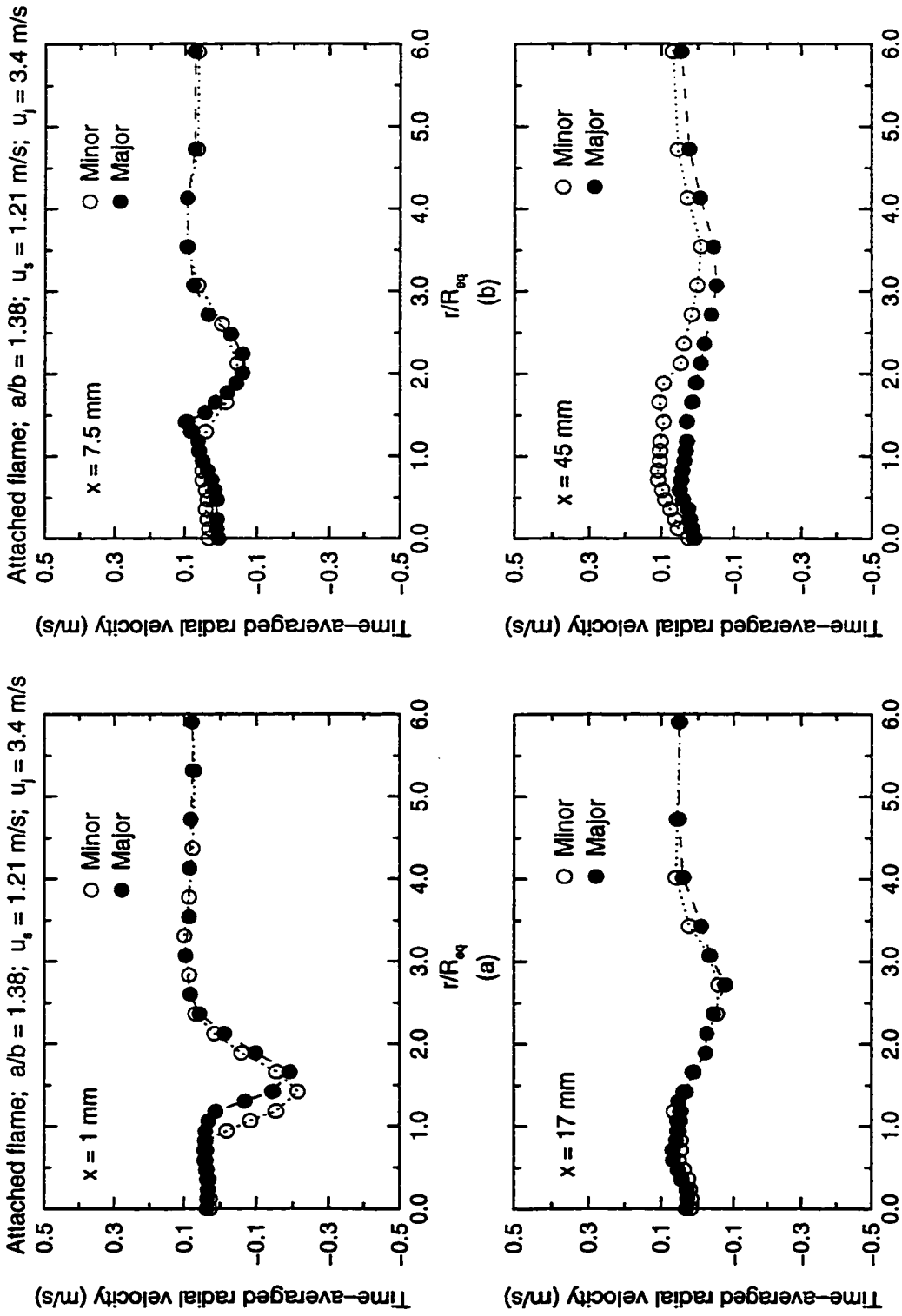

Fig. 5.6.23 Time–averaged radial velocity profiles within attached flames with an aspect ratio of 1.38 (R_{eq} = 2.15 mm).

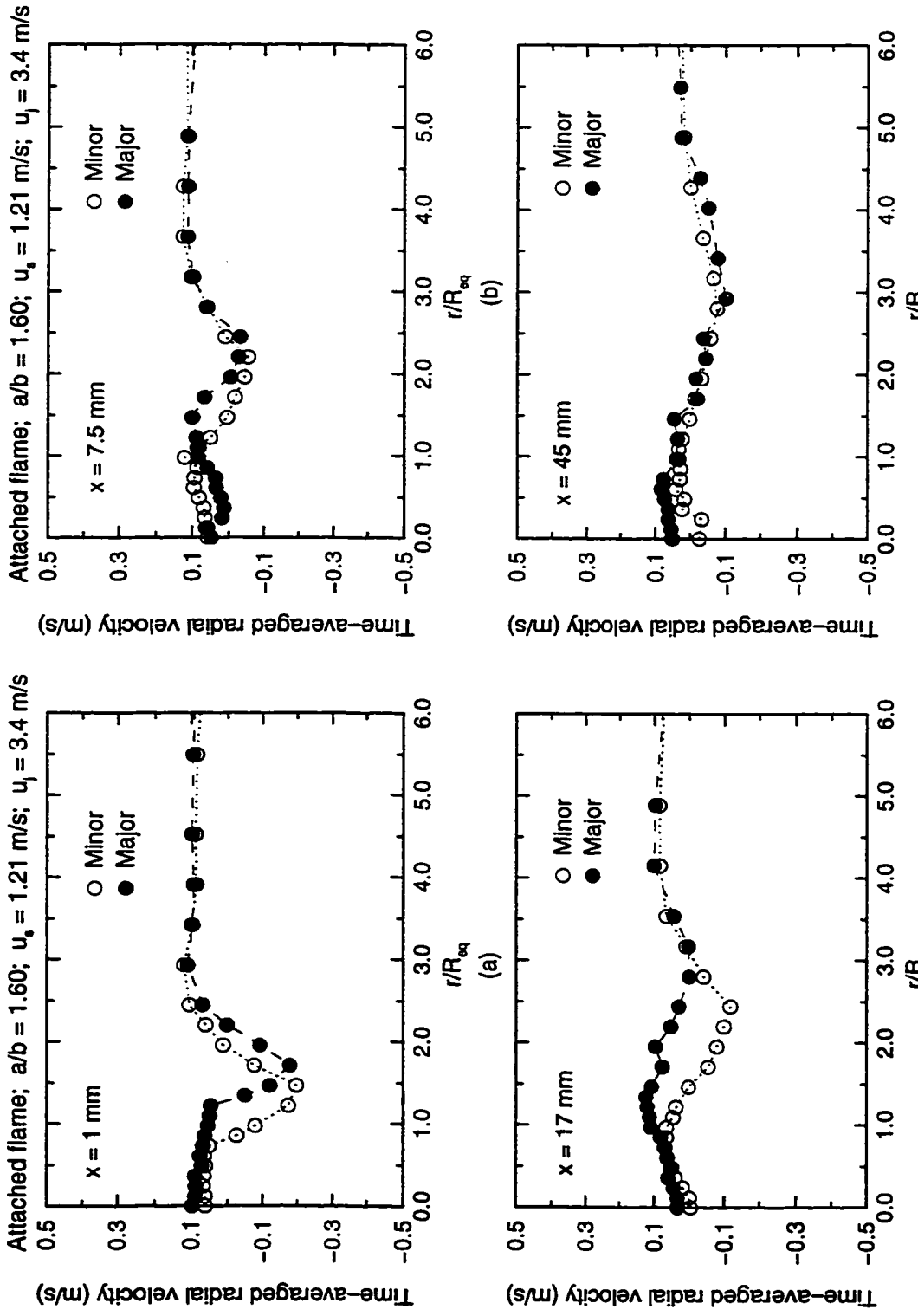

Fig. 5.6.24 Time–averaged radial velocity profiles within attached flames with an aspect ratio of 1.60 (R_{eq} = 2.08 mm).

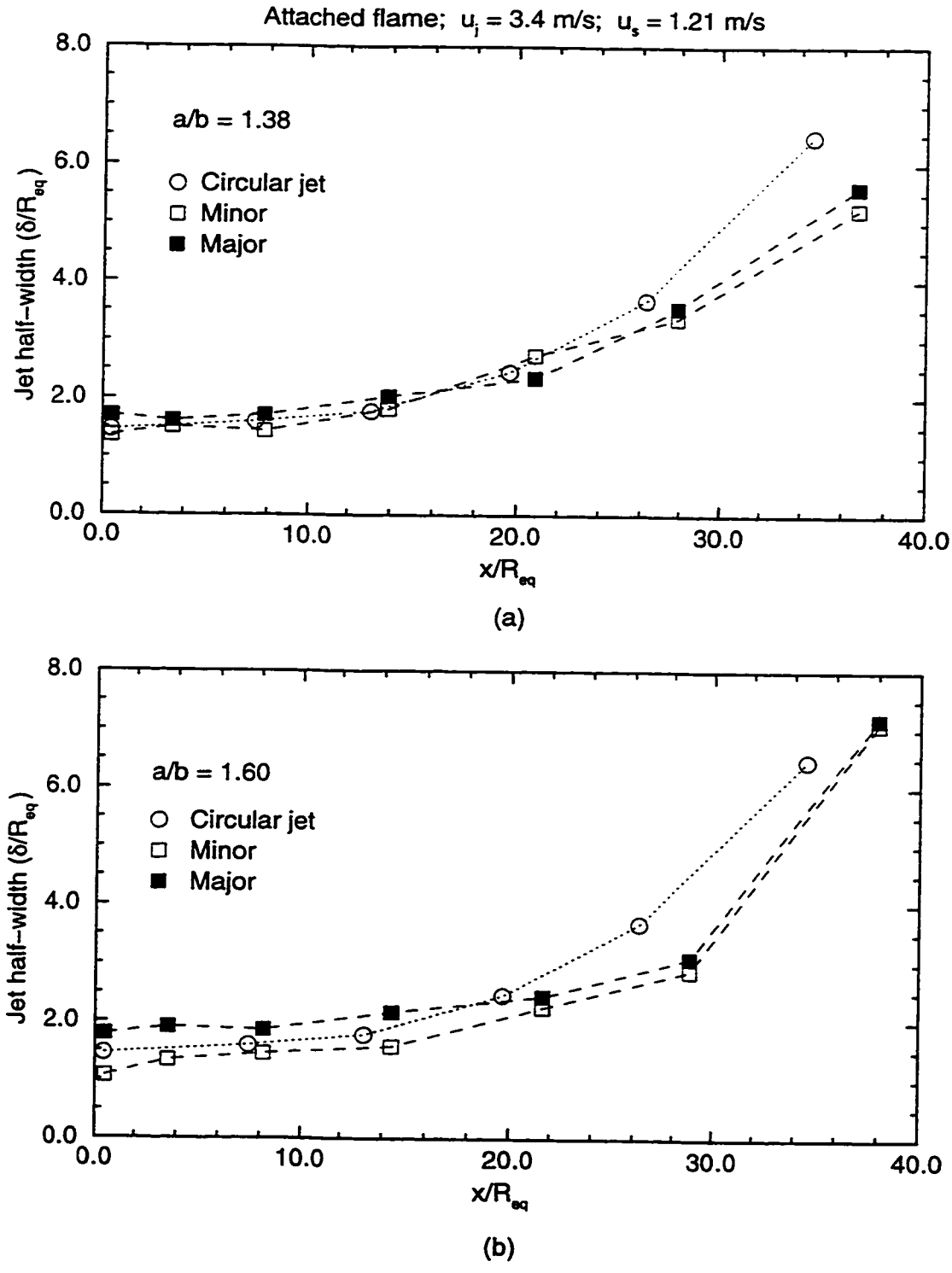

Fig. 5.6.25 A comparison of the jet half–width of attached flames issuing from elliptic nozzles of aspect ratios (a) 1.38 and (b) 1.60.

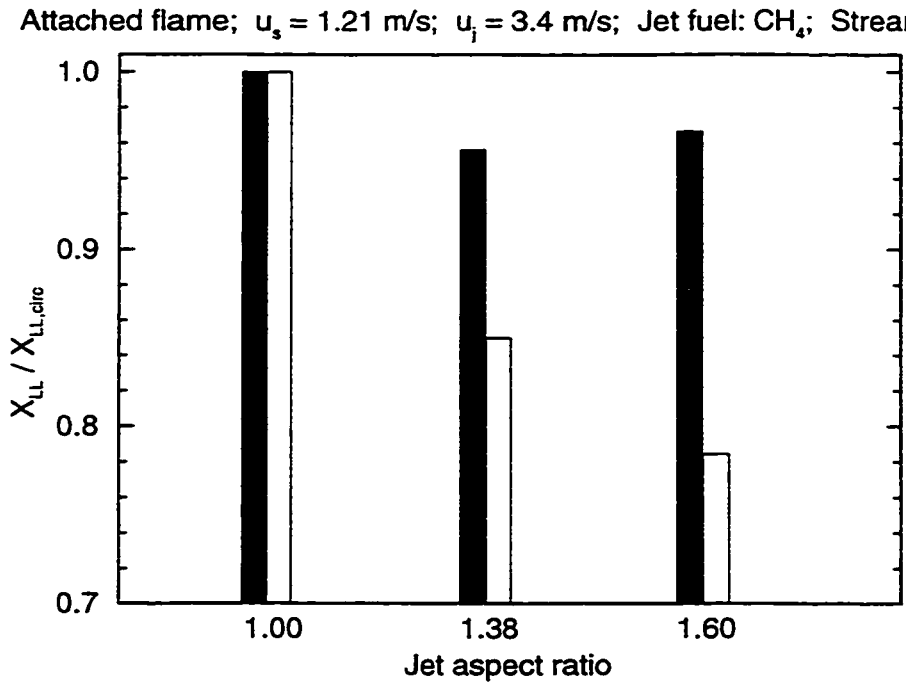

Fig. 5.6.26 The axial distance where the fuel–air concentration equalled the lower flammability limit as a function of the jet aspect ratio. Solid bars: attached flame. Open bars: cold jet.

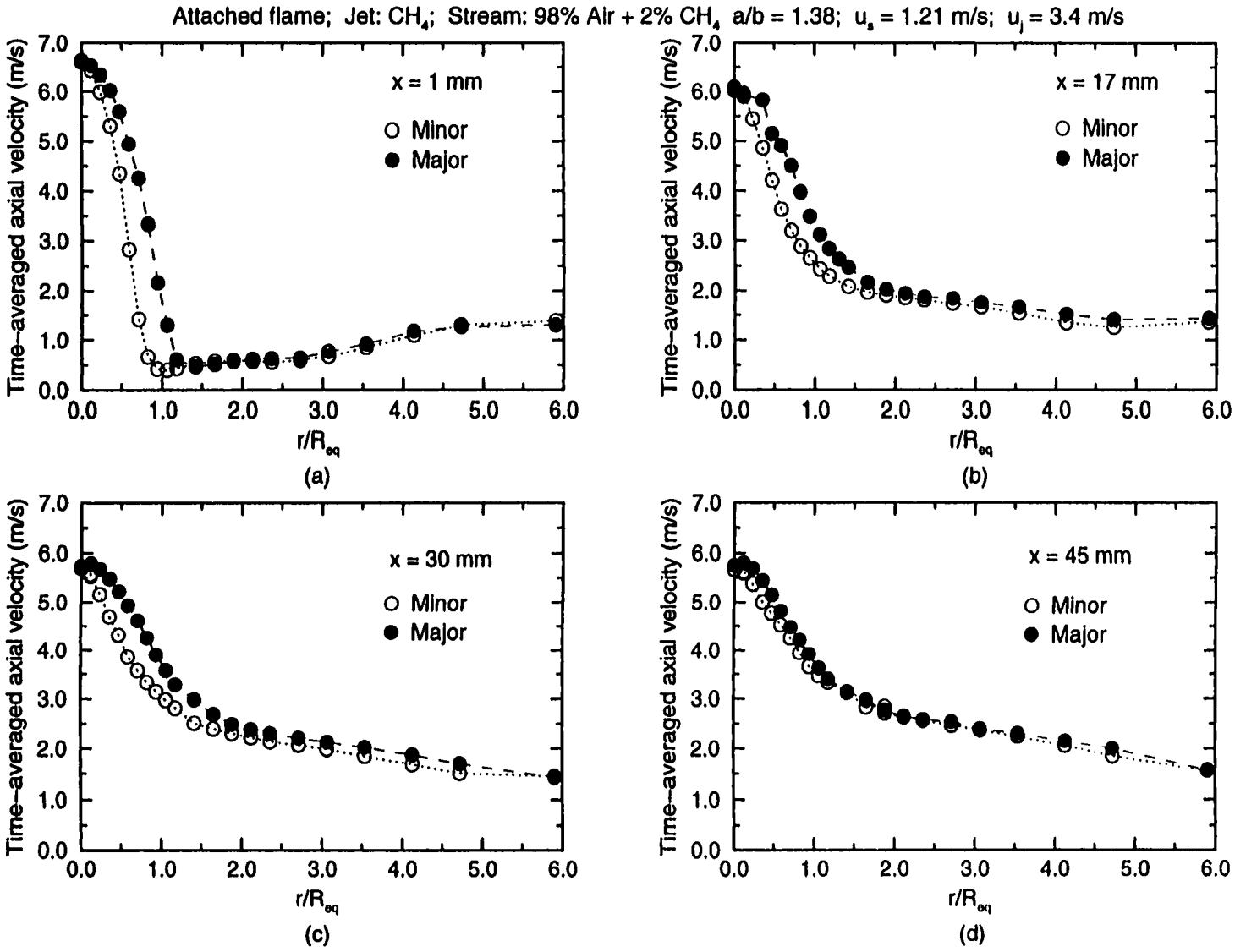

Fig. 5.6.27 Time-averaged axial velocity profiles within attached flames with an aspect ratio of 1.38 in a co-flowing stream of air premixed with 2.0% (by volume) methane (R_{eq} = 2.15 mm).

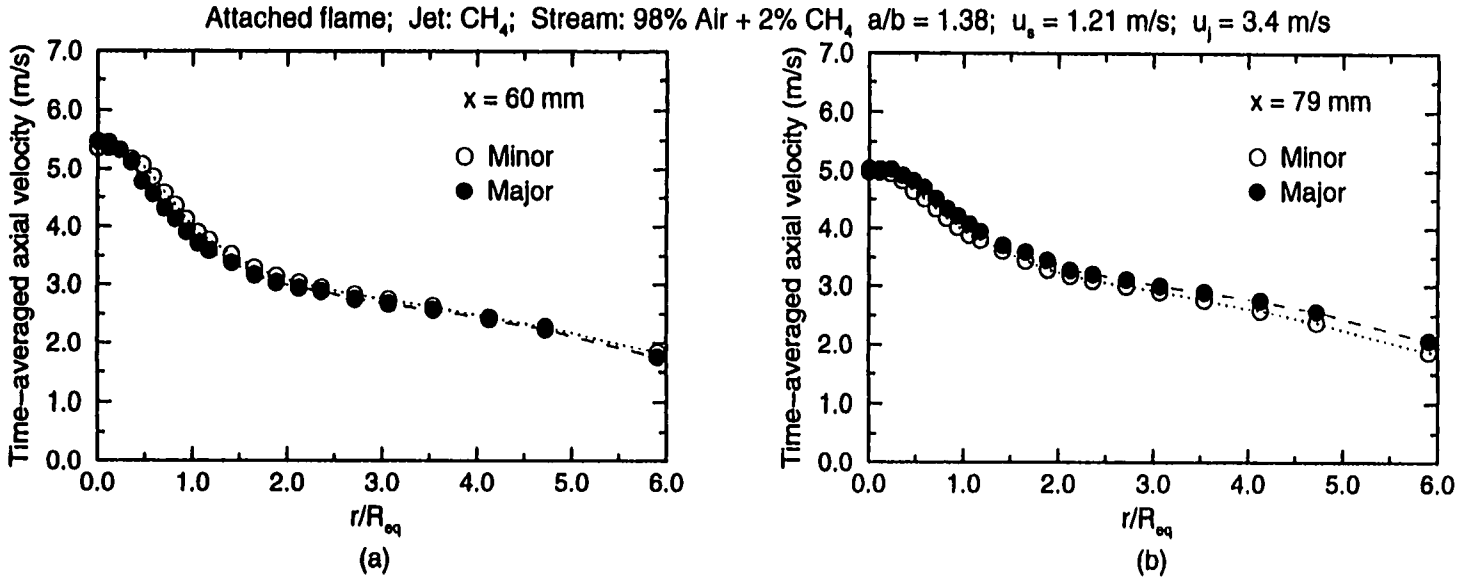

Fig. 5.6.28 Time–averaged axial velocity profiles within attached flames with an aspect ratio of 1.38 in a co–flowing stream of air premixed with 2.0% (by volume) methane (R_{eq} = 2.15 mm).

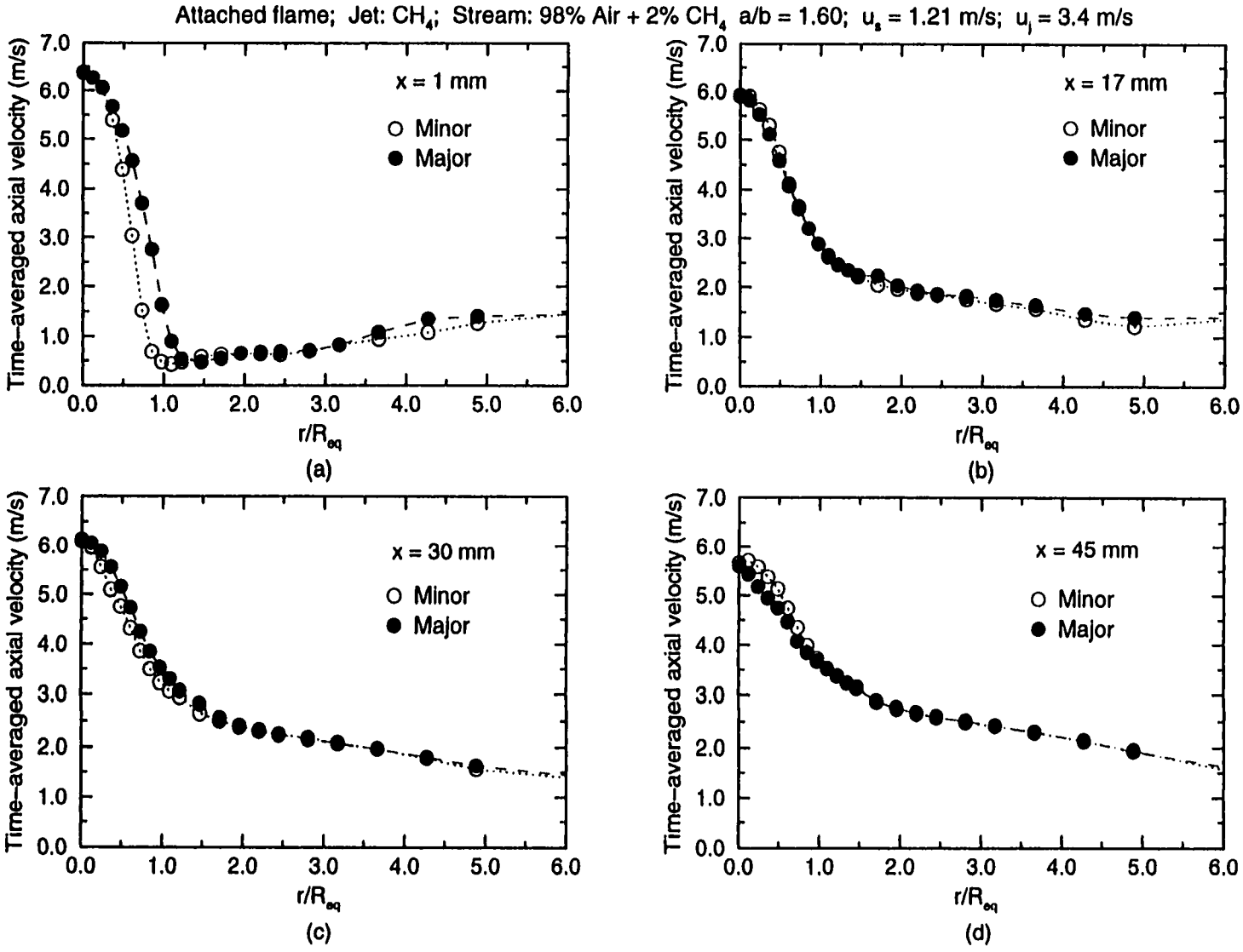

Fig. 5.6.29 Time-averaged axial velocity profiles within attached flames with an aspect ratio of 1.60 in a co-flowing stream of air premixed with 2.0% (by volume) methane (R_{eq} = 2.08 mm).

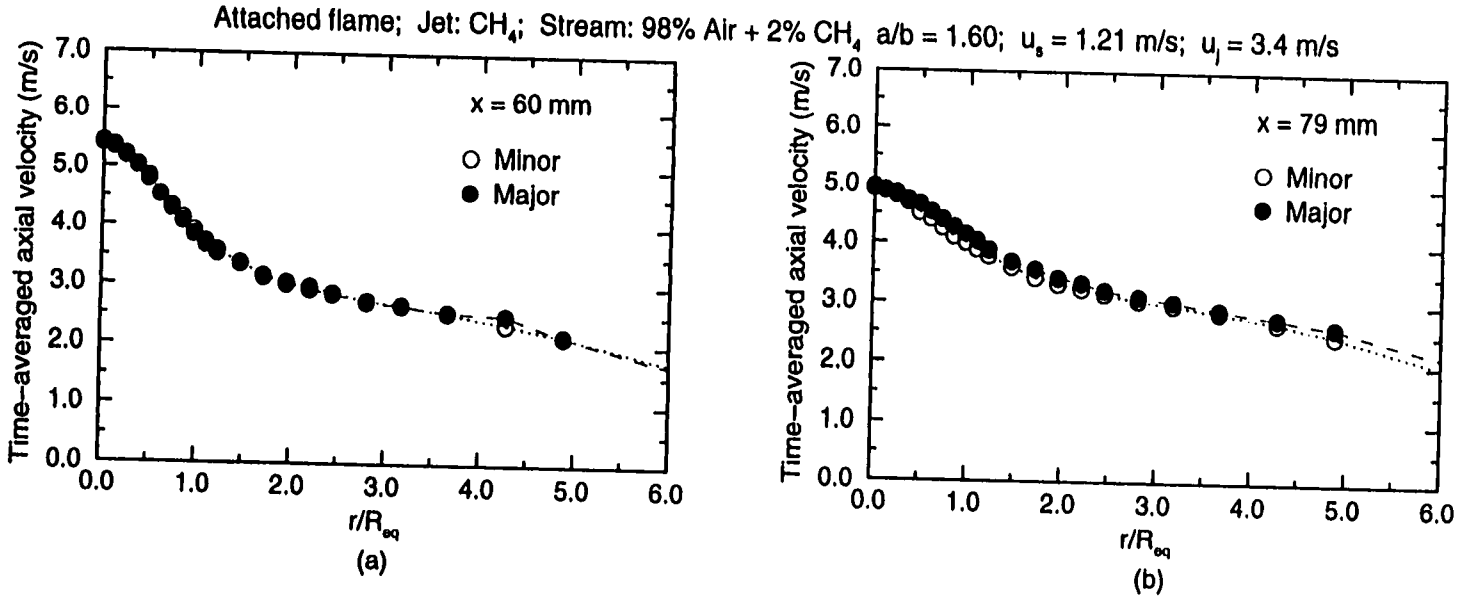

Fig. 5.6.30 Time-averaged axial velocity profiles within attached flames with an aspect ratio of 1.60 in a co-flowing stream of air premixed with 2.0% (by volume) methane (R_{eq} = 2.08 mm).

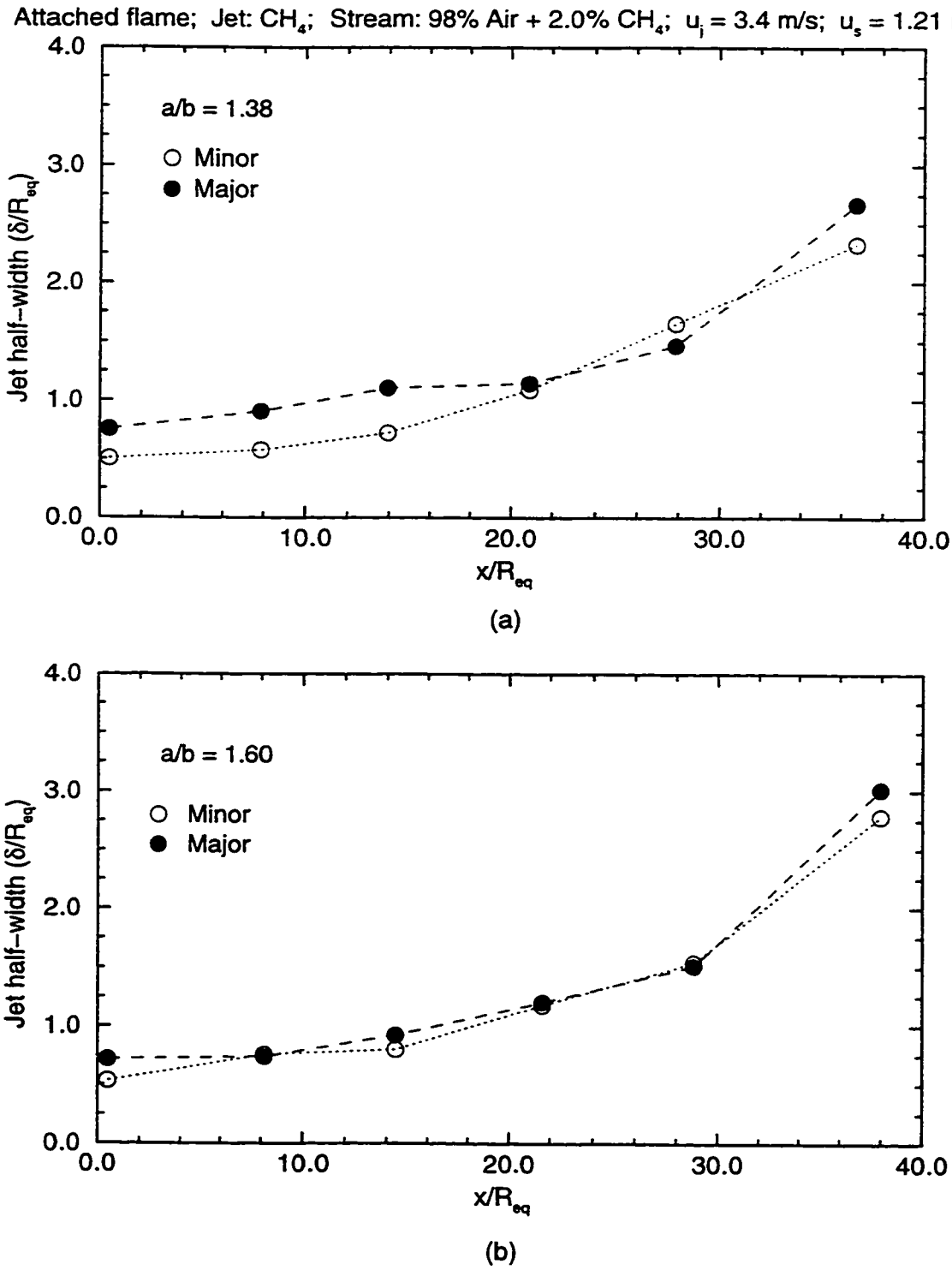

Fig. 5.6.31 The variation of the jet half–width with dimensionless downstream distance for attached flames issuing from two different elliptic jets into a co–flowing air stream premixed with 2.0% (by volume) methane.

reversed for these two jets in comparison with that in a stream of pure air. For the jet with aspect ratio 1.60, the rate of jet spread in the minor axis plane near the nozzle was greater than that in the major axis plane and the jet already became approximately circular at a downstream distance of $x/R_{eq} = 8.1$ (in comparison to the distance of $x/R_{eq} = 21.6$ in an air only stream). The resulting enhanced mixing contributed to the greatest improvement in the blowout limits for the 1.60 aspect ratio jet. These findings indicate that the existing complex flame-flow interactions remain to be fully understood.

5.7 Nondimensional Correlations

Far-field. Attempts were made to correlate the experimental results for the time-averaged axial velocity in the self-similar (far-field) region of the jet for different operating conditions. The cold circular jet with a discharge velocity of 11.5 m/s became self-similar at downstream distances greater than 60 mm (Fig. 5.7.1). The experimentally established axial velocity profiles compared well with the profiles calculated using correlations proposed by Antonia and Bilger [55] and Steward and Guruz [60] for cold turbulent jets in the self-preserving region; however, there are some deviations at the jet boundary. The axial velocity profiles for jets of different discharge velocities and different co-flowing stream velocities at the axial distance of 79 mm were also reasonably correlated in terms of dimensionless velocity and jet half-width as shown in Fig. 5.7.2. The effect of variations in the jet density is also well correlated in these terms. The correlation can be used for the cold region of lifted jet flames, however, it is not applicable in the presence of the flame

(Fig. 5.7.3).

The non-dimensional relation applied to attached flame jets when they were turbulent and in the self-preserving region as shown in Fig. 5.7.4 (a) for a jet with a discharge velocity of 11 m/s. The non-dimensional relation failed to predict the velocity profile when the flame was laminar (i.e., at $u_j = 3.4$ m/s) (Fig. 5.7.4 (b)).

Near-field. The correlations developed for a fully developed (self-preserving) flow are not applicable in the near-field region of the jet. Accordingly, an attempt was made in correlating the experimentally established axial velocity profiles of cold as well as ignited jets of different shapes using as a basis the non-dimensional relations suggested for cold free laminar elliptic jets by Hussain and Husain [45]. Modifications were made in order to take into account the presence of the co-flowing air stream. Dimensionless axial velocity, $(u - u_s) / (u_{cl} - u_s)$, was plotted as a function of a dimensionless radial distance, $(r - \delta) \bullet (\partial u/\partial r)_{max} / u_{cl}$.

The correlated axial velocity profiles for different cold jets discharged with velocities of 3.4 and 7.2 m/s into a co-flowing stream of velocity 1.21 m/s are shown in Figs. 5.7.5 for two different downstream distances and two different jet discharge velocities (at a distance of x = 1 mm). The correlated axial velocity profiles for ignited jets are shown in Figs. 5.7.6 and 5.7.7. The relation appeared to correlate satisfactorily the axial velocity profiles for jets with different aspect ratios at the same downstream axial distance and the same bulk jet velocity: it was not as successful at correlating velocity profiles at different axial distances or different bulk jet velocities, particularly at values of $(r - \delta) \bullet (\partial u/\partial r)_{max} /$

u_{cl} larger than 0.1. The presence of a co-flowing stream as well as the existence of flame-flow interactions created additional flow structure complexities (particularly at the jet boundary) that have not been accounted for in the correlations suggested by Hussain and Husain [45] for cold jets.

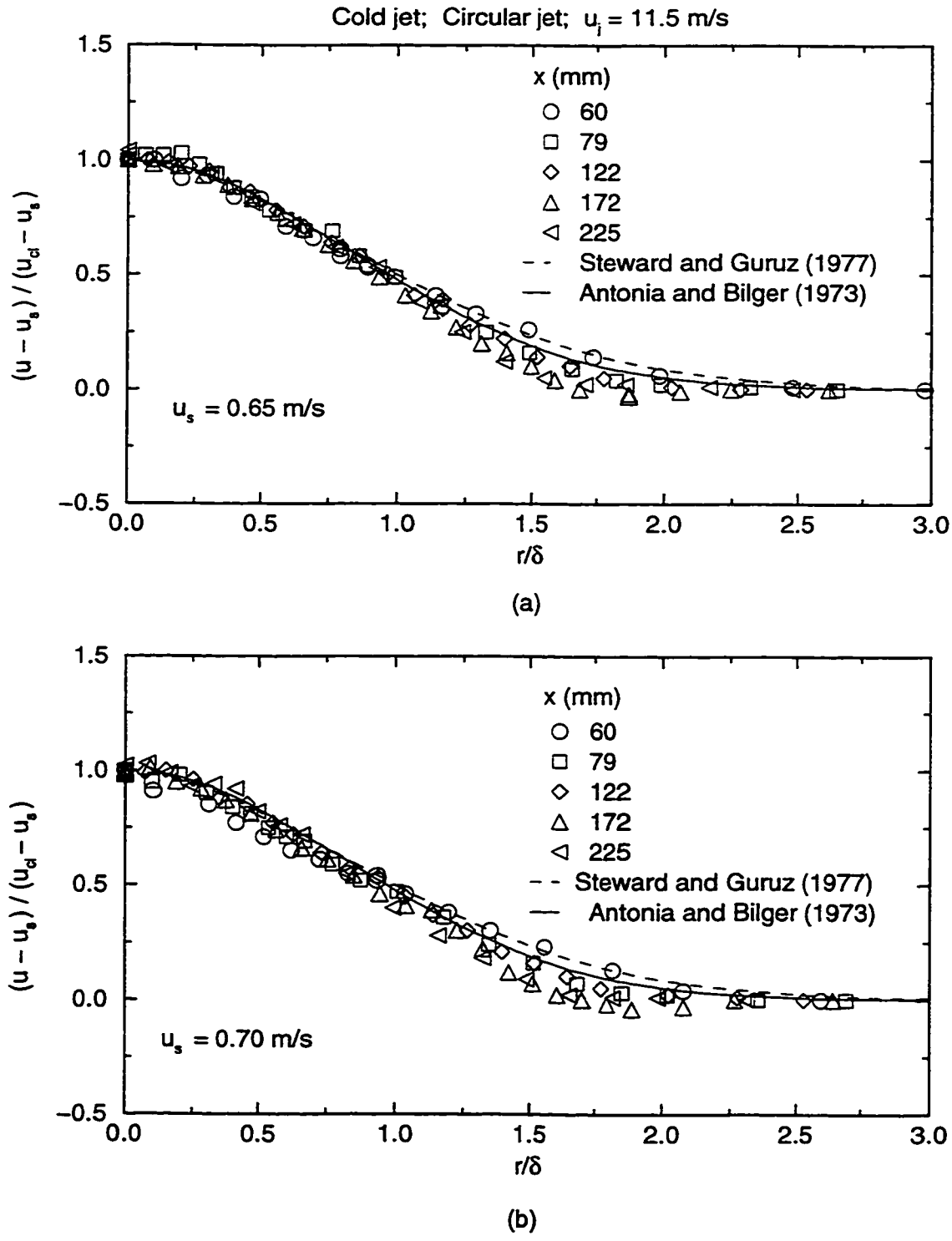

Fig. 5.7.1 A comparison of dimensionless velocity profiles in the far–field region of a cold circular jet (d_j = 4.57 mm).

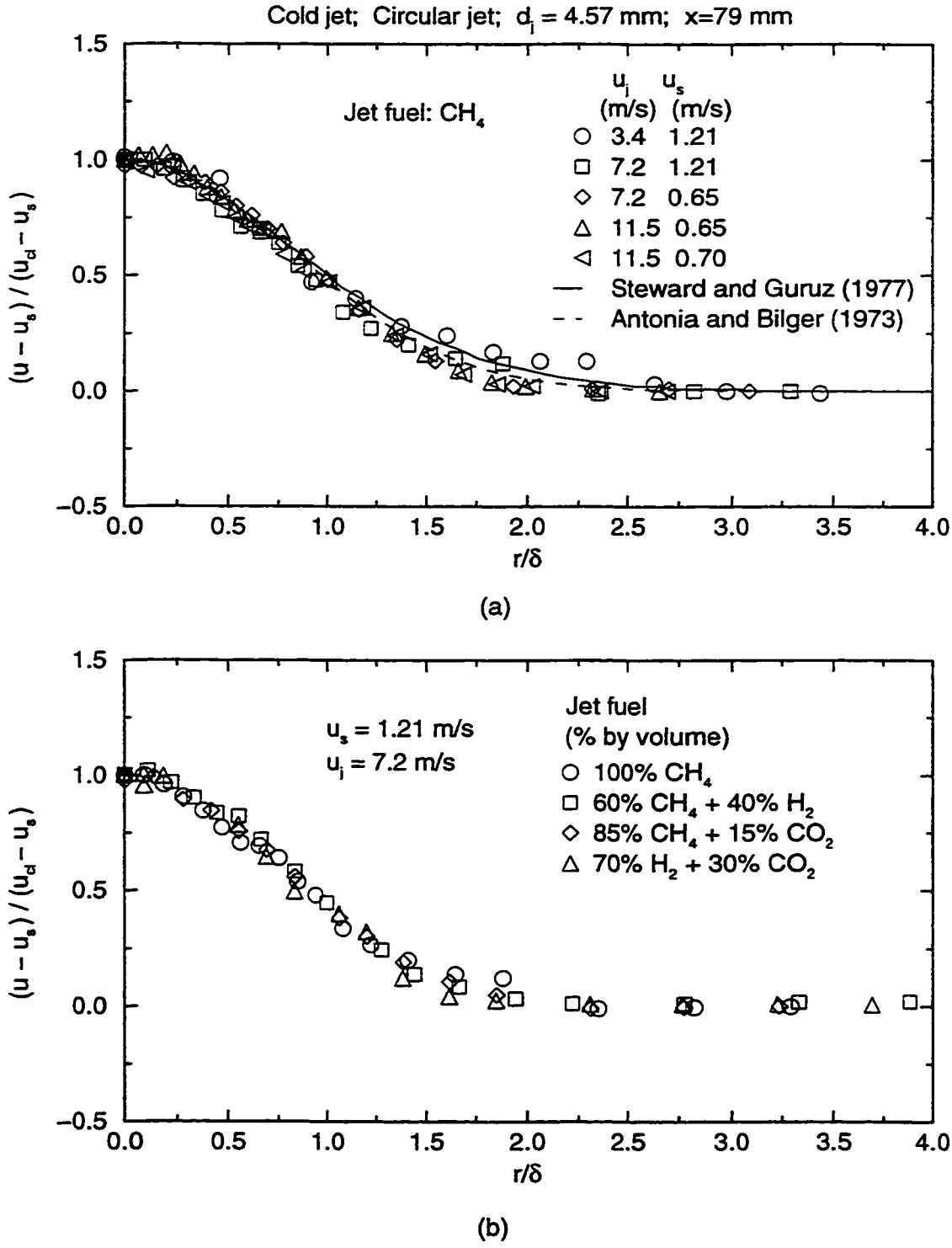

Fig. 5.7.2 A comparison of dimensionless velocity profiles in the far–field region of a cold circular jet with (a) different jet discharge and co–flowing stream velocities and (b) different jet fuel compositions.

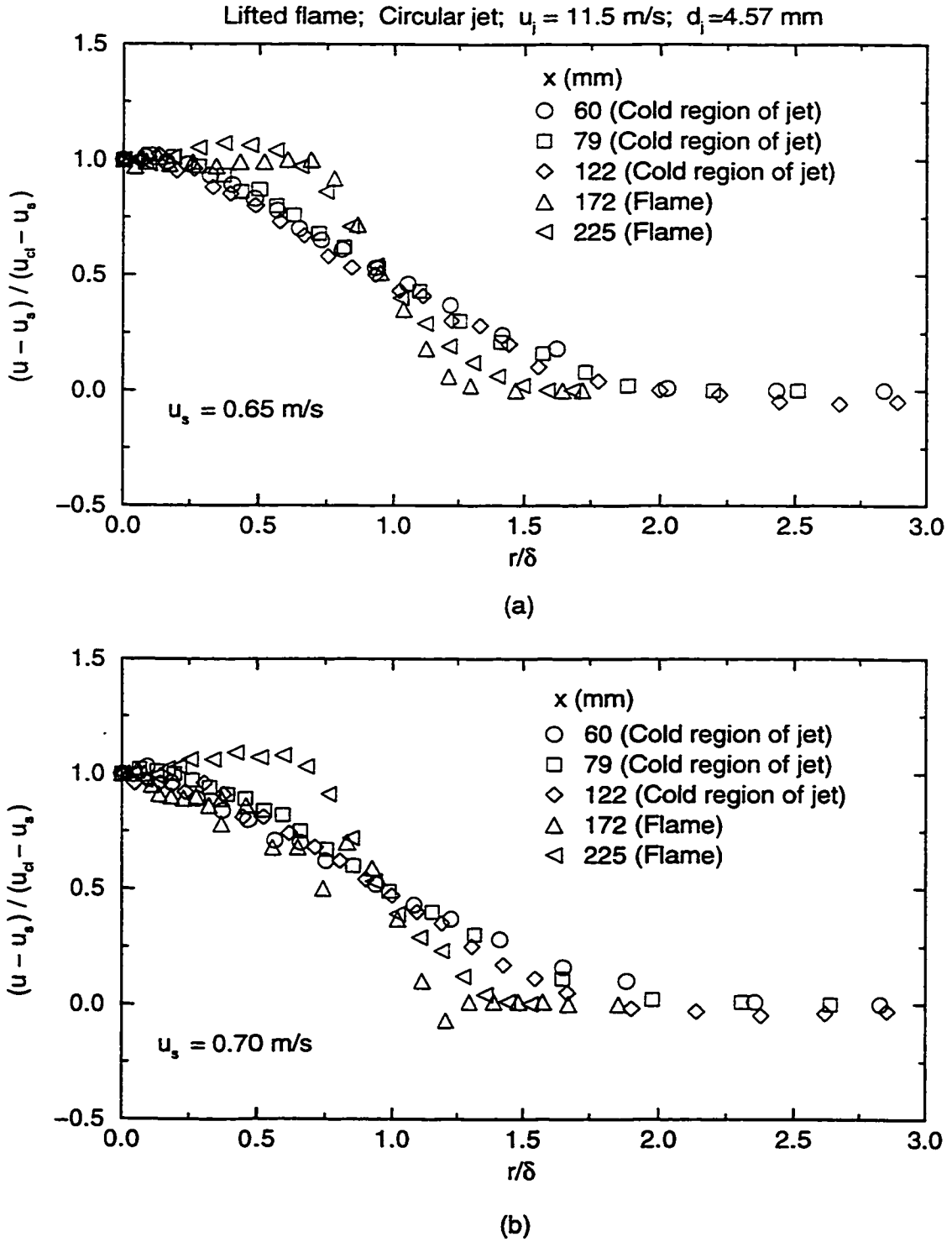

Fig. 5.7.3 A comparison of dimensionless velocity profiles in the far–field region of lifted flames in a co–flowing stream of velocity (a) 0.65 m/s and (b) 0.70 m/s.

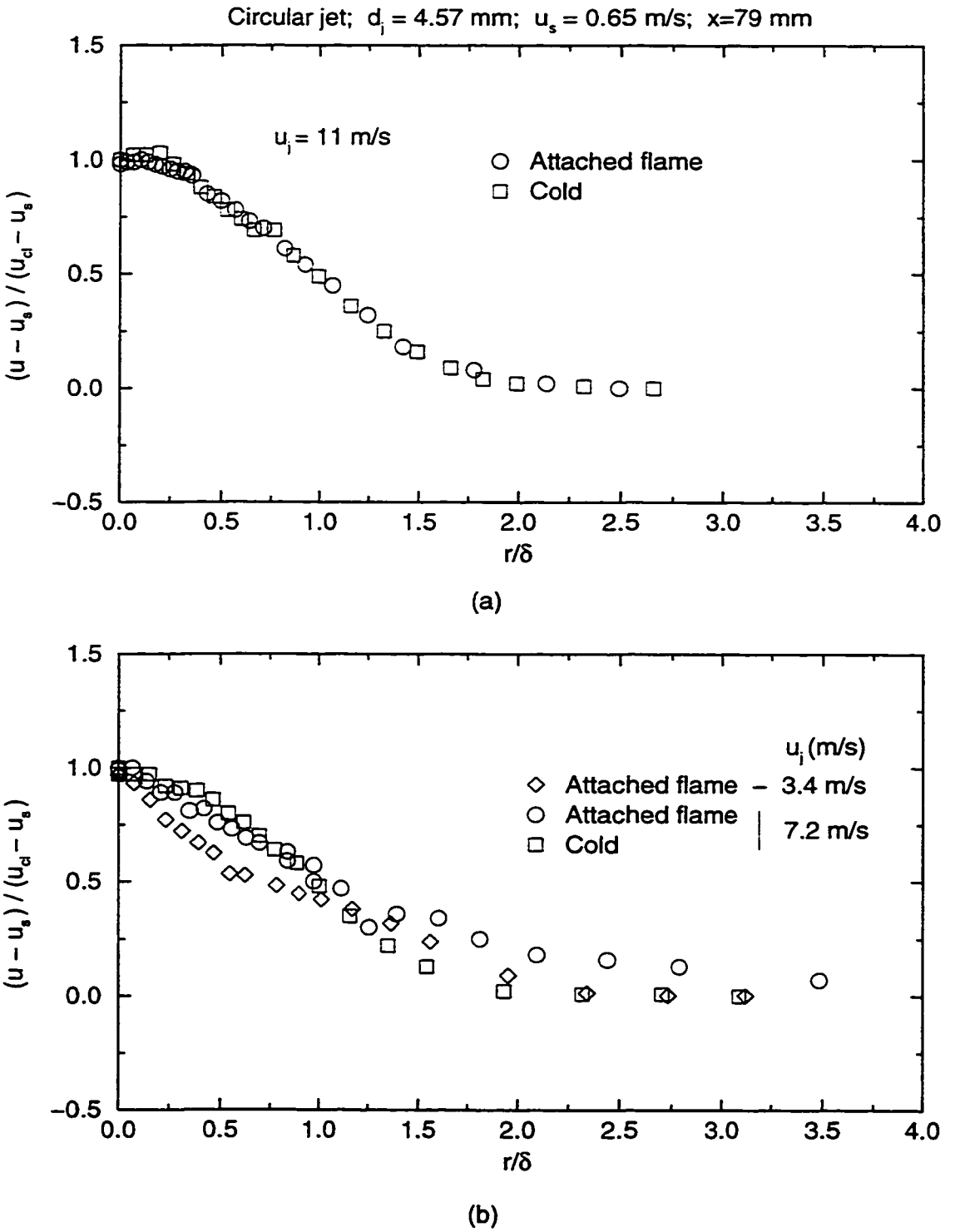

Fig. 5.7.4 A comparison of dimensionless velocity profiles in the far–field region of cold jets and attached flames.

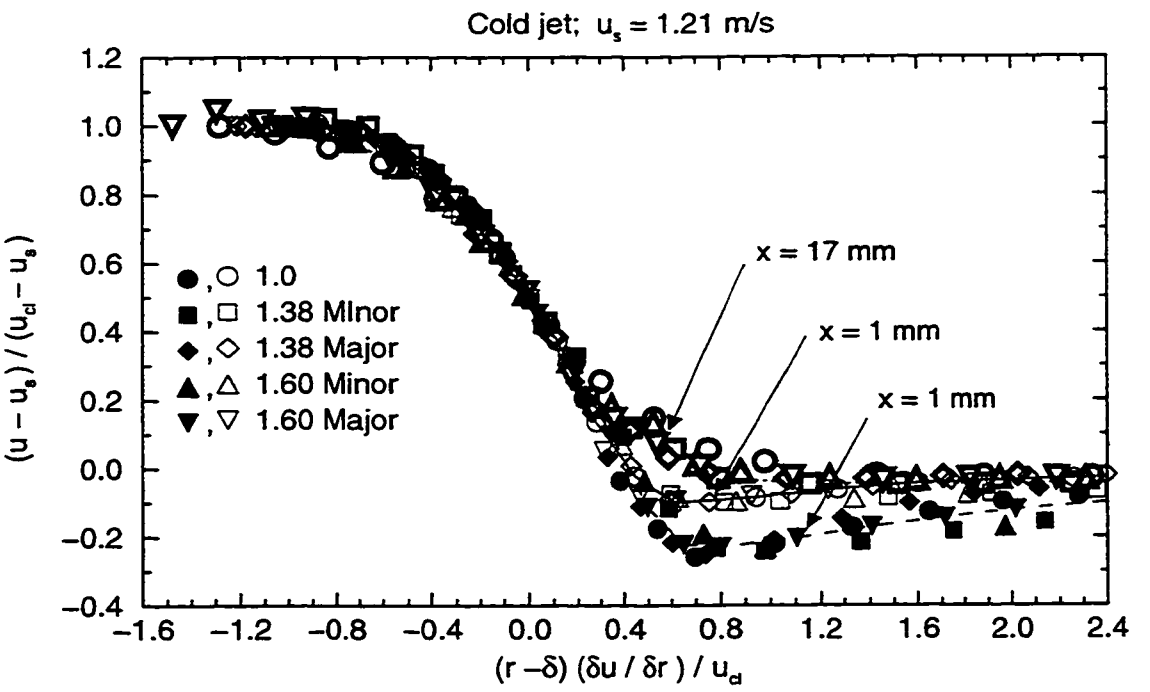

Fig. 5.7.5 Dimensionless velocity profiles from nozzles of various aspect ratios in the near–field region of the jet. Solid symbols: u_j = 3.4 m/s. Open symbols: u_j = 7.2 m/s.

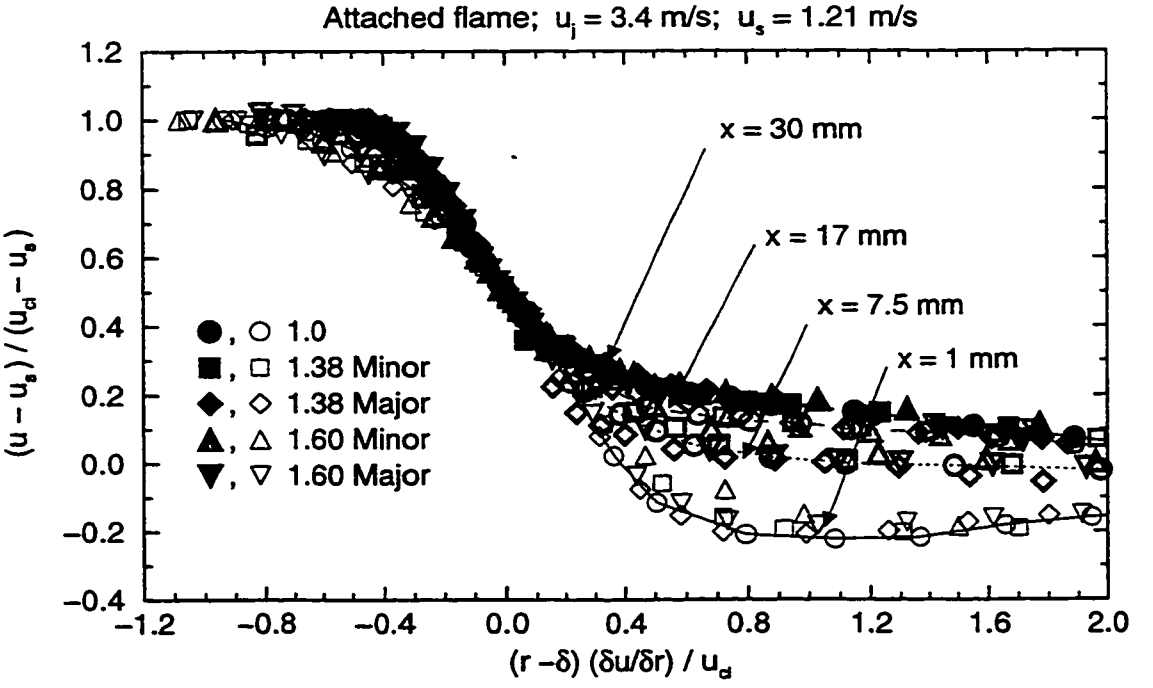

Fig. 5.7.6 Dimensionless velocity profiles from nozzles of various aspect ratios in the near–field region of the jet.

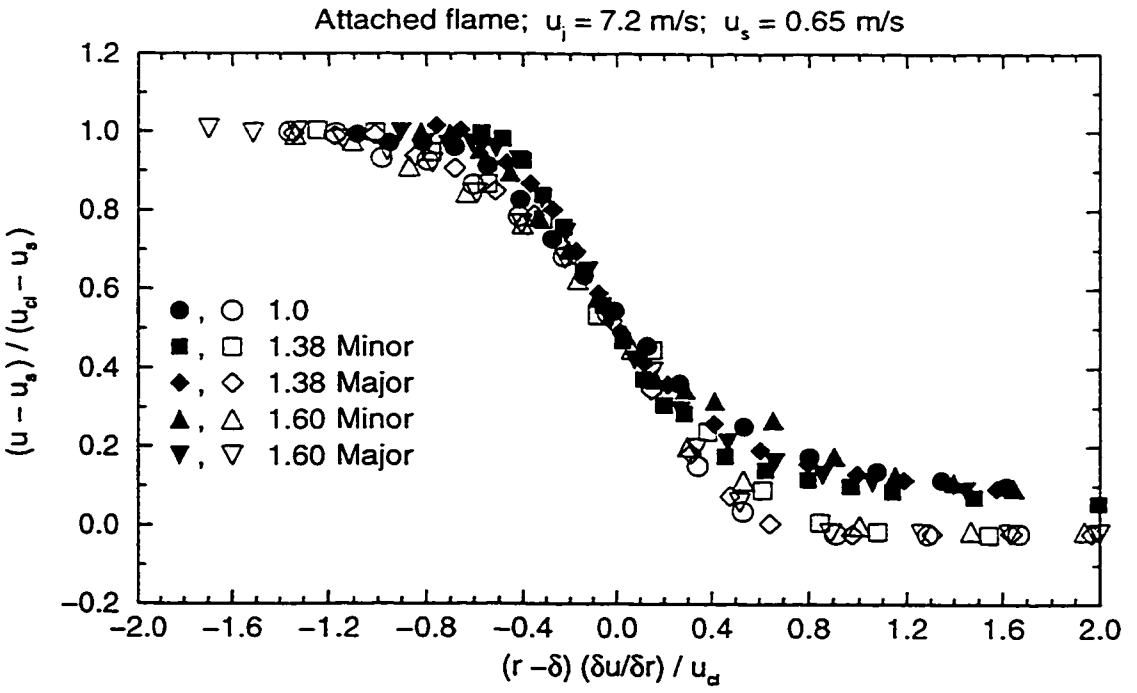

Fig. 5.7.7 Dimensionless velocity profiles from nozzles of various aspect ratios in the near–field region of the jet. Open symbols: x = 1 mm. Solid symbols: x = 30 mm.

CHAPTER 6

CONCLUSIONS

6.1 General Conclusions

A number of conclusions can be made from the results obtained in this study and may be summarized as follows:

- There were two distinct regions in which the flame extinguishes as either a lifted flame or an attached flame, depending on the value of the co-flowing stream velocity. The flame blew out as a lifted flame in low co-flowing stream velocities while attached flame blowout occurred at relatively higher co-flowing stream velocities.
- A number of parameters such as the nozzle lip thickness and ellipticity, jet fuel additives and the type and concentration of auxiliary fuel in the co-flowing stream of air affected the blowout of jet diffusion flames. The effect was dependent on whether the flame was lifted or attached at blowout.
- Generally, the blowout limits of jet diffusion flames decrease with an increase in the co-flowing stream velocity. The rate of decrease in the blowout velocity with an increase in the co-flowing stream velocity was considerably greater for lifted flames than for attached flames.
- The effect the co-flowing stream velocity on the lift-off velocity was rather small.
- The jet blowout velocities of lifted flames increased considerably with an increase

in the jet discharge area, however, the blowout velocities of attached flames were lower for large diameter jets than those of smaller jets.

- A variation in the nozzle geometry (i.e., lip thickness and ellipticity) for the same discharge area had little effect on the blowout limits of lifted flames.
- The nozzle geometry significantly affected the blowout limits of attached flames. The range of co-flowing stream velocities, in which such flames can be stabilized without additional external devices, was extended with an increase in the nozzle lip thickness. The stability limits of attached flames were also dependent on the nozzle ellipticity. The existence of an optimum aspect ratio with respect to the blowout limits was observed with the highest blowout limits recorded for jet nozzles with an aspect ratio of 1.32 (Nozzle Type 1) and 1.38 (Nozzle Type 2).
- The limiting stream velocity separating the regions of lifted from attached flame blowout was independent of the nozzle shape (i.e., lip thickness and ellipticity) but was dependent on the jet discharge area and jet fuel quality. The limiting stream velocity was found to increase with an increase in the jet diameter and calorific value of the fuel.
- The introduction of hydrogen into the methane jet significantly improved the blowout limits in both the lifted and attached flame regions. The addition of the diluents, carbon dioxide or nitrogen, into the methane jet decreased considerably the stability of lifted flames and, to a much lesser degree, the stability of attached flames.

- The effect of the addition of an auxiliary fuel into the surrounding air stream on the blowout limits of a jet flame depended on the co-flowing stream velocity and the type of auxiliary fuel employed. At low co-flowing stream velocities, the addition of an auxiliary fuel into the air stream improved the blowout limits; beyond a certain auxiliary fuel concentration, the formerly attached flame lifted off the nozzle rim, and the blowout limit was rapidly enhanced with further small increases in the auxiliary fuel concentration.
- At higher co-flowing stream velocities, the improvement in the blowout limits of attached flames with small concentrations of an auxiliary fuel into the air stream was more significant than at lower co-flowing stream velocities. A further increase in the auxiliary fuel concentration was either beneficial or detrimental to flame stability depending on the type of auxiliary fuel employed. For high burning velocity fuels such as hydrogen and ethylene, the formerly attached flame lifted off the nozzle rim, and stability improved rapidly with a further small increase in the fuel concentration. However, for fuels such as methane and propane having relatively low burning velocities, increasing their concentration did not cause the attached flame to lift off. Further increases in the concentration of these fuels resulted in a decrease in the flame blowout limit.
- The effect of the nozzle ellipticity on the blowout limits of a methane jet flame in a co-flowing stream of homogeneous fuel-air mixtures was also observed only in the attached flame blowout region. Although the greatest improvement in the

blowout limits was observed with the higher aspect ratio jets (i.e., a/b = 2.70 for Nozzle Type 1 and a/b = 1.60 for Nozzle Type 2), the blowout limits of these jets were still the lowest.

- Separate correlations for lifted and attached flames in different operating conditions were proposed due to their very different flame stabilization mechanisms. The blowout limits of lifted flames were correlated well, while the correlations for attached flames had limited application due to the effect of many additional factors.
- The flow structure, i.e., the axial and radial velocity and intensity of turbulence profiles, of jet diffusion flames issuing into a co-flowing stream were established in order to explain the experimentally observed behaviour of the blowout limits.
- Generally, an increase in the co-flowing stream velocity was found to decrease the axial distance where the jet centerline methane concentration in air equalled the lean flammability limit and to increase the axial velocity profile which distorted the balance between the local jet and burning velocity, and caused the flame to blowout earlier.
- The addition of hydrogen to the methane jet increased the rate of jet spread and the decay of the centerline jet velocity.
- The addition of auxiliary methane into a co-flowing stream of air increased the jet axial velocities and the rate of jet spread. It also caused an increase in the flame envelope and shifted the stoichiometric zone radially outward.
- The introduction of small amounts of carbon dioxide (3% by volume) into the

surrounding air stream was found to have very little affect on the flow structure of attached flames. The significant reduction in the blowout limits for flames in an air-CO_2 stream was, therefore, most likely the combined result of a reduction in the oxygen concentration in the stream and a change in the thermochemical properties of the fuel-air-diluent mixture such as the heat capacity, burning velocity and flammability limits.

- Generally, all of the cold elliptic jets tested experienced a higher jet spread in the minor axis than that in the major axis, which led to axis-switching. The degree of this jet spread was dependent on the operating conditions. The presence of a flame reduced the jet spread in the minor axis and as a result delayed axis-switching in elliptic jets.
- In the presence of a flame, the axis-switching phenomenon was observed in the jet with an aspect ratio of 1.38 but not for the jet with an aspect ratio of 1.60 (within the measuring range).
- An increase in the jet aspect ratio enhanced the entrainment rate of air into cold elliptic jets; however, very different results were obtained in the presence of a flame. Measurements of the jet centerline concentration indicated that the jet with an aspect ratio of 1.38 became fuel lean more quickly than the 1.60 aspect ratio jet.
- An attempt was made in correlating the experimentally established axial velocity profiles in the near-nozzle region of cold as well as ignited jets. The relation appeared to correlate satisfactorily the axial velocity profiles for jets with different

aspect ratios at the same downstream axial distance and the same discharge jet velocity.

- The addition of methane into a co-flowing stream of air delayed axis-switching in the 1.38 aspect ratio jet, while enhancing the rate of jet spread in the minor axis plane for the jet with an aspect ratio of 1.60.

6.2 Practical Implications

An experimental database of the blowout limits in a wide range of operating conditions is of considerable importance for a better understanding of the mechanism of flame stabilization and can be used in many practical applications. There is, to the best knowledge of the author, no data in the literature with a complete blowout limit curve with respect to the co-flowing stream velocity, different nozzle geometries and jet fuel compositions. Such a database can be used to validate existing lifted flame blowout models and help create models for attached flame blowout. In the meantime, the non-dimensional correlations developed can be used to predict the blowout limits of jet diffusion flames in many operating conditions. The present results also confirm the importance of a detailed design of the geometry of the jet outlet.

Furthermore, the study of the mixing of cold and ignited jets with a co-flowing oxidizing stream gives a useful insight into the stability of jet diffusion flames. Even if the present experimental data refer only to particular geometrical and flow conditions, it gives a description of the mixing process and creates an adequate experimental data base. It also

provides a characterization of the mean and fluctuating velocity fields of a geometrically simple but fluid dynamically complex configuration. These measurements may be used for the validation of CFD codes and for analyzing the performance of the employed turbulence models.

6.3 Future Work

It was shown that there exist many factors contributing to or detracting from the stability of jet diffusion flames issuing into a co-flowing air stream. However, due to the complexity of such systems, further experimentation is still required to fully understand the processes involved in flame stabilization, particularly in the region of attached flame blowout. At present, there are many parameters requiring investigation but the more pressing inquiries will be mentioned. For instance, it is not clear how the results are affected by scaling the combustion chamber and nozzles to different sizes and thus, despite the laborious nature of such work, necessitates further detailed studies. Moreover, studies on the preferential diffusion of a multi-component jet fuel or co-flowing air stream is needed to delineate its effect on flame stability. More experiments are also required to understand *why* an optimum aspect ratio exists with respect to axis-switching, air entrainment and hence the blowout limits.

It was also shown that many different parameters affect the flame-flow interactions which control the mechanism of flame stabilization. No model for the stabilization of attached flames and their blowout limits is available at present. It would be useful to

attempt a numerical simulation of this process.

References

[1] Feikema, D., R.H. Chen and Driscoll, J.F., "Blowout of Nonpremixed Flames: Maximum Coaxial Air Velocities Achievable, with and without Swirl," *Combustion and Flame*, Vol. 86, 1991, pp. 347-358.

[2] Wierzba, I. and Oladipo, A.B., "Blowout of Jet Diffusion Flames in Co-flowing Air Stream," *Emerging Energy Technology, ASME*, Vol, 57, 1994, pp. 29-33.

[3] Vanquickenborne, L. and van Tiggelen, A. "The Stabilization Mechanism of Lifted Diffusion Flames," *Combustion and Flame*, Vol. 10, 1966, pp. 59-69.

[4] Byggstoyl, S. and Magnussen, B.F., "A Model for Flame Extinction in Turbulent Flow," *Turbulent Shear Flows 4. International Symposium on Turbulent Shear Flows*, Berlin, 1985.

[5] Broadwell, J.E., Dahm, W.J.A. and Mungal, M.G., "Blowout of Turbulent Diffusion Flames," *Twentieth Symposium (International) on Combustion, The Combustion Institute*, 1984, pp. 303-310.

[6] Dahm, W.J.A. and Dibble, R.W., "Coflowing Turbulent Jet Diffusion Flame Blowout," *Twenty-Second Symposium (International) on Combustion*, 1988, pp. 801-808.

[7] Karbassi, M., "Analytical and Experimental Studies of the Stability Limits of Nonpremixed Flames in a Co-Flowing Stream," Ph.D. Dissertation, Department of Mechanical Engineering, University of Calgary, Sep. 1997.

[8] Kalghatgi, G.T., "Blowout Stability of Gaseous Jet Diffusion Flames Part III:

Effect of Burner Orientation to Wind Direction," *Combustion Science and Technology*, Vol. 28, 1982, pp. 241-245.

[9] Karim, G.A., Wierzba, I. and Hanna, M., "The Blowout Limit of a Jet Diffusion Flame in a Co-flowing Stream of Lean Gaseous Fuel-Air Mixtures," *Combustion and Flame*, Vol. 57, 1984, pp. 283-288.

[10] Kibrya, M.G., "An Experimental and Analytical Examination of Jet Diffusion Flames in Non-Quiescent Environments of Fuel and Air," Ph.D. Dissertation, Department of Mechanical Engineering, University of Calgary, Jan. 1987

[11] Wierzba, I., Kar, K. and Karim, G.A., "An Experimental Investigation of the Blowout Limits of a Jet Diffusion Flame in Co-flowing Streams of Different Velocity and Composition," *Transactions of the ASME*, Vol. 115, June 1993, pp. 142-147.

[12] Gutmark, E. and Ho, C.M. "On a Forced Elliptic Jet," *Fourth Symposium on Turbulent Shear Flows*, 1983, p.7-13.

[13] Ho, C.M. and Gutmark, E., "Vortex Induction and Mass Entrainment in a Small-Aspect-Ratio Elliptic Jet," *Journal of Fluid Mechanics*, Vol. 179, 1987, pp. 383-405.

[14] Vranos, A., E.D. Taback and Shipman, C.W., "An Experimental Study of the Stability of Hydrogen-Air Diffusion Flames," *Combustion and Flame*, Vol. 12, 1968, pp. 253-260.

[15] Takahashi, F. and Schmoll, W.J., "Lifting Criteria of Jet Diffusion Flames,"

Twenty-Third Symposium (International) on Combustion, The Combustion Institute, 1990, pp. 677-683.

[16] Feikema, D., R.H. Chen and Driscoll, J.F., "Enhancement of Flame Blowout Limits by Use of Swirl," *Combustion and Flame*, Vol. 80, 1990, pp. 183-195.

[17] Takahashi, F., Mizomoto, M., Ikai, S., and Tsuruyama, K., "Stability Limits of Hydrogen/Air Coflow Jet Diffusion Flames," *Proceedings of the 28th Aerospace Sciences Meeting*, Paper AIAA-90-0034, January 1990.

[18] Takahashi, F. and Goss, L.P., "Near-Field Turbulent Structures and the Local Extinction of Jet Diffusion Flames," *Twenty-Fourth Symposium (International) on Combustion, The Combustion Institute*, 1992, pp. 351-359.

[19] Takahashi, F., Mizomoto, M. and Ikai, S., "Stability of Hydrogen Jet Diffusion Flames," *Hydrogen Energy Progress, Proceedings of the 3rd World Hydrogen Energy Conference*, Tokyo, Japan, 1980, pp. 1165-1176.

[20] Yoon, Y., Donbar, J.M. and Driscoll, J.F., "Blowout Stability Limits of a Hydrogen Jet Flame in a Supersonic, Heated, Coflowing Air Stream," *Combustion Science and Technology*, Vol. 97, 1994, pp. 137-156.

[21] Takeno, T. and Kotani, Y., "An Experimental Study on the Stability of Jet Diffusion Flame," *Acta Astronautica*, Vol. 2, 1975, pp. 999-1008.

[22] Seaba, J.P., Chen, L.-D. and Roquemore, W.M., "Liftoff Characteristics of Methane Jet Diffusion Flames," *Journal of Propulsion and Power*, Vol. 9, No. 4, 1993, pp. 654-656.

[23] Chen, T.H., Goss, L.P., Talley, D.G. and Mikolaitis, D.W., "Dynamic Stabilization Zone Structure of Jet Diffusion Flames from Liftoff to Blowout," *Journal of Propulsion and Power*, Vol. 8, No. 3, May-June 1992, pp. 548-552.

[24] Prasad, A., Gundavelli, S. and Gollahalli, S.R., "Characteristics of Diluent-Caused Lifted Gas Jet Flames," *Journal of Propulsion and Power*, Vol. 7, No. 5, 1991, pp. 659-667.

[25] Oladipo, A.B., "Experimental Investigation of a Jet Diffusion Flame and Flame Flashback within Streams of Homogeneous Fuel-Air Mixtures," M.Sc. Thesis, Department of Mechanical Engineering, University of Calgary, Dec. 1992.

[26] Kalghatgi, G.T., "Blow-Out Stability of Gaseous Jet Diffusion Flames. Part 1: In Still Air." *Combustion Science and Technology*. Vol. 26, 1981, pp. 233-239.

[27] Chao, Y.C. and Jeng, H.S., "Behaviour of the Lifted Jet Flame Under Acoustic Excitation," *Twenty-Fourth Symposium (International) on Combustion, The Combustion Institute*, 1992, pp. 333-340.

[28] Schadow, K.C., Gutmark, E., Parr, T.P., Parr, D.M., Wilson, K.J. and Ferrel, G.B., "Enhancement of Fine-Scale Turbulence for Improving Fuel-Rich Plume Combustion," *Journal of Propulsion and Power*, Vol. 6, No. 4, July-August 1990, pp. 357-363.

[29] Chen, R.H., Driscoll, J.F., Kelly, J., Namazian, M. and Schefer, R.W., "A Comparison of Bluff-Body and Swirl-Stabilized Flames," *Combustion Science and Technology*, Vol. 71, 1990, pp. 197-217.

[30] Coats, C.M. and Zhao, H., "Transition and Stability of Turbulent Jet Diffusion Flames," *Twenty-Second Symposium (International) on Combustion, The Combustion Institute*, 1988, pp. 685-692.

[31] Gollahalli, S.R., Khanna, T. and Prabhu, N., "Diffusion Flames of Gas Jets Issued from Circular and Elliptic Nozzles," *Combustion Science and Technology*, Vol. 86, 1992, pp. 267-288.

[32] Kalghatgi, G.T., "Lift-off Heights and Visible Lengths of Vertical Turbulent Jet Diffusion Flames in Still Air." *Combustion Science and Technology*, Vol. 41, 1984, pp. 17-29.

[33] Savas, O. and Gollahalli, S.R., "Stability of Lifted Laminar Round Gas-jet Flame," *Journal of Fluid Mechanics*, Vol. 165, 1986, pp. 297-318.

[34] Gollahalli, S.R., Savas, O., Huang, R.F. and Rodriquez Azara, J.L., "Structure of Attached and Lifted Gas Jet Flames in Hysteresis Region," *Twenty-First Symposium (International) on Combustion, The Combustion Institute*, 1986, pp. 1463-1471.

[35] Shekarachi, S., Savas, O. and Gollahalli, S.R., "Structure of a Split Gas Flame," *Combustion and Flame*, Vol. 73, No. 3, 1988, pp. 221-232.

[36] Trentacoste, N. and Sforza, P., "Further Experimental Results for Three-Dimensional Free Jets," *AIAA Journal*, Vol. 5, No. 5, May 1967, pp. 885-891.

[37] Krothapalli, A., Baganoff, D. and Karamcheti, K., "On the Mixing of a Rectangular

Jet," *Journal of Fluid Mechanics*, Vol. 107, 1981, pp. 201-220.

[38] Quinn, W.R., "Passive Near-Field Mixing Enhancement in Rectangular Jet Flows," *AIAA Journal*, Vol. 29, No. 4, April 1991, pp. 515-519.

[39] Schadow, K.C., Gutmark, E., Parr, D.M. and Wilson, K.J., "Selective Control of Flow Coherence in Triangular Jets," *Experiments in Fluids*, Vol. 6, 1988, pp. 129-135.

[40] Koshigoe, S., Gutmark, E., Schadow, K.C. and Tubis, A., "Initial Development of Noncircular Jet Leading to Axis Switching," *AIAA Journal*, Vol. 27, No. 4, April 1989.

[41] Gutmark, E., Schadow, K.C. and Wilson, K.J., "Noncircular Jet Dynamics in Supersonic Combustion," *Journal of Propulsion and Power*, Vol. 5, No. 5, Sept-Oct. 1989, pp. 529-533.

[42] Gutmark, E., Schadow, K.C. and Wilson, K.J., "Subsonic and Supersonic Combustion using Noncircular Injectors," *Journal of Propulsion and Power*, Vol. 7, No. 2, 1991, pp. 240-249.

[43] Crighton, D.G., "Instability of an Elliptic Jet," *Journal of Fluid Mechanics*, Vol. 59, Part 4, 1973, pp. 665-672.

[44] Gutmark, E. and Ho, C.M., "Visualization of a Forced Elliptic Jet," *AIAA Journal*, Vol. 24, No. 4, 1985, pp. 684-685.

[45] Hussain, F. and Husain, H.S., "Elliptic Jets. Part 1. Characteristics of Unexcited and Excited Jets," *Journal of Fluid Mechanics*, Vol. 208, 1989, pp. 257-320.

[46] Gollahalli, S.R., "Jet Flames from Noncircular Burners," *Sadana - Academy Proceedings in Engineering Sciences*, Vol. 22, 1997, pp. 369-382.

[47] Schadow, K.C., Wilson, K.J., Lee, M.J., and Gutmark, E., "Enhancement of Mixing in Ducted Rockets with Elliptic Gas-Generator Nozzles," *Proceedings to an AIAA Conference*, Paper No. 84-1260, 1984.

[48] Gollahalli, S.R. and Subba, S., "Partially Premixed Laminar Gas Flames from Triangular Burners," *Journal of Propulsion and Power*, Vol. 13, No. 2, 1997, pp. 226-232.

[49] Kamal, A. and Gollahalli, S., "Numerical Analysis of the Near-nozzle Structure of Gas Jet Flames from Circular and Rectangular Nozzles," *Proceedings of the 1996 International Joint Power Generation Conference. Part 1, ASME*, Houston, Texas, 1996, pp. 273-277.

[50] Kamal, A. and Gollahalli, S.R., "Effects of Noncircular Fuel Nozzles on the Pollutant Emission Characteristics of Natural Gas Burners for Residential Furnaces," *Proceedings of the 1993 International Joint Power Generation Conference*, Vol. 17, 1993, pp. 41-50.

[51] Prabhu, N. and Gollahalli, S.R., "Effect of Aspect Ratio on Combustion Characteristics of Elliptic Nozzle Flames," *Emerging Energy Technology, Proceedings of the 14th Annual Energy-Sources Technology Conference and Exhibition, ASME*, Vol. 36, 1991, pp. 51-56.

[52] Gollahalli, S.R. and Prabhu, N., "Differences in the Structure of Lifted Gas Jet

Flames with Laminar Base over Circular and Elliptic Nozzles", *Proceedings of Energy Sources Technology Conference and Exhibition, ASME*, New Orleans, 1990.

[53] Dan-Zhi, C., "A Modelling Theory of Combustion Chambers," *Combustion Science and Technology*, Vol. 24, 1981, pp. 221-226.

[54] Abramovich, G.N., *The Theory of Turbulence Jets*, M.I.T. Press, 1963.

[55] Antonia, R.A. and Bilger, R.W., "An Experimental Investigation of an Axisymmetric Jet in a Co-flowing Air Stream," *Journal of Fluid Mechanics*, Vol. 61, Part 4, 1973, pp. 805-822.

[56] Becker, H.A., Hottel, H.C. and Williams, G.C., "Mixing and Flow in Ducted Turbulent Jets," *Ninth Symposium (International) on Combustion, The Combustion Institute*, 1963, pp. 7-20.

[57] Bradbury, L.J.S., "The Structure of a Self-Preserving Turbulent Plane Jet," *Journal of Fluid Mechanics*, Vol. 23, 1965, pp. 31-64.

[58] Bradbury, L.J.S. and Riley, J., "The Spread of a Turbulent Plane Jet Issuing into a Parallel Moving Airstream." *Journal of Fluid Mechanics*, Vol. 27, Part 2, 1967, pp. 381-394.

[59] Biringen, S., "An Experimental Study of a Turbulent Axisymmetric Jet Issuing into a Coflowing Airstream," *vonKarman Institute for Fluid Dynamics*, Technical Notes 110, April 1975.

[60] Steward, F.R. and Guruz, A.G., "Aerodynamics of a Confined Jet with Variable

Density," *Combustion Science and Technology*, Vol. 16, 1977, pp. 29-45.

[61] Forstall, W. Jr., and Shapiro, A.H., "Momentum and Mass Transfer in Coaxial Gas Jets," *Journal of Applied Mechanics*, Vol. 17, 1950, pp. 399-408.

[62] Antonia, R.A. and Bilger, R.W., "The Heated Round Jet in a Coflowing Stream," *AIAA Journal*, Vol. 14, No. 11, 1976.

[63] Schefer, R.W., Hartmann, V. and Dibble, R.W., "Conditional Sampling of Velocity in a Turbulent Nonpremixed Propane Jet," Sandia Report SAND87-8610, Sandia National Laboratories, 1987.

[64] Gladnick, P.G., Enotiadis, A.C., LaRue, J.C. and Samuelsen, G.S. "Near-field Characteristics of a Turbulent Co-flowing Jet," *AIAA Journal*, Vol. 28, No. 8, 1990, pp. 1405-1414.

[65] Buresti, G., Talamelli, A. and Petagna, P., "Experimental Characterization of the Velocity Field of a Coaxial Jet Configuration," *Experimental Thermal and Fluid Science*, Vol. 9, 1994, pp. 135-146.

[66] Ribeirio, M.M. and Whitelaw, J.H., "Turbulent Mixing of Coaxial Jets with Particular Reference to the Near-Exit Region," *Journal of Fluids Engineering*, Vol. 98, 1976, pp. 284-291.

[67] Dibble, R.W., Magre, P, Schefer, R.W. and Chen, J.Y., "Measurement of Joint Probability of Velocity and Concentrations in a Turbulent Nonpremixed Flame," Sandia Report SAND85-8234, Sandia National Laboratories, 1987.

[68] Starner, S.H. and Bilger, R.W., "Measurements of Velocity and Concentration in

Turbulent Diffusion Flames with Pressure Gradients," *AIAA 18th Aerospace Sciences Meeting*, Paper No. AIAA-80-0205.

[69] Gunther, R. And Lenze, B., "The Stability of Free Jet Diffusion Flames," *Proceedings of the Fourteenth World Gas Conference, International Gas Union*, Toronto, 1979, pp 1-15.

[70] Miake-Lye, R.C. and Hammer, J.A., "Lifted Turbulent Jet Flames: A Stability Criterion Based on the Jet Large-scale Structure," *Twenty-Second Symposium (International) on Combustion, The Combustion Institute*, 1988, pp. 817-824.

[71] Peters, N., "Partially Premixed Diffusion Flamelets in Non-Premixed Turbulent Combustion," *Twentieth Symposium (International) on Combustion, The Combustion Institute*, 1984, pp. 353-360.

[72] Pitts, W.M., "Assessment of Theories for the Behaviour and Blowout of Lifted Turbulent Jet Diffusion Flames," *Twenty-Second Symposium (International) on Combustion, The Combustion Institute*, 1988, pp. 809-816.

[73] Eickhoff, H., Lenze, B. and Leuckel, W., "Experimental Investigation on the Stabilization Mechanism of Jet Diffusion Flames," *Twentieth Symposium (International) on Combustion, The Combustion Institute*, 1984, pp. 311-318.

[74] Kaplan, C.R., Oran, E.S. and S.W. Baek. "Stabilization Mechanism of Lifted Jet Diffusion Flames," *Twenty-Fifth International Symposium on Combustion, The Combustion Institute*, 1994, pp. 1183-1189.

[75] Lewis, B. and von Elbe, G., "Stability and Structure of Burner Flames," *Journal*

of Chemical Physics, Vol. 11, 1943, pp. 75-97.

[76] Karlovitz, B., Denniston, D.W., Knapschafer, D.H., and Wells, F.E., "Studies on Turbulent Flames," *Fourth Symposium (International) on Combustion, The Combustion Institute*, 1953, pp. 613-620.

[77] Sanders, J.P.H. and Lamers, A.P.G.G., "Modelling and Calculation of Turbulent Lifted Diffusion Flames," *Combustion and Flame*, Vol. 96, 1994, pp. 22-33.

[78] Peters, N. and Williams, F.A., "Liftoff Characteristics of Turbulent Jet Diffusion Flames," *AIAA Journal*, Vol. 21, No. 3, March 1983, pp. 423-429.

[79] Schefer, R.W., Namazian, M., Filtopoulos, E.E.J. and Kelly, J., "Temporal Evolution of Turbulence/Chemistry Interactions in Lifted, Turbulent-Jet Flames," *Twenty-Fifth Symposium (International) on Combustion, The Combustion Institute*, 1994, pp. 1223-1231.

[80] Chelliah, H.K., Law, C.K, Ueda, T., Smooke, M.D. and Williams, F.A., "An Experimental and Theoretical Investigation of the Dilution, Pressure and Flow-field Effects on the Extinction Condition of Methane-Air-Nitrogen Diffusion Flames," *Twenty-Third Symposium (International) on Combustion, The Combustion Institute*, 1990, pp. 503-511.

[81] Kalghatgi, G.T., "Blowout Stability of Gaseous Jet Diffusion Flames Part II: Effect of Cross Wind," *Combustion Science and Technology*, Vol. 26, 1981, pp. 241-244.

[82] Peters, N., "Local Quenching Due to Flame Stretch and Non-Premixed Turbulent Combustion," *Combustion Science and Technology*, Vol. 30, 1983, pp. 1-17.

[83] Bradley, D., Gaskell, P.H. and Lau, A.K.C., "A Mixedness-Reactedness Flamelet Model for Turbulent Diffusion Flames," *Twenty-Third Symposium (International) on Combustion, The Combustion Institute*, 1990, pp. 685-692.

[84] Muller, C.M., Breitbach, H. and Peters, N., "Partially Premixed Turbulent Flame Propagation in Jet Flames," *Twenty-Fifth Symposium (International) on Combustion, The Combustion Institute*, 1994, pp. 1099-1106.

[85] Cuenot, B. and Poinsot, T., "Effects of Curvature and Unsteadiness in Diffusion Flames. Implications for Turbulent Diffusion Combustion," *Proceedings of the Twenty-Fifth International Symposium on Combustion*, Irvine, Paper no. 25-200, 1994.

[86] Broadwell, J.E. and Dimotakis, P.E., "Implications of Recent Experimental Results for Modelling Reactions in Turbulent Flows," *AIAA Journal*, Vol. 24, No. 6, June 1986, pp. 885-889.

[87] Dahm, W.J.A. and Mayman, A.G., "Blowout Limits of Turbulent Jet Diffusion Flames for Arbitrary Source Conditions," *AIAA Journal*, Vol. 28, No. 7, July 1990.

[88] Glass, M. and Kennedy, I.M., "An Improved Seeding Method for High Temperature Laser Doppler Velocimetry," *Combustion and Flame*, Vol. 29, 1977, pp. 333-335.

[89] Fristrom, R.M. and Westenburg, A.A., *Flame Structure*, McGraw-Hill, New York, 1965.

[90] Takahashi, F., Mizomoto, M., Ikai, S. and Futaki, N., "Lifting Mechanism of Free

Jet Diffusion Flames," *Twentieth Symposium (International) on Combustion, The Combustion Institute, 1984*, pp. 295-302.

[91] Haniff, M.S., Melvin, A., Smith, D.B. and Williams, A., "The Burning Velocities of Methane and SNG Mixtures of Air," *Journal of the Institute of Energy*, Vol. LXII, No. 435, 1989, pp. 229-236.

[92] Reed, S.B., Mineur, J. and McNaughton, J.P., "The Effect on the Burning Velocity of Methane of Vitiation on Combustion Air," *Journal of the Institute of Fuel*, Vol. 44, 1971, pp. 149-155.

[93] Fells, I. and Rutherford, A.G., "Burning Velocity of Methane-air Flames," *Combustion and Flame*, Vol. 13, 1969, pp. 130-138.

[94] Gerry, H.M. and Walter, R.K., "Some Effect of Inert Diluents on Flame Speeds and Temperatures," *Fourth Symposium (International) on Combustion, The Combustion Institute,* 1952, pp. 313-320.

[95] Savas, O. and Gollahalli, S.R., "Flow Structure in Near-Nozzle Region of Gas Jet Flames," *AIAA Journal*, Vol. 24, No. 7, 1986, pp. 1137-1140.

[96] Browand, F.K. and Ho, C.M., "The Mixing Layer: An Example of Quasi-two-dimensional Turbulence," *Journal de Mechanique Theorique et Appliquee* (numero special), pp. 99-120.

[97] Kar, K., "Experimental Study of Flame-Blowout and Flashback in a System Involving Fuel Jet within Homogeneous Turbulent Stream of Air and Fuel," M.Sc. Thesis, Department of Mechanical Engineering, University of Calgary, Dec. 1990.

APPENDIX I

LDV Measurements:

Effect of Co-flowing Stream Velocity

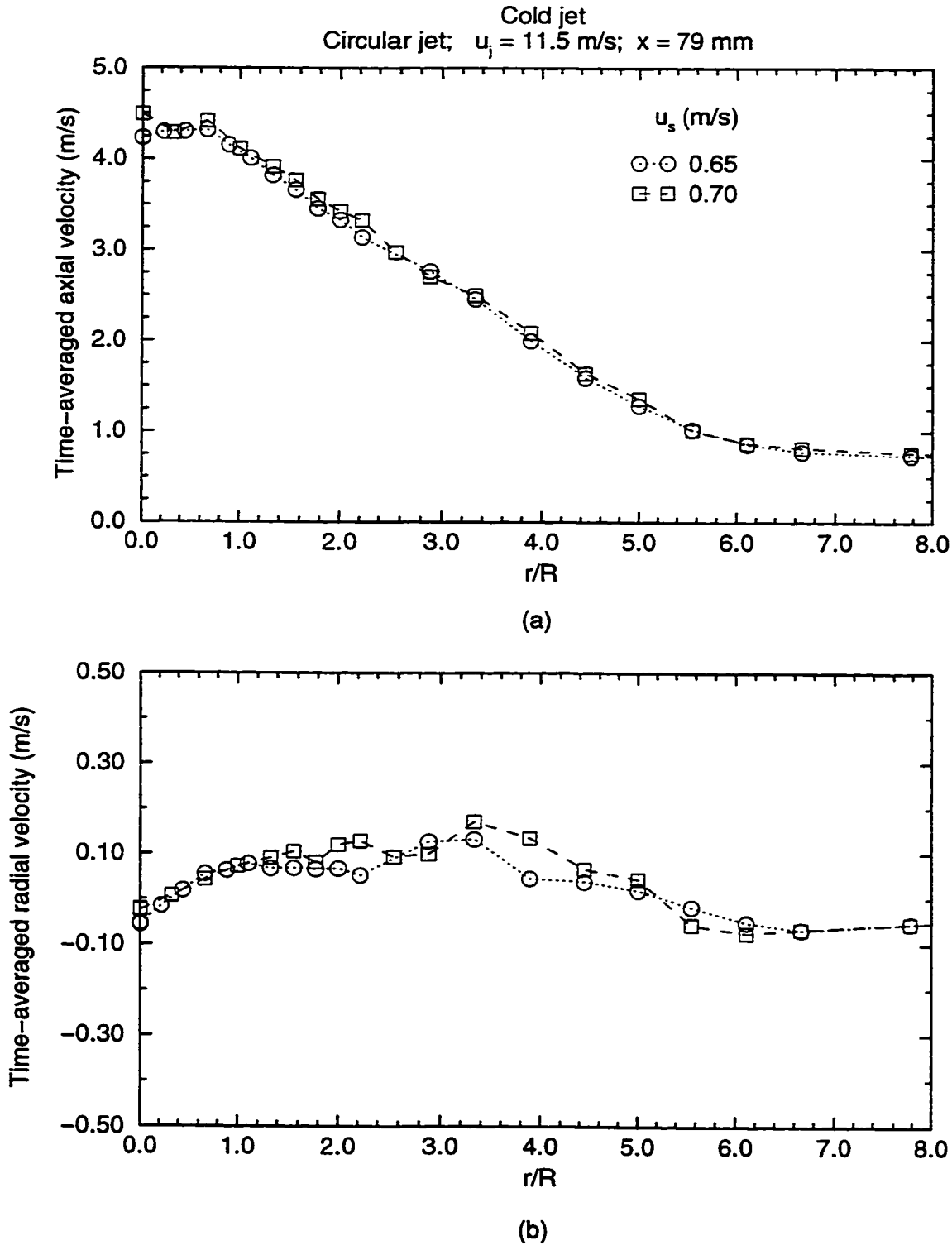

Fig. A.1.1 Time–averaged axial and radial velocity profiles within a cold circular jet at a downstream distance of 79 mm for two different co–flowing stream velocities (R = 2.29 mm).

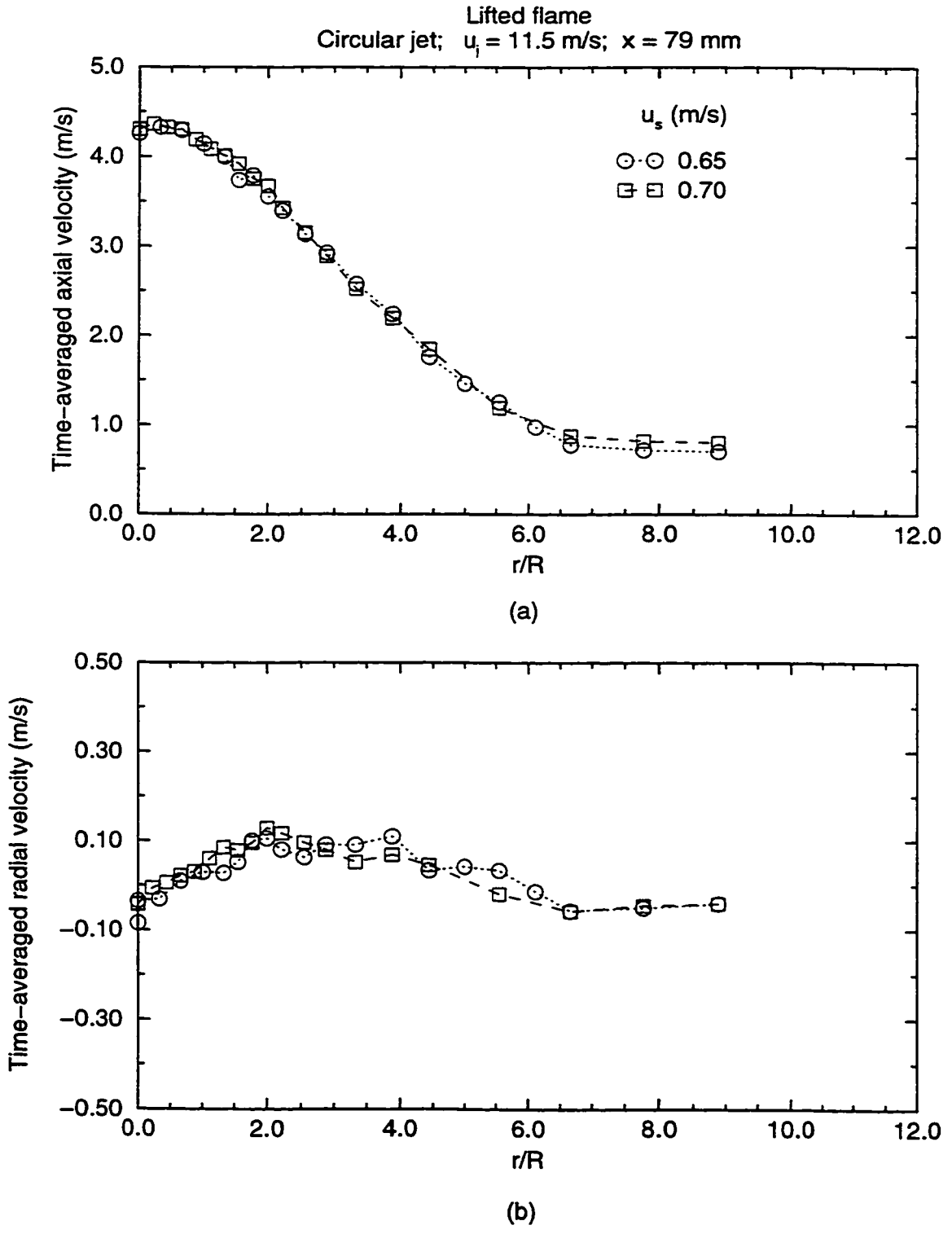

Fig. A.1.2 Time–averaged axial and radial velocity profiles within a lifted flame at a downstream distance of 79 mm for two different co–flowing stream velocities.

APPENDIX II

LDV Measurements:

Effect of Jet Discharge Velocity

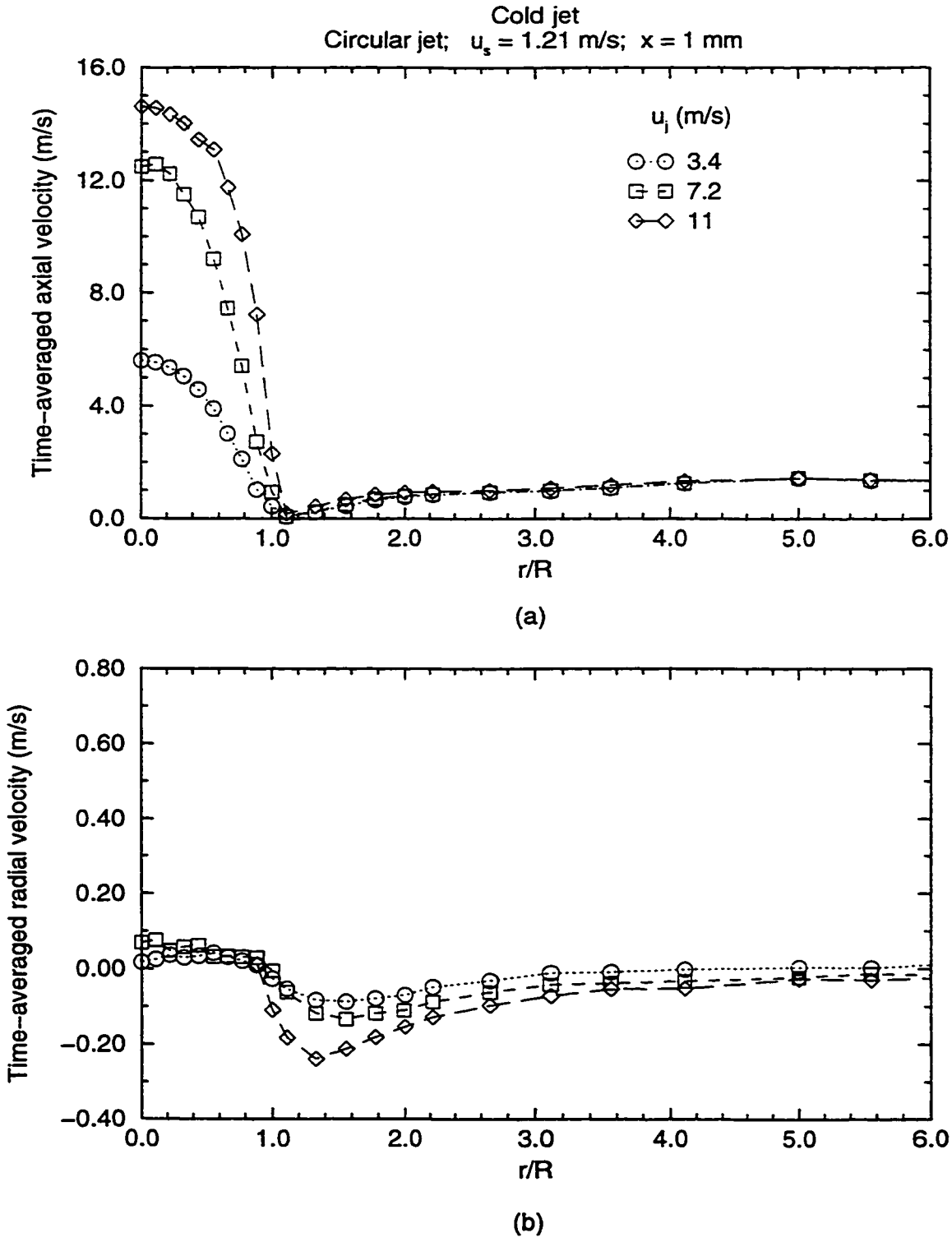

Fig. A.2.1 Time–averaged axial and radial velocity profiles within a cold circular jet at a downstream distance of 1 mm for different jet discharge velocities (R = 2.29 mm).

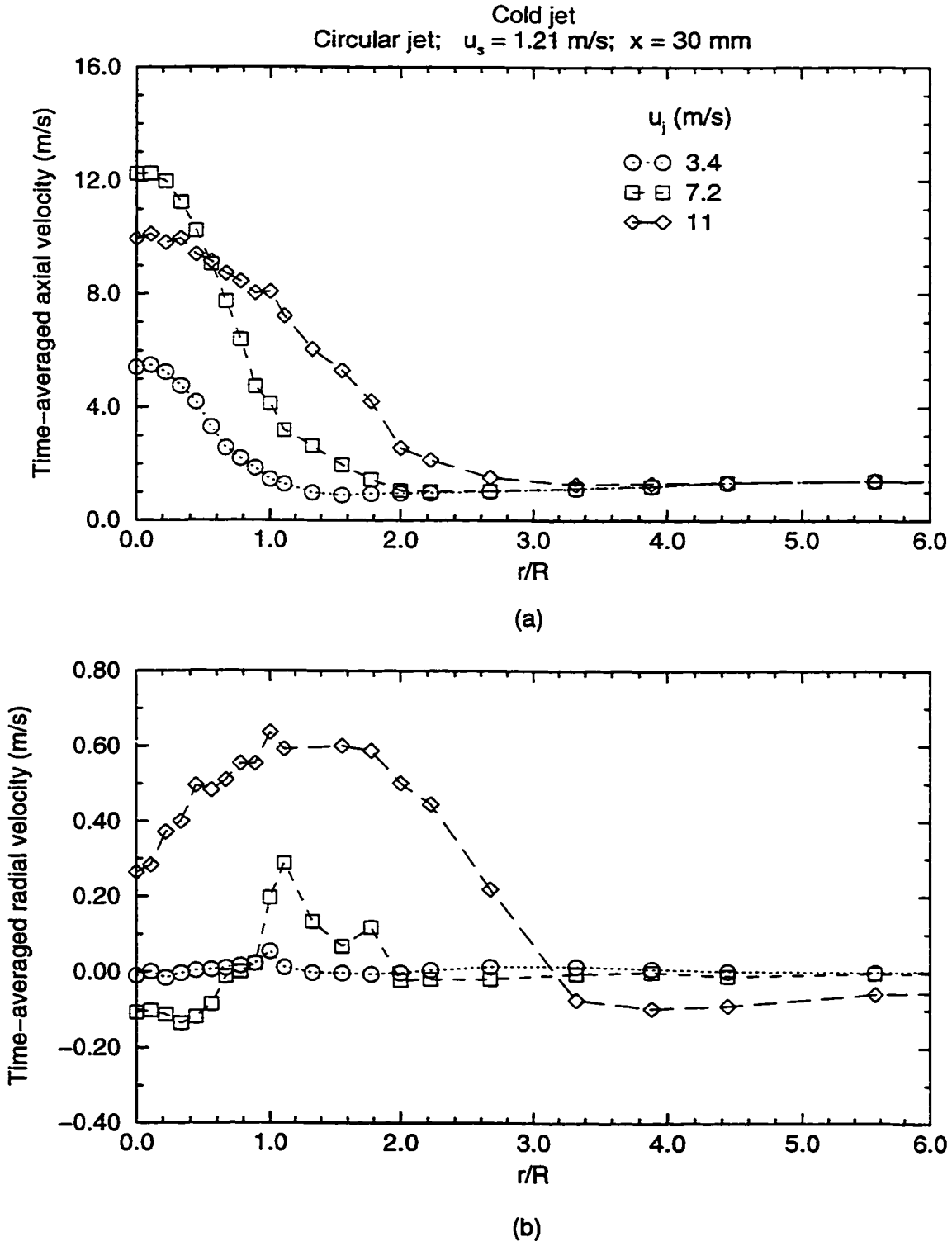

Fig. A.2.2 Time-averaged axial and radial velocity profiles within a cold circular jet at a downstream distance of 30 mm with different discharge velocities (R = 2.29 mm).

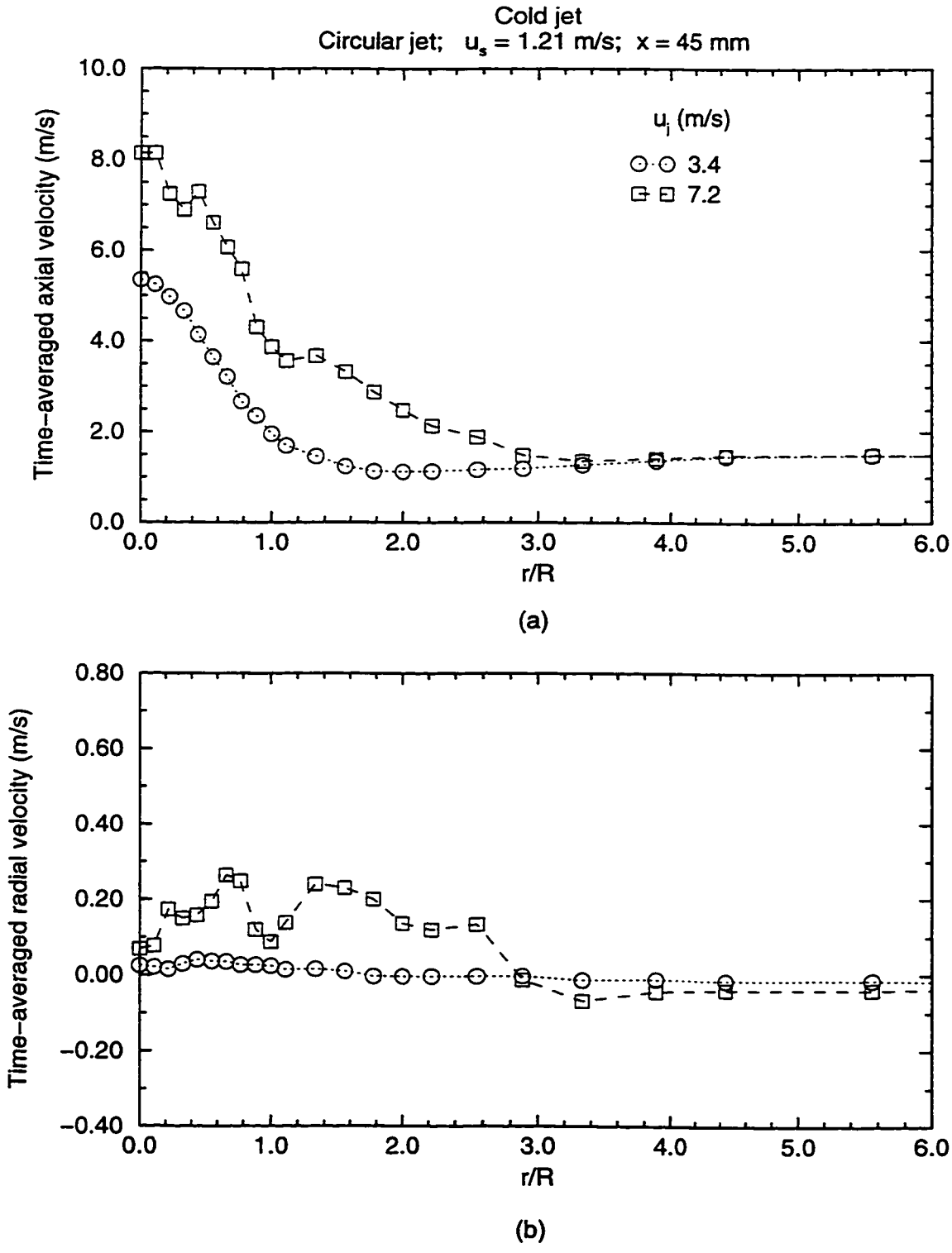

Fig. A.2.3 Time–averaged axial and radial velocity profiles within a cold circular jet at a downstream distance of 45 mm with different discharge velocities.

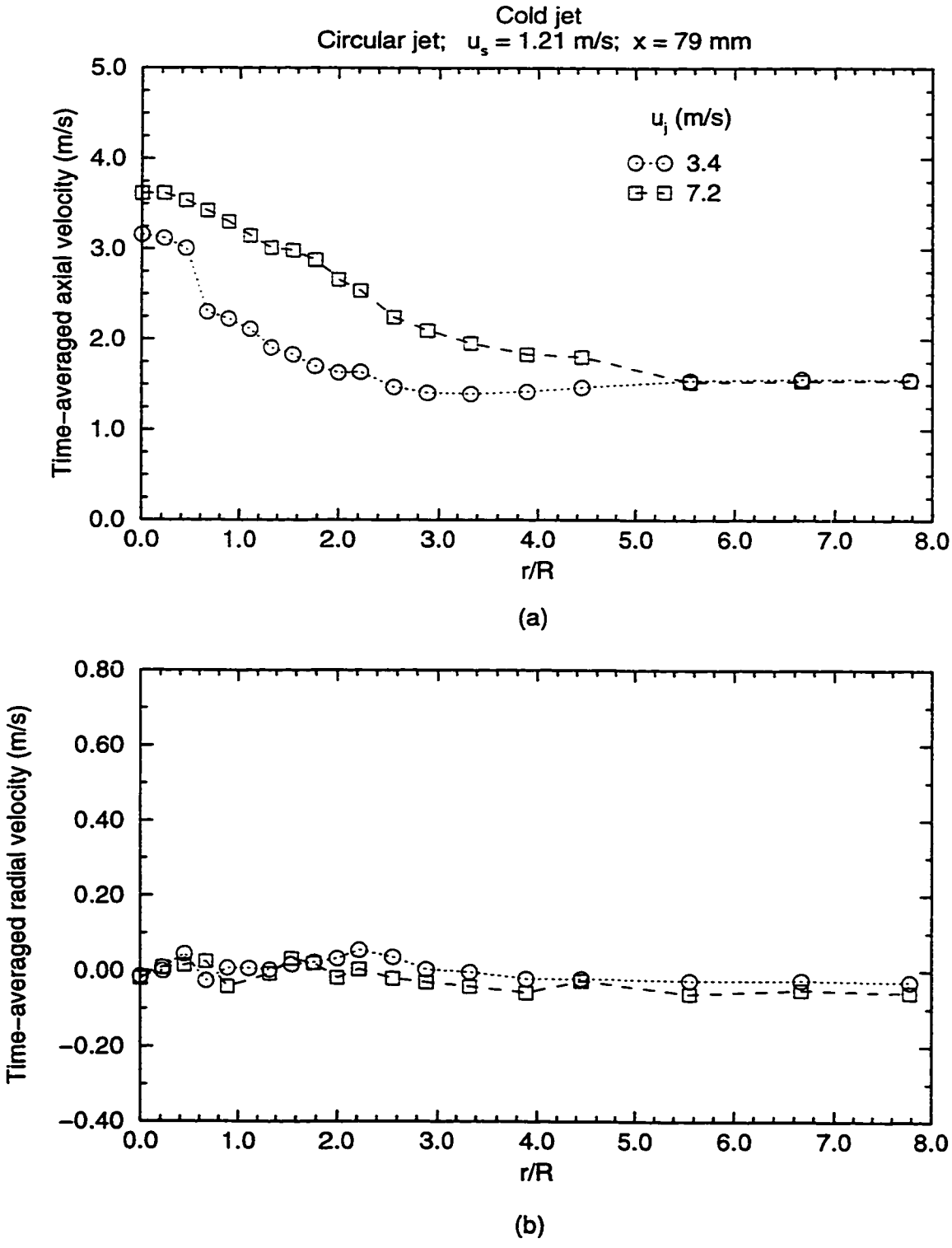

Fig. A.2.4 Time–averaged axial and radial velocity profiles within a cold circular jet at a downstream distance of 79 mm with different discharge velocities (R = 2.29 mm).

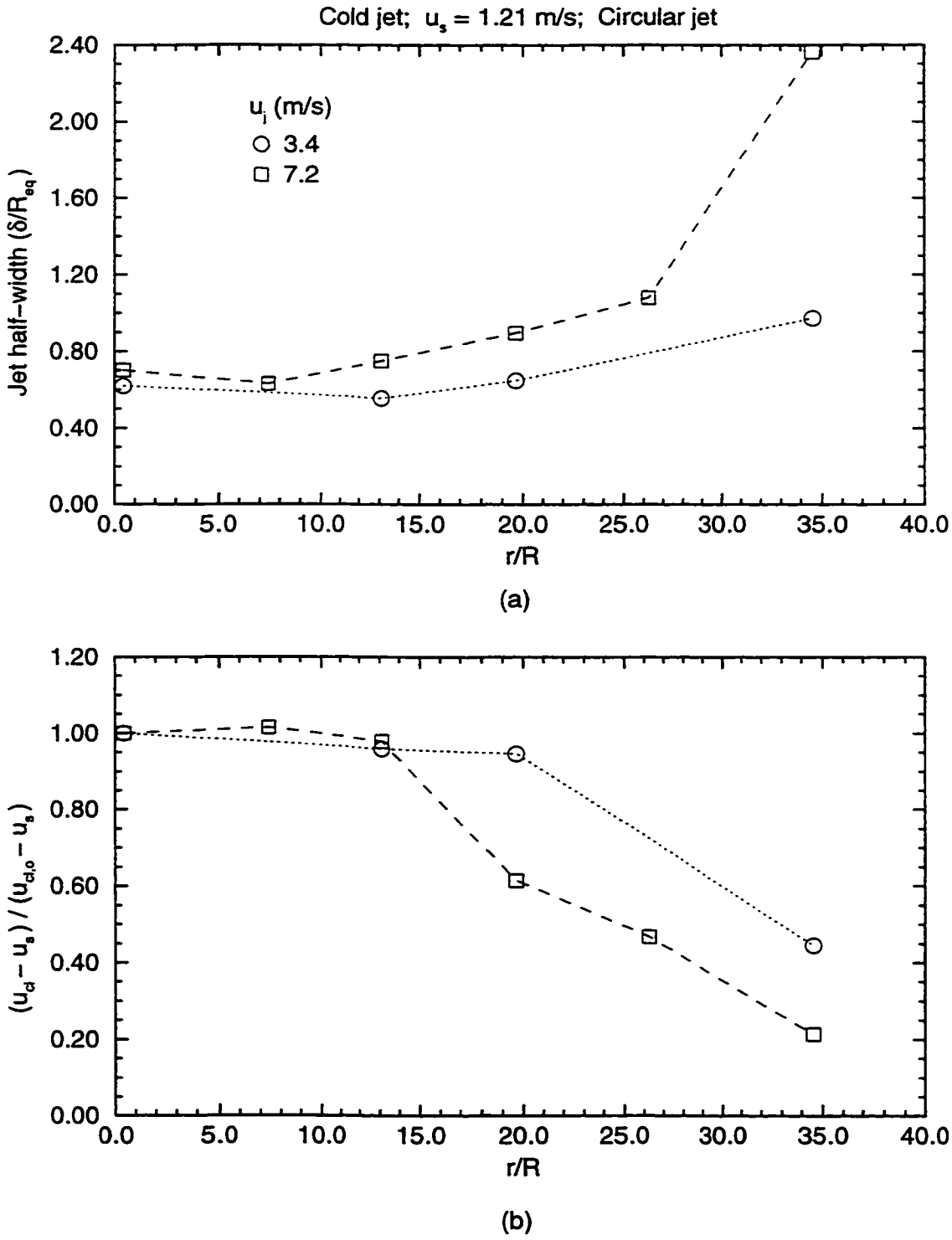

Fig. A.2.5 A comparison of (a) the jet half–width and (b) the centerline velocity with downstream distance for cold jets with two different discharge velocities (R = 2.29 mm).

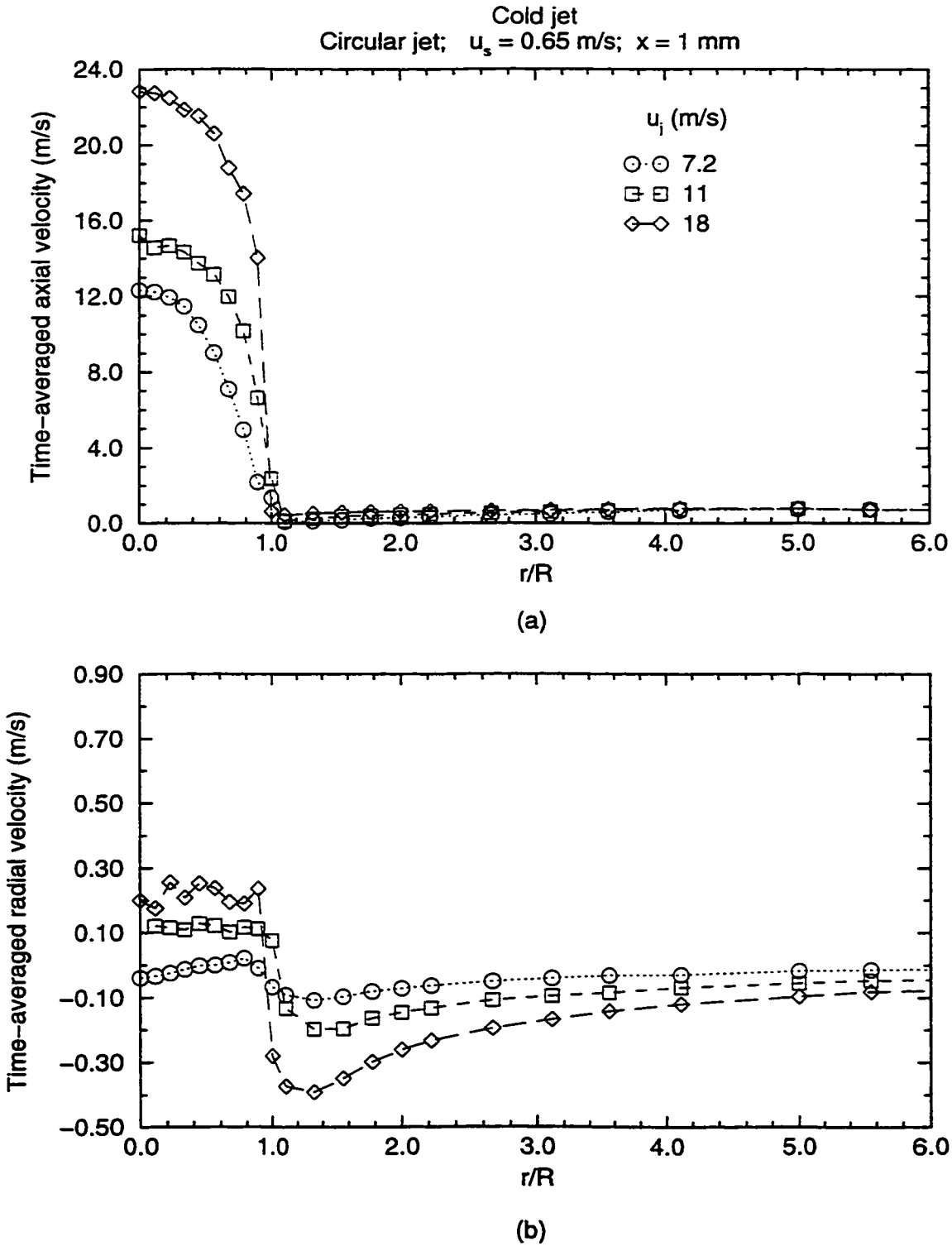

Fig. A.2.6 Time–averaged axial and radial velocity profiles within cold jets at a downstream distance of 1 mm with different discharge velocities (R = 2.29 mm).

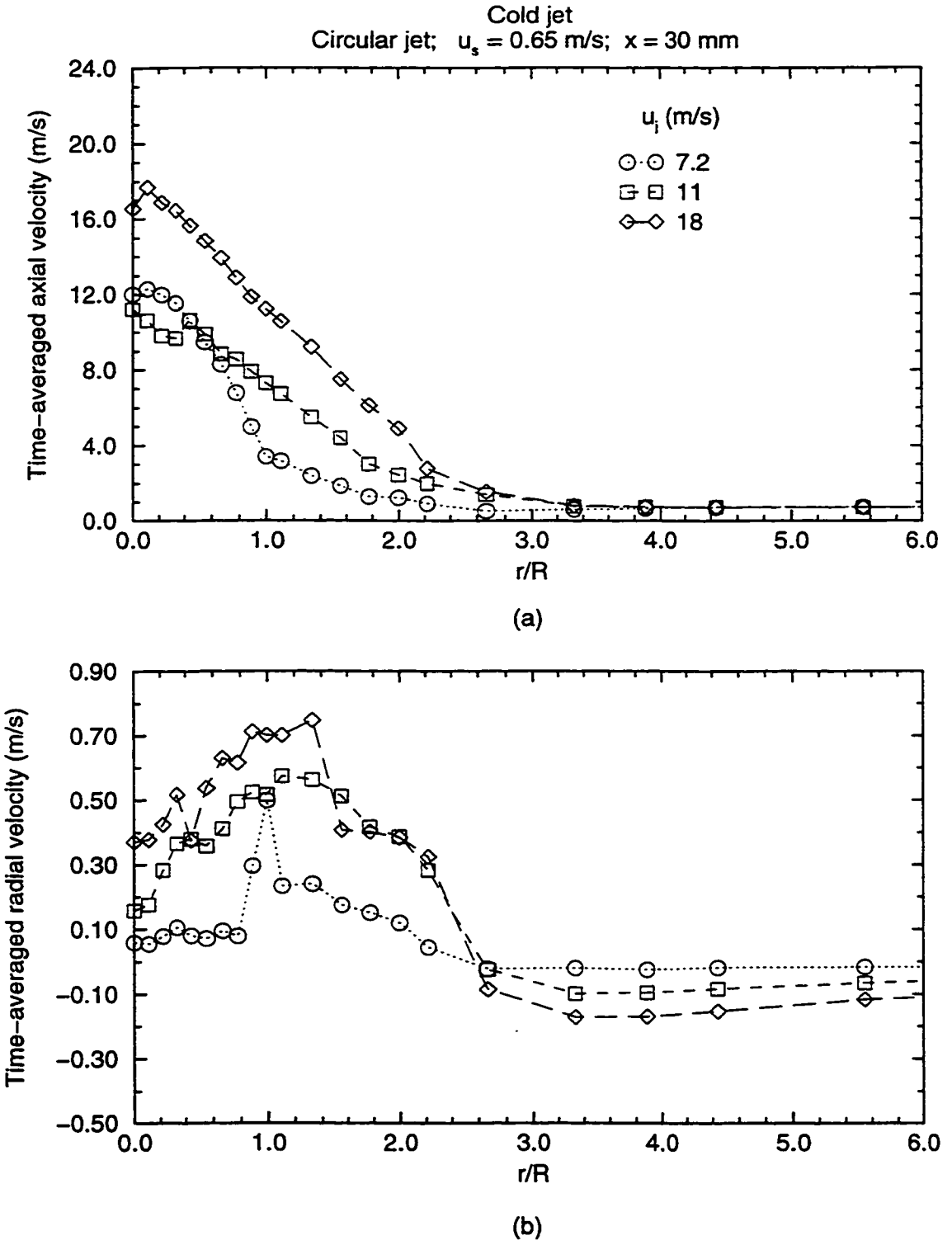

Fig. A.2.7 Time–averaged axial and radial velocity profiles within cold jets at a downstream distance of 30 mm with different discharge velocities (R = 2.29 mm).

Cold jet; Circular jet; u_s = 1.21 m/s

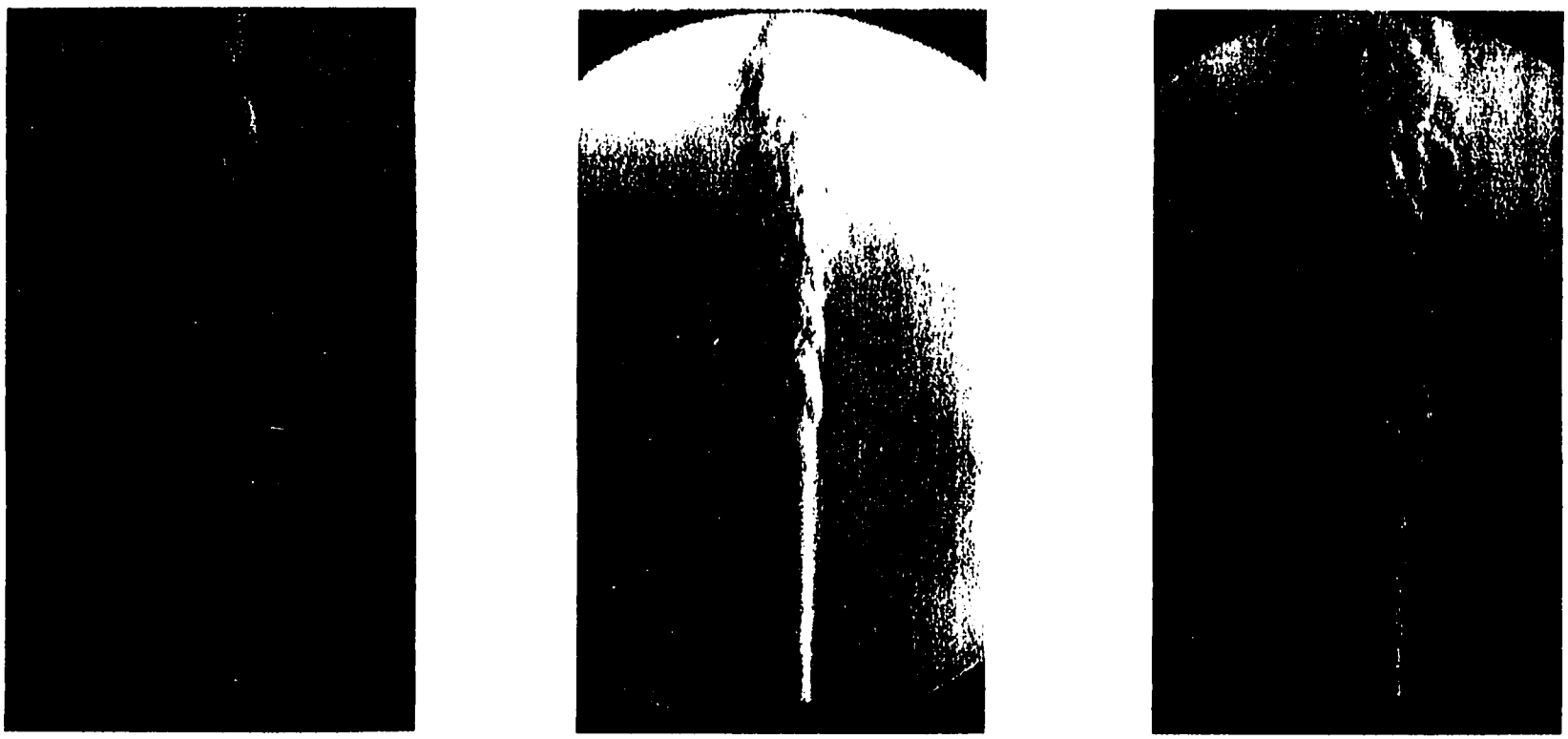

(a)
u_j = 3.4 m/s (Re_j = 816)

(b)
u_j = 7.2 m/s (Re_j = 1722)

(c)
u_j = 11 m/s (Re_j = 2630)

Scale: 1 cm

Fig. A.2.8 Schlieren photographs showing the effect of varying jet velocities on the flow structure of cold jets in a co-flowing stream of velocity 1.21 m/s (d_j = 4.57 mm).

APPENDIX III

LDV Measurements:

Effect of Hydrogen Addition

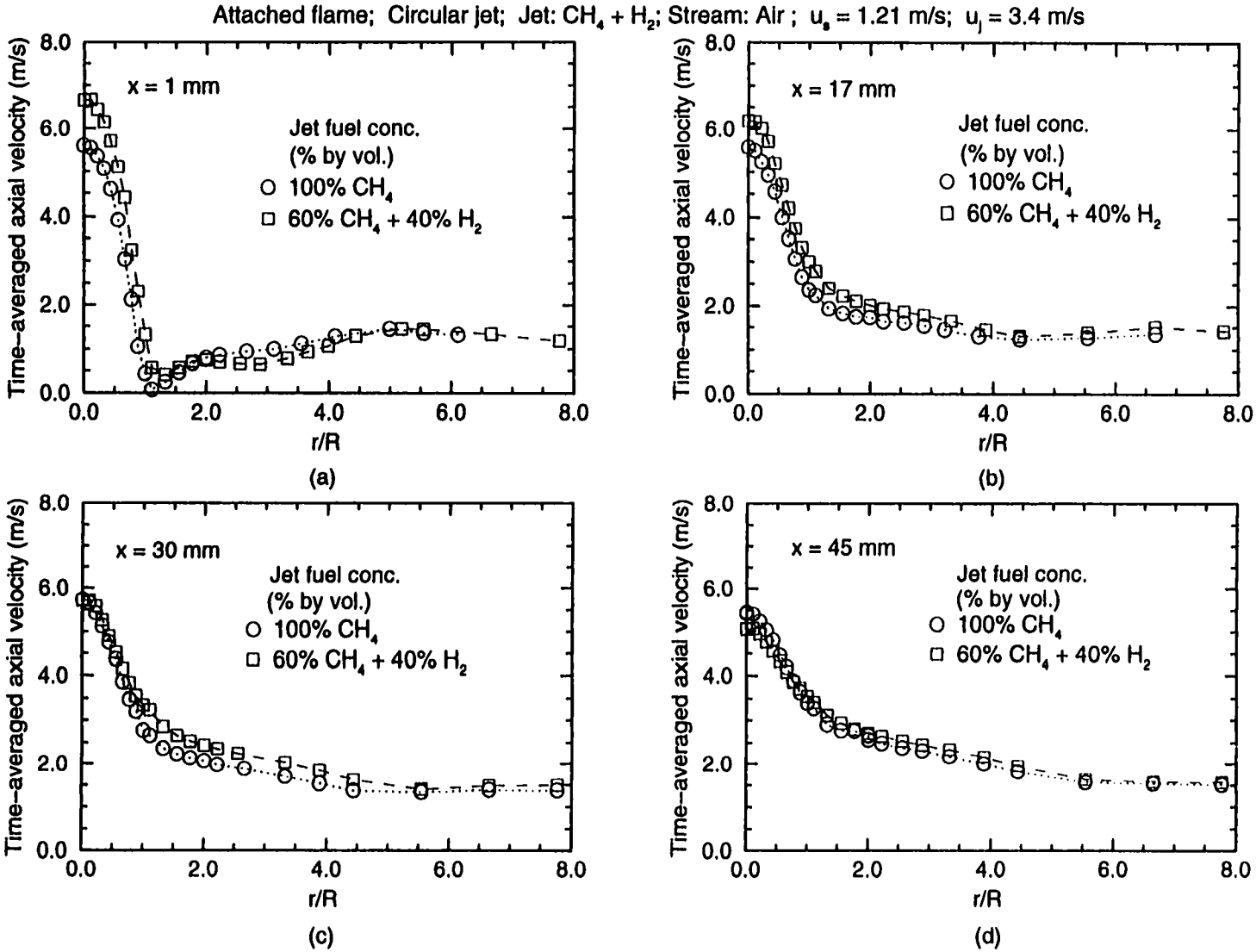

Fig. A.3.1 Time-averaged axial velocity profiles within attached flames of different fuel compositions.

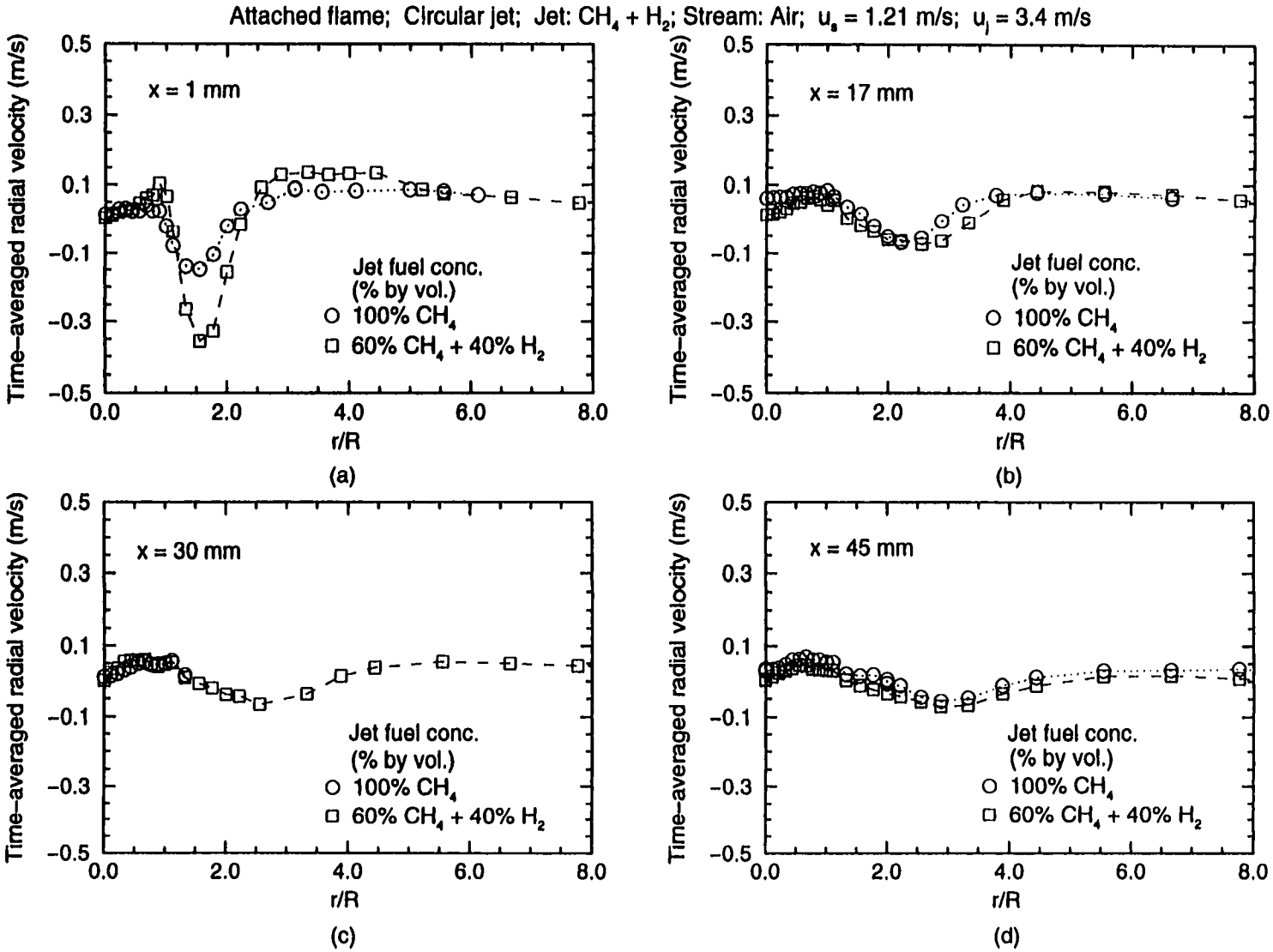

Fig. A.3.2 Time-averaged radial velocity profiles within attached flames for different fuel compositions.

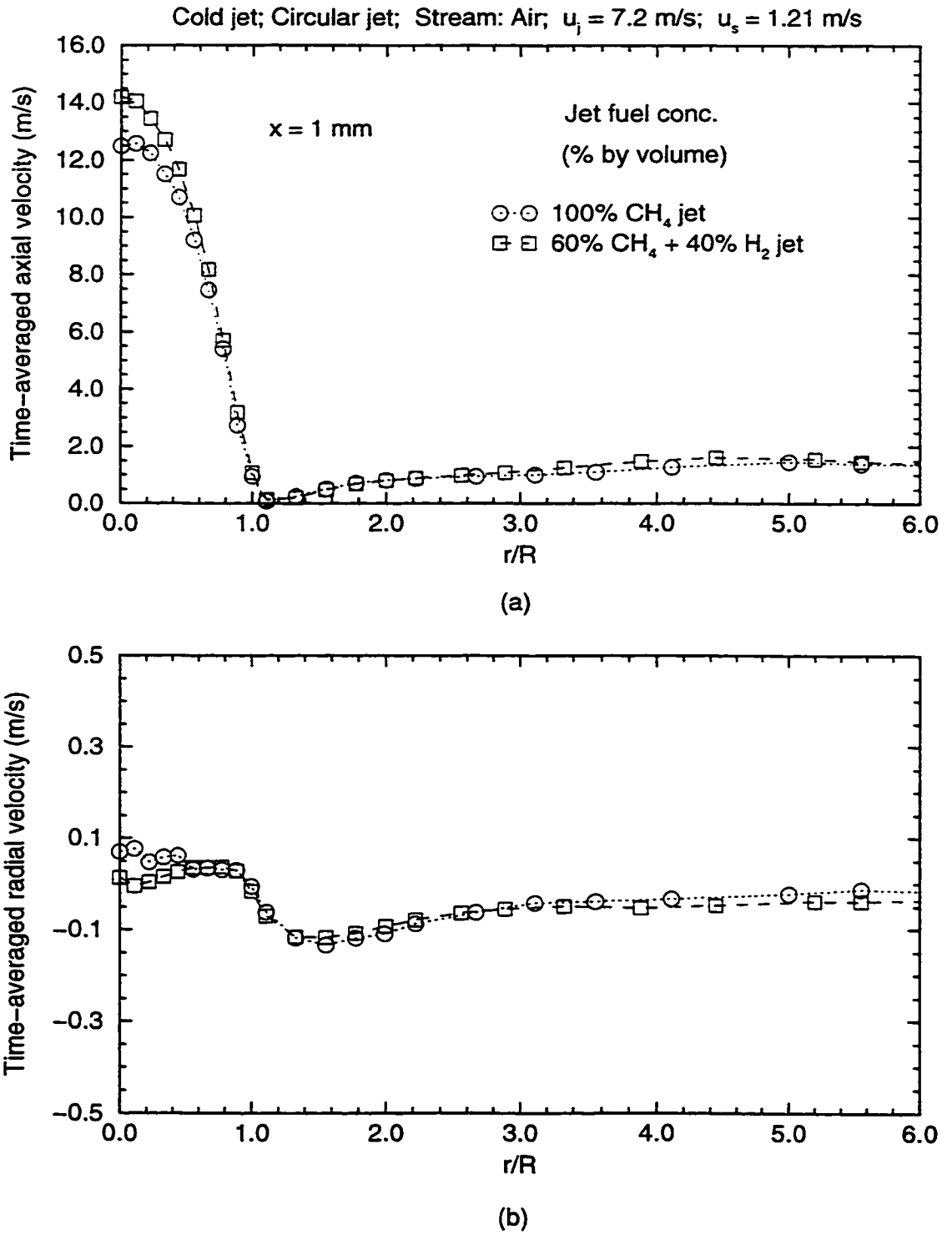

Fig. A.3.3 Time–averaged axial and radial velocity profiles for jets of different fuel compositions.

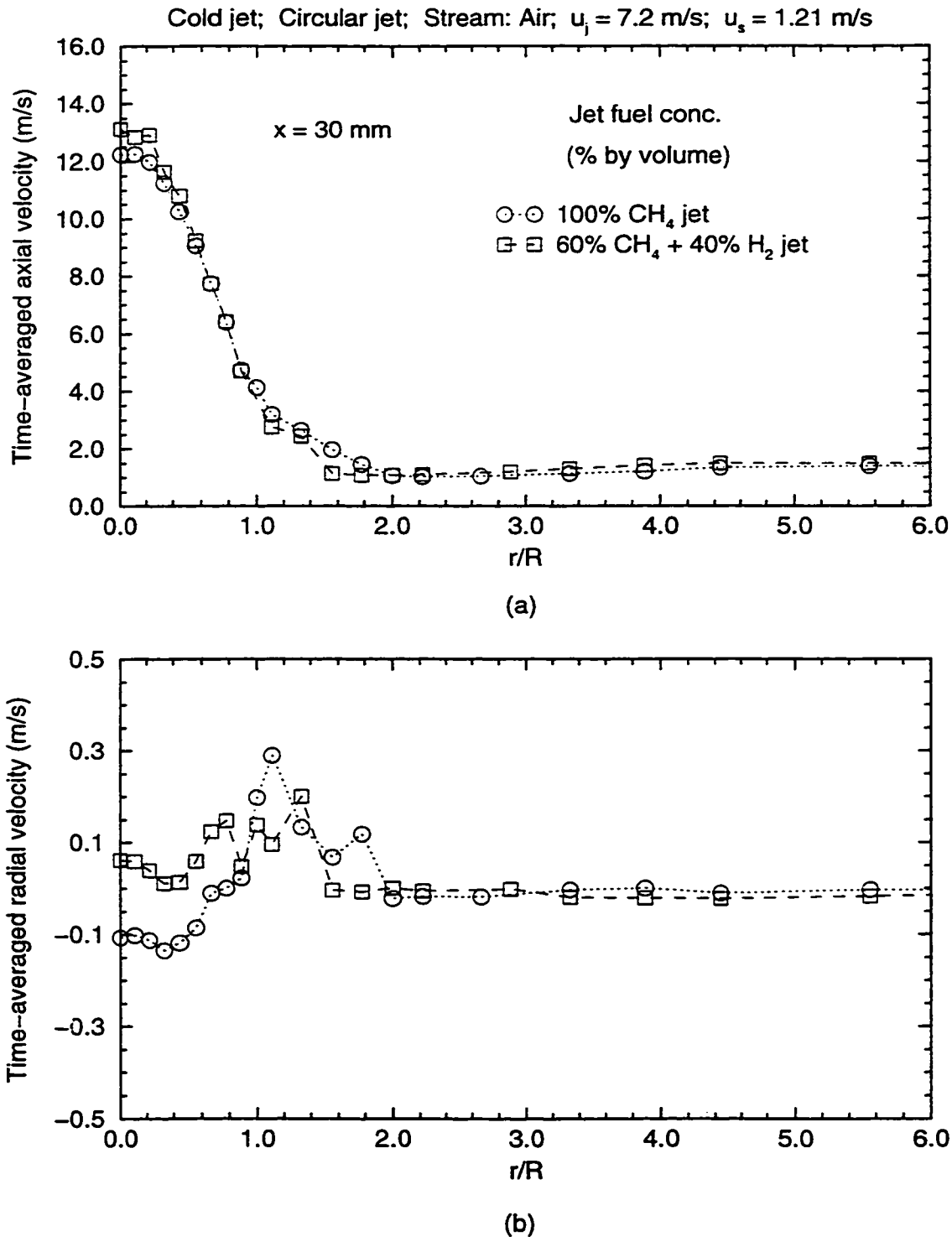

Fig. A.3.4 Time–averaged axial and radial velocity profiles within jets of different fuel compositions.

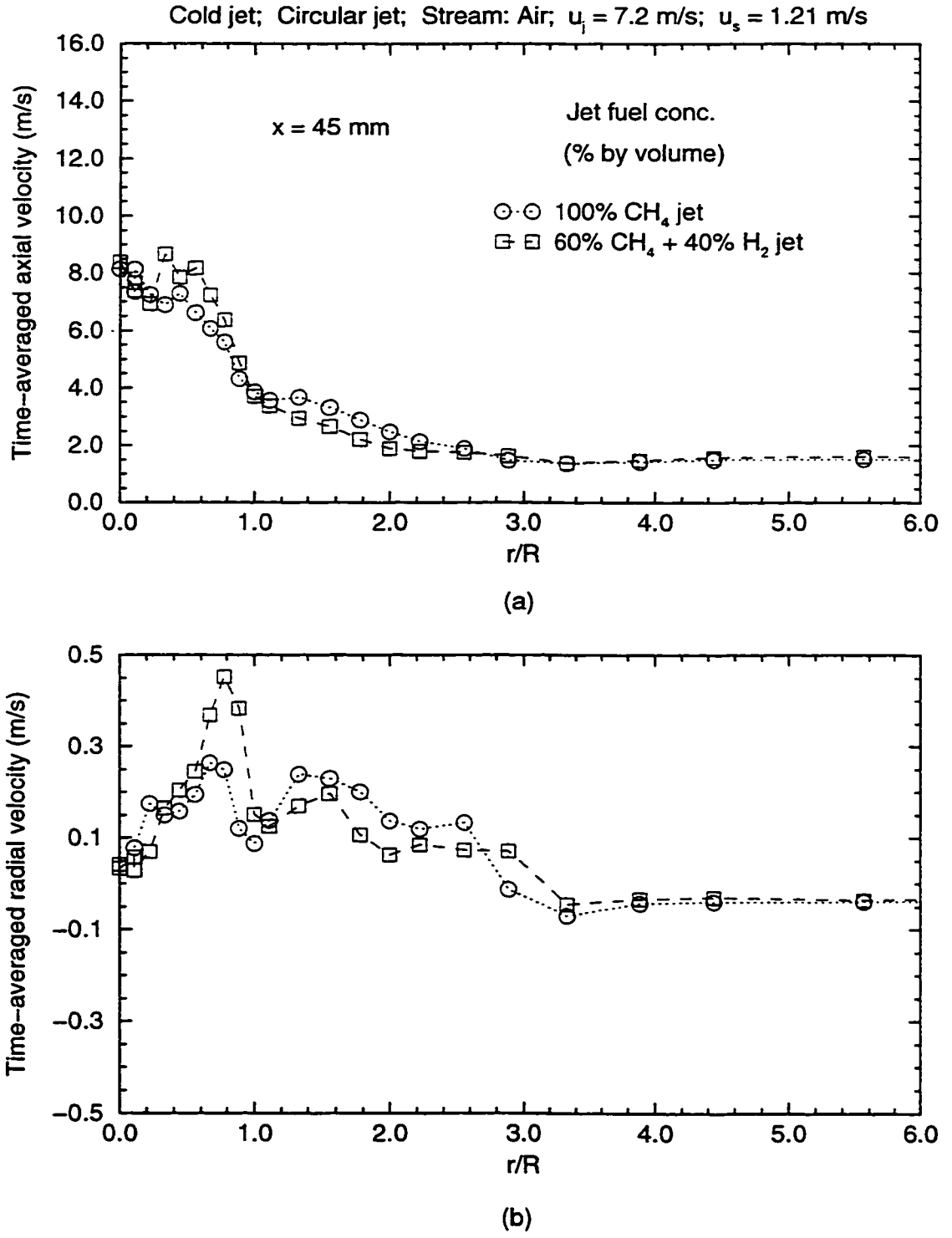

Fig. A.3.5 Time–averaged axial and radial velocity profiles within jets of different fuel compositions.

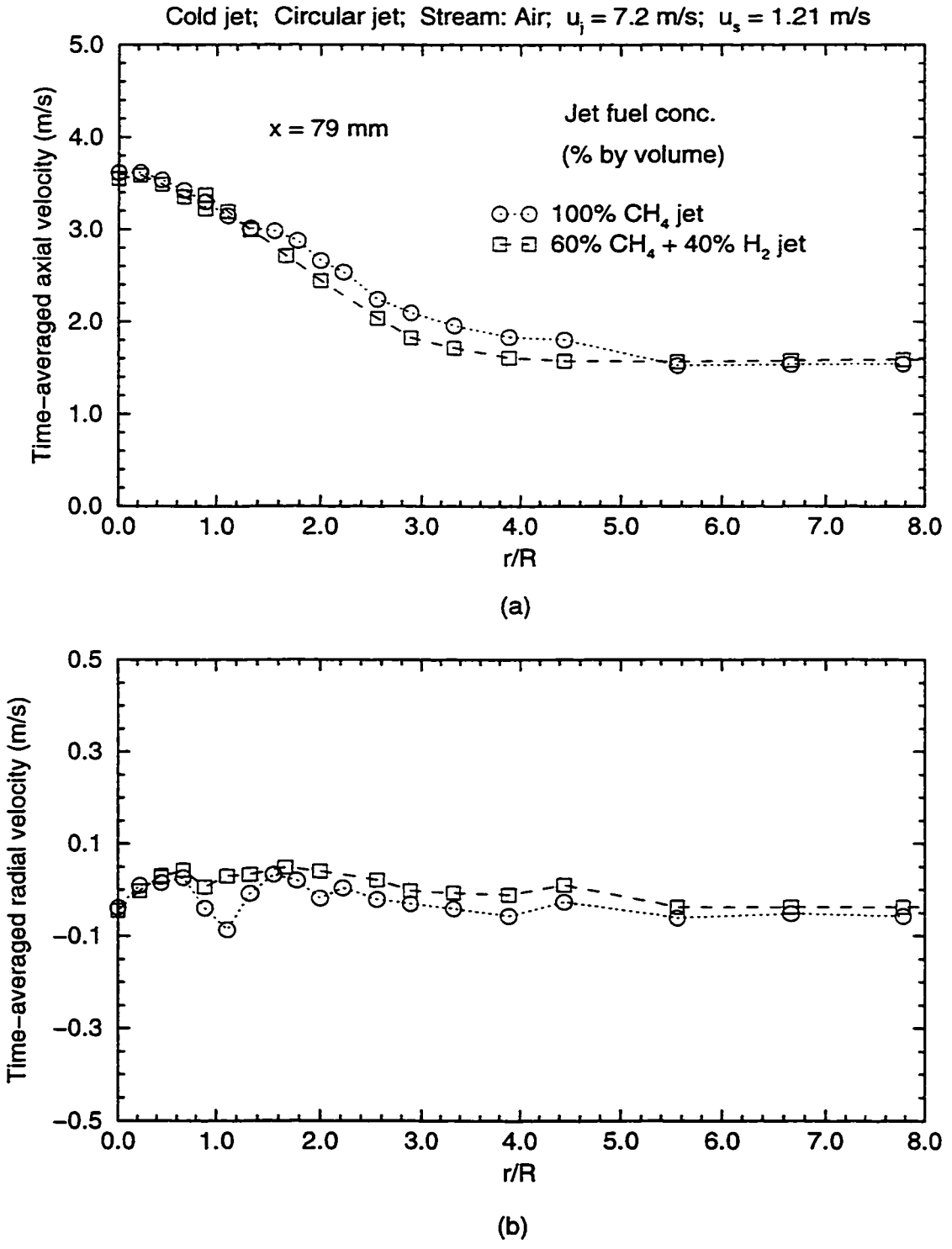

Fig. A.3.6 Time–averaged axial and radial velocity profiles within jets of different fuel compositions.

APPENDIX IV

LDV Measurements:

Effect of Auxiliary Methane in the Co-flowing Air Stream

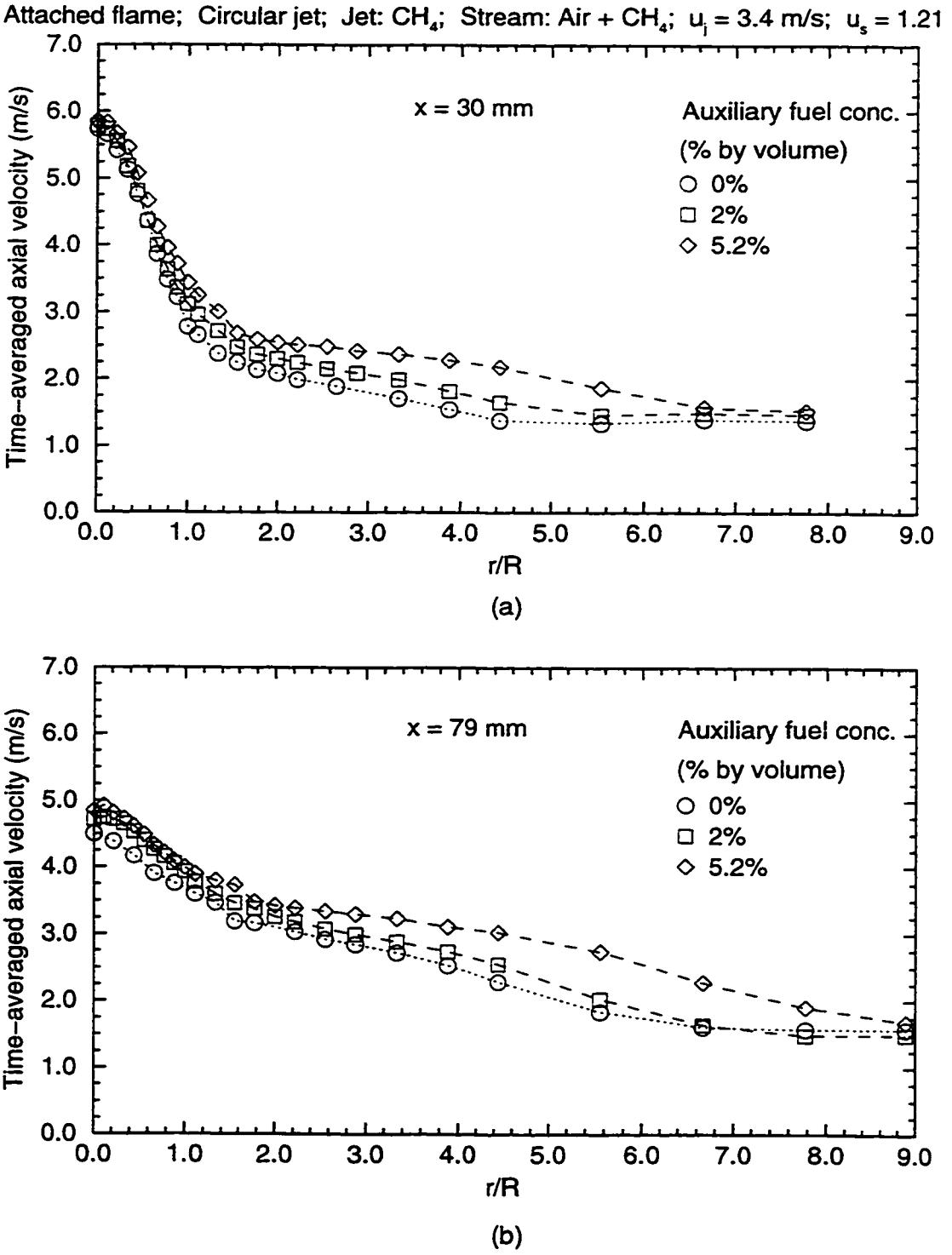

Fig. A.4.1 Time–averaged axial velocity profiles within attached flames issuing into a co–flowing air stream premixed with CH_4.

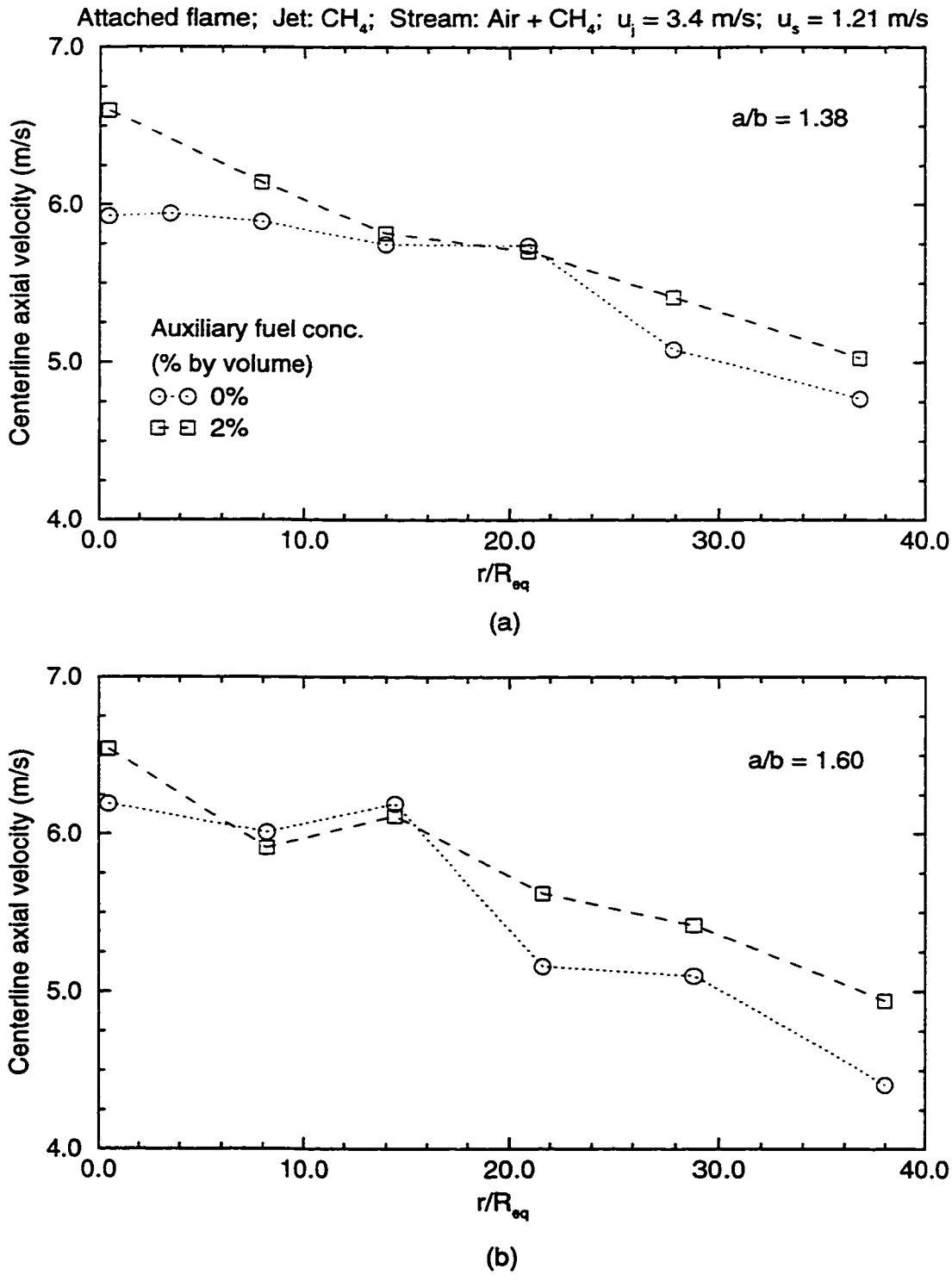

Fig. A.4.2 The variation of the axial velocity at the jet axis with downstream distance for attached flames issuing from two different elliptic jets into a co–flowing air stream premixed with 2.0% (by volume) CH_4.

APPENDIX V

LDV Measurements:

Effect of a Diluent in the Co-flowing Air Stream

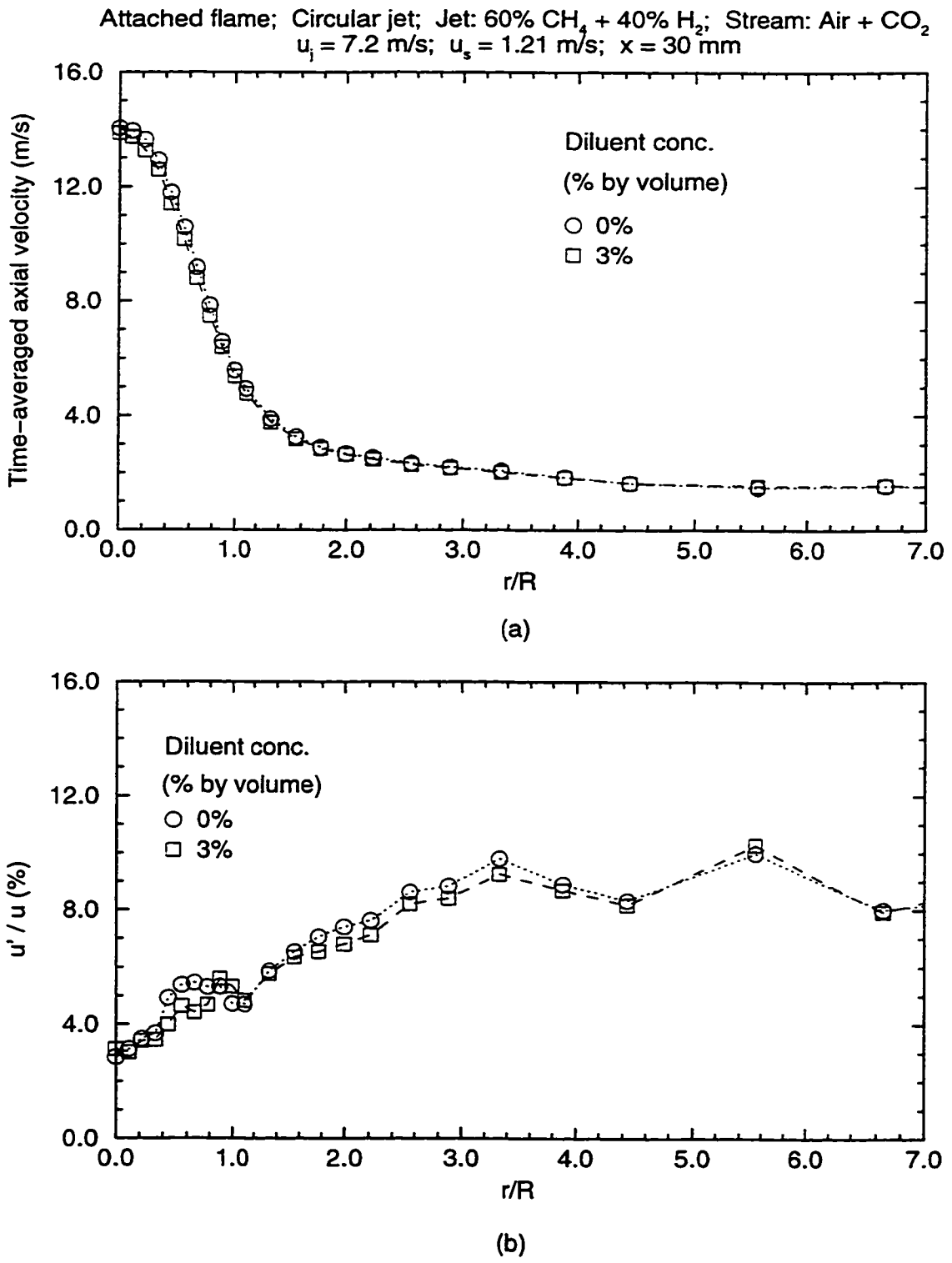

Fig. A.5.1 Time-averaged axial velocity profiles of attached flames issuing into a co-flowing air stream premixed with CO_2.

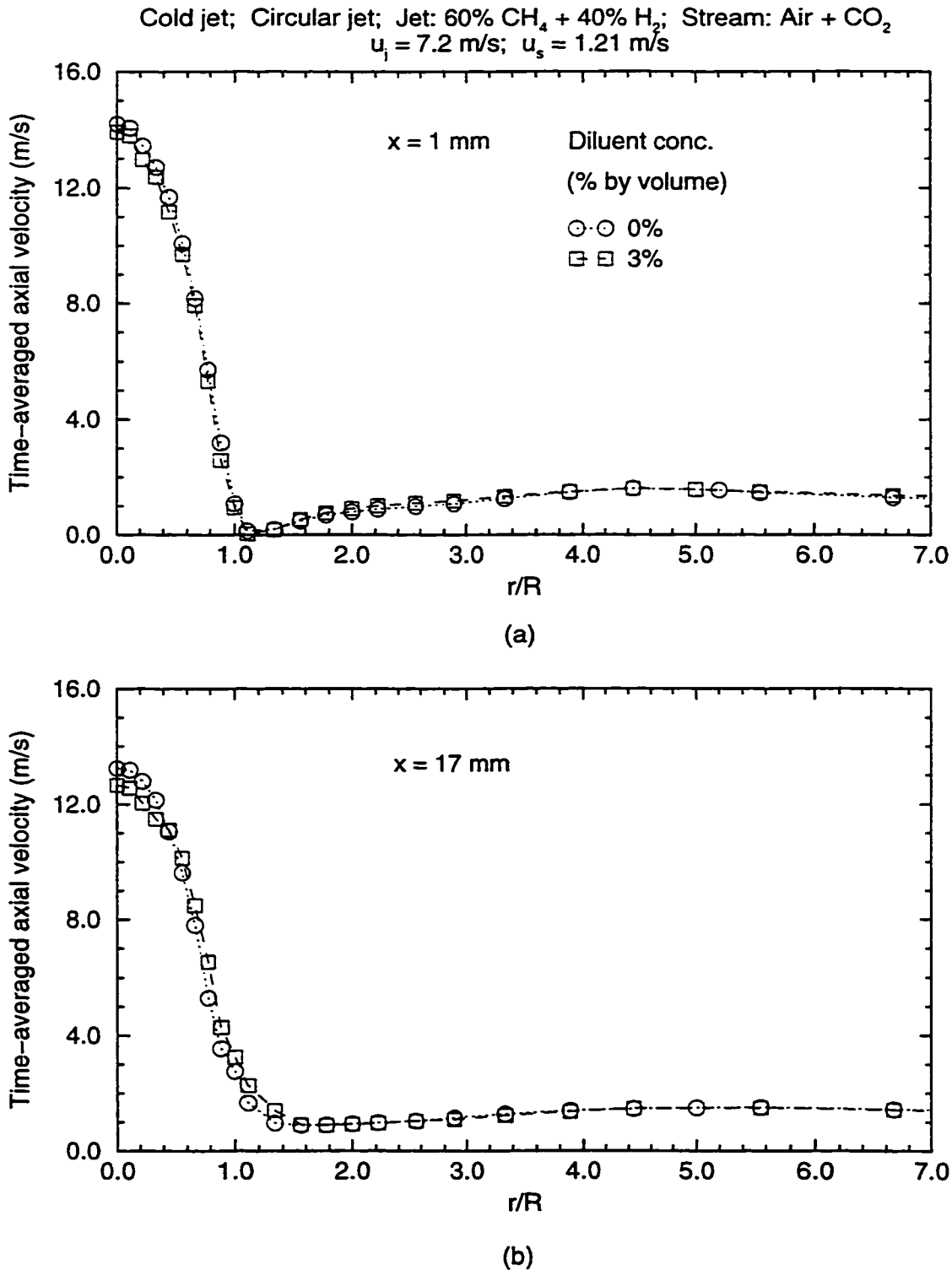

Fig. A.5.2 Turbulence intensity profiles within cold jets issuing into a co–flowing stream of air premixed with CO_2.

APPENDIX VI

LDV Measurements:

Effect of Jet Nozzle Ellipticity

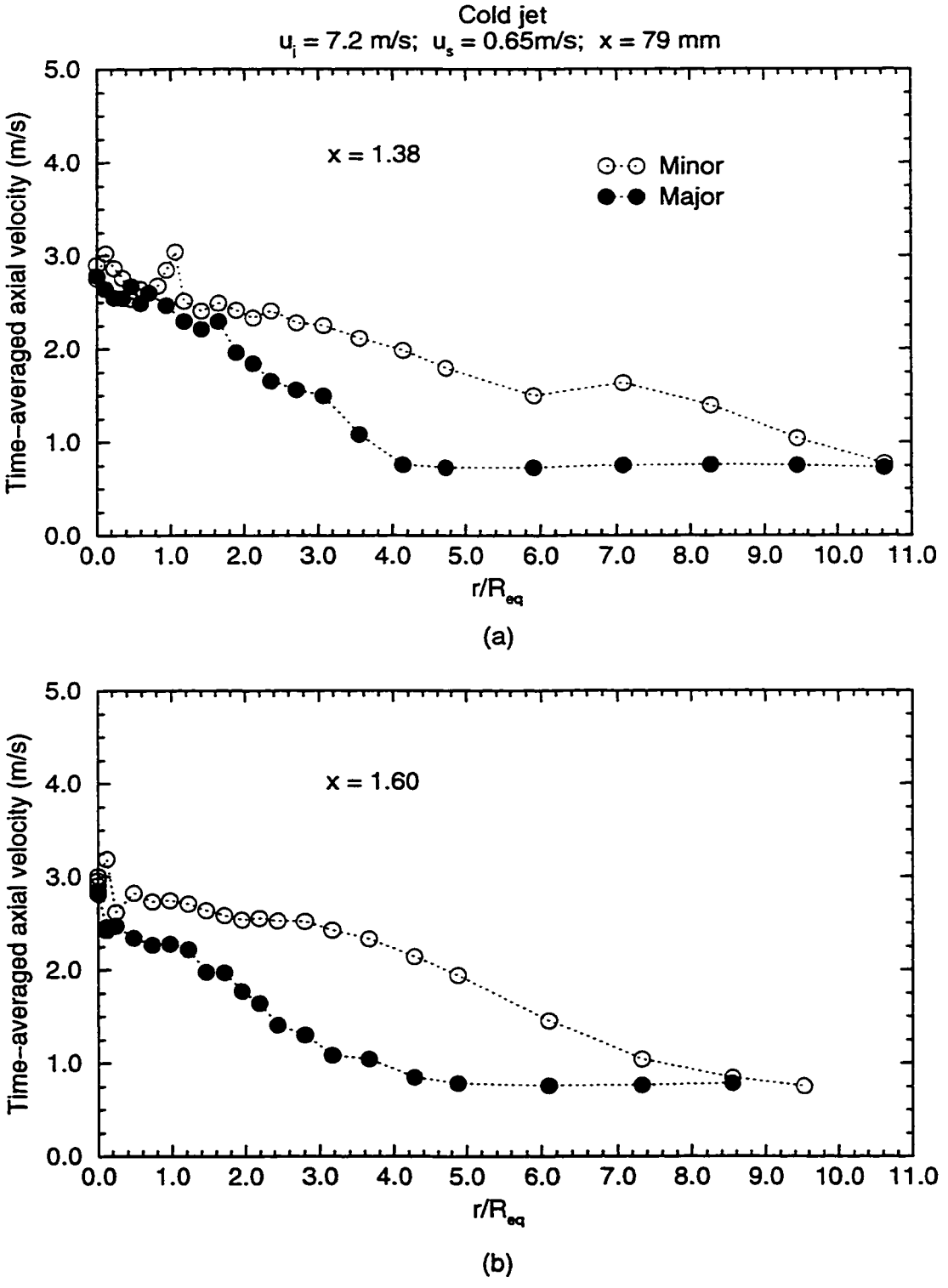

Fig. A.6.1 Time–averaged axial velocity profiles for elliptic jets of aspect ratios (a) 1.38 and (b) 1.60.

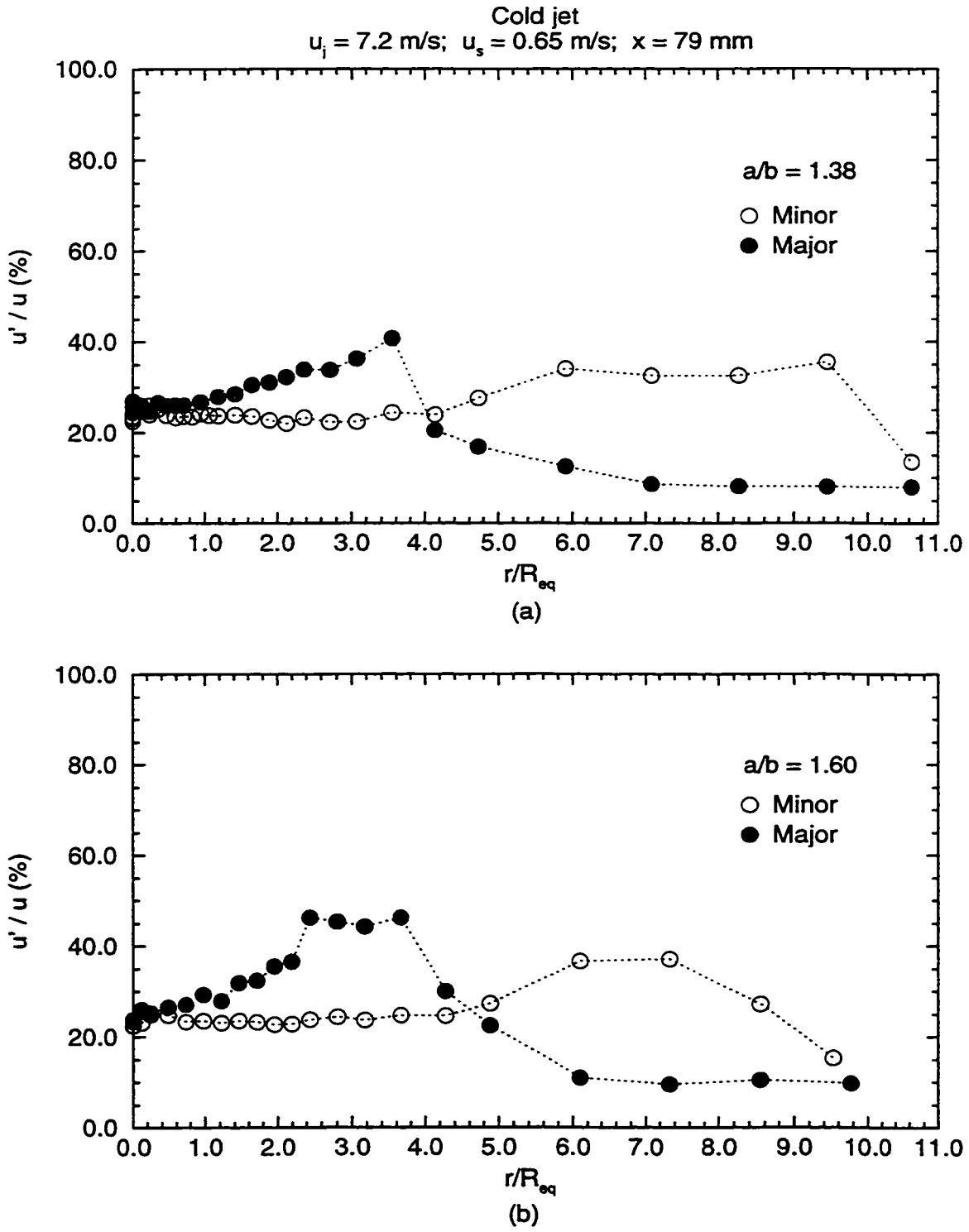

Fig. A.6.2 Turbulence intensity profiles within cold elliptic jets of aspect ratios (a) 1.38 and (b) 1.60.

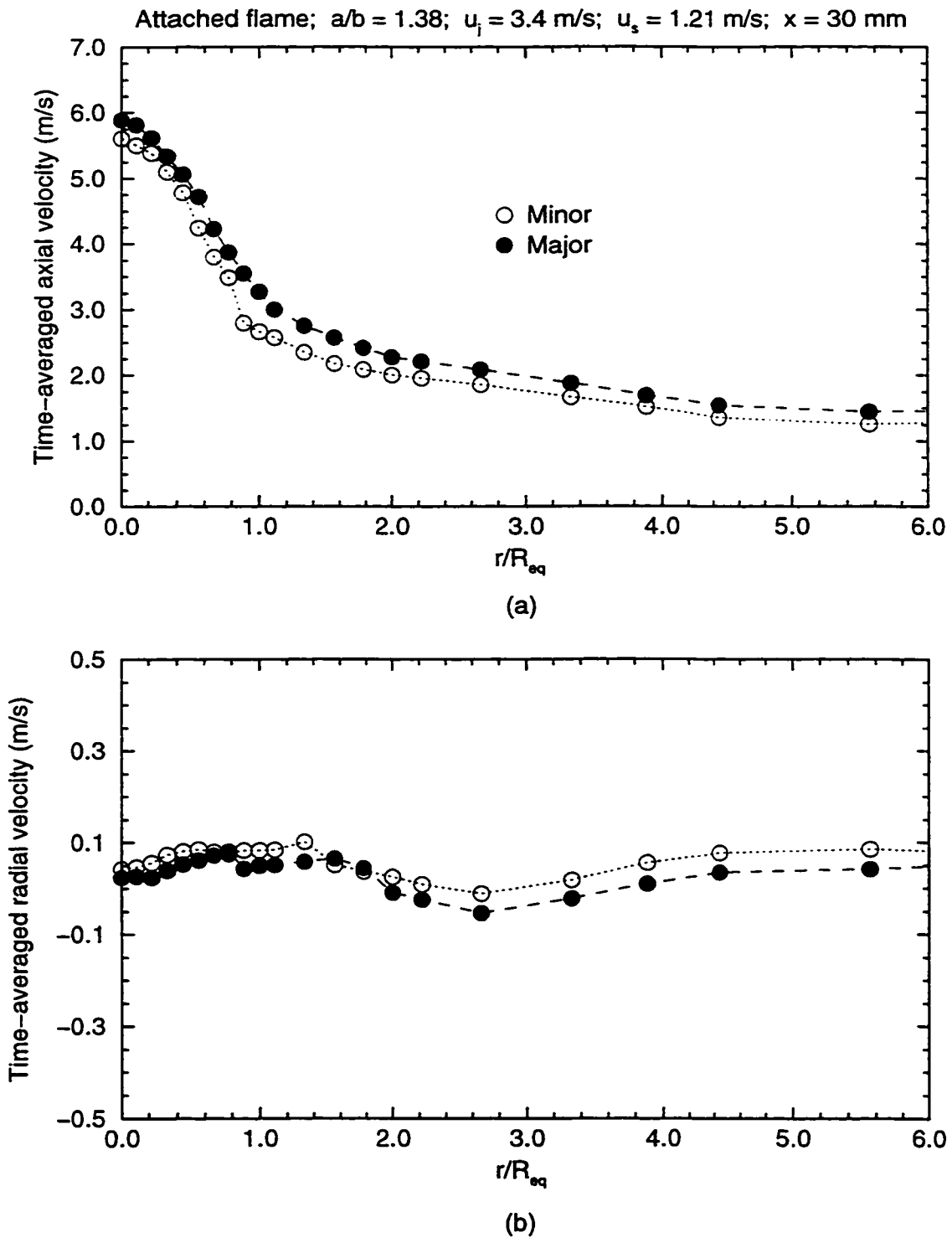

Fig. A.6.3 Time–averaged axial and radial velocity profiles within an attached flame discharging from an elliptic nozzle of aspect ratio 1.38.

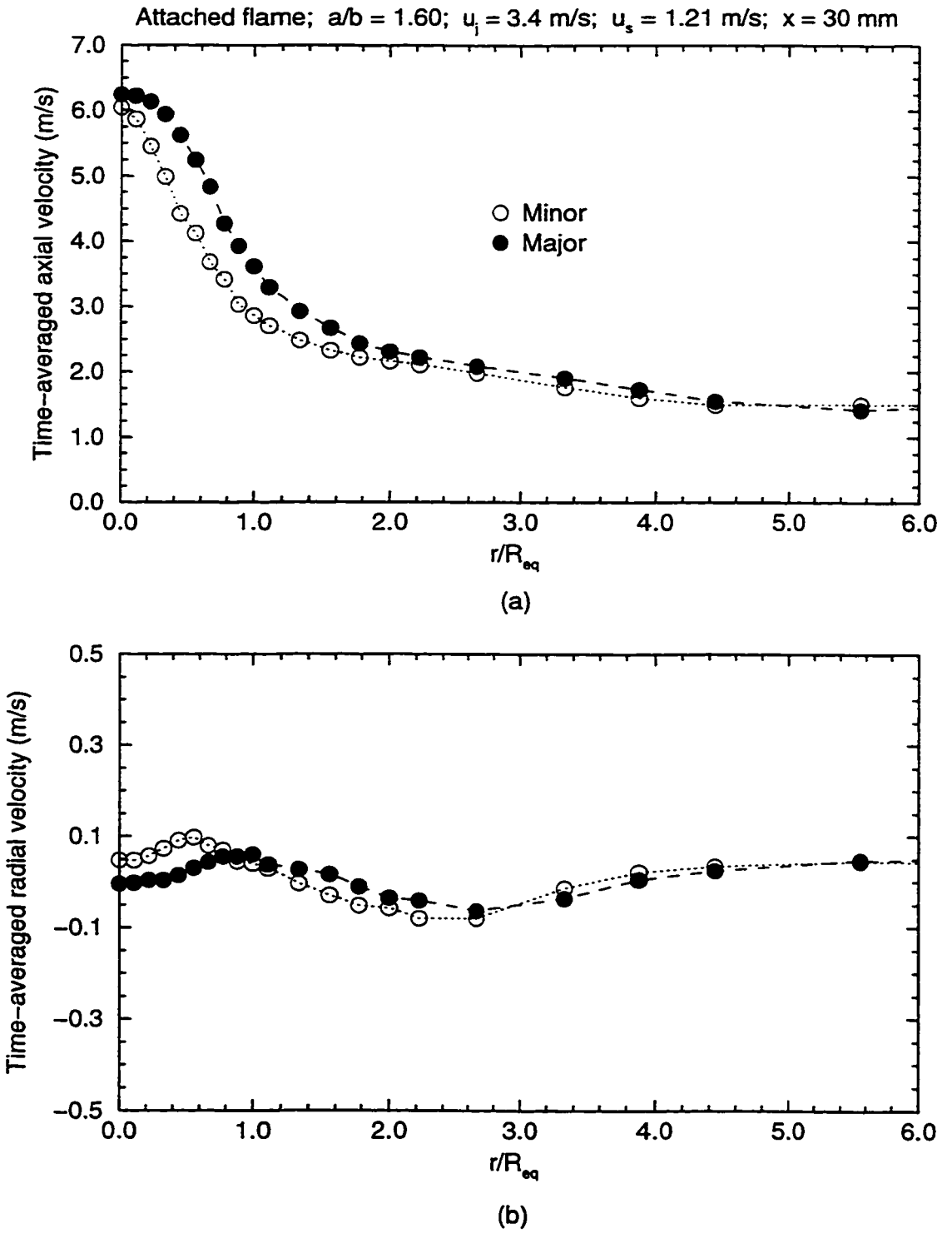

Fig. A.6.4 Time–averaged axial and radial velocity profiles within an attached flame discharging from an elliptic jet of aspect ratio 1.60.

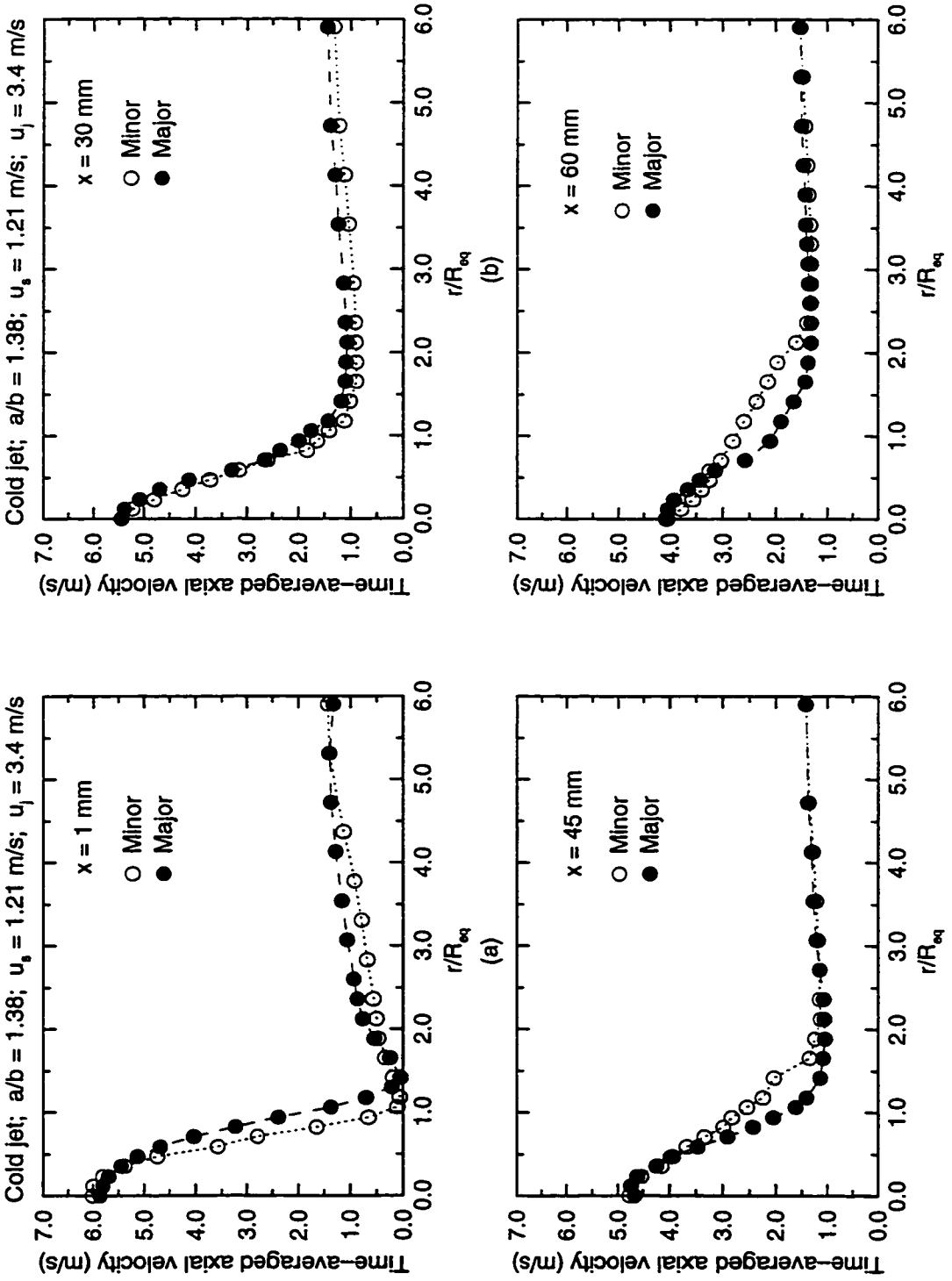

Fig. A.6.5 Time–averaged axial velocity profiles within a cold jet of aspect ratio 1.38 (R_{eq} = 2.15 mm).

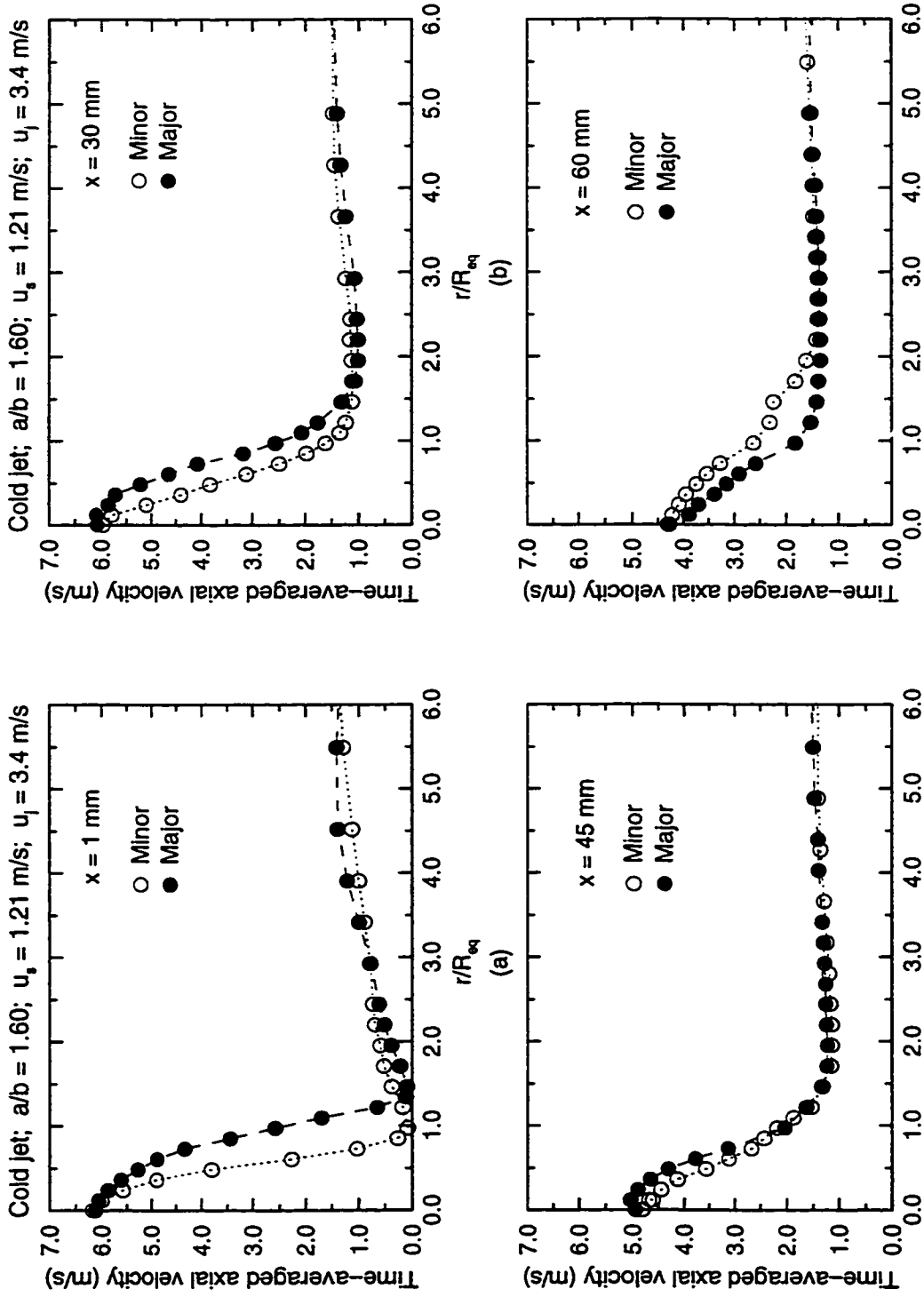

Fig. A.6.6 Time–averaged axial velocity profiles within a cold jet with an aspect ratio of 1.60 (R_{eq} = 2.08 mm).

IMAGE EVALUATION TEST TARGET (QA-3)

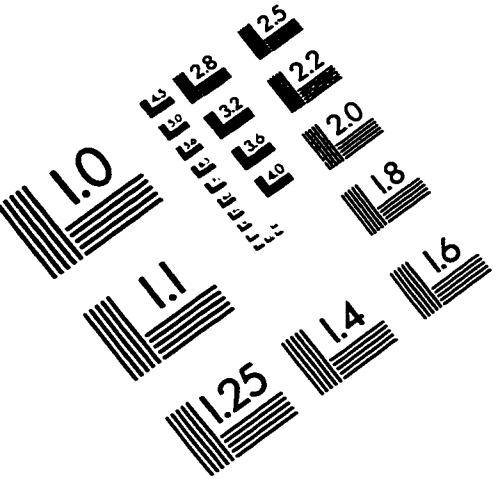

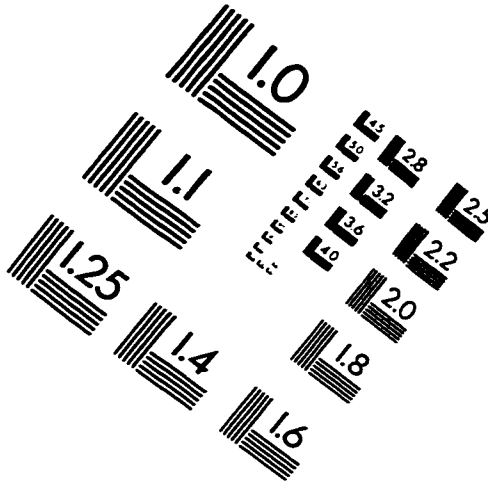

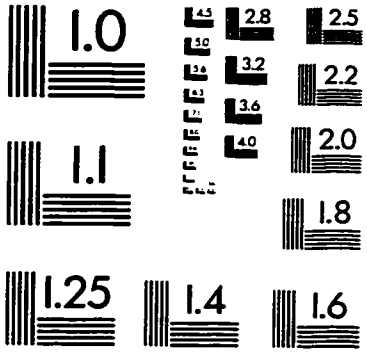

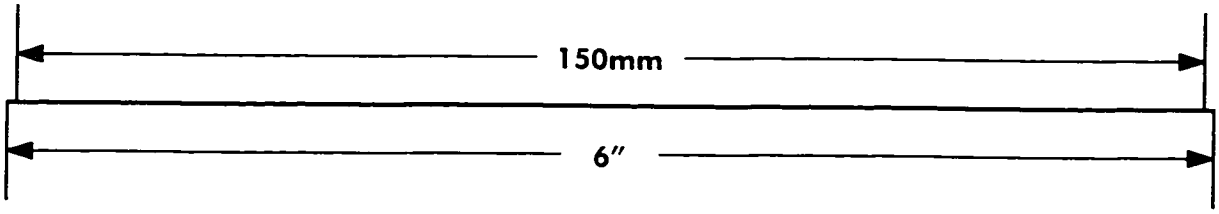

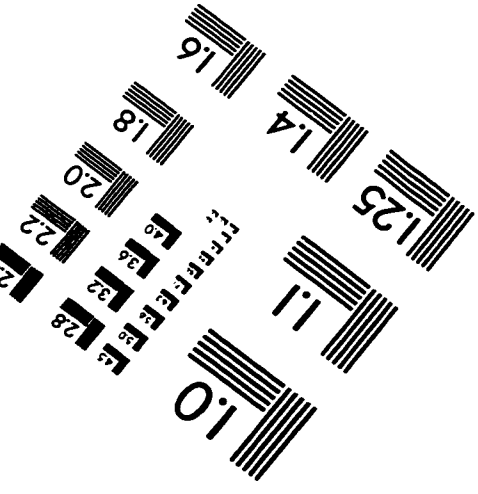

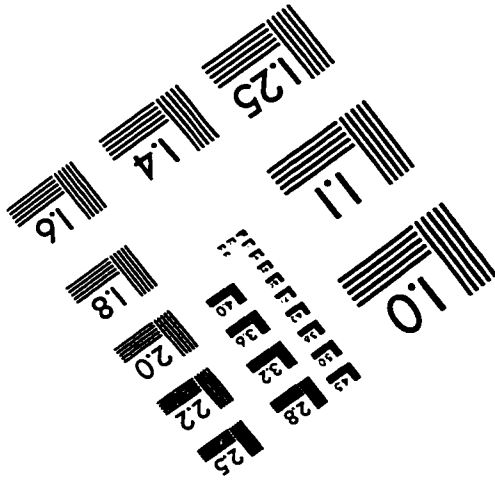

APPLIED IMAGE, Inc
1653 East Main Street
Rochester, NY 14609 USA
Phone: 716/482-0300
Fax: 716/288-5989

© 1993, Applied Image, Inc., All Rights Reserved